## **BULLETIN OF RUSSIAN STATE MEDICAL UNIVERSITY**

## BIOMEDICAL JOURNAL OF PIROGOV RUSSIAN NATIONAL RESEARCH MEDICAL UNIVERSITY

EDITOR-IN-CHIEF Denis Rebrikov, DSc, professor

**DEPUTY EDITOR-IN-CHIEF** Alexander Oettinger, DSc, professor

EDITORS Valentina Geidebrekht, PhD; Nadezda Tikhomirova

TECHNICAL EDITOR Evgeny Lukyanov

TRANSLATORS Nadezda Tikhomirova, Vyacheslav Vityuk

**DESIGN AND LAYOUT** Marina Doronina



SUBMISSION

#### **EDITORIAL BOARD**

Averin VI, DSc, professor (Minsk, Belarus)

Azizoglu M, MD PhD (Istanbul, Turkey)

Alipov NN, DSc. professor (Moscow Russia)

Belousov VV, DSc, professor (Moscow, Russia)

Bozhenko VK, DSc, CSc, professor (Moscow, Russia)

Bylova NA, CSc, docent (Moscow, Russia)

Gainetdinov RR, CSc (Saint-Petersburg, Russia)

Gendlin GYe, DSc, professor (Moscow, Russia)

Ginter EK, member of RAS, DSc (Moscow, Russia)

Gorbacheva LR, DSc, professor (Moscow, Russia)

Gordeev IG. DSc. professor (Moscow, Russia)

Gudkov AV, PhD, DSc (Buffalo, USA)

Gulyaeva NV, DSc, professor (Moscow, Russia)

Gusev EI, member of RAS, DSc, professor (Moscow, Russia)

Danilenko VN, DSc, professor (Moscow, Russia)

Zarubina TV, DSc, professor (Moscow, Russia)

Zatevakhin II, member of RAS, DSc, professor (Moscow, Russia)

Kagan VE, professor (Pittsburgh, USA)

Kzyshkowska YuG, DSc, professor (Heidelberg, Germany)

Kobrinskii BA, DSc, professor (Moscow, Russia)

Kozlov AV, MD PhD, (Vienna, Austria)

Kotelevtsev YuV, CSc (Moscow, Russia)

Lebedev MA, PhD (Darem, USA)

Manturova NE, DSc (Moscow, Russia)

Milushkina OYu, DSc, professor (Moscow, Russia)

Mitupov ZB, DSc, professor (Moscow, Russia)

Moshkovskii SA, DSc, professor (Moscow, Russia)

Munblit DB, MSc, PhD (London, Great Britain)

Negrebetsky VV, DSc, professor (Moscow, Russia) Novikov AA, DSc (Moscow, Russia)

Pivovarov YuP, member of RAS, DSc, professor (Moscow, Russia) Polunina NV, corr. member of RAS, DSc, professor (Moscow, Russia)

Poryadin GV, corr. member of RAS, DSc, professor (Moscow, Russia)

Razumovskii AYu, corr. member of RAS, DSc, professor (Moscow, Russia)

Rebrova OYu. DSc (Moscow, Russia)

Rudoy AS, DSc, professor (Minsk, Belarus)

Rylova AK, DSc, professor (Moscow, Russia)

Semiglazov VF, corr. member of RAS, DSc, professor (Saint-Petersburg, Russia)

Skoblina NA, DSc. professor (Moscow, Russia)

Slavyanskaya TA, DSc, professor (Moscow, Russia)

Smirnov VM, DSc, professor (Moscow, Russia)

Spallone A, DSc, professor (Rome, Italy)

Starodubov VI. member of RAS. DSc. professor (Moscow, Russia)

Stepanov VA, corr. member of RAS, DSc, professor (Tomsk, Russia)

Suchkov SV, DSc, professor (Moscow, Russia)

Takhchidi KhP, member of RAS, DSc, professor (Moscow, Russia)

Trufanov GE, DSc, professor (Saint-Petersburg, Russia)

Tumanova UN, MD (Moscow, Russia)

Favorova OO, DSc, professor (Moscow, Russia)

Filipenko ML, CSc, leading researcher (Novosibirsk, Russia)

Khazipov RN, DSc (Marsel, France)

Chundukova MA, DSc, professor (Moscow, Russia)

Schegolev AI, MD, professor (Moscow, Russia)

Shimanovskii NL, corr. member of RAS, Dsc, professor (Moscow, Russia)

Shishkina LN, DSc, senior researcher (Novosibirsk, Russia) Yakubovskaya RI, DSc, professor (Moscow, Russia)

SUBMISSION http://vestnik.rsmu.press/login?lang=en CORRESPONDENCE editor@rsmu.press

**COLLABORATION** manager@rsmu.press

ADDRESS ul. Ostrovityanova, d. 1, Moscow, Russia, 117997

Indexed in Scopus. CiteScore 2024: 0.7







SCImago Journal & Country Rank 2024: 0.166

SJR

Scimago Journal & Country Rank

Indexed in DOAJ



Open access to archive



Issue DOI: 10.24075/brsmu.2025-05

Mass media registration certificate No. 012769, issued on July 29, 1994. ISSN (Print): 2500-1094, ISSN (Online): 2542-1204

Founder and publisher: Pirogov Russian National Research Medical University (Moscow, Russia).

The journal is indexed in the following scientific databases: Scopus, Web of Science, Google Scholar, SJR, DOAJ, Scilit, CyberLeninka, Embase, EZB, Lens.org, MIT Libraries, OpenAlex, Research4Life, Scholia, Wikidata, and ZDB.

The journal is distributed under the terms of the Creative Commons Attribution 4.0 International License (www.creativecommons.org).



Approved for print 31.10.2025 Circulation: 100 copies. Printed by Print.Formula www.print-formula.ru

## ВЕСТНИК РОССИЙСКОГО ГОСУДАРСТВЕННОГО МЕДИЦИНСКОГО УНИВЕРСИТЕТА

НАУЧНЫЙ МЕДИЦИНСКИЙ ЖУРНАЛ РНИМУ ИМ. Н. И. ПИРОГОВА

ГЛАВНЫЙ РЕДАКТОР Денис Ребриков, д. б. н., профессор

ЗАМЕСТИТЕЛЬ ГЛАВНОГО РЕДАКТОРА Александр Эттингер, д. м. н., профессор

РЕДАКТОРЫ Валентина Гейдебрехт, к. б. н.; Надежда Тихомирова

ТЕХНИЧЕСКИЙ РЕДАКТОР Евгений Лукьянов

ПЕРЕВОДЧИКИ Надежда Тихомирова, Вячеслав Витюк

ДИЗАЙН И ВЕРСТКА Марины Дорониной



ПОДАЧА РУКОПИСЕЙ

#### РЕДАКЦИОННАЯ КОЛЛЕГИЯ

- В. И. Аверин, д. м. н., профессор (Минск, Белоруссия)
- М. Азизоглу, MD PhD (Стамбул, Турция)
- Н. Н. Алипов, д. м. н., профессор (Москва, Россия)
- В. В. Белоусов, д. б. н., профессор (Москва, Россия)
- В. К. Боженко, д. м. н., к. б. н., профессор (Москва, Россия)
- Н. А. Былова, к. м. н., доцент (Москва, Россия)
- Р. Р. Гайнетдинов, к. м. н. (Санкт-Петербург, Россия)
- Г. Е. Гендлин, д. м. н., профессор (Москва, Россия)
- Е. К. Гинтер, академик РАН, д. б. н. (Москва, Россия)
- Л. Р. Горбачева, д. б. н., профессор (Москва, Россия)
- И. Г. Гордеев, д. м. н., профессор (Москва, Россия)
- А. В. Гудков, PhD, DSc (Буффало, США)
- Н. В. Гуляева, д. б. н., профессор (Москва, Россия)
- Е. И. Гусев, академик РАН, д. м. н., профессор (Москва, Россия)
- В. Н. Даниленко, д. б. н., профессор (Москва, Россия)
- Т. В. Зарубина, д. м. н., профессор (Москва, Россия)
- И. И. Затевахин, академик РАН, д. м. н., профессор (Москва, Россия)
- В. Е. Каган, профессор (Питтсбург, США)
- Ю. Г. Кжышковска, д. б. н., профессор (Гейдельберг, Германия)
- Б. А. Кобринский, д. м. н., профессор (Москва, Россия)
- А. В. Козлов, MD PhD (Вена, Австрия)
- Ю. В. Котелевцев, к. х. н. (Москва, Россия)
- **М. А. Лебедев,** PhD (Дарем, США)
- Н. Е. Мантурова, д. м. н. (Москва, Россия)
- О. Ю. Милушкина, д. м. н., доцент (Москва, Россия)
- 3. Б. Митупов, д. м. н., профессор (Москва, Россия)
- С. А. Мошковский, д. б. н., профессор (Москва, Россия)
- **Д. Б. Мунблит,** MSc, PhD (Лондон, Великобритания)

- В. В. Негребецкий, д. х. н., профессор (Москва, Россия)
- А. А. Новиков, д. б. н. (Москва, Россия)
- Ю. П. Пивоваров, д. м. н., академик РАН, профессор (Москва, Россия)
- Н. В. Полунина, член-корр. РАН, д. м. н., профессор (Москва, Россия)
- Г. В. Порядин, член-корр. РАН, д. м. н., профессор (Москва, Россия)
- А. Ю. Разумовский, член-корр. РАН, д. м. н., профессор (Москва, Россия)
- О. Ю. Реброва, д. м. н. (Москва, Россия)
- А. С. Рудой, д. м. н., профессор (Минск, Белоруссия)
- А. К. Рылова, д. м. н., профессор (Москва, Россия)
- В. Ф. Семиглазов, член-корр. РАН, д. м. н., профессор (Санкт-Петербург, Россия)
- Н. А. Скоблина, д. м. н., профессор (Москва, Россия)
- Т. А. Славянская, д. м. н., профессор (Москва, Россия)
- В. М. Смирнов, д. б. н., профессор (Москва, Россия)
- А. Спаллоне, д. м. н., профессор (Рим, Италия)
- В. И. Стародубов, академик РАН, д. м. н., профессор (Москва, Россия)
- В. А. Степанов, член-корр. РАН, д. б. н., профессор (Томск, Россия)
- С. В. Сучков, д. м. н., профессор (Москва, Россия)
- Х. П. Тахчиди, академик РАН, д. м. н., профессор (Москва, Россия)
- Г. Е. Труфанов, д. м. н., профессор (Санкт-Петербург, Россия)
- У. Н. Туманова, д. м. н. (Москва, Россия)
- О. О. Фаворова, д. б. н., профессор (Москва, Россия)
- М. Л. Филипенко, к. б. н. (Новосибирск, Россия)
- Р. Н. Хазипов, д. м. н. (Марсель, Франция)
- М. А. Чундокова, д. м. н., профессор (Москва, Россия)
- Н. Л. Шимановский, член-корр. РАН, д. м. н., профессор (Москва, Россия)
- Л. Н. Шишкина, д. б. н. (Новосибирск, Россия)
- А. И. Щеголев, д. м. н., профессор (Москва, Россия)
- Р. И. Якубовская, д. б. н., профессор (Москва, Россия)

ПОДАЧА РУКОПИСЕЙ https://vestnik.rsmu.press/login?lang=ru

ПЕРЕПИСКА С РЕДАКЦИЕЙ editor@rsmu.press

**СОТРУДНИЧЕСТВО** manager@rsmu.press

АДРЕС РЕДАКЦИИ ул. Островитянова, д. 1, г. Москва, 117997

Журнал включен в Scopus. CiteScore 2024: 0,7

Журнал включен в WoS. JIF 2024: 0,4

Индекс Хирша (h<sup>6</sup>) журнала по оценке Google Scholar: 1



WEB OF SCIENCE



SJR SCImago Journal & Country Rank 2024: 0,166

Журнал включен в DOAJ

Зпесь науолится открытый эруир условая

SJR

Scimago Journal & Country Rank





DOI выпуска: 10.24075/vramu.2025-05

Свидетельство о регистрации средства массовой информации № 012769 от 29 июля 1994 г. ISSN (Print): 2500-1094, ISSN (Online): 2542-1204.

Учредитель и издатель — Российский национальный исследовательский медицинский университет имени Н. И. Пирогова (Москва, Россия).

Журнал индексируется в научных базах Scopus, Web of Science, Google Scholar, SJR, DOAJ, Scilit,

CyberLeninka, Embase, EZB, Lens.org, MITLibaries, OpenAlex, Research4Life, Scholia, Wikidata, ZDB.

Журнал распространяется по лицензии Creative Commons Attribution 4.0 International (www.creativecommons.org).



Подписано в печать 31.10.2025 Тираж 100 экз. Отпечатано в типографии Print.Formula www.print-formula.ru

## **BULLETIN OF RSMU** 5, 2025

BECTHUK PEN	1)	/
-------------	----	---

## Contents

Содержание

ORIGINAL RESEARCH	5
Age-related alterations in the immune system of aging mice  Matveeva KS, Shevyrev DV	
<b>Возрастные изменения в иммунной системе стареющих мышей</b> К. С. Матвеева, Д. В. Шевырев	
ORIGINAL RESEARCH	12
Panel of IFN-I-induced genes in systemic scleroderma: a stratification biomarker potential Shagina IA, Turchaninova MA, Golovina OA, Bufeeva LS, Zhurina TI, Saifullin RF, Myshkin MYu, Mutovina ZYu, Britanova OV	
Панель IFN-I-индуцируемых генов при системной склеродермии: потенциал биомаркера стратификации И. А. Шагина, М. А. Турчанинова, О. А. Головина, Л. С. Буфеева, Т. И. Журина, Р. Ф. Сайфуллин, М. Ю. Мышкин, З. Ю. Мутовина, О. В. Британова	
ORIGINAL RESEARCH	22
Alterations in mitochondrial and lysosomal compartments under chemotherapy-induced senescence Shatalova RO, Shevyrev DV	
<b>Изменения митохондриального и лизосомного компартментов в условиях химиоиндуцированной сенесцентности</b> Р. О. Шаталова, Д. В. Шевырев	
CLINICAL CASE	32
Morphological, immunohistochemistry and molecular analysis of differentiated high-grade carcinoma  Makhachev DR, Bulanov DV, Shovkhalov MM, Bekmurziev BZ, Geroev IA, Netsvetova AM, Zhusupova AR, Gubich DS, Manovski AM	
Морфологический, иммуногистохимический и молекулярный анализ дифференцированной высокозлокачественной карциномы Д. Р. Махачев, Д. В. Буланов, М. М. Шовхалов, Б. З. Бекмурзиев, И. А. Героев, А. М. Нецветова, А. Р. Жусупова, Д. С. Губич, А. М. Мановски	
ORIGINAL RESEARCH	38
Revival of radioimmunoassay for determination of insulin autoantibodies Timofeev AV, Galimov RR, Kolesnikova EA, Artyuhov AS, Skoblov YuS, Taktarov SV	
Реанимация радиоиммунологического метода определения аутоантител к инсулину А. В. Тимофеев, Р. Р. Галимов, Е. А. Колесникова, А. С. Артюхов, Ю. С. Скоблов, С. В. Тактаров	
OPINION	44
Prospects of finding pathologically based therapies for epilepsy associated with brain glioma  Ashkhatsava TI, Kalinin VA, Yakunina AV, Poverennova IE	
Перспективы поиска патогенетически обоснованной терапии эпилепсии, ассоциированной с глиомой головного мозга Т. И. Ашхацава, В. А. Калинин, А. В. Якунина, И. Е. Повереннова	
ORIGINAL RESEARCH	48
Transcriptomic features of FAP+ cells across molecular subtypes of breast cancer Kalinchuk AYu, Patskan IA, Stadelman MM, Grigorieva ES, Tashireva LA	
Особенности транскриптомного профиля FAP*-клеток в опухолях молочной железы различных молекулярно-биологических подт А. Ю. Калинчук, И. А. Пацкан, М. М. Штадельман, Е. С. Григорьева, Л. А. Таширева	гипов
ORIGINAL RESEARCH	55
Optimization of human B cell culture conditions for expansion of activated or differentiated B cells Sokolova SR, Grigorova IL	
Оптимизация условий культивирования В-клеток человека для экспансии активированных или дифференцированных В-клеток С. Р. Соколова, И. Л. Григорова	
ORIGINAL RESEARCH	65
Comparative analysis of metallic endovascular coil frame designs Chepeleva EV, Kozyr KV, Borodin VP, Khakhalkin VV, Vladimirov SV, Makhmudov MA, Badoian AG, Baranov AA, Krestyaninov OV	
Сравнительный анализ конструкций металлических каркасов эндоваскулярных спиралей Е. В. Чепелева, К. В. Козырь, В. П. Бородин, В. В. Хахалкин, С. В. Владимиров, М. А. Махмудов, А. Г. Бадоян, А. А. Баранов, О. В. Крестьянинов	
ORIGINAL RESEARCH	74
Cytocompatibility of pressureless sintered porous B <sub>4</sub> C-ceramics assessed <i>in vitro</i> Chepeleva EV, Kozyr KV, Vaver AA, Khakhalkin VV	
Цитосовместимость свободноспеченной пористой В₄С-керамики при исследовании <i>in vitro</i> Е. В. Чепелева, К. В. Козырь, А. А. Вавер, В. В. Хахалкин	

ORIGINAL RESEARCH 81 Susceptibility of the nontuberculous mycobacteria circulating in Russia to bedaquiline Smirnova TG, Andreevskaya SN, Larionova EE, Zaytseva AS, Kiseleva EA, Ustinova VV, Chernousova LN, Ergeshov AE Чувствительность к бедаквилину нетуберкулезных микобактерий, циркулирующих на территории России Т.Г. Смирнова, С. Н. Андреевская, Е. Е. Ларионова, А. С. Зайцева, Е. А. Киселева, В. В. Устинова, Л. Н. Черноусова, А. Э. Эргешов 86 ORIGINAL RESEARCH Neurophysiological markers of the illusion caused by the mirror visual feedback Mokienko OA, Bobrov PD, Soloveva AA, Isaev MR, Kerechanin YaV, Ratnikova VYu, Kataitsev VA, Shagina ED, Nikishina VB Нейрофизиологические маркеры иллюзии, вызванной зеркальной визуальной обратной связью О. А. Мокиенко, П. Д. Бобров, А. А. Соловьева, М. Р. Исаев, Я. В. Керечанин, В. Ю. Ратникова, В. А. Катайцев, Е. Д. Шагина, В. Б. Никишина ORIGINAL RESEARCH 94 Molecular cytogenetic characterization of a rare recombinant chromosome 22 caused by a maternal intrachromosomal insertion Yurchenko DA, Markova ZhG, Petukhova MS, Matyushchenko GN, Shilova NV Молекулярно-цитогенетическая характеристика редкого случая рекомбинантной хромосомы 22 вследствие материнской **интрахромосомной инсерции** Д. А. Юрченко, Ж. Г. Маркова, М. С. Петухова, Г. Н. Матющенко, Н. В. Шилова

OPINION

The terms "Ideminant" and "vecessive" should be avaided due to gone therepy

The terms "dominant" and "recessive" should be avoided due to gene therapy

В медицине следует избегать терминов «доминантный» и «рецессивный» из-за развития генной терапии А. М. Гамисония, Д. В. Ребриков

102

#### AGE-RELATED ALTERATIONS IN THE IMMUNE SYSTEM OF AGING MICE

Matveeva KS, Shevyrev DV <sup>™</sup>

Sirius University of Science and Technology, Sirius Federal Territory, Krasnodarsky Krai, Russia

Accumulation of senescent cells in the tissues is associated with functional impairment and the development of age-related disorders. The key role in this process is played by the senescence-associated secretory phenotype (SASP) contributing to chronic systemic inflammation, which is associated with the increased risk of autoimmune disorders and cancer, as well as the decreased resistance to infections. Normally, the immune system eliminates senescent cells, but the effectiveness of this process decreases with age, including due to the immune system aging. The study aimed to assess age-related alterations in the main lymphocyte and myelocyte populations in the spleen and bone marrow samples of senile mice. The study involved groups of young (n = 8) and elderly (n = 4) C57BL/6 mice. Populations were tested by flow cytometry using the fluorescence-labeled antibodies. The aging phenotype was assessed based on the  $\beta$ -Gal enzyme activity with pre-treatment with bafilomycin A1, ensuring lysosomal alkalinization and allowing one to detect the increased enzyme activity typical for the aging cells (SA- $\beta$ -Gal). As a result, the significantly increased levels of myeloid populations, CD11c $^+$ B cells, double-negative T cells, along with the decreased levels of the CD8 $\alpha$  $^+$  dendritic cells, were reported in elderly mice. Furthermore, aging was associated with the significant increase in the levels of SA- $\beta$ -Gal-positive cells, especially in the populations of myeloid cells. The data obtained suggest that the age-related alterations are of systemic nature and reflect the so-called myeloid shift, as well as accumulation of pro-inflammatory populations in the myeloid and lymphoid compartments.

Keywords: aging, senescence, immune system aging,  $\beta$ -galactosidase, SA- $\beta$ -Gal, lymphocytes, myelocytes, mice

Funding: the study was supported by the Russian Science Foundation pa6ora, project No. 24-15-20003 https://rscf.ru/project/24-15-20003/ (date of access: August 19, 2025).

Author contribution: Matveeva KS — experimental procedure, data processing, manuscript formatting, Shevyrev DV — experimental procedure, statistical analysis, manuscript reviewing.

Compliance with ethical standards: the study was approved by the Ethics Committee of the Sirius University of Science and Technology (protocol No. 7.1 dated 12 April 2024).

Correspondence should be addressed: Daniil V. Shevyrev Olimpiysky prospekt, 1, Sochi, 354349, Russia; dr.daniil25@mail.ru

Received: 27.08.2025 Accepted: 23.09.2025 Published online: 30.09.2025

DOI: 10.24075/brsmu.2025.043

Copyright: © 2025 by the authors. Licensee: Pirogov University. This article is an open access article distributed under the terms and conditions of the Creative Commons Attribution (CC BY) license (https://creativecommons.org/licenses/by/4.0/).

## ВОЗРАСТНЫЕ ИЗМЕНЕНИЯ В ИММУННОЙ СИСТЕМЕ СТАРЕЮЩИХ МЫШЕЙ

К. С. Матвеева, Д. В. Шевырев

Научно-технологический университет «Сириус», Федеральная территория «Сириус», Краснодарский край, Россия

Накопление сенесцентных клеток в тканях связано с функциональным ухудшением и развитием возраст-ассоциированных патологий. Ключевую роль в этом процессе играет сенесцент-ассоциированный секреторный фенотип (SASP), способствующий хроническому вялотекущему системному воспалению, которое ассоциировано с повышенным риском аутоиммунных и онкологических заболеваний, а также снижением устойчивости к инфекциям. В норме иммунная система удаляет сенесцентные клетки, однако с возрастом эффективность этого процесса падает, в том числе по причине старения иммунной системы. Целью исследования было изучить возрастные изменения в основных популяциях лимфоцитов и миелоцитов в образцах селезенки и костного мозга мышей преклонного возраста. Исследование проводили на группах молодых (*n* = 8) и пожилых (*n* = 4) мышей линии C57BL/6. Анализ популяций проводили с использованием флуоресцентно-меченых антител методом проточной цитометрии. Фенотип старения оценивали по активности фермента β-Gal с предварительной обработкой бафиломицином A1, который обеспечивает защелачивание лизосом и позволяет выявить повышенную активность фермента, типичную для стареющих клеток (SA-β-Gal). В результате у пожилых мышей было выявлено значимое повышение содержания миелоидных популяций, CD11c<sup>\*</sup>B-клеток, дважды негативных Т-лимфоцитов, а также снижение CD8α<sup>\*</sup> дендритных клеток. Кроме того, при старении значимо возрастало содержание клеток позитивных по SA-β-Gal, особенно в популяциях миелоидных клеток. Полученные данные указывают, что возрастные изменения носят системный характер и отражают так называемый миелоидный сдвиг, а также накопление провоспалительных популяций в миелоидном и лимфоидном компартментах.

Ключевые слова: старение, сенесцентность, старение иммунной системы, β-галактозидаза, SA-β-Gal, лимфоциты, миелоциты, мыши

Финансирование: данная работа выполнена при поддержке Российского Научного Фонда, проект № 24-15-20003 https://rscf.ru/project/24-15-20003/ (дата доступа 19 августа 2025 г.).

Вклад авторов: К. С. Матвеева — проведение экспериментов, обработка данных, оформление рукописи, Д. В. Шевырев — проведение экспериментов, статистический анализ, рецензирование рукописи.

Соблюдение этических стандартов: исследование одобрено этическим комитетом Университета «Сириус» (протокол № 7.1 от 12 апреля 2024 г.).

 Для корреспонденции: Даниил Вадимович Шевырев Олимпийский проспект, д. 1, г. Сочи, 354349, Россия; dr.daniil25@mail.ru

Статья получена: 27.08.2025 Статья принята к печати: 23.09.2025 Опубликована онлайн: 30.09.2025

DOI: 10.24075/vramu.2025.043

Авторские права: © 2025 принадлежат авторам. Лицензиат: PHИMУ им. Н. И. Пирогова. Статья размещена в открытом доступе и распространяется на условиях лицензии Creative Commons Attribution (CC BY) (https://creativecommons.org/licenses/by/4.0/).

## ОРИГИНАЛЬНОЕ ИССЛЕДОВАНИЕ І ИММУНОЛОГИЯ

Cellular senescence is a complex, multifactorial process triggered by diverse stressors, including DNA damage, telomere attrition, retrotransposon activation, oxidative and mechanical stress, as well as adverse physical, chemical, and biological factors [1, 2]. The accumulation of mutations and various types of molecular damage in aging cells increases the risk of neoplastic transformation. Currently, entry into a senescent state is recognized as one of the key tumor-suppressive mechanisms [3, 4]. Senescence is orchestrated through the convergence of several signaling cascades, primarily the p53/p21<sup>CIP1</sup> and p16<sup>INK4a/RB</sup> pathways [5]. These pathways are activated in response to telomere shortening and DNA damage (DNA damage response, DDR), oncogene activation, epigenetic alterations, chromatin architecture disruption, excessive reactive oxygen species (ROS) production due to organelle dysfunction — particularly mitochondrial dysfunction as well as specific inflammatory and paracrine signals [6, 7]. Stress-induced activation of the NF-kB and mTOR pathways drives senescent cells to secrete a broad spectrum of proinflammatory mediators (the senescence-associated secretory phenotype, SASP) and impairs autophagy [8, 9]. Concurrently, upregulation of anti-apoptotic BCL-2 family proteins — BCL-2, BCL-XL, and MCL-1 — inhibits apoptosis [10]. Collectively, these alterations define the hallmark features of senescent cells: irreversible cell cycle arrest, apoptosis resistance, a pro-inflammatory SASP, mitochondrial dysfunction, and proteostasis impairment [11]. A morphofunctional manifestation of the metabolic imbalance and lysosomal dysfunction characteristic of senescent cells is the hypertrophy of the lysosomal compartment and elevated activity of the lysosomal enzyme  $\beta$ -galactosidase ( $\beta$ -Gal) [12]. Consequently, the high concentration of this enzyme within enlarged lysosomes results in detectable enzymatic activity at a suboptimal pH of 6.0, enabling its use as a biomarker for senescent cells - termed senescence-associated  $\beta$ -galactosidase (SA- $\beta$ -Gal) [13, 14]. Traditionally, chromogenic substrates have been employed to assess  $\beta$ -Gal activity; however, these are incompatible with multiparametric phenotypic analysis of senescent cells by fluorescence-based techniques, including flow cytometry. The recent development of fluorogenic β-Gal substrates has substantially expanded the utility of this marker, allowing simultaneous quantification of SA-β-Gal activity across distinct immune cell populations via flow cytometry [15]. To date, limited data exist regarding age-related changes in SA-β-Gal activity across different immune cell subsets. Evaluating SA-β-Gal activity in lymphoid and myeloid populations from both central (bone marrow) and peripheral (spleen) compartments of the immune system is therefore of considerable interest for understanding immunosenescence. Given that the immune system is continuously exposed throughout life to stressors of varying nature and intensity, distinct lymphoid and myeloid subsets are expected to exhibit heterogeneous trajectories and rates of aging. An increased senescent burden within the immune system exacerbates "inflammaging," heightens the risk of autoimmune and neoplastic disorders, and enhances susceptibility to infections [16]. Consequently, a detailed characterization of age-associated alterations in the immune system provides a critical foundation for developing targeted strategies to restore immune competence in the elderly. Thus, the aim of this study was to perform a comparative analysis of SA-β-Gal activity in major immune cell populations isolated from the spleen and bone marrow of young (3-month-old) and very old (26-month-old) C57BL/6 mice. This approach enabled us to map the distribution of senescent-like cells within the aged immune system and to directly compare central and peripheral immune compartments with respect to their senescent cell content.

#### **METHODS**

#### Mice

The study involved 12 C57BL/6 mice: 8 mice aged 3 months and 4 elderly mice aged 26 months. The animals were kept in the vivarium with the 12-h ligh/dark cycle, unlimited access to water and balanced laboratory feed. Euthanasia compliant with the principles of animal welfare was performed under deep isoflurane anesthesia by cervical dislocation. Appropriate biomaterial was collected immediately after euthanasia.

#### Splenocyte isolation

After euthanasia the spleen was retrieved, put it in the glass homogenizer with cold PBS (1% FCS, 0.02% EDTA), and gently grinded with the glass pestle to obtain the homogenous suspension. The resulting cell suspension was twice filtered though the nylon filter (70  $\mu m$ ) with PBS washing. The filtered material was centrifuged for 5 min at 300 g and 8 °C. Precipitate was resuspended in 5 mL of buffer for 2 min to lyse red blood cells. Then it was supplemented with 10 mL of PBS with 1% FBS and centrifuged again. After elimination of supernatant, the cells were resuspended to the desired concentration in the RPMI-1640 complete medium or PBS, depending on the goal.

#### Bone marrow cell isolation

Bone marrow cells were isolated from the mouse femur and tibia by washing the bone marrow out of the bone cavity with the PBS solution using a syringe (27 G). The resulting suspension was twice filtered though the 70  $\mu m$  nylon filter, washed in PBS (0.02% EDTA) by centrifugation for 5 min at 300 g and 8 °C. Then red blood cells were lysed (see above) and resuspended in the complete medium or PBS.

The splenocyte and bone marrow cell viability was assessed by the fluorescent method using acridine orange and propidium iodide; the average viability was 98%.

#### SA-β-Gal staining

To estimate SA-β-Gal activity in living cells, the SPiDER-βGal vital dye was used (Cellular Senescence Detection Kit, Dojindo Laboratories, Japan), which represents a fluorogenic substrate specific for  $\beta$ -Gal. The bone marrow cells or splenocytes,  $2 \times 10^5$ cells per well, were incubated in the flat-bottom 96-well plate (NEST Biotechnologies, China), in 200 µL of the RPMI-1640 complete medium supplemented with bafilomycin A1 (Sigma Aldrich, USA) to the final concentration of 100 nM as a lizosome alkalinizing agent, for 1 h in the CO2 incubator at 37°. Then the cells were added the substrate to the final concentration of 1 µmol/L and incubated under the same conditions for 1 h. Then the cells were washed by centrifugation for 5 min at 300 g, 20 °C, stained with the FVS780 dye (BD Biosciences, USA) in accordance with the manufacturer's protocol to eliminate the dead cells from the further analysis, and antibody-labeled. As a positive control, the cells were simultaneously incubated with the substrate not supplemented with bafilomycin. As a negative control, the cells were incubated with added bafilomycin without the substrate.

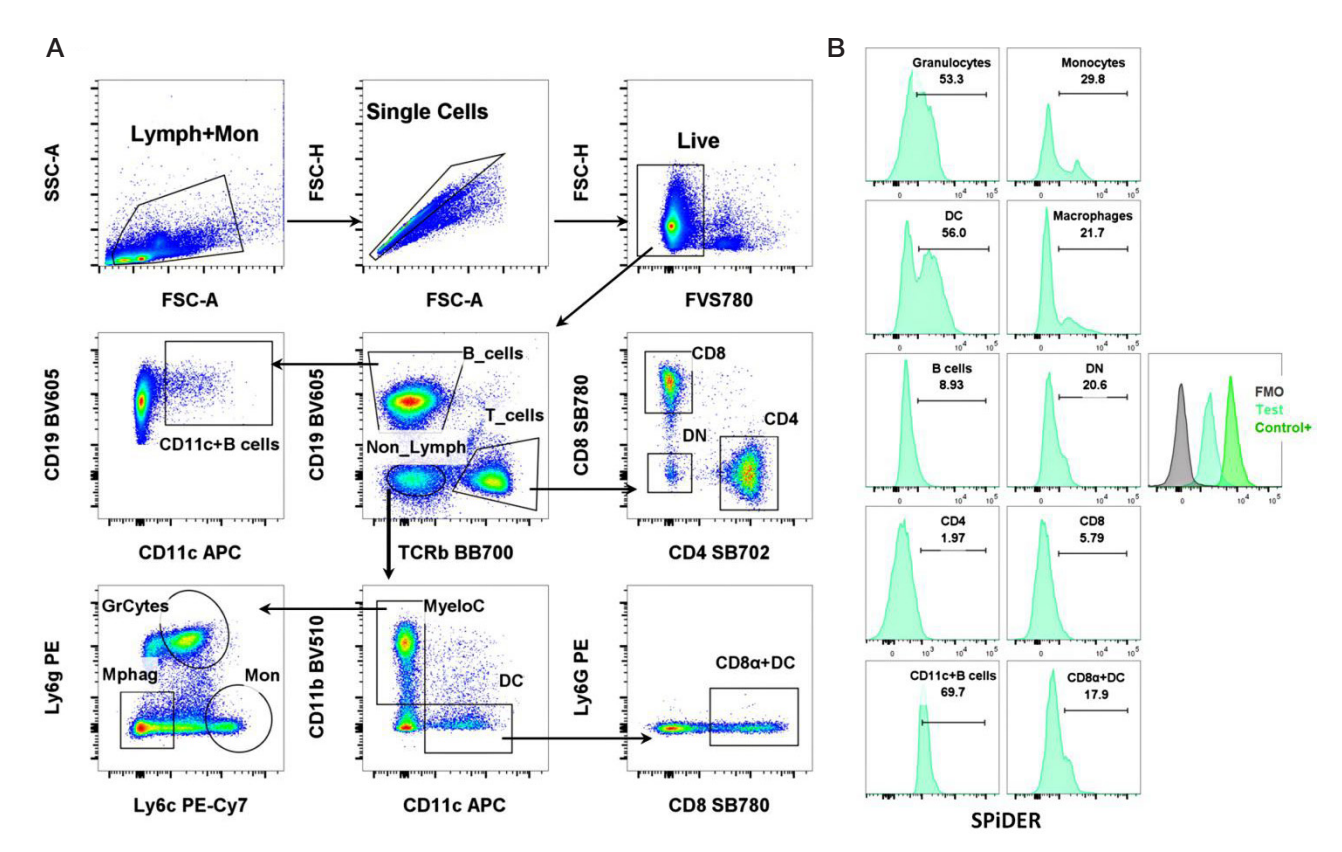


Fig. 1. Gating strategies for lymphoid and myeloid populations in spleen and bone marrow samples from mice (A) and quantification of the proportion of SA-β-Galpositive cells within each analyzed population (B). The histogram on the right shows SPiDER fluorescence intensity in the 488-530/30 nm detection channel for the FMO control (without fluorogenic substrate) and the positive control (Control+, without bafilomycin A1)

#### Phenotyping

For antibody staining a total of  $2\times10^5$  cells were resuspended in 200 µL of the FACS buffer, added 50 µL of the antibody mixture, mixed thoroughly by pipetting, and incubated at 4 °C for 30 min in the dark. The anti-mouse antibodies used were as follows: TCR $\beta$  BB700 (#745846, BD Biosciences, USA), CD19 BV605 (#563148, BD Biosciences, USA), CD11c APC (#550261, BD Biosciences, USA), CD11b BV510 (#562950, BD Biosciences, USA), Ly6G PE (#12-9668-82, ThermoFisher, USA), Ly6C PE-Cy7 (#560593, BD Biosciences, USA), CD4 SB702 (#67-0041-82, ThermoFisher, USA), CD8 SB780 (#78-0081-82, ThermoFisher, USA). Then the cells were twice washed for 5 min at 300 g with the FACS buffer and resuspended in 300 µL. Then these were analyzed using the BD LSRFortessa flow cytometer (BD Biosciences, USA).

#### Statistical analysis

Flow cytometry data were analyzed using FlowJo software (version 10.8.1; BD Biosciences, USA). Statistical analyses were performed with GraphPad Prism (version 9.3.1; GraphPad Software, USA). The normality of data distributions was assessed using the Shapiro–Wilk test. Comparisons between young and aged mouse groups were carried out using the non-parametric Mann–Whitney U test. Data are presented as medians with interquartile ranges.

#### **RESULTS**

Multiparameter flow cytometry enabled the assessment of SA- $\beta$ -Gal activity across ten distinct immune cell populations. These populations were broadly categorized by lineage into lymphoid (T and B cells) and myeloid subsets (conventional

dendritic cells, monocytes, macrophages, and granulocytes). The gating strategy is illustrated in Fig. 1A. Within each defined population, the proportion of cells exhibiting elevated SA- $\beta$ -Gal activity was quantified. The gating threshold was established using fluorescence-minus-one (FMO) controls, in which cells were treated with bafilomycin A1 but without the fluorogenic substrate SPiDER- $\beta$ Gal (Fig. 1B). This control is particularly critical, as bafilomycin A1 itself can alter cellular autofluorescence levels, thereby influencing background signal in the absence of the substrate.

The analysis of the data obtained for the mouse spleen revealed a significant increase in the counts of monocytes (8.2% (5.6-12.4) vs. 23.7% (17.3-29.2), p < 0.05), dendriticcells (12.9% (12-14.2) vs. 27.9% (18.2-29.5), p < 0.05), and B cells (53.5% (49.8–57.5) vs. 66.4% (64.9–69.5), p < 0.05) in the group of elderly mice (Fig. 2A). It is interesting to note that the counts of CD11c+ B cells increased significantly with age (0.39% (0.32–0.47) vs. 2.18% (1.33–2.58), p < 0.01). This is a fairly recently described population of B cells associated with aging. Furthermore, despite the increase in the general dendritic cell population, the counts of CD8 $\alpha$ <sup>+</sup>DC significantly decreased (31.9% (29–33) vs. 23.8% (19.3–31.2), p < 0.01). The bone marrow samples also showed the increase in the counts of monocytes (18.2% (14-20) vs. 23.7% (22-28.2), p < 0.05) and decrease in B cell counts (32.9% (29.9–36.3) vs. 26.2% (22.8–27.5), p < 0.05), while the counts of CD11c<sup>+</sup> B cells increased (0.03% (0.025-0.048) vs. 0.26% (0.18-0.4), p < 0.01) and that of CD8 $\alpha$ <sup>+</sup>DC decreased (21.6% (19.1–24) vs. 6.5% (4.9–7.1), p < 0.01), like in the splenic samples (Fig. 2B).

In the next phase, we assessed the distribution of cells showing the increased SA- $\beta$ -Gal activity across lymphoid and myeloid populations. Samples of the spleen showed a considerable increase in the counts of SA- $\beta$ -Gal-positive

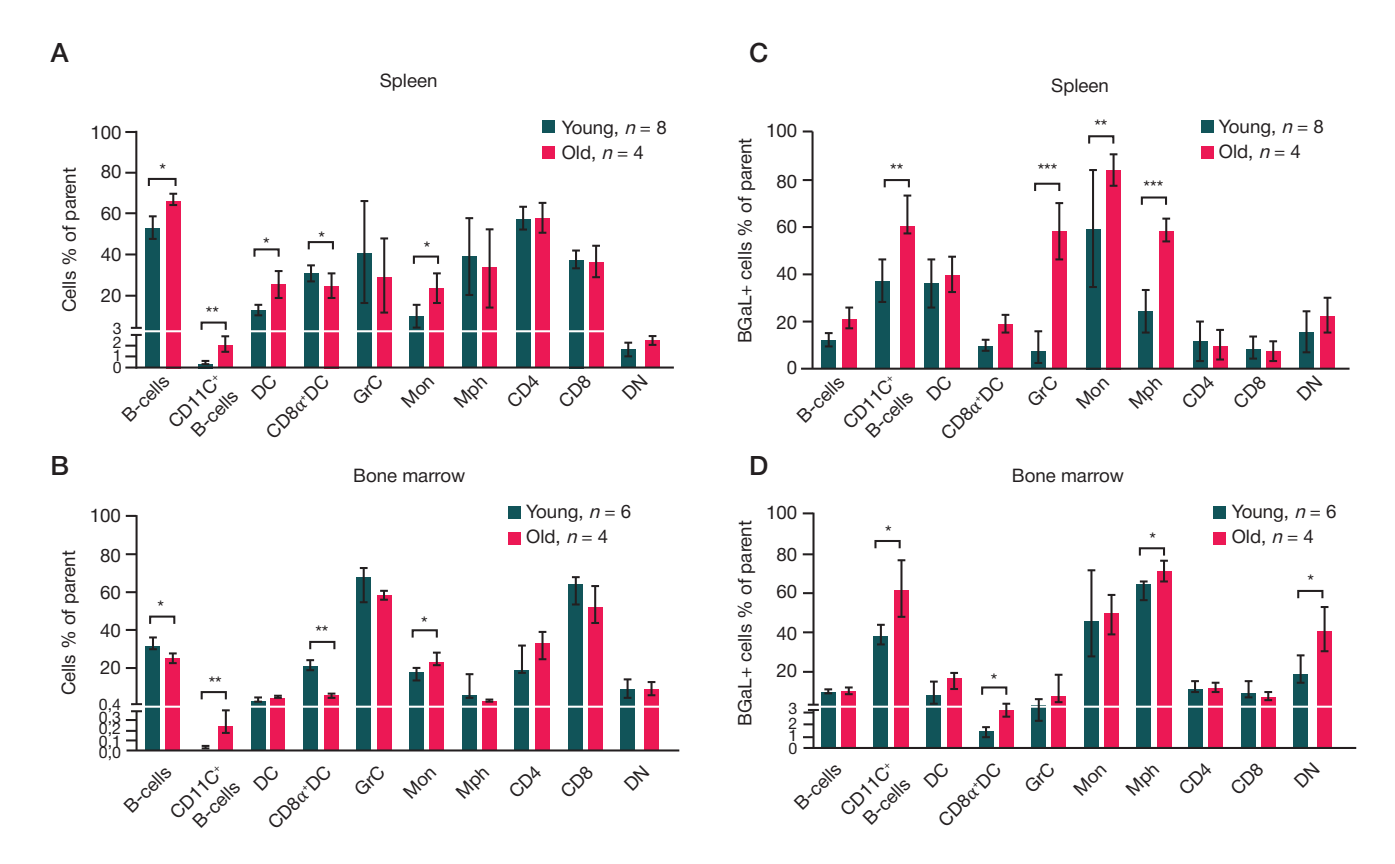


Fig. 2. Proportions of lymphoid and myeloid populations in spleen (A) and bone marrow (B) samples. Additionally, the frequency of senescent-like cells positive for the SA-β-Gal marker in spleen (C) and bone marrow (D) is shown. Abbreviations: DC — dendritic cells; GrC — granulocytes; Mon — monocytes; Mph — macrophages; DN – double-negative T cells. Group comparisons were performed usin the Mann–Whitney U-test. Data are presented as Me  $\pm$  interquartile range (IQR); \* — p < 0.05, \*\* — p < 0.001

granulocytes (7.2% (2.4–15.5) vs. 62.5% (45.8–66.1), p < 0.001), macrophages (23.8% (16.8–29.1) vs. 57.2% (55.1–63.5), p < 0.001), and monocytes (50.5% (43.8–86) vs. 85.1% (77.7–90.2), p < 0.01), as well as CD11c+B cells (39.2% (35.4–43) vs. 60.5% (57.5–73.3), p < 0.01) in the group of elderly mice (Fig. 2C). The bone marrow showed the age-related increase in the counts of SA- $\beta$ -Gal-positive macrophages (64.4% (56.8–65.8) vs. 70.9% (66.1–76.5), p < 0.05), CD8 $\alpha$ +DC (1.5% (0.96–1.7) vs. 3.25% (2.71–4.26), p < 0.05), double negative lymphocytes (19.5% (15.2–28.3) vs. 41% (30.9–53.3), p < 0.05), and CD11c+B cells (38.4% (34.2–43.6) vs. 62% (47.8–76.8), p < 0.05) (Fig. 2D).

Thus, the study revealed age-related alterations in the major populations of lymphoid and myeloid cells, associated with the larger share of cells showing the increased SA- $\beta$ -Gal activity. In the bone marrow, as a primary lymphoid organ, these alterations were less prominent.

#### DISCUSSION

The findings showed that physiological aging of the immune system is uneven [17] and is accompanied by significant quantitative changes in the populations of B cells, dendritic cells, and monocytes. Furthermore, the cells showing the increased SA- $\beta$ -Gal activity are accumulated faster in myeloid populations, than in the lymphoid compartment.

The increase in B-cell counts in the spleen of elderly mice can reflect the life-long history of antigenic challenges, and accumulation of the age-associated CD11c<sup>+</sup> B cells is considered to be associated with aging and the increased risk of autoimmune disorders, as well as the inflammaging phenomenon [18, 19]. These cells with impaired functions, which contribute to acquisition of pro-inflammatory phenotype

by macrophages, show the increased counts in various autoimmune disorders and can constitute a large proportion of the mature B-cell population in the elderly body [20].

In contrast, the bone marrow showed the decrease in B-cell counts reflecting the age-related decline in B-cell production, which is likely to negatively affect the immune system capability of responding to new antigenic challenges [21]. Furthermore, despite reduction of the general B-cell population, the CD11c+ B-cell counts were increased, like in the spleen. The agerelated increase in the counts of the CD11c+ dendritic cells in the spleen and monocytes in the bone marrow is likely to reflect the so-called "myeloid shift" representing the typical feature of the immune system aging described in detail in the recent reports [22-24]. The detected increase in the share of SA-β-Gal-positive granulocytes, monocytes, and macrophages in the spleen of elderly mice is of special interest. The age-related accumulation of SA-β-Gal-positive cells in myeloid populations is likely to contribute to chronic low-grade inflammation, i.e. inflammaging resulting primarily from production of SASP factors by senescent myeloid cells [25, 26]. The increased counts of SA-β-Gal-positive macrophages, DN T cells, and especially CD11c+ B cells in the bone marrow suggest involvement of the central immune system departments in the aging processes. In this context it should be noted, that the close relationship between the aging macrophages/CD11c+ B cells and hematopoietic stem cells (HSCs) can have a negative effect on the microenvironment in the niches due to SASP production and result in the HSC functional depletion and lymphopoietic potential reduction [27]. This can create a vicious circle, when accumulation of the cells showing signs of senescence in the bone marrow negatively affects hematopoiesis, which, in turn, enhances accumulation of dysfunctional and aging cells [28].

We observed a significant increase in SA-B-Gal activity across multiple lymphoid and myeloid cell populations in aged mice, which – taken together with existing evidence – supports the utility of this marker for investigating immunosenescence. However, certain limitations of our study should be noted. The data obtained are based on the assessment of SA-B-Gal activity as the main cellular senescence marker, but this marker is not absolutely specific and can increase with activation and alteration of metabolism in some types of cells, as well as in the phase of the cell transition to the senescent state [29, 30]. Moreover, we did not assess the functional potential of the studied populations and did not use additional senescence markers, such as p16INK4a, p21CIP1, HMGB1 [5] or SASP components [31], which limits interpretation of the phenomena observed exclusively in the context of the cellular senescence. However, aging is a complex, multifaceted process that is not limited to the cell transition to the senescent state. Thus, the reported quantitative changes in the counts of lymphoid and myeloid subpopulations in the group of elderly mice, along with the changes in SA-β-Gal activity, are likely to reflect the most prominent age-related alterations in the immune system. That is why further comprehensive research is required including transcriptome and proteome assessment and functional tests aimed at investigation of various aspects of the immune system aging. Such an approach will contribute to better understanding of the immune aging mechanisms and the development of strategies aimed at restoring the immune system competence in the elderly.

#### **CONCLUSIONS**

Our findings support the hypothesis of heterogeneous aging across different compartments of the immune system and highlight myeloid skewing as a hallmark feature of immunosenescence. Importantly, age-related alterations were observed not only in the peripheral immune compartment but also in the bone marrow. Specifically, the decline in B-cell frequency reflects age-associated suppression of B-lymphopoiesis, while the marked increase in pro-inflammatory CD11c<sup>+</sup> B cells and SA-β-Gal-positive double-negative (DN) T lymphocytes, macrophages, and CD8 $\alpha^+$  dendritic cells indicates active involvement of central immune organs in the aging process [27]. Notably, the accumulation of SA-β-Galpositive cells occurs in the bone marrow in close proximity to hematopoietic stem cells (HSCs). In this microenvironment, SASP factor secretion may disrupt the functional integrity of HSC niches, impair lymphopoietic potential, and thereby perpetuate a vicious cycle of age-related immune dysfunction [27, 28]. These observations expand current understanding of the dynamic remodeling of the immune system during aging. Consequently, further investigation of age-associated immune alterations — using a multimodal approach that includes SA-β-Gal assessment — holds significant translational potential. Such research could guide the development of targeted strategies for the selective elimination of pro-inflammatory senescent cells, restoration of lymphopoietic capacity, and enhancement of overall immune competence in the elderly.

#### References

- Ajoolabady A, Pratico D, Bahijri S, Tuomilehto J, Uversky VN, Ren J. Hallmarks of cellular senescence: biology, mechanisms, regulations. Exp Mol Med. 2025; 57 (7): 1482–91. DOI: 10.1038/s12276-025-01480-7. Epub 2025 Jul 10. PMID: 40634753; PMCID: PMC12322015.
- Kumari R, Jat P. Mechanisms of Cellular Senescence: Cell Cycle Arrest and Senescence Associated Secretory Phenotype. Front Cell Dev Biol. 2021; 9: 645593. DOI: 10.3389/fcell.2021.645593. PMID: 33855023; PMCID: PMC8039141.
- Hornsby PJ. Senescence as an anticancer mechanism. J Clin Oncol. 2007; 25 (14): 1852–7. DOI: 10.1200/JCO.2006.10.3101. PMID: 17488983.
- Baz-Martínez M, Da Silva-Álvarez S, Rodríguez E, Guerra J, El Motiam A, et al. Cell senescence is an antiviral defense mechanism. Sci Rep. 2016; 6: 37007. DOI: 10.1038/srep37007. PMID: 27849057; PMCID: PMC51111111.
- Prieur A, Besnard E, Babled A, Lemaitre JM. p53 and p16(INK4A) independent induction of senescence by chromatin-dependent alteration of S-phase progression. Nat Commun. 2011; 2: 473. DOI: 10.1038/ncomms1473. PMID: 21915115.
- Dasgupta N, Arnold R, Equey A, Gandhi A, Adams PD. The role of the dynamic epigenetic landscape in senescence: orchestrating SASP expression. NPJ Aging. 2024; 10 (1): 48. DOI: 10.1038/s41514-024-00172-2. PMID: 39448585; PMCID: PMC11502686.
- Miwa S, Kashyap S, Chini E, von Zglinicki T. Mitochondrial dysfunction in cell senescence and aging. J Clin Invest. 2022; 132 (13): e158447. DOI: 10.1172/JCI158447. PMID: 35775483; PMCID: PMC9246372.
- 8. Kwon Y, Kim JW, Jeoung JA, Kim MS, Kang C. Autophagy Is Pro-Senescence When Seen in Close-Up, but Anti-Senescence in Long-Shot. Mol Cells. 2017; 40 (9): 607–12. DOI: 10.14348/molcells.2017.0151. Epub 2017 Sep 20. PMID: 28927262; PMCID: PMC5638768.
- 9. Tilstra JS, Clauson CL, Niedernhofer LJ, Robbins PD. NF-κB in

- Aging and Disease. Aging Dis. 2011; 2 (6): 449–65. Epub 2011 Dec 2. PMID: 22396894; PMCID: PMC3295063.
- Yosef R, Pilpel N, Tokarsky-Amiel R, Biran A, Ovadya Y, Cohen S, et al. Directed elimination of senescent cells by inhibition of BCL-W and BCL-XL. Nat Commun. 2016; 7: 11190. DOI: 10.1038/ncomms11190. PMID: 27048913; PMCID: PMC4823827.
- Dodig S, Čepelak I, Pavić I. Hallmarks of senescence and aging. Biochem Med (Zagreb). 2019; 29 (3): 030501. DOI: 10.11613/BM.2019.030501. Epub 2019 Aug 5. PMID: 31379458; PMCID: PMC6610675.
- Debacq-Chainiaux F, Erusalimsky JD, Campisi J, Toussaint O. Protocols to detect senescence-associated beta-galactosidase (SA-betagal) activity, a biomarker of senescent cells in culture and in vivo. Nat Protoc. 2009; 4 (12): 1798–806. DOI: 10.1038/nprot.2009.191. PMID: 20010931.
- Dimri GP, Lee X, Basile G, Acosta M, Scott G, Roskelley C, et al. A biomarker that identifies senescent human cells in culture and in aging skin in vivo. Proc Natl Acad Sci USA. 1995; 92 (20): 9363–7. DOI: 10.1073/pnas.92.20.9363. PMID: 7568133; PMCID: PMC40985.
- 14. Yegorov YE, Akimov SS, Hass R, Zelenin AV, Prudovsky IA. Endogenous beta-galactosidase activity in continuously nonproliferating cells. Exp Cell Res. 1998; 243 (1): 207–11. DOI: 10.1006/excr.1998.4169. PMID: 9716464.
- Doura T, Kamiya M, Obata F, Yamaguchi Y, Hiyama TY, Matsuda T, et al. Detection of LacZ-Positive Cells in Living Tissue with Single-Cell Resolution. Angew Chem Int Ed Engl. 2016 Aug 8;55(33):9620–4. DOI: 10.1002/anie.201603328. Epub 2016 Jul 12. PMID: 27400827.
- Franceschi C, Garagnani P, Parini P, Giuliani C, Santoro A. Inflammaging: a new immune-metabolic viewpoint for age-related diseases. Nat Rev Endocrinol. 2018; 14 (10): 576–90. DOI: 10.1038/s41574-018-0059-4. PMID: 30046148.
- Liu Z, Liang Q, Ren Y, Guo C, Ge X, Wang L, et al. Immunosenescence: molecular mechanisms and diseases. Signal Transduct Target Ther. 2023; 8 (1): 200. DOI: 10.1038/s41392-023-01451-2.

## ОРИГИНАЛЬНОЕ ИССЛЕДОВАНИЕ І ИММУНОЛОГИЯ

- PMID: 37179335; PMCID: PMC10182360.
- Frasca D, Diaz A, Romero M, Landin AM, Blomberg BB. Age effects on B cells and humoral immunity in humans. Ageing Res Rev. 2011; 10 (3): 330–5. DOI: 10.1016/j.arr.2010.08.004. Epub 2010 Aug 20. PMID: 20728581; PMCID: PMC3040253.
- Carey A, Nguyen K, Kandikonda P, Kruglov V, Bradley C, Dahlquist KJV, et al. Age-associated accumulation of B cells promotes macrophage inflammation and inhibits lipolysis in adipose tissue during sepsis. Cell Rep. 2024; 43 (3): 113967. DOI: 10.1016/j.celrep.2024.113967. Epub 2024 Mar 15. PMID: 38492219: PMCID: PMC11014686.
- Mouat IC, Goldberg E, Horwitz MS. Age-associated B cells in autoimmune diseases. Cell Mol Life Sci. 2022; 79 (8): 402. DOI: 10.1007/s00018-022-04433-9. PMID: 35798993; PMCID: PMC9263041.
- Zharhary D. Age-related changes in the capability of the bone marrow to generate B cells. J Immunol. 1988; 141 (6): 1863–9. PMID: 3262642.
- 22. Pang WW, Price EA, Sahoo D, Beerman I, Maloney WJ, Rossi DJ, et al. Human bone marrow hematopoietic stem cells are increased in frequency and myeloid-biased with age. Proc Natl Acad Sci USA. 2011; 108 (50): 20012–7. DOI: 10.1073/pnas.1116110108. Epub 2011 Nov 28. PMID: 22123971; PMCID: PMC3250139.
- Yamamoto R, Nakauchi H. In vivo clonal analysis of aging hematopoietic stem cells. Mech Ageing Dev. 2020; 192: 111378.
   DOI: 10.1016/j.mad.2020.111378. Epub 2020 Oct 3. PMID: 33022333; PMCID: PMC7686268.
- 24. Ross JB, Myers LM, Noh JJ, Collins MM, Carmody AB, Messer RJ, et al. Depleting myeloid-biased haematopoietic stem cells rejuvenates aged immunity. Nature. 2024; 628 (8006): 162–170. DOI: 10.1038/s41586-024-07238-x. Epub 2024 Mar 27. PMID: 38538791; PMCID: PMC11870232.
- Kovtonyuk LV, Fritsch K, Feng X, Manz MG, Takizawa H. Inflamm-Aging of Hematopoiesis, Hematopoietic Stem Cells, and the

- Bone Marrow Microenvironment. Front Immunol. 2016; 7: 502. DOI: 10.3389/fimmu.2016.00502. PMID: 27895645; PMCID: PMC5107568.
- 26. Bleve A, Motta F, Durante B, Pandolfo C, Selmi C, Sica A. Immunosenescence, Inflammaging, and Frailty: Role of Myeloid Cells in Age-Related Diseases. Clin Rev Allergy Immunol. 2023; 64 (2): 123–44. DOI: 10.1007/s12016-021-08909-7. Epub 2022 Jan 15. PMID: 35031957; PMCID: PMC8760106.
- Pappert M, Khosla S, Doolittle M. Influences of Aged Bone Marrow Macrophages on Skeletal Health and Senescence. Curr Osteoporos Rep. 2023; 21 (6): 771–78. DOI: 10.1007/s11914-023-00820-8. Epub 2023 Sep 9. PMID: 37688671; PMCID: PMC10724341.
- Hou J, Chen KX, He C, Li XX, Huang M, Jiang YZ, et al. Aged bone marrow macrophages drive systemic aging and agerelated dysfunction via extracellular vesicle-mediated induction of paracrine senescence. Nat Aging. 2024; 4 (11): 1562–81. DOI: 10.1038/s43587-024-00694-0. Epub 2024 Sep 12. PMID: 39266768; PMCID: PMC11564114.
- de Mera-Rodríguez JA, Álvarez-Hernán G, Gañán Y, Martín-Partido G, Rodríguez-León J, Francisco-Morcillo J. Is Senescence-Associated β-Galactosidase a Reliable in vivo Marker of Cellular Senescence During Embryonic Development? Front Cell Dev Biol. 2021; 9: 623175. DOI: 10.3389/fcell.2021.623175. PMID: 33585480; PMCID: PMC7876289.
- Severino J, Allen RG, Balin S, Balin A, Cristofalo VJ. Is betagalactosidase staining a marker of senescence in vitro and in vivo? Exp Cell Res. 2000; 257 (1): 162–71. DOI: 10.1006/excr.2000.4875. PMID: 10854064.
- Coppé JP, Desprez PY, Krtolica A, Campisi J. The senescenceassociated secretory phenotype: the dark side of tumor suppression. Annu Rev Pathol. 2010; 5: 99–118. DOI: 10.1146/annurev-pathol-121808-102144. PMID: 20078217; PMCID: PMC4166495.

## Литература

- Ajoolabady A, Pratico D, Bahijri S, Tuomilehto J, Uversky VN, Ren J. Hallmarks of cellular senescence: biology, mechanisms, regulations. Exp Mol Med. 2025; 57 (7): 1482–91. DOI: 10.1038/s12276-025-01480-7. Epub 2025 Jul 10. PMID: 40634753; PMCID: PMC12322015.
- Kumari R, Jat P. Mechanisms of Cellular Senescence: Cell Cycle Arrest and Senescence Associated Secretory Phenotype. Front Cell Dev Biol. 2021; 9: 645593. DOI: 10.3389/fcell.2021.645593. PMID: 33855023; PMCID: PMC8039141.
- Hornsby PJ. Senescence as an anticancer mechanism. J Clin Oncol. 2007; 25 (14): 1852–7. DOI: 10.1200/JCO.2006.10.3101. PMID: 17488983.
- Baz-Martínez M, Da Silva-Álvarez S, Rodríguez E, Guerra J, El Motiam A, et al. Cell senescence is an antiviral defense mechanism. Sci Rep. 2016; 6: 37007. DOI: 10.1038/srep37007. PMID: 27849057; PMCID: PMC5111111.
- Prieur A, Besnard E, Babled A, Lemaitre JM. p53 and p16(INK4A) independent induction of senescence by chromatin-dependent alteration of S-phase progression. Nat Commun. 2011; 2: 473. DOI: 10.1038/ncomms1473. PMID: 21915115.
- Dasgupta N, Arnold R, Equey A, Gandhi A, Adams PD. The role of the dynamic epigenetic landscape in senescence: orchestrating SASP expression. NPJ Aging. 2024; 10 (1): 48. DOI: 10.1038/s41514-024-00172-2. PMID: 39448585; PMCID: PMC11502686
- Miwa S, Kashyap S, Chini E, von Zglinicki T. Mitochondrial dysfunction in cell senescence and aging. J Clin Invest. 2022; 132 (13): e158447. DOI: 10.1172/JCI158447. PMID: 35775483; PMCID: PMC9246372.
- Kwon Y, Kim JW, Jeoung JA, Kim MS, Kang C. Autophagy Is Pro-Senescence When Seen in Close-Up, but Anti-Senescence in Long-Shot. Mol Cells. 2017; 40 (9): 607–12. DOI: 10.14348/molcells.2017.0151. Epub 2017 Sep 20. PMID: 28927262; PMCID: PMC5638768.
- 9. Tilstra JS, Clauson CL, Niedernhofer LJ, Robbins PD. NF-κB in

- Aging and Disease. Aging Dis. 2011; 2 (6): 449–65. Epub 2011 Dec 2. PMID: 22396894; PMCID: PMC3295063.
- Yosef R, Pilpel N, Tokarsky-Amiel R, Biran A, Ovadya Y, Cohen S, et al. Directed elimination of senescent cells by inhibition of BCL-W and BCL-XL. Nat Commun. 2016; 7: 11190. DOI: 10.1038/ncomms11190. PMID: 27048913; PMCID: PMC4823827.
- Dodig S, Čepelak I, Pavić I. Hallmarks of senescence and aging. Biochem Med (Zagreb). 2019; 29 (3): 030501. DOI: 10.11613/BM.2019.030501. Epub 2019 Aug 5. PMID: 31379458; PMCID: PMC6610675.
- Debacq-Chainiaux F, Erusalimsky JD, Campisi J, Toussaint O. Protocols to detect senescence-associated beta-galactosidase (SA-betagal) activity, a biomarker of senescent cells in culture and in vivo. Nat Protoc. 2009; 4 (12): 1798–806. DOI: 10.1038/nprot.2009.191. PMID: 20010931.
- 13. Dimri GP, Lee X, Basile G, Acosta M, Scott G, Roskelley C, et al. A biomarker that identifies senescent human cells in culture and in aging skin in vivo. Proc Natl Acad Sci USA. 1995; 92 (20): 9363–7. DOI: 10.1073/pnas.92.20.9363. PMID: 7568133; PMCID: PMC40985.
- Yegorov YE, Akimov SS, Hass R, Zelenin AV, Prudovsky IA. Endogenous beta-galactosidase activity in continuously nonproliferating cells. Exp Cell Res. 1998; 243 (1): 207–11. DOI: 10.1006/excr.1998.4169. PMID: 9716464.
- 15. Doura T, Kamiya M, Obata F, Yamaguchi Y, Hiyama TY, Matsuda T, et al. Detection of LacZ-Positive Cells in Living Tissue with Single-Cell Resolution. Angew Chem Int Ed Engl. 2016 Aug 8;55(33):9620–4. DOI: 10.1002/anie.201603328. Epub 2016 Jul 12. PMID: 27400827.
- Franceschi C, Garagnani P, Parini P, Giuliani C, Santoro A. Inflammaging: a new immune-metabolic viewpoint for age-related diseases. Nat Rev Endocrinol. 2018; 14 (10): 576–90. DOI: 10.1038/s41574-018-0059-4. PMID: 30046148.
- Liu Z, Liang Q, Ren Y, Guo C, Ge X, Wang L, et al. Immunosenescence: molecular mechanisms and diseases. Signal Transduct Target Ther. 2023; 8 (1): 200. DOI: 10.1038/s41392-023-01451-2.

## ORIGINAL RESEARCH I IMMUNOLOGY

- PMID: 37179335; PMCID: PMC10182360.
- Frasca D, Diaz A, Romero M, Landin AM, Blomberg BB. Age effects on B cells and humoral immunity in humans. Ageing Res Rev. 2011; 10 (3): 330–5. DOI: 10.1016/j.arr.2010.08.004. Epub 2010 Aug 20. PMID: 20728581; PMCID: PMC3040253.
- Carey A, Nguyen K, Kandikonda P, Kruglov V, Bradley C, Dahlquist KJV, et al. Age-associated accumulation of B cells promotes macrophage inflammation and inhibits lipolysis in adipose tissue during sepsis. Cell Rep. 2024; 43 (3): 113967. DOI: 10.1016/j.celrep.2024.113967. Epub 2024 Mar 15. PMID: 38492219: PMCID: PMC11014686.
- Mouat IC, Goldberg E, Horwitz MS. Age-associated B cells in autoimmune diseases. Cell Mol Life Sci. 2022; 79 (8): 402. DOI: 10.1007/s00018-022-04433-9. PMID: 35798993; PMCID: PMC9263041.
- Zharhary D. Age-related changes in the capability of the bone marrow to generate B cells. J Immunol. 1988; 141 (6): 1863–9. PMID: 3262642.
- 22. Pang WW, Price EA, Sahoo D, Beerman I, Maloney WJ, Rossi DJ, et al. Human bone marrow hematopoietic stem cells are increased in frequency and myeloid-biased with age. Proc Natl Acad Sci USA. 2011; 108 (50): 20012–7. DOI: 10.1073/pnas.1116110108. Epub 2011 Nov 28. PMID: 22123971; PMCID: PMC3250139.
- 23. Yamamoto R, Nakauchi H. In vivo clonal analysis of aging hematopoietic stem cells. Mech Ageing Dev. 2020; 192: 111378. DOI: 10.1016/j.mad.2020.111378. Epub 2020 Oct 3. PMID: 33022333; PMCID: PMC7686268.
- 24. Ross JB, Myers LM, Noh JJ, Collins MM, Carmody AB, Messer RJ, et al. Depleting myeloid-biased haematopoietic stem cells rejuvenates aged immunity. Nature. 2024; 628 (8006): 162–170. DOI: 10.1038/s41586-024-07238-x. Epub 2024 Mar 27. PMID: 38538791; PMCID: PMC11870232.
- Kovtonyuk LV, Fritsch K, Feng X, Manz MG, Takizawa H. Inflamm-Aging of Hematopoiesis, Hematopoietic Stem Cells, and the

- Bone Marrow Microenvironment. Front Immunol. 2016; 7: 502. DOI: 10.3389/fimmu.2016.00502. PMID: 27895645; PMCID: PMC5107568.
- Bleve A, Motta F, Durante B, Pandolfo C, Selmi C, Sica A. Immunosenescence, Inflammaging, and Frailty: Role of Myeloid Cells in Age-Related Diseases. Clin Rev Allergy Immunol. 2023; 64 (2): 123–44. DOI: 10.1007/s12016-021-08909-7. Epub 2022 Jan 15. PMID: 35031957; PMCID: PMC8760106.
- Pappert M, Khosla S, Doolittle M. Influences of Aged Bone Marrow Macrophages on Skeletal Health and Senescence. Curr Osteoporos Rep. 2023; 21 (6): 771–78. DOI: 10.1007/s11914-023-00820-8. Epub 2023 Sep 9. PMID: 37688671; PMCID: PMC10724341.
- 28. Hou J, Chen KX, He C, Li XX, Huang M, Jiang YZ, et al. Aged bone marrow macrophages drive systemic aging and agerelated dysfunction via extracellular vesicle-mediated induction of paracrine senescence. Nat Aging. 2024; 4 (11): 1562–81. DOI: 10.1038/s43587-024-00694-0. Epub 2024 Sep 12. PMID: 39266768; PMCID: PMC11564114.
- de Mera-Rodríguez JA, Álvarez-Hernán G, Gañán Y, Martín-Partido G, Rodríguez-León J, Francisco-Morcillo J. Is Senescence-Associated β-Galactosidase a Reliable in vivo Marker of Cellular Senescence During Embryonic Development? Front Cell Dev Biol. 2021; 9: 623175. DOI: 10.3389/fcell.2021.623175. PMID: 33585480; PMCID: PMC7876289.
- Severino J, Allen RG, Balin S, Balin A, Cristofalo VJ. Is betagalactosidase staining a marker of senescence in vitro and in vivo? Exp Cell Res. 2000; 257 (1): 162–71. DOI: 10.1006/excr.2000.4875. PMID: 10854064.
- Coppé JP, Desprez PY, Krtolica A, Campisi J. The senescenceassociated secretory phenotype: the dark side of tumor suppression. Annu Rev Pathol. 2010; 5: 99–118. DOI: 10.1146/annurev-pathol-121808-102144. PMID: 20078217; PMCID: PMC4166495.

### PANEL OF IFN-I-INDUCED GENES IN SYSTEMIC SCLERODERMA: A STRATIFICATION BIOMARKER POTENTIAL

Shagina IA1.2.5, Turchaninova MA2.5, Golovina OA3, Bufeeva LS2.5, Zhurina TI3, Saifullin RF1.4, Myshkin MYu2.5, Mutovina ZYu3, Britanova OV2.5

- <sup>1</sup> Pirogov Russian National Research Medical University, Moscow, Russia
- <sup>2</sup> MyLaboratory LLC, Moscow, Russia
- <sup>3</sup> Moscow City Research Center Hospital No. 52, Moscow, Russia
- <sup>4</sup> Federal Scientific and Clinical Center of Resuscitation and Rehabilitation, Moscow, Russia
- <sup>5</sup> Shemyakin and Ovchinnikov Institute of Bioorganic Chemistry of the Russian Academy of Sciences, Moscow, Russia

Systemic scleroderma (SS) remains a disease with a high mortality rate; validated biomarkers for stratification and disease monitoring are still lacking. The study aimed to assess the expression of the developed panel of IFN-I-induced genes (*IFI27*, *IFI44*, *IFIT3*, *ISG15*, *XAF1*) in peripheral blood and affected skin of patients with SS. We tested samples of 48 SS patients and 31 healthy donors. Gene expression was analyzed using RT-qPCR ( $\Delta\Delta$ Ct) method (with normalization to the reference housekeeping gene TBP). The SFRP4 gene expression was used as a marker of skin fibrosis. Expression values of the IFN-I-induced genes were significantly ( $\rho$  < 0.1) increased in both blood and skin of SS patients compared to healthy donors. Comparison between compartments revealed that the expression levels of *XAF1*, *IFI44*, *IFIT3*, *ISG15* in the patients' blood are higher ( $\rho$  < 0.01), than those in skin samples. The *IFI27* gene expression, in contrast, is higher in the skin ( $\rho$  < 0.01). The findings show that the test system developed for interferon signature assessment can potentially be used as a noninvasive tool for stratifying SS patients by analysis of RNA from peripheral blood samples, to substantiate the prescription of therapy with the IFN-I receptor blockers.

Keywords: systemic scleroderma, SS, Type I interferon, IFN-I-signature, anifrolumab, qRT-PCR, noninvasive diagnosis

Funding: the study was supported by the grant from the Moscow Government (R&D project No. 1603-47/23 dated 08.06.2023), sponsored by the Moscow Center for Innovative Technologies in Healthcare.

Author contribution: Mutovina ZYu — concept; Zhurina TI, Saifullin RF — acquisition of rheumatology and medicine data; literature review; Myshkin MYu — data analysis; Bufeeva LS — sample collection, RNA extraction; Shagina IA — RT-qPCR optimization and procedure, primary data analysis, manuscript writing, literature review; Turchaninova MA, Golovina OA, Britanova OV — manuscript writing, literature review.

Compliance with ethical standards: the study was conducted in accordance with the Declaration of Helsinki. The informed consent for biomaterial collection and testing during inpatient assessment settings was obtained from all patients.

Correspondence should be addressed: Olga V. Britanova — Miklukho-Maklaya, 16/10, Moscow, 117997, Russia; olbritan@gmail.com; Zinaida Yu. Mutovina — Pekhotnaya, 3, Moscow, 123182, Russia, zmutovina@mail.ru

Received: 06.09.2025 Accepted: 08.10.2025 Published online: 21.10.2025

DOI: 10.24075/brsmu.2025.047

Copyright: © 2025 by the authors. Licensee: Pirogov University. This article is an open access article distributed under the terms and conditions of the Creative Commons Attribution (CC BY) license (https://creativecommons.org/licenses/by/4.0/).

# ПАНЕЛЬ IFN-I-ИНДУЦИРУЕМЫХ ГЕНОВ ПРИ СИСТЕМНОЙ СКЛЕРОДЕРМИИ: ПОТЕНЦИАЛ БИОМАРКЕРА СТРАТИФИКАЦИИ

И. А. Шагина<sup>1,2,5</sup>, М. А. Турчанинова<sup>2,5</sup>, О. А. Головина<sup>3</sup>, Л. С. Буфеева<sup>2,5</sup>, Т. И. Журина<sup>3</sup>, Р. Ф. Сайфуллин<sup>1,4</sup>, М. Ю. Мышкин<sup>2,5</sup>, З. Ю. Мутовина<sup>3</sup>, О. В. Британова<sup>2,5</sup> ⊠

- 1 Российский национальный исследовательский медицинский университет имени Н. И. Пирогова, Москва, Россия
- <sup>2</sup> ООО «МайЛаборатори», Москва, Россия
- <sup>3</sup> Московский городской научно-исследовательский центр Больница № 52, Москва, Россия
- 4 Федеральный научно-клинический центр реаниматологии и реабилитологии, Москва, Россия
- <sup>5</sup> Институт биоорганической химии имени М. М. Шемякина и Ю. А. Овчинникова Российской академии наук, Москва, Россия

Системная склеродермия (ССД) остается заболеванием с высокой летальностью; валидированных биомаркеров для стратификации и мониторинга недостаточно. Целью работы было изучить экспрессию разработанной панели IFN-I-индуцируемых генов (IFI27, IFI44, IFI73, ISG15, XAF1) в периферической крови и пораженной коже при ССД. Исследовали образцы 48 пациентов с ССД и 31 здорового донора. Экспрессию генов определяли методом RT-qPCR ( $\Delta\Delta$ Ct) с нормировкой по референсному гену «домашнего хозяйства»; экспрессию гена SFRP4 использовали как маркер кожного фиброза. Экспрессия IFN-I-индуцируемых генов была достоверно (p < 0,1) повышена как в крови, так и в коже пациентов с ССД относительно образцов здоровых доноров. Сопоставление экспрессии между компартментами показало, что уровни экспрессии генов XAF1, IFI44, IFI73, ISG15 в крови пациентов выше (p < 0,01), чем в образцах кожи. Экспрессия гена IFI27, напротив, более выражена в коже (p < 0,01). Результаты исследования показывают, что разработанная тест-система оценки интерфероновой сигнатуры потенциально может быть использована как неинвазивный инструмент стратификации пациентов с ССД по анализу РНК, полученной из образца крови, в том числе для обоснования назначения терапии блокаторами рецептора IFN-I.

Ключевые слова: системная склеродермия, интерферон I типа, интерфероновая сигнатура, анифролумаб, qRT-PCR, неинвазивная диагностика

Финансирование: исследование выполнено на средства гранта Правительства Москвы (НИР № 1603-47/23 от 08.06.2023), спонсор — АНО «Московский центр инновационных технологий в здравоохранении».

Вклад авторов: 3. Ю. Мутовина — концепция; Т. И. Журина, Р. Ф. Сайфуллин — сбор данных в сфере ревматологии и медицины; анализ литературы М. Ю. Мышкин — анализ данных; Л. С. Буфеева — сбор образцов, выделение РНК; И. А. Шагина — оптимизация и проведение RT-qPCR, первичный анализ данных, подготовка рукописи, анализ литературы. М. А.Турчанинова, О. А. Головина, О. В. Британова — подготовка рукописи, анализ литературы.

Соблюдение этических стандартов: исследование проведено в соответствии с требованиями Хельсинкской декларации. От всех пациентов получено добровольное информационное согласие в рамках прохождения обследования в стационаре (на взятие образцов биоматериала и проведение анализов).

Для корреспонденции: Ольга Владимировна Британова — ул. Миклухо-Маклая, д. 16/10, 117997, г. Москва, Россия, olbritan@gmail.com; Зинаида Юрьевна Мутовина — ул. Пехотная, д. 3, 123182, г. Москва, Россия, zmutovina@mail.ru

Статья получена: 06.09.2025 Статья принята к печати: 08.10.2025 Опубликована онлайн: 21.10.2025

DOI: 10.24075/vrgmu.2025.047

Авторские права: © 2025 принадлежат авторам. Лицензиат: РНИМУ им. Н. И. Пирогова. Статья размещена в открытом доступе и распространяется на условиях лицензии Creative Commons Attribution (CC BY) (https://creativecommons.org/licenses/by/4.0/).

## ОРИГИНАЛЬНОЕ ИССЛЕДОВАНИЕ І ИММУНОЛОГИЯ

Systemic scleroderma (SS) is a systemic autoimmune disorder characterized by vasculopathy followed by progressive fibrosis of the skin and internal organs manifestations [1] and high mortality rate: 25% of patients die within the first 5 years after making the diagnosis, 37.5% die within the first 10 years [2-5]. The mean life expectancy of SS patients is 16-34 years less than the population average [4]. The disease prevalence varies between 38 and 341 per million population annually, and the disease incidence varies between 8 and 56 individuals per million per year based on the data from different countries [6-11]. The most common cause of death associated with SS in damage to internal organs: the lung, heart, gastrointestinal tract [4, 5]. In addition to these manifestations, in 35% of patients the disease course is complicated by digital ulcers, which, in turn, often leading to gangrene and fingers amputation, which causes severe functional impairment in such patients [12–13].

Although the disease is multisystemic, skin lesion is a distinctive feature that determines the clinical and prognostic stratification. SS is classified based on the extent of skin involvement into the diffuse (dSS) and limited (ISS) forms that have different progression rate, disease course features, and prognosis [1].

The molecular mechanisms that underlie the development of SS are poorly understood. This hinders the selection of targeted therapy selection. Currently, the range of potential treatment options is extremely limited, necessitating the search for new therapies. Although the T cell responses of types Th2 and Th17 play an important role in the SS pathogenesis [15, 16], it has been shown that activation of interferon pathways, especially type I, is more strongly associated with SS, than immune responses of other types [17, 18].

Recent studies have shown similar expression of the genes involved in the interferon cascade in patients with systemic lupus erythematosus and SS [19–21]. Upregulation of the IFN-associated genes is also typical for rheumatoid arthritis, Sjogren's syndrome, and polymyositis [23–29].

Activation of the IFN-I pathway and, as a result, the "interferon" gene signature are observed in blood and skin of a large number of patients with even early-stage SS and, according to some data, are associated with severity of lesions (including pulmonary and skin lesions) [30, 31]. The conclusion about the relationship between the expression of IFN-induced genes and the disease severity was disproven by subsequent research [28, 32].

The up-to-date EULAR guidelines (updated 2023) reflect a shift towards targeted approaches to SS, which increases the importance of the validated stratification biomarkers [33]. Such observations raise the question about the potential effectiveness of the interferon-mediated pathway blocking in some patients with SS.

The study aimed to assess the expression of interferondependent genes in peripheral blood cells and affected skin areas of SS patients in order to estimate the potential for patient stratification and the prognosis of a promising, but not yet approved therapy with antibodies against interferon receptors in SS [34]. The hypothesis was tested that the IFN-I-signature can be reflected in peripheral blood of patients with SS, the analysis of which can become an alternative to repeated skin biopsy when performing patient stratification and monitoring.

**METHODS** 

## Patients

The patients aged 21-77 with the limited or diffuse cutaneous systemic scleroderma form, who were admitted to the

Rheumatology Department of the Moscow City Research Center Hospital No. 52 from April 2023 to February 2025 and met the ACR/EULAR2013 criteria, were included in the study [35].

Inclusion criteria: detection of the antinuclear factor in patient's blood by the indirect immunufluorescence method. When detecting the antinuclear factor, the range of nuclear antibodies was tested by immunoblotting (Table 1).

Exclusion criteria: another systemic autoimmune disorder (such as rheumatoid arthritis, idiopathic inflammatory myopathy, systemic lupus erythematosus); signs of infectious disease (upon physical examination).

The patients having no specific antibodies or negative immunoblot test results were not excluded from the study, since:

1) according to the ACR/EULAR criteria, the fact of having specific antibodies is not a mandatory criterion for establishing the diagnosis of SS [35];

2) antibodies against RNA polymerase III, which are not detected in the Russian Federation, are also typical for SS; furthermore, SS can be associated with the antibodies that are outside the spectrum assessed.

The screening tests for antinuclear antibodies were performed by enzyme-linked immunoassay (ELISA) with the Multiscan FC semi-automatic ELISA analyzer (Thermo Fisher Scientific Inc., USA) using the ANA-Screen ELISA IgG reagent kit (Euroimmun AG, Germany) in accordance with the manufacturer's instructions. Confirmatory testing for specific antinuclear antibodies was performed by immunoblotting using the ANA profile 1 IgG reagent kit (Euroimmun AG, Germany) in accordance with the manufacturer's instructions.

The clinical and immunological assessment of patients was conducted that included the following: assessment of disease activity based on EScSG (Table 1) [36], evaluation of the capillaroscopic pattern at the time of examination, and laboratory testing for specific antibodies. All the patients were tested for the presence/absence of damage to possible target organs: skin (Rodnan skin score was assessed), joints (the number of painful and swollen joints was estimated), lung (all the patients underwent chest multislice computed tomography (MSCT)), heart and pulmonary artery (electrocardiography, echocardiography and gastrointestinal catheterization (e.g. barium swallow test in one patient) were performed).

## Biomaterial selection and RNA extraction

Sample collection was performed in the clinic during general patient examination at admission to the hospital. A total of 48 patients with SS were included in the study. In 25 patients, peripheral blood samples only were collected as biomaterial for testing. In another 10 patients, both the affected skin specimens and peripheral blood samples were collected; in 13 patients, the affected skin specimens only were collected. Skin biopsy specimens were collected from the forearm (area with the thickest skin) by incisional biopsy.

The healthy skin samples collected from three donors not diagnosed with SS were used as the reference samples, along with the peripheral venous blood samples of 31 healthy donors aged 20–54 years. A total of 20% of the cohort of healthy donors were males.

The affected skin samples 4 mm in diameter were placed in the MACS® Tissue Storage Solution (Miltenyi, USA) at +4 °C and transferred to the laboratory for RNA extraction. The resulting samples were ground in liquid nitrogen with RLT lysis buffer added simultaneously. RNA extraction was performed using the HiPure Total RNA Kit (Magen, China) in accordance with the

## ORIGINAL RESEARCH I IMMUNOLOGY

**Table 1.** Results of clinical and immunological assessment of SS patients (n = 48)

Indicator	Values	Standard deviation
Average age	61 (21–77)	61.4
Sex	Males 5/48 (10%), females 43/48 (90%)	0.31
Disease duration	13.5 years (0.5–47)	13.6
Course	acute — 3/48 (6%) subacute — 5/48 (10%) chronic — 40/48 (84%)	0.24 0.31 0.37
Form	Limited — 30/48 (62.5%), diffuse — 18/48 (37.5%)	0.48
Organ damage		
Interstitial lung disease	27/48 (56%)	0.50
- CT pattern for organizing pneumonia	2/48 (4%)	0.20
- CT pattern for nonspecific interstitial pneumonia	25/48 (52%)	0.50
Primary pulmonary hypertension	12/48 (25%)	0.43
Kidney disease	2/48 (4%)	0.20
Heart disease	14/48 (29%)	0.45
- Pericarditis	12/48 (25%)	0.42
- Myocarditis	3/48 (6%)	0.24
Esophageal lesion	34/48 (71%)	0.45
Intestinal lesion	6/48 (12.5%)	0.33
Muscle lesion	9/48 (19%)	0.39
Joint lesion	28/48 (58%)	0.49
Skin manifestations	46/48 (96%)	0.20
- digital ulcers	15/48 (31%)	0.46
Signs of Raynaud's phenomenon	47/48 (98%)	0.14
Capillaroscopic pattern	late — 27/48 (56%), active — 16/48 (33%) early — 3/48 (6%) myopathic — 2/48 (4%)	0.50 0.47 0.24 0.20
Telangiectasia	27/48 (56%)	0.49
Rodnan score, points	7 (0–37)	6.90
Laboratory tests		
Anti-centromere antibodies (ACAs)	25/48 (52%)	0.50
Anti-Sc-70 antibodies	14/48 (29%)	0.45
Anti-PM/Scl antibodies	1/48 (2%)	0.14
Anti-RNP70 antibodies	1/48 (2%)	0.14
Anti-SSA antibodies	1/48 (2%)	0.14
No specific antibodies	6/48 (12.5%)	0.33
Therapy (at the time of sample	collection)	
Mycophenolate mofetii (MMF) — $14/48$ (29%), low-dose glucocorticoids (GC (27%), rituximab (RTX) — $11/48$ (23%), nintedanib — $3/48$ (6%), cyclophosp (4%), no therapy — $8/48$ (16.7%)		
Low-intensity immunosuppressive therapy (HC and/or low dose GCs)	18/48 (37.5%)	0.48
High-intensity immunosuppressive therapy (MMF and/or RTX and/or MT)	22/48 (46%)	0.50

manufacturer's instructions. RNA concentration was measured using the Qubit 3.0 fluorometer and the reagent kit (Thermo Fisher Scientific, USA).

Blood samples (4 mL) were collected into the EDTA-coated tubes (final concentration of 2 mg/mL).

After collection, whole blood was stored at 4 °C until mononuclear cells were isolated. Mononuclear cells were isolated from peripheral blood by sedimentation (Ficoll-Paque density gradient centrifugation (density 1.077 g/cm³)) (PanEco, Russia). The resulting cell fraction was placed in the RLT lysis buffer (Qiagen, Germany) and stored at -80 °C until total RNA was extracted. The total RNA was extracted using the HiPure Total RNA Kit (Magen, China) in accordance with the manufacturer's instructions.

The RNA concentration was measured using the Qubit 3.0 fluorometer (USA) and the reagent kit (Thermo Fisher Scientific, USA). The quality of the RNA sample extracted was evaluated by agarose gel electrophoresis. The extracted RNA was frozen and stored at the temperature of –80 °C until the reverse transcription and real-time PCR were launched.

## RT-PCR and data analysis

The one-tube quantitative RT-PCR (reverse transcription PCR) was performed using the One-Tube RT-PCR TaqMan reagent kit (Evrogen, Russia) [37]. The kit contains a ready-to-use master mix comprising a reaction buffer for RT and

## ОРИГИНАЛЬНОЕ ИССЛЕДОВАНИЕ І ИММУНОЛОГИЯ

PCR, nucleotide triphosphates, and the hot start Taq DNA polymerase. In the first phase, during the first-strand cDNA synthesis, the Taq polymerase was inactivated by monoclonal antibodies; heating at 95 °C prior to PCR ensured the rapid hot start. The modified MMLV reverse transcriptase was provided to the reaction mixture separately. Primers for first-strand cDNA synthesis and subsequent PCR amplification were added to the reaction in a concentration of 0.4  $\mu$ M. Real-time PCR product accumulation imaging was performed using the TaqMan type fluorescent probes. The probes were added to the reaction at a concentration of 0.1  $\mu$ M. All the oligonucleotides specific for the test and reference genes were selected such that optimal performance was achieved under a single, versatile RT-PCR protocol.

Reverse transcription: 55 °C, 15 min, one cycle, without fluorescence acquisition. This was followed by a reverse transcriptase inactivation/polymerase activation step: 95 °C, 1 min, one cycle, without reading. Amplification was carried out for 40 cycles: denaturation — 95 °C, 15 s (without acquisition); annealing — 60 °C, 20 s (with fluorescence acquisition); elongation — 72 °C, 20 s (without acquisition).

To analyze the interferon signature, the expression of *IFIT1*, *IFIT3*, *IFI27*, *IFI44*, *ISG15*, *XAF1* was assessed, that was previously validated in the peripheral blood samples of patients with systemic lupus erythemathosus (SLE), along with that of the TBP reference gene [29, 31].

The same method was used to assess the expression of the SFRP4 marker gene which is a recognized marker associated with fibrosis progression in scleroderma [22].

Assessment of the relative expression of the interferondependent genes involved normalization to the expression of the TBP housekeeping gene.

Relative expression was determined by the  $\Delta\Delta$ Ct method with normalization to the reference gene amplified in the same PCR. Relative expression of the test gene was determined based on the amplification effeciency and the difference in cycle thresholds ( $\Delta$ Ct) between the target and reference gene.

#### Statistical data processing

The nonparametric methods (appropriate for small sample sizes) were used for statistical processing.

The Mann-Whitney test was used to compare gene expression in the donor samples of the experimental (SS patients) and control groups. When comparing gene expression values of the skin and blood samples, the significance of differences between samples was estimated using the paired Wilcoxon signed-rank test. All *p*-values were further adjusted using the Benjamini-Hochberg (False Discovery Rate (FDR)) procedure. Spearman's rank correlation coefficient was used to assess correlations between variables.

The IFN-I signature value was calculated as the mean of the standardized scores (z-score) of relative expression of five genes (IFIT3, IFI27, IFI44, ISG15, XAF1).

The standardized scores for the IFN-I signature (averaged between skin and blood) were calculated for the subgroup of patients from whom paired blood and skin samples were obtained (n = 10).

The standardized scores of the IFN-I signature values in SS patients were calculated relative to healthy donors, separately in blood and skin samples).

Mean values and the standard deviation were calculated for clinical data (Tables 2 and 3). However, due to the indicators' limited applicability to small samples (with the unproven hypothesis about the normally distributed values) the median and interquartile range were also calculated.

The standard deviation of binary types of data (such as clinical mainfestations) was calculated for the Bernoulli distribution.

Work with the tables, data correction, charting, and statistical analysis were accomplished using the R integrated features and supplementary libraries: tidyverse, ggplot2, and corrplot.

#### **RESULTS**

The study included 48 SS patients, mostly females (90%), a mean age 61 years, and mean disease duration 13.5 of years, primarily with the disease chronic course (84%) and limited cutaneous form (62.5%). The leading organ damage and manifestations: interstitial lung disease (56%, mainly NSIP); esophageal (71%) and joint (58%) lesions. were observed. The average skin activity was low (mRSS 7), the Raynaud's phenomenon was diagnosed in almost all patients (98%), digital ulcers were present in 31%. The results of the clinical and immunological assessment of SS patients are presented in Table 1.

The integrated IFN-I signature assessment involved the use of the modified test system conprising five genes (IFI27, XAF1, IFI44, IFIT3, ISG15) using one reference gene instead of two, which had been previously tested in peripheral blood samples of patients with SLE [32, 38]. SFRP4 (secreted frizzled-related protein) was used as a marker gene of the disease, the expression levels of which are associated with skin fibrosis in SS [22].

Significant differences in expression levels of all five test genes between the groups of SS patients and healthy donors were observed in the RNA samples obtained from the skin; significant differences in expression of 4 test genes out of 5 (except IFI27) between the groups of SS patients and healthy donors were reported for blood samples (Fig. 1A, B; Table 2.). The SFRP4 expression levels were higher in the skin samples of patients with SS compared to the skin samples of healthy donors (Fig. 1A).

Comparison of expression levels between compartments performed for the paired blood/skin samples (Fig. 2; Table 3) showed that the XAF1, IFI44, IFIT3, ISG15 expression levels in patients' blood were significantly higher than in skin samples. The IF127 gene expression, in contrast, was more pronounced in the skin (Fig. 2A, C). The direction of changes was consistent across both sample types, which supports the effectiveness of using both skin biopsy samples and blood samples for the diagnosis and dynamic monitoring (Fig. 2B, D). The IFN-I integral index of patients with SS was significantly higher compared to the reference threshold interval calculated based on the healthy donors' values in both peripheral blood samples and the affected skin biopsy samples (Fig. 2E, F). A limitation of the skin IFN-I signature index comparison is associated with the small number of samples collected from healthy donors. The integral index based on blood samples showed that the values were above the reference interval in 62% (22 patients).

The correlation analysis of clinical parameters and gene expression (Fig. 3; Table 4) has shown that the IFN-I signature genes (*IFIT3*, *IFI27*, *IFI44*, *ISG15*, *XAF1*) form a tightly coexpressed module (Rs between 0.52 and 0.87; p < 0.05 for the skin) with the significant positive correlations between genes, while SFRP4 exhibited little association with this module reflecting a distinct fibrosis-associated component.

In blood samples, the *IFIT3*, *IFI27*, *ISG15*, *XAF1* genes also form a correlation cluster with each other, but the correlation values are lower (Rs between 0.38 and 0.63). The *IFIT27* gene

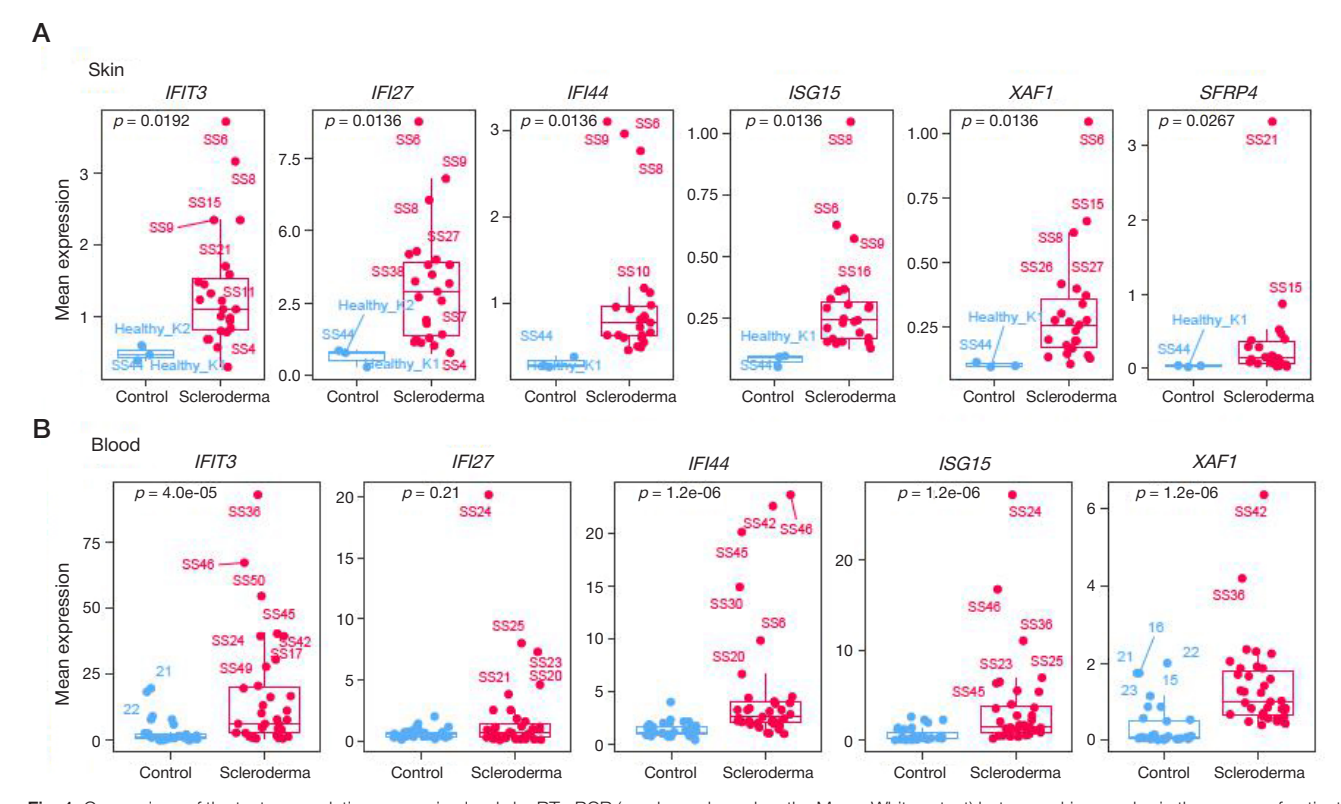


Fig. 1. Comparison of the test gene relative expression levels by RT-qPCR (p-value — based on the Mann–Whitney test) between skin samples in the groups of patients with SS (n = 23) and healthy donors (n = 3) (A), between peripheral blood samples in the groups of patients with SS (n = 35) and healthy donors (n = 31) (B)

is most closely correlated to ISG15 (Rs = 0.77), but it is outside the common correlation cluster (Rs with *IFIT3*, *IFI27*, *ISG15*, XAF1 < 0.15).

Clinical indicators of disease severity (activity based on EScSG, progression, diffuse form) significantly correlate with each other.

The IFN-I signature genes demonstrate a non-significant correlation with the diffuse disease form: in skin samples, Rs is between 0.23 and 0.34, skin samples show a slight correlation for ISG15 and IFIT27 only (0.21 and 0.27, respectively). Age shows a weak negative association with the expression of the IFN-I-induced genes (Rs between -0.32 and -0.36) in skin samples; the correlations for blood are insignificant (0 to -0.13).

#### DISCUSSION

Recently, determination of the expression of the IFN-I-stimulated genes by PCR is increasingly used in clinical trials. Various diagnostic test systems for assessment of the IFN signature expression have been developed. Expression levels of the genes IFI44L, IFI44, MX1, MX2, OAS1, OAS2, OAS3, SIGLEC1, IFI35 are most often determined when determining the IFN signature [39]. Russian scientists have also proposed solutions in this area [40, 41]. In particular, one system involves the analysis of three genes (RIG-1, IFIT-1, IFIH-1). However, the expression normalization approach used in these panels seems to be suboptimal: HPRT is used as a reference gene

**Table 2.** Gene expression levels in skin samples in the groups of patients with SS (n = 23) and healthy donors (n = 3) **(A)**, in peripheral blood samples in the groups of patients with SS (n = 35) and healthy donors (n = 31) **(B)** 

			A. Skin	samples		B. Blood samples				
Gene	Group	Mean	SD	Median	iqr*	Mean	SD	Median	iqr*	
IFIT3	Control	0.47	0.11	0.46	0.1	3.15	4.87	1.15	1.76	
IFIT3	SS	1.36	0.84	1.1	0.72	16.37	21.17	6.35	17.24	
IFI27	Control	0.64	0.31	0.78	0.28	0.59	0.39	0.54	0.35	
IFI27	SS	3.11	2.02	2.89	2.56	1.91	3.69	0.72	1.07	
IFI44	Control	0.31	0.06	0.28	0.06	1.38	0.69	1.15	0.68	
IFI44	SS	1.03	0.78	0.78	0.35	4.9	5.98	2.58	1.93	
ISG15	Control	0.08	0.02	0.09	0.02	0.65	0.76	0.31	0.71	
ISG15	SS	0.3	0.21	0.24	0.15	3.63	5.33	1.48	2.94	
XAF1	Control	0.1	0.01	0.1	0.01	0.37	0.57	0.08	0.47	
XAF1	SS	0.31	0.22	0.26	0.18	1.39	1.17	1	1.13	
SFRP4	Control	0.03	0.01	0.04	0.01	n/a	n/a	n/a	n/a	
SFRP4	SS	0.36	0.69	0.14	0.28	n/a	n/a	n/a	n/a	

Note: \* iqr — interquartile range.

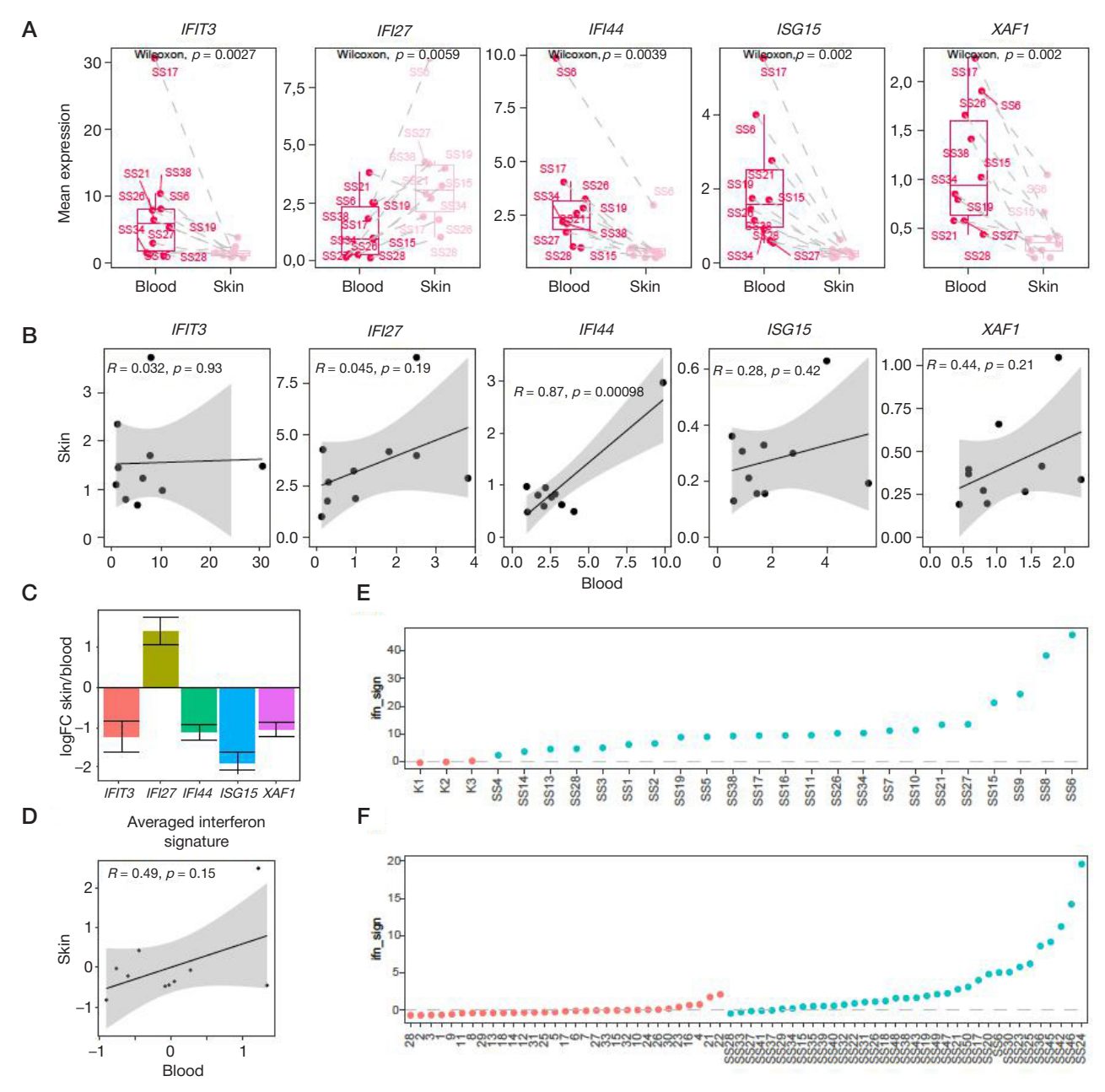


Fig. 2. Comparison of interferon signature in blood and skin of patients with SS. A. Comparison of relative expression levels of the test genes *IFIT3*, *IFI27*, *IFI24*, *ISG15*, *XAF1* in the RNA samples obtained from the skin and peripheral blood of SS patients (n = 10) represented as a box-plot. The Wilcoxon signed-rank test was used. B. Pairwise correlation of the IFN-I panel gene expression between blood and skin. C. A bar chart shows the mean log fold change) for the skin and blood. Negative values indicate higher expression in blood, and positive values indicate higher expression in the skin. D. Correlation of the averaged IFN-I signature of blood and skin for paired samples (n = 10), (R = 0.49; p = 0.15). B, D Spearman's rank correlation coefficient is used (*grey areas* — 95% CI). E. IFN-I signature values (z-score, standardized against donor values) in skin biopsy samples: red dots — healthy donors (n = 3), blue dots — SS patients (n = 23). F. IFN-I signature values (z-score, standardization by healthy donors) in peripheral blood samples. Red dots — healthy donors (n = 31), Red dots — SS patients (n = 35, including 10 paired skin/blood samples). The dashed line shows the threshold interval

in the first one, but standardization by  $\Delta Ct$  is not described, it is proposed to use GAPDH as a reference gene in the second one, which can result in artifacts due to the presence of numerous pseudogenes in the human genome. In this study, we used integrated assessment of the IFN-I signature using the test system of five genes: IFI27, XAF1, IFI44, IFIT3, ISG15 with normalization to one reference gene. Previously, we tested these genes individually and as a test system in peripheral blood samples from patients with SLE [32, 38].

According to the findings, the SS patients showed the increased expression of the IFN-induced genes compared to healthy donors in both skin and peripheral blood samples. These data confirming involvement of type I interferons in the disease pathogenesis are consistent with the previously

reported results for SS [17, 21, 30]. Based on the results of our analysis the expression of IFN-I-induced genes shows a trend toward correlation in blood and affected skin samples. Such a trend has been earlier demonstrated in the large cohort of SS patients using the transcriptome profiling (microarray). It has been shown that the expression of the IFN-associated genes in the skin is consistent with similar changes in peripheral blood [42]. These and other observations suggest the informativeness of assessing IFN-I signature in blood samples of patients with SS [18].

Clinical indicators of the disease severity (activity based on EScSG, progression, diffuse form) significantly correlate with each other, but demonstrate only weak and heterogeneous correlations with the IFN-I signature. Thus, the applicability of

## ORIGINAL RESEARCH I IMMUNOLOGY

Table 3. Expression of the test genes IFI73, IFI27, IFI44, ISG15, XAF1 in the RNA samples obtained from peripheral blood of the same SS patients (n = 10)

Gene	Sample	Mean valus	Standard deviation	Median	lqr*
IFIT3	Blood	7.48	8.73	5.81	6.17
IFIT3	Skin	1.55	0.91	1.34	0.64
IFI27	Blood	1.34	1.27	0.96	2.07
IFI27	Skin	3.48	2.16	3.07	2.03
IFI44	Blood	3.05	2.57	2.39	1.34
IFI44	Skin	0.95	0.73	0.79	0.32
ISG15	Blood	2.04	1.62	1.57	1.54
ISG15	Skin	0.28	0.15	0.26	0.16
XAF1	Blood	1.15	0.62	0.94	0.97
XAF1	Skin	0.42	0.26	0.35	0.14

Note: \* — interquartile range.

the developed test system for patient stratification and predicting the success of therapy with the IFN-I receptor inhibitors should be assessed independently from the disease severity and form.

Since the levels of the assessed IFN-I signature in some SS patients are within the range close to that of controls (Fig. 2), and there is no correlation between gene expression and the disease severity (Fig. 3), it can be assumed that SS patients have various immunological patterns, in addition to the type I interferon activation patterns (by analogy to the patterns reported for SLE [26]). The fact that SS patients have both significantly higher and lower (at the level of the control group) expression levels of the IFN-induced genes suggests the need for patient stratification to predict the response to therapy) with the interferon receptor antibodies with the interferon receptor antibodies.

Given the current clinical trials of the IFN-I receptor inhibitor in SS (DAISY; NCT05631227) [37], the elevated IFN-I signature value can potentially be a criterion for patient selection and the tool to monitor the effectiveness of the response to therapy with the interferon receptor blocker (anifrolumab). Similarity of the interferon-associated pathways in SS and SLE [14, 23, 42] together with the available data on the anifrolumab efficacy in

SLE [43] suggest that the use of this drug in SS can be highly effective in patients having high interferon signature values.

#### CONCLUSIONS

SS patients show the increased expression of interferoninduced genes in both skin and peripheral blood samples compared to healthy donors, which suggests the involvement of type I interferons in the SS pathogenesis. The expression levels of the IFN-I-induced genes show a trend toward correlation in blood samples and affected skin areas. The RT-qPCR panel developed that comprises the IFN-I-induced genes (IFI27, IFI44, IFIT3, ISG15, XAF1) has a potential for stratification of SS patients, as well as for assessment of the efficacy of target therapy with the interferon receptor blockers (in case such therapy is approved for SS). To verify this conclusion it is required to conduct further research focused on the correlation between the decrease in the interferon signature levels and the condition improvement in SS patients treated with the antibodies against the interferon receptor. We recommend using peripheral blood from SS patients for IFN-I-

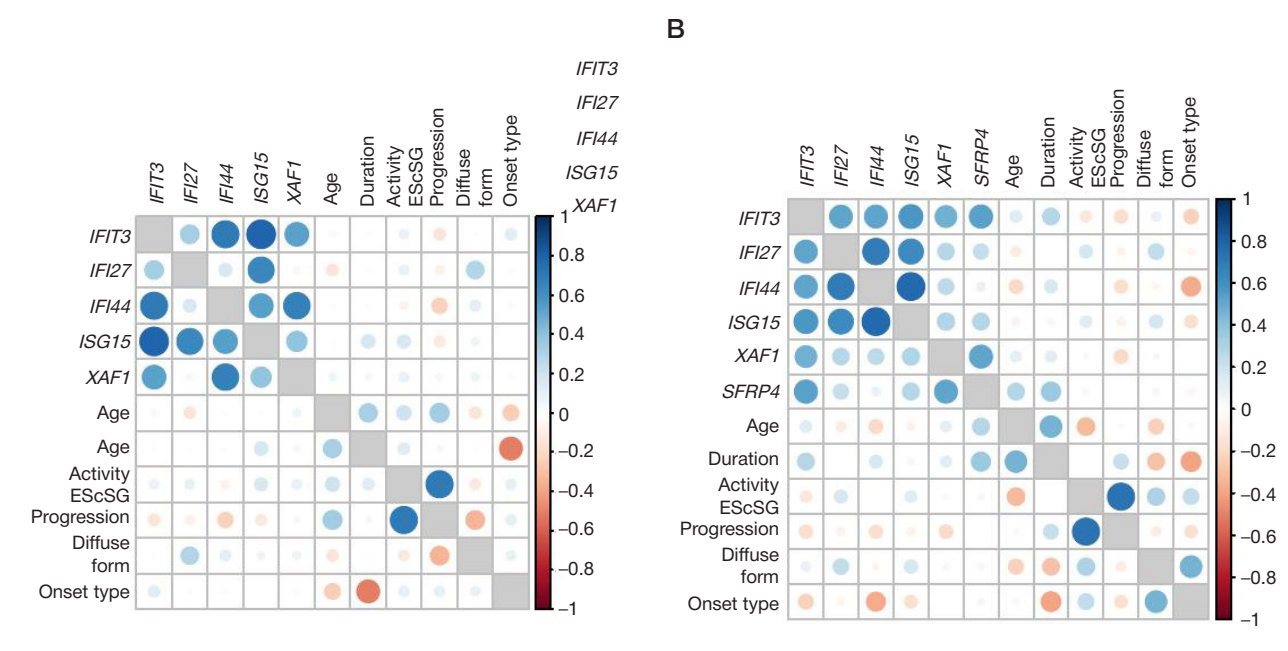


Fig. 3. Correlation matrix for expression levels of the IFN-I signature genes (IF144, IF173, ISG15, IF127, XAF1) in the samples and clinical signs of the group of SS patients for peripheral blood (n = 35) (A) and affected skin samples (n = 23) (B). The SFRP4 gene expression was added as a disease marker. The circle color indicates the correlation sign and strength: bIue — positive, red — negative; the more saturated the color, the closer |r| to 1. The circle size is proportional to the Spearman's rank correlation module (coefficient)

Α

### ОРИГИНАЛЬНОЕ ИССЛЕДОВАНИЕ І ИММУНОЛОГИЯ

**Table 4.** Values of the correlation between the expression of the IFN-I signature genes (IFI44, IFIT3, ISG15, IFI27, XAF1) in the samples and clinical signs of the group of SS patients for blood (n = 35), (4A) and skin (n = 23) samples (4B)

4A	IFIT3	IFIT2	?7 IF	TT44	ISG15	XAF1	Age	Duration	Activity (EScSG)	Progression	Diffuse form	Onset type
IFIT3	1.00	0.16	6 (	).49	0.63	0.63	0.03	0.01	0.24	0.06	0.08	0.11
IFIT27	0.16	1.00	) –	0.04	0.77	-0.17	-0.03	0.10	0.06	0.03	0.27	-0.09
IFIT44	0.49	-0.0	4	.00	0.38	0.64	-0.13	-0.22	-0.08	-0.08	-0.13	0.24
ISG15	0.63	0.77	7 (	.38	1.00	0.24	0.00	0.00	0.16	0.08	0.21	0.06
XAF1	0.63	-0.1	7 (	).64	0.24	1.00	-0.08	0.04	0.06	-0.13	0.04	0.00
Age	0.03	-0.0	3 –	0.13	0.00	-0.08	1.00	0.31	0.18	0.32	-0.12	-0.16
Duration	0.01	0.10	) -	0.22	0.00	0.04	0.31	1.00	0.15	0.07	-0.14	-0.36
Activity (EScSG)	0.24	0.06	3 -	0.08	0.16	0.06	0.18	0.15	1.00	0.60	-0.02	0.20
Progression	0.06	0.03	3 –	0.08	0.08	-0.13	0.32	0.07	0.60	1.00	-0.34	0.12
Diffuse form	0.08	0.27	7 –	0.13	0.21	0.04	-0.12	-0.14	-0.02	-0.34	1.00	0.15
Onset type	0.11	-0.0	9 (	).24	0.06	0.00	-0.16	-0.36	0.20	0.12	0.15	1.00
4B	IFIT3	IFIT27	IFIT44	1001	1				Activity			
			11 11 44	ISG18	5 XAF1	SFRP4	Age	Duration	(EScSG)	Progression	Diffuse form	Onset type
IFIT3	1.00	0.79	0.82	0.80	0.79	0.22	Age -0.36	Duration 0.13		Progression -0.15	Diffuse form 0.23	
IFIT3	1.00								(EScSG)	ŭ		type
-		0.79	0.82	0.80	0.79	0.22	-0.36	0.13	(EScSG) 0.01	-0.15	0.23	type -0.19
IFIT27	0.79	0.79	0.82	0.80	0.79	0.22	-0.36 -0.36	0.13	(EScSG) 0.01 0.15	-0.15 -0.09	0.23 0.34	-0.19 -0.08
IFIT27 IFIT44	0.79	0.79 1.00 0.87	0.82 0.87 1.00	0.80 0.74 0.87	0.79 0.59 0.52	0.22 0.03 -0.05	-0.36 -0.36 -0.51	0.13 -0.09 -0.07	(EScSG)  0.01  0.15  0.13	-0.15 -0.09 -0.09	0.23 0.34 0.28	type -0.19 -0.08 -0.24
IFIT27 IFIT44 ISG15	0.79 0.82 0.8	0.79 1.00 0.87 0.74	0.82 0.87 1.00 0.87	0.80 0.74 0.87 1.00	0.79 0.59 0.52 0.54	0.22 0.03 -0.05 0.05	-0.36 -0.36 -0.51 -0.57	0.13 -0.09 -0.07 -0.04	(EScSG)  0.01  0.15  0.13  0.21	-0.15 -0.09 -0.09 0.02	0.23 0.34 0.28 0.31	type -0.19 -0.08 -0.24 -0.20
IFIT27 IFIT44 ISG15 XAF1	0.79 0.82 0.8 0.79	0.79 1.00 0.87 0.74 0.59	0.82 0.87 1.00 0.87 0.52	0.80 0.74 0.87 1.00 0.54	0.79 0.59 0.52 0.54 1.00	0.22 0.03 -0.05 0.05	-0.36 -0.36 -0.51 -0.57 -0.32	0.13 -0.09 -0.07 -0.04 0.16	(EScSG)  0.01  0.15  0.13  0.21  0.02	-0.15 -0.09 -0.09 0.02 -0.19	0.23 0.34 0.28 0.31 0.16	type -0.19 -0.08 -0.24 -0.20 -0.12
IFIT27 IFIT44 ISG15 XAF1 SFRP4	0.79 0.82 0.8 0.79 0.22	0.79 1.00 0.87 0.74 0.59 0.03	0.82 0.87 1.00 0.87 0.52 -0.05	0.80 0.74 0.87 1.00 0.54 0.05	0.79 0.59 0.52 0.54 1.00 0.22 -0.32	0.22 0.03 -0.05 0.05 0.22 1.00	-0.36 -0.36 -0.51 -0.57 -0.32 0.37	0.13 -0.09 -0.07 -0.04 0.16 0.22	(EScSG)  0.01  0.15  0.13  0.21  0.02  -0.07	-0.15 -0.09 -0.09 0.02 -0.19	0.23 0.34 0.28 0.31 0.16 0.17	-0.19 -0.08 -0.24 -0.20 -0.12 -0.15
IFIT27 IFIT44 ISG15 XAF1 SFRP4 Age	0.79 0.82 0.8 0.79 0.22 -0.36	0.79 1.00 0.87 0.74 0.59 0.03 -0.36	0.82 0.87 1.00 0.87 0.52 -0.05	0.80 0.74 0.87 1.00 0.54 0.05	0.79 0.59 0.52 0.54 1.00 0.22 -0.32	0.22 0.03 -0.05 0.05 0.22 1.00 0.37	-0.36 -0.36 -0.51 -0.57 -0.32 0.37	0.13 -0.09 -0.07 -0.04 0.16 0.22 0.34	(EScSG)  0.01  0.15  0.13  0.21  0.02  -0.07  -0.25	-0.15 -0.09 -0.09 0.02 -0.19 0.13 -0.02	0.23 0.34 0.28 0.31 0.16 0.17 -0.19	-0.19 -0.08 -0.24 -0.20 -0.12 -0.15 0.05
IFIT27 IFIT44 ISG15 XAF1 SFRP4 Age Duration	0.79 0.82 0.8 0.79 0.22 -0.36 0.13	0.79 1.00 0.87 0.74 0.59 0.03 -0.36	0.82 0.87 1.00 0.87 0.52 -0.05 -0.51	0.80 0.74 0.87 1.00 0.54 0.05 -0.57	0.79 0.59 0.52 0.54 1.00 0.22 -0.32 0.16	0.22 0.03 -0.05 0.05 0.22 1.00 0.37 0.22	-0.36 -0.36 -0.51 -0.57 -0.32 0.37 1.00	0.13 -0.09 -0.07 -0.04 0.16 0.22 0.34 1.00	(EScSG)  0.01  0.15  0.13  0.21  0.02  -0.07  -0.25  -0.01	-0.15 -0.09 -0.09 0.02 -0.19 0.13 -0.02 0.16	0.23 0.34 0.28 0.31 0.16 0.17 -0.19 -0.39	-0.19 -0.08 -0.24 -0.20 -0.12 -0.15 0.05 -0.34

signature analysis by RT-PCR with the proposed gene panel, as this biomaterial is more accessible, less invasive and more

reproducible; it also shows the informativeness potentially comparable with that of skin samples.

#### References

- Elhai M, Meune C, Avouac J, Kahan A, Allanore Y. Trends in mortality in patients with systemic sclerosis over 40 years: a systematic review and meta-analysis of cohort studies. Rheumatology (Oxford). 2012; 51 (6): 1017–26. DOI: 10.1093/rheumatology/ker269. PMID: 21900368.
- Rubio-Rivas M, Royo C, Simeón CP, Corbella X, Fonollosa V. Mortality and survival in systemic sclerosis: systematic review and meta-analysis. Semin Arthritis Rheum. 2014; 44 (2): 208–19. DOI: 10.1016/j.semarthrit.2014.05.010.
- Nikpour M, Baron M. Mortality in systemic sclerosis: lessons learned from population-based and observational cohort studies. Curr Opin Rheumatol. 2014; 26 (2): 131–7. DOI: 10.1097/BOR.0000000000000027.
- Elhai M, Meune C, Boubaya M, et al. EUSTAR group. Mapping and predicting mortality from systemic sclerosis. Ann Rheum Dis. 2017; 76 (11): 1897–905. DOI: 10.1136/annrheumdis-2017-211448.
- Rosa JE, Soriano ER, Narvaez-Ponce L, et al. Incidence and prevalence of systemic sclerosis in a healthcare plan in Buenos Aires. J Clin Rheumatol. 2011; 17 (2): 59–63. DOI: 10.1097/RHU.0b013e31820e7e8d.
- Furst DE, Fernandes AW, lorga SR, Greth W, Bancroft T. Epidemiology of systemic sclerosis in a large US managed care population. J Rheumatol. 2012; 39 (4): 784–6. DOI: 10.3899/jrheum.111106.
- 7. Horimoto AMC, Matos ENN, Costa MRD, et al. Incidence and prevalence of systemic sclerosis in Campo Grande, Brazil. Rev Bras Reumatol (Engl Ed). 2017; 57 (2): 107–14. DOI: 10.1016/j.rbre.2016.09.005.
- 8. Hoffmann-Vold AM, Midtvedt Ø, Molberg Ø, Garen T, Gran JT. Prevalence of systemic sclerosis in south-east Norway. Rheumatology

- (Oxford). 2012; 51 (9): 1600–5. DOI: 10.1093/rheumatology/kes076.
   Bajraktari IH, Berisha I, Berisha M, et al. Incidence, prevalence and clinical manifestations of systemic sclerosis in Dukagjini plain. Mater Sociomed. 2013; 25 (1): 14–18. DOI: 10.5455/msm.2013.25.14-18.
- El Adssi H, Cirstea D, Virion JM, Guillemin F, de Korwin JD. Estimating the prevalence of systemic sclerosis in Lorraine, France, by the capture-recapture method. Semin Arthritis Rheum. 2013; 42 (5): 530–38. DOI: 10.1016/j.semarthrit.2012.10.001.
- 11. Meier FM, Frommer KW, Dinser R, et al. EUSTAR Co-authors. Update on the profile of the EUSTAR cohort. Ann Rheum Dis. 2012; 71 (8): 1355–60. DOI: 10.1136/annrheumdis-2011-200742.
- Matucci-Cerinic M, Krieg T, Guillevin L, et al. Burden of recurrent and chronic digital ulcers in systemic sclerosis: long-term results from the DUO Registry. Ann Rheum Dis. 2016; 75 (10): 1770–6. DOI: 10.1136/annrheumdis-2015-208121.
- Tyndall AJ, Bannert B, Vonk M, et al. Causes and risk factors for death in systemic sclerosis: EUSTAR database study. Ann Rheum Dis. 2010; 69 (10): 1809–15. DOI: 10.1136/ard.2009.114264.
- Assassi S, Mayes MD, Arnett FC, et al. Systemic sclerosis and lupus: points in an interferon-mediated continuum. Arthritis Rheum. 2010; 62 (2): 589–98. DOI: 10.1002/art.27224.
- Gasparini G, Cozzani E, Parodi A. Interleukin-4 and interleukin-13 as possible therapeutic targets in systemic sclerosis. Cytokine. 2020; 125: 154799. DOI: 10.1016/j.cyto.2019.154799.
- Wei L, Abraham D, Ong V. The Yin and Yang of IL-17 in systemic sclerosis.
   Front Immunol. 2022; 13: 885609. DOI: 10.3389/fimmu.2022.885609.
- 17. Skaug B, Assassi S. Type I interferon dysregulation in systemic

## ORIGINAL RESEARCH I IMMUNOLOGY

18. Farutin V, Pradines JR, Cilfone NA, Ghavami A, Kurtagic E, Guess J, et al. Multiomic study of skin, peripheral blood, and serum: is serum

sclerosis, Cytokine, 2020; 132; 154635, DOI: 10.1016/j.cyto.2018.12.018.

- proteome a reflection of disease process at the end-organ level in systemic sclerosis? Arthritis Res Ther. 2021; 23 (1): 259. DOI: 10.1186/s13075-021-02633-5.
- Nasonov EL. Sovremennaya koncepciya autoimmuniteta v revmatologii. Nauchno-prakticheskaya revmatologiya. 2023; 61 (4): 397-420. DOI: 10.47360/1995-4484-2023-397-420. Russian.
- Paradowska-Gorycka A, Wajda A, Stypinska B, et al. Endosomal TLRs and interferons expression in SLE, SSc and MCTD. Clin Exp Immunol. 2021; 204 (1): 49-63. DOI: 10.1111/cei.13566.
- Yin H, Distler O, Shen L, et al. Endothelial response to type I interferon contributes to vasculopathy and fibrosis and predicts progression in systemic sclerosis. Arthritis Rheumatol. 2024; 76 (1): 78-91. DOI: 10.1002/art.42662. PMID: 37488975.
- 22. Tinazzi I, Mulipa P, Colato C, et al. SFRP4 expression is linked to immune-driven fibrotic conditions and correlates with skin and lung fibrosis in SSc. J Clin Med. 2021; 10 (24): 5820. DOI: 10.3390/jcm10245820.
- 23. Nasonov EL, Avdeeva AS. Immunovospalitel'nye revmaticheskie zabolevaniya, svyazannye s interferonom tipa I: novye dannye. Nauchno-prakticheskaya revmatologiya. 2019; 57 (4): 452-61.
- 24 Avdeeva AS, CHetina EV, CHerkasova MV, Markova GA, Artyuhov AS, Dashinimaev EB, et al. Ekspressiya interferon-stimulirovannyh genov (interferonovyj «avtograf») u pacientov s revmatoidnym artritom: predvaritel'nye rezul'taty. Nauchno-prakticheskaya revmatologiya. 2020; 58 (6): 673-7. Dostupno po ssylke: https://doi. org/10.47360/1995-4484-2020-673-677. Russian.
- Avdeeva AS, CHetina EV, Markova GA, Nasonov EL. Ekspressiya interferon-stimulirovannyh genov u pacientov s revmatoidnym artritom na fone anti-V-kletochnoj terapii (predvaritel'nye rezul'taty) Sovremennaya revmatologiya. 2021; 15 (5): 12-17. Russian.
- Avdeeva AS, Aleksankin AP, Chetina EV, Gorbunova YuN, Popkova TV, Markova GA, et al. Immunophenotypes of systemic lupus erythematosus — features of clinical and laboratory disorders. Doklady Biochemistry and Biophysics. 2025; 522 (1): 315-22
- Panafidina TA, Popkova TV, Gorbunova YuN, Kondrateva LV, CHetina EV, Avdeeva AS, et al. Klinicheskoe znachenie interferonovogo statusa u pacientov s sistemnoj krasnoj volchankoj. Nauchno-prakticheskaya revmatologiya. 2025; 63 (1): 95-103. Russian.
- Aliev DB, Gajdukova IZ. Interferon- $\alpha$  i osobennosti sistemnoj krasnoj volchanki u pacientov s yuvenil'nym i vzroslym nachalom zabolevaniya. RMZH. 2022; 6: 3-6. Russian.
- Avdeeva AS, CHetina EV, Gorbunova YuN, Panafidina TA, Popkova TV. Interferonovyj «avtograf» u pacientov s sistemnoj krasnoj volchankoj - vzaimosvyaz' s laboratornymi i klinicheskimi pokazatelyami. Klinicheskaya laboratornaya diagnostika. 2025; 70 (8): 530-5. Russian.
- Brkic Z, van Bon L, Cossu M, van Helden-Meeuwsen CG, Vonk MC, Knaapen H, et al. The interferon type I signature is present in

- systemic sclerosis before overt fibrosis and might contribute to its pathogenesis through high BAFF gene expression and high collagen synthesis. Ann Rheum Dis. 2016; 75 (8): 1567-73. DOI: 10.1136/annrheumdis-2015-207392.
- Kakkar V, Assassi S, Allanore Y, et al. Type 1 interferon activation in systemic sclerosis: a biomarker, a target or the culprit. Curr Opin Rheumatol. 2022; 34 (6): 357-64. DOI: 10.1097/BOR.0000000000000907.
- Mutovina Z, Golovina O, Zhurina T, Zagrebneva A, Shagina I, Myshkin M, et al. Increased type 1 interferon signature in systemic scleroderma patients suggests unexplored therapeutic options. International Journal of Rheumatic Diseases: Volume 27, Issue S3 Special Issue: APLAR 26th Asia-Pacific League of Associations for Rheumatology Congress, 21–25 August 2024.
- Del Galdo F, Lescoat A, Conaghan PG, et al. EULAR recommendations for the treatment of SSc: 2023 update. Ann Rheum Dis. 2025; 84 (1): 29-40. DOI: 10.1136/ard-2024-226430.
- Khanna D, Denton CP, Assassi S, et al. DAISY study design and rationale: anifrolumab in SSc (phase 3). Clin Exp Rheumatol. 2024; 42 (8): 1635-44. DOI: 10.55563/clinexprheumatol/s8qcyu.
- van den Hoogen F, et al. 2013 classification criteria for systemic sclerosis. Arthritis Rheum. 2013; 65 (11): 2737-47. DOI: 10.1002/art.38098.
- Valentini G, et al. EScSG preliminary activity criteria: construct validity. Ann Rheum Dis. 2003; 62: 901-03. DOI: 10.1136/ard.62.9.901.
- Bong D, et al. Brief guide to RT-qPCR. Molecules and Cells. 2024; 47 (12): 100141. DOI: 10.1016/j.mocell.2024.100141.
- Chudakov DM, Turchaninova MA, Britanova OV, Shagina IA, Mutovina ZYu, avtory. Diagnosticheskaya test-sistema dlya ocenki funkcional'nogo sostoyaniya sistemy interferona pri autoimmunnyh vospalitel'nyh zabolevaniyah. Patent 2845958 ot 28.08.2025 g. Dostupno po ssylke: https://fips.ru/EGD/22f31495-c376-4c27-9260-553d619511a9, Russian,
- Schneider WM, Chevillotte MD, Rice CM. Interferon-stimulated genes: a complex web of host defenses. Annu Rev Immunol. 2014; 32: 513-45. DOI: 10.1146/annurev-immunol-032713-120231.
- Lozhkov AA, Plotnikova MA, Egorova MA, Baranovskaya IL, Elpaeva EA, Klotchenko SA, et al. Simultaneous Detection of RIG-1, MDA5, and IFIT-1 Expression Is a Convenient Tool for Evaluation of the Interferon-Mediated Response. Viruses. 2022; 14 (10): 2090. DOI: 10.3390/v14102090.
- 41. Egorova MA, Plotnikova MA, Lozhkov AA, Vlasov PK, Vasin AV, avtory. Mnogoparametricheskaya testovaya sistema dlya kolichestvennogo opredele niya mRNK genov RIG-1, IFIT-1, IFIH-1 metodom OT-PCR v real'nom vremeni. Patent RU2782428C1. 09.03.2023. Dostupno po ssylke: https://patents.google.com/ patent/RU2782428C1/ru. Russian.
- Higgs BW, Liu Z, White B, Zhu W, White WI, Morehouse C, et al. Patients with systemic lupus erythematosus, myositis, rheumatoid arthritis and scleroderma share activation of a common type I interferon pathway. Ann Rheum Dis. 2011; 70 (11): 2029-36. DOI: 10.1136/ard.2011.150326.
- 43. Morand EF, et al. Efficacy of anifrolumab across organ domains in SLE (TULIP-1/2). Lancet Rheumatol. 2022; 4 (4): e282-e292. DOI: 10.1016/S2665-9913(21)00317-9.

#### Литература

- Elhai M, Meune C, Avouac J, Kahan A, Allanore Y. Trends in mortality in patients with systemic sclerosis over 40 years: a systematic review and meta-analysis of cohort studies. Rheumatology (Oxford). 2012; 51 (6): 1017-26. DOI: 10.1093/rheumatology/ker269. PMID: 21900368.
- Rubio-Rivas M, Royo C, Simeón CP, Corbella X, Fonollosa V. Mortality and survival in systemic sclerosis: systematic review and meta-analysis. Semin Arthritis Rheum. 2014; 44 (2): 208-19. DOI: 10.1016/j.semarthrit.2014.05.010.
- Nikpour M, Baron M. Mortality in systemic sclerosis: lessons learned from population-based and observational cohort studies. Curr Opin Rheumatol. 2014; 26 (2): 131-7. DOI: 10.1097/BOR.0000000000000027.
- Elhai M, Meune C, Boubaya M, et al. EUSTAR group. Mapping and predicting mortality from systemic sclerosis. Ann Rheum Dis. 2017;

- 76 (11): 1897-905. DOI: 10.1136/annrheumdis-2017-211448.
- Rosa JE, Soriano ER, Narvaez-Ponce L, et al. Incidence and prevalence of systemic sclerosis in a healthcare plan in Buenos Aires. J Clin Rheumatol. 2011; 17 (2): 59-63. DOI: 10.1097/RHU.0b013e31820e7e8d.
- Furst DE, Fernandes AW, lorga SR, Greth W, Bancroft T. Epidemiology of systemic sclerosis in a large US managed care population. J Rheumatol. 2012; 39 (4): 784-6. DOI: 10.3899/jrheum.111106.
- Horimoto AMC, Matos ENN, Costa MRD, et al. Incidence and prevalence of systemic sclerosis in Campo Grande, Brazil. Rev Bras Reumatol (Engl Ed). 2017; 57 (2): 107-14. DOI: 10.1016/j.rbre.2016.09.005.
- Hoffmann-Vold AM, Midtvedt Ø, Molberg Ø, Garen T, Gran JT. Prevalence of systemic sclerosis in south-east Norway. Rheumatology (Oxford). 2012; 51 (9): 1600-5. DOI: 10.1093/rheumatology/kes076.

### ОРИГИНАЛЬНОЕ ИССЛЕДОВАНИЕ І ИММУНОЛОГИЯ

- Bajraktari IH, Berisha I, Berisha M, et al. Incidence, prevalence and clinical manifestations of systemic sclerosis in Dukagjini plain. Mater Sociomed. 2013; 25 (1): 14–18. DOI: 10.5455/msm.2013.25.14-18.
- El Adssi H, Cirstea D, Virion JM, Guillemin F, de Korwin JD. Estimating the prevalence of systemic sclerosis in Lorraine, France, by the capture-recapture method. Semin Arthritis Rheum. 2013; 42 (5): 530–38. DOI: 10.1016/j.semarthrit.2012.10.001.
- Meier FM, Frommer KW, Dinser R, et al. EUSTAR Co-authors. Update on the profile of the EUSTAR cohort. Ann Rheum Dis. 2012; 71 (8): 1355–60. DOI: 10.1136/annrheumdis-2011-200742.
- Matucci-Cerinic M, Krieg T, Guillevin L, et al. Burden of recurrent and chronic digital ulcers in systemic sclerosis: long-term results from the DUO Registry. Ann Rheum Dis. 2016; 75 (10): 1770–6. DOI: 10.1136/annrheumdis-2015-208121.
- Tyndall AJ, Bannert B, Vonk M, et al. Causes and risk factors for death in systemic sclerosis: EUSTAR database study. Ann Rheum Dis. 2010; 69 (10): 1809–15. DOI: 10.1136/ard.2009.114264.
- Assassi S, Mayes MD, Arnett FC, et al. Systemic sclerosis and lupus: points in an interferon-mediated continuum. Arthritis Rheum. 2010; 62 (2): 589–98. DOI: 10.1002/art.27224.
- Gasparini G, Cozzani E, Parodi A. Interleukin-4 and interleukin-13 as possible therapeutic targets in systemic sclerosis. Cytokine. 2020; 125: 154799. DOI: 10.1016/j.cyto.2019.154799.
- Wei L, Abraham D, Ong V. The Yin and Yang of IL-17 in systemic sclerosis.
   Front Immunol. 2022; 13: 885609. DOI: 10.3389/fimmu.2022.885609.
- Skaug B, Assassi S. Type I interferon dysregulation in systemic sclerosis. Cytokine. 2020; 132: 154635. DOI: 10.1016/j.cyto.2018.12.018.
- Farutin V, Pradines JR, Cilfone NA, Ghavami A, Kurtagic E, Guess J, et al. Multiomic study of skin, peripheral blood, and serum: is serum proteome a reflection of disease process at the end-organ level in systemic sclerosis? Arthritis Res Ther. 2021; 23 (1): 259. DOI: 10.1186/s13075-021-02633-5.
- Насонов Е. Л. Современная концепция аутоиммунитета в ревматологии. Научно-практическая ревматология. 2023; 61 (4): 397–420. DOI: 10.47360/1995-4484-2023-397-420.
- Paradowska-Gorycka A, Wajda A, Stypinska B, et al. Endosomal TLRs and interferons expression in SLE, SSc and MCTD. Clin Exp Immunol. 2021; 204 (1): 49–63. DOI: 10.1111/cei.13566.
- Yin H, Distler O, Shen L, et al. Endothelial response to type I interferon contributes to vasculopathy and fibrosis and predicts progression in systemic sclerosis. Arthritis Rheumatol. 2024; 76 (1): 78–91. DOI: 10.1002/art.42662. PMID: 37488975.
- Tinazzi I, Mulipa P, Colato C, et al. SFRP4 expression is linked to immune-driven fibrotic conditions and correlates with skin and lung fibrosis in SSc. J Clin Med. 2021; 10 (24): 5820. DOI: 10.3390/jcm10245820.
- 23. Насонов Е. Л., Авдеева А. С. Иммуновоспалительные ревматические заболевания, связанные с интерфероном типа I: новые данные. Научно-практическая ревматология. 2019; 57 (4): 452–61
- Авдеева А. С., Четина Е. В., Черкасова М. В., Маркова Г. А., Артюхов А. С., Дашинимаев Э. Б., и др. Экспрессия интерферонстимулированных генов (интерфероновый «автограф») у пациентов с ревматоидным артритом: предварительные результаты. Научно-практическая ревматология. 2020; 58 (6): 673–7. Доступно по ссылке: https://doi.org/10.47360/1995-4484-2020-673-677.
- 25. Авдеева А. С., Четина Е. В., Маркова Г. А., Насонов Е. Л. Экспрессия интерферон-стимулированных генов у пациентов с ревматоидным артритом на фоне анти-В-клеточной терапии (предварительные результаты). Современная ревматология. 2021; 15 (5): 12–17.
- Avdeeva AS, Aleksankin AP, Chetina EV, Gorbunova YuN, Popkova TV, Markova GA, et al. Immunophenotypes of systemic lupus erythematosus — features of clinical and laboratory disorders. Doklady Biochemistry and Biophysics. 2025; 522 (1): 315–22.
- 27. Панафидина Т. А., Попкова Т. В., Горбунова Ю. Н., Кондратьева Л. В.,

- Четина Е. В., Авдеева А. С., и др. Клиническое значение интерферонового статуса у пациентов с системной красной волчанкой. Научно-практическая ревматология. 2025; 63 (1): 95–103.
- Алиев Д. Б., Гайдукова И. З. Интерферон-α и особенности системной красной волчанки у пациентов с ювенильным и взрослым началом заболевания. РМЖ. 2022; 6: 3–6.
- Авдеева А. С., Четина Е. В., Горбунова Ю. Н., Панафидина Т. А., Попкова Т. В. Интерфероновый «автограф» у пациентов с системной красной волчанкой — взаимосвязь с лабораторными и клиническими показателями. Клиническая лабораторная диагностика. 2025; 70 (8): 530–5.
- Brkic Z, van Bon L, Cossu M, van Helden-Meeuwsen CG, Vonk MC, Knaapen H, et al. The interferon type I signature is present in systemic sclerosis before overt fibrosis and might contribute to its pathogenesis through high BAFF gene expression and high collagen synthesis. Ann Rheum Dis. 2016; 75 (8): 1567–73. DOI: 10.1136/annrheumdis-2015-207392.
- Kakkar V, Assassi S, Allanore Y, et al. Type 1 interferon activation in systemic sclerosis: a biomarker, a target or the culprit. Curr Opin Rheumatol. 2022; 34 (6): 357–64. DOI: 10.1097/BOR.00000000000000907.
- 32. Mutovina Z, Golovina O, Zhurina T, Zagrebneva A, Shagina I, Myshkin M, et al. Increased type 1 interferon signature in systemic scleroderma patients suggests unexplored therapeutic options. International Journal of Rheumatic Diseases: Volume 27, Issue S3 Special Issue: APLAR 26th Asia–Pacific League of Associations for Rheumatology Congress, 21–25 August 2024.
- Del Galdo F, Lescoat A, Conaghan PG, et al. EULAR recommendations for the treatment of SSc: 2023 update. Ann Rheum Dis. 2025; 84 (1): 29–40. DOI: 10.1136/ard-2024-226430.
- Khanna D, Denton CP, Assassi S, et al. DAISY study design and rationale: anifrolumab in SSc (phase 3). Clin Exp Rheumatol. 2024; 42 (8): 1635–44. DOI: 10.55563/clinexprheumatol/s8qcyu.
- van den Hoogen F, et al. 2013 classification criteria for systemic sclerosis. Arthritis Rheum. 2013; 65 (11): 2737–47. DOI: 10.1002/art.38098.
- 36. Valentini G, et al. EScSG preliminary activity criteria: construct validity. Ann Rheum Dis. 2003; 62: 901–03. DOI: 10.1136/ard.62.9.901.
- 37. Bong D, et al. Brief guide to RT-qPCR. Molecules and Cells. 2024; 47 (12): 100141. DOI: 10.1016/j.mocell.2024.100141.
- Чудаков Д. М, Турчанинова М. А., Британова О. В., Шагина И. А, Мутовина З. Ю., авторы. Диагностическая тест-система для оценки функционального состояния системы интерферона при аутоиммунных воспалительных заболеваниях. Патент 2845958 от 28.08.2025 г. Доступно по ссылке: https://fips.ru/EGD/22f31495-c376-4c27-9260-553d619511a9.
- 39. Schneider WM, Chevillotte MD, Rice CM. Interferon-stimulated genes: a complex web of host defenses. Annu Rev Immunol. 2014; 32: 513–45. DOI: 10.1146/annurev-immunol-032713-120231.
- Lozhkov AA, Plotnikova MA, Egorova MA, Baranovskaya IL, Elpaeva EA, Klotchenko SA, et al. Simultaneous Detection of RIG-1, MDA5, and IFIT-1 Expression Is a Convenient Tool for Evaluation of the Interferon-Mediated Response. Viruses. 2022; 14 (10): 2090. DOI: 10.3390/v14102090.
- 41. Егорова М. А., Плотникова М. А., Ложков А. А., Власов П. К., Васин А. В., авторы. Многопараметрическая тестовая система для количественного определения мРНК генов RIG-1, IFIT-1, IFIH-1 методом ОТ-ПЦР в реальном времени. Патент RU2782428C1. 09.03.2023. Доступно по ссылке: https://patents.google.com/patent/RU2782428C1/ru.
- 42. Higgs BW, Liu Z, White B, Zhu W, White WI, Morehouse C, et al. Patients with systemic lupus erythematosus, myositis, rheumatoid arthritis and scleroderma share activation of a common type I interferon pathway. Ann Rheum Dis. 2011; 70 (11): 2029–36. DOI: 10.1136/ard.2011.150326.
- 43. Morand EF, et al. Efficacy of anifrolumab across organ domains in SLE (TULIP-1/2). Lancet Rheumatol. 2022; 4 (4): e282–e292. DOI: 10.1016/S2665-9913(21)00317-9.

# ALTERATIONS IN MITOCHONDRIAL AND LYSOSOMAL COMPARTMENTS UNDER CHEMOTHERAPY-INDUCED SENESCENCE

Shatalova RO, Shevyrev DV ™

Translational Medicine Research Center, Sirius University of Science and Technology, Sirius Federal Territory, Krasnodar Krai, Russia

Cellular senescence is associated with the accumulation of senescent cells characterized by functional alterations, telomere shortening, cell cycle arrest, resistance to apoptosis, and metabolic dysregulation. In recent years, senescence has been extensively investigated not only in the context of aging but also in relation to cancer therapy, as senescence induction in various tumor cell types may differentially influence disease progression. The aim of this study was to comparatively evaluate commonly used chemotherapeutic agents with respect to their ability to induce senescence and their effects on mitochondrial and lysosomal compartments in primary dermal fibroblasts isolated from C57BL/6 mice. Cellular senescence was assessed using both chromogenic and fluorescent assays for β-galactosidase (β-Gal) activity. Mitochondria were labeled with the potential-sensitive dye MitoTracker® Orange, and lysosomes were stained with LysoTracker® Red. Flow cytometry analysis was performed using a BD LSRFortessa cytometer. Our results revealed a significant decrease in mitochondrial membrane potential and an increase in lysosomal fluorescence intensity in cells undergoing chemotherapy-induced senescence. Using an integrative senescence induction index developed in our laboratory, we demonstrated that doxorubicin exerts a more pronounced effect on senescence induction and on mitochondrial and lysosomal compartments compared to cisplatin, bleomycin, and etoposide.

Keywords: senescence, β-galactosidase, SA-β-Gal, mitochondria, lysosomes, doxorubicin, cisplatin, bleomycin, etoposide

Funding: This work was supported by Russian Science Foundation, Project No. 24-15-20003 (https://rscf.ru/project/24-15-20003/ accessed September 3, 2025).

Author contribution: Shatalova RO — optimization of cell culture conditions, cell staining; Shevyrev DV — manuscript preparation, flow cytometry experiments, cytometry data processing, statistical analysis, conceptualization.

Compliance with ethical standards: The study was approved by the Ethics Committee of Sirius University (Protocol No. 7.1, April 12, 2024) and conducted in accordance with the principles of the Declaration of Helsinki.

Correspondence should be addressed: Daniil V. Shevyrev

1 Olimpiyskiy Avenue, Sochi, 354349, Russia; Email: dr.daniil25@mail.ru; shevyrev.dv@talantiuspeh.ru

Received: 06.09.2025 Accepted: 06.10.2025 Published online: 19.10.2025

DOI: 10.24075/brsmu.2025.045

Copyright: © 2025 by the authors. Licensee: Pirogov University. This article is an open access article distributed under the terms and conditions of the Creative Commons Attribution (CC BY) license (https://creativecommons.org/licenses/by/4.0/).

## ИЗМЕНЕНИЯ МИТОХОНДРИАЛЬНОГО И ЛИЗОСОМНОГО КОМПАРТМЕНТОВ В УСЛОВИЯХ ХИМИОИНДУЦИРОВАННОЙ СЕНЕСЦЕНТНОСТИ

Р. О. Шаталова, Д. В. Шевырев ⊠

Научный центр трансляционной медицины, Научно-технологический университет «Сириус», Федеральная территория «Сириус», Краснодарский край, Россия

Старение связано с накоплением сенесцентных клеток, для которых характерно изменение функций, укорочение теломер, остановка клеточного цикла, устойчивость к апоптозу и метаболические нарушения. В последние годы широко изучают различные аспекты сенесцентности не только в контексте старения, но и в отношении терапии опухолей, так как сенесцентность в различных клетках опухоли может по-разному влиять на ход патологического процесса. Целью исследования было провести сравнительный анализ распространенных химиотерапевтических препаратов в контексте индукции сенесцентности и влияния на митохондриальный и лизосомный компартменты фибробластов, выделенных из кожи мышей линии С57BL/6. Сенесцентность клеток оценивали с помощью хромогенного и флуоресцентного методов определения активности фермента β-Gal. Окрашивание митохондрий проводили с использованием потенциалзависимого красителя MitoTracker® Orange, лизосомы окрашивали с помощью LysoTracker® Red. Для анализа использовали проточный цитометр BD LSRFortessa. В результате было выявлено значительное снижение митохондриального потенциала и усиление интенсивности флуоресценции лизосом в клетках с химиоиндуцированной сенесцентностью. Использование разработанного нами интегрального индекса индукции сенесцентности позволило установить, что влияние доксорубицина с точки зрения индукции сенесцентности и влияния на митохондриальный и лизосомный компартменты выражено сильнее, чем у цисплатина, блеомицина и этопозида.

Ключевые слова: сенесцентность, β-галактозидаза, SA-β-Gal, митохондрии, лизосомы, доксорубицин, цисплатин, блеомицин, этопозид

Финансирование: данная работа выполнена при поддержке Российского Научного Фонда, проект № 24-15-20003 https://rscf.ru/project/24-15-20003/ (дата доступа 03 сентября 2025 г.).

**Вклад авторов:** Р. О. Шаталова — отработка условий культивирования, окрашивание клеток; Д. В. Шевырев — оформление рукописи, проведение проточной цитометрии, обработка данных цитометрии, статистическая обработка данных, концептуализация.

Соблюдение этических стандартов: исследование одобрено этическим комитетом университета «Сириус» (протокол заседания № 7.1 от 12 апреля 2024 г.), проведено в соответствии с требованиями Хельсинкской декларации.

**Для корреспонденции:** Даниил Вадимович Шевырев

Олимпийский проспект, д. 1, г. Сочи, 354349, Россия; dr.daniil25@mail.ru; shevyrev.dv@talantiuspeh.ru

Статья получена: 06.09.2025 Статья принята к печати: 06.10.2025 Опубликована онлайн: 19.10.2025

DOI: 10.24075/vrgmu.2025.045

Авторские права: © 2025 принадлежат авторам. **Лицензиат:** PHИМУ им. Н. И. Пирогова. Статья размещена в открытом доступе и распространяется на условиях лицензии Creative Commons Attribution (CC BY) (https://creativecommons.org/licenses/by/4.0/).

## ОРИГИНАЛЬНОЕ ИССЛЕДОВАНИЕ І ГЕРОНТОЛОГИЯ

In recent years, interest in the study of cellular aging and senescence has markedly increased. The age-related accumulation of senescent cells impairs tissue homeostasis and, at the systemic level, contributes to chronic low-grade inflammation due to the secretion of a range of pro-inflammatory factors collectively known as the senescence-associated secretory phenotype (SASP) [1, 2]. In the context of oncogenesis, the role of senescence is dual: while it can halt tumor growth, it may simultaneously promote tumor cell survival and create a microenvironment conducive to metastasis [3, 4]. For instance, senescent tumor-associated fibroblasts generate a pro-inflammatory, angiogenic, and metabolically active niche that supports tumor survival and progression [5, 6]. Entry into senescence can be triggered by diverse stressors — ranging from replicative exhaustion to exposure to adverse physical, chemical, or biological agents that induce various disruptions in the cellular molecular machinery [7]. Metabolic alterations in senescent cells are closely linked to mitochondrial dysfunction, a shift toward anaerobic glycolysis, and impaired autophagy [8, 9]. Specifically, downregulation of genes involved in mitochondrial fission (e.g., FIS1, DRP1, MFF) coupled with upregulation of fusion genes (MFN1, MFN2) disrupts mitochondrial dynamics in senescent cells [10, 11]. This results in mitochondrial mass expansion and the formation of an elongated, tubular mitochondrial network, which overall enhances resistance to oxidative stress via the PINK1-mediated pathway [12]. Such morphological changes are sometimes interpreted as an adaptive response to cellular stress. Notably, during the early stages of senescence, when mitochondrial aerobic activity is still preserved, the increased mitochondrial mass may lead to excessive production of reactive oxygen species (ROS). Consequently, this mitochondrial remodeling itself exacerbates cellular stress and contributes to the development of the pro-inflammatory SASP [13]. Progressive mitochondrial dysfunction is further characterized by diminished oxidative phosphorylation and a metabolic shift toward anaerobic glycolysis. This is reflected in a decline in mitochondrial membrane potential, reduced ATP production, and elevated ROS generation [14]. Excess ROS combined with ATP deficiency impairs the activity of vacuolar ATPase (v-ATPase), leading to lysosomal alkalinization and consequent dysfunction of acid hydrolases (e.g., proteases, lipases, nucleases) [15, 16]. As a result, autophagic efficiency declines, causing the accumulation of damaged proteins and organelles — including mitochondria — which further intensifies cellular stress [17]. Stress-induced activation of the PI3K/Akt pathway, autocrine signaling by SASP factors, and the buildup of damaged proteins converge to activate mTOR, which in turn suppresses TFEB — the master transcriptional regulator of lysosomal biogenesis and regeneration [18]. This suppression impairs autophagosome content degradation, leading to the accumulation of dysfunctional, alkalinized lysosomes that lose their degradative capacity and instead function primarily as storage compartments [15, 19]. Hypertrophy of the lysosomal compartment is accompanied by a compensatory increase in  $\beta$ -galactosidase activity, which becomes detectable at a suboptimal pH near 6.0 - hence termed senescence-associated β-galactosidase (SA-β-Gal) [20]. This enzymatic activity serves as a widely used biomarker for identifying senescent cells [21].

Currently, various models — both *in vivo* and *in vitro* — are employed to study cellular senescence. The aim of this study was to perform a comparative analysis of commonly used chemotherapeutic agents — doxorubicin, cisplatin, bleomycin, and etoposide — with respect to their capacity to induce senescence in primary mouse dermal fibroblast cultures. Additionally, we sought to characterize concomitant alterations

in the mitochondrial and lysosomal compartments, as these organelles reflect critical aspects of the cell's metabolic and functional status and play a pivotal role in the establishment and maintenance of the senescent phenotype.

#### **METHODS**

Primary dermal fibroblasts isolated from male C57BL/6 mice aged 4 and 19 months were used in this study. Animals were housed in a vivarium under a 12-hour light-dark cycle and provided ad libitum access to water and standard balanced laboratory chow. Euthanasia was performed in accordance with the principles of humane care for laboratory animals: under deep isoflurane-induced anesthesia followed by cervical dislocation. Biological samples were collected immediately after euthanasia. Cells derived from both young (4-month-old) and aged (19-month-old) mice were included in the analysis. However, preliminary experiments revealed no significant differences between fibroblasts from mice of different ages when compared at the same passage number; therefore, data from both age groups were pooled for subsequent analyses.

#### Isolation of Dermal Fibroblasts

The dorsal skin was shaved using an animal trimmer, followed by disinfection with 70% ethanol for 2 minutes, allowing the alcohol to fully evaporate. A 2 × 2 cm skin fragment was aseptically excised using sterile scissors and immediately transferred into ice-cold phosphate-buffered saline (PBS) supplemented with 1% penicillin-streptomycin and 0.1% chlorhexidine for 5 minutes. The tissue was then rinsed with sterile PBS and placed in a Petri dish containing cold PBS. Using sterile instruments, subcutaneous adipose tissue was carefully removed. The dermal tissue was minced into fragments of approximately 1 mm<sup>2</sup>. Enzymatic dissociation was performed in DMEM/F12 medium (PanEco, Russia) containing 0.2% collagenase IV (Gibco, USA) at 37 °C for 3 hours with periodic gentle agitation. Following incubation, enzymatic activity was neutralized by adding 100% fetal bovine serum (FBS; Capricorn Scientific, Germany) to a final concentration of 20%. The resulting cell suspension was filtered through a 40-µm cell strainer and centrifuged at 300g for 5 minutes. The pellet was gently resuspended and seeded into six-well tissue culture plates (Fudan Biotech, China) in DMEM/F12 medium supplemented with 10% FBS and 1% penicillin-streptomycin. Cells were maintained at 37 °C in a humidified atmosphere containing 5% CO<sub>2</sub> and subcultured upon reaching 85% confluence.

## Assessment of SA-β-Gal Activity

Senescence-associated  $\beta$ -galactosidase (SA- $\beta$ -Gal) activity was evaluated using the chromogenic substrate 5-bromo-4-chloro-3-indolyl- $\beta$ -D-galactopyranoside (X-Gal), which yields an intense blue precipitate upon enzymatic hydrolysis. Although  $\beta$ -galactosidase is constitutively present in lysosomes of most cell types and exhibits optimal activity at pH ~4.2, SA- $\beta$ -Gal activity in senescent cells is detectable at a suboptimal pH of ~6.0 due to lysosomal hypertrophy and increased enzyme expression. To selectively identify senescent cells, staining was therefore performed at pH 6.0. Cells were washed with PBS and fixed with 0.2% glutaraldehyde for 10 minutes at room temperature, followed by three PBS washes. Staining was carried out in a solution containing: 2 mM citrate—phosphate buffer (pH 6.0), 50 mM potassium ferricyanide [K $_{\circ}$ Fe(CN) $_{\circ}$ ],

50 mM potassium ferrocyanide [K $_4$ Fe(CN) $_e$ ], 5 mM NaCl, 1 mM MgCl $_2$ , and 20 mg/mL X-Gal (dissolved in DMSO; SibEnzyme, Russia). After addition of the staining solution, plates were incubated at 37 °C in ambient air for 20–24 hours. Cells were then washed twice with PBS and visualized using an AxioScope 5 light microscope (Carl Zeiss, Germany). The percentage of SA- $\beta$ -Gal-positive (blue-stained) cells was determined manually by counting at least three microscopic fields from three independent wells per experimental condition.

For live-cell assessment of SA- $\beta$ -Gal activity, the vital fluorescent probe SPiDER- $\beta$ Gal (Cellular Senescence Detection Kit, Dojindo Laboratories, Japan) was employed. Fibroblasts cultured in 24-well plates (NEST Biotechnology, China) were incubated for 1 hour at 37 °C in a CO $_2$  incubator with 1 mL of complete medium supplemented with bafilomycin A1 (final concentration as per manufacturer's instructions), which alkalinizes lysosomes by inhibiting vacuolar ATPase and thereby enhances probe retention and signal specificity. Subsequently, SPiDER- $\beta$ Gal was added to a final concentration of 1  $\mu$ M, and cells were incubated under the same conditions for an additional hour. Excess probe was removed by PBS washes, and cells were detached using 0.25% trypsin–EDTA. Fluorescence intensity was quantified by flow cytometry using a BD LSRFortessa instrument (BD Biosciences, USA).

#### **Induction of Senescence**

To induce senescence, we used chemotherapeutic agents commonly employed in the treatment of malignant diseases: doxorubicin, cisplatin, bleomycin, and etoposide. Doxorubicin is an anthracycline antitumor antibiotic whose mechanism of action involves intercalation between DNA strands and inhibition of topoisomerase II, leading to replication arrest. In addition, doxorubicin enhances the production of quinonetype free radicals and displaces histones from transcriptionally active chromatin [22]. Overall, its action results in DNA damage as well as transcriptomic and epigenetic disturbances. Cells are most sensitive to this drug during the S and G2 phases of the cell cycle [22]. Cisplatin is an alkylating cytotoxic agent that induces intra- and interstrand DNA crosslinks, thereby disrupting replication and transcription. Cisplatin causes cell cycle arrest at the G1, S, or G2 phase [23]. Bleomycin is an antitumor glycopeptide antibiotic that induces DNA strand breaks, presumably through the generation of free radicals. It blocks the cell cycle at the early G2 phase [24]. Etoposide is an antitumor agent that binds to topoisomerase II and inhibits its activity, preventing the resealing of DNA strand breaks normally introduced by topoisomerase II to relax DNA supercoils. Etoposide acts predominantly during the G2 and S phases of the cell cycle [25]. In general, these drugs induce genotoxic stress — one of the primary triggers of senescence.

Based on published data, a range of concentrations was selected for each inducer: 250, 350, and 450 nM for doxorubicin; 5, 10, and 20 μM for cisplatin; 10, 14, and 25 μM for bleomycin; and 5, 10, and 20 μM for etoposide. At medium and high concentrations, all inducers exhibited pronounced cytotoxic effects, resulting in the death of the majority of cells within the first 3–4 days of culture — conditions inconsistent with the aims of the study. Cell viability was assessed using an EVOS<sup>TM</sup> M5000 laser scanning microscope (Thermo Fisher Scientific, USA) with acridine orange (AO), which visualizes all nucleated cells, and propidium iodide (PI), which stains dead cells. At low doses, the cytotoxic effect was less pronounced; most cells survived and acquired morphological and biochemical features characteristic of senescence, as confirmed by X-Gal staining.

Ultimately, the lowest tested concentration for each inducer that maintained cell viability above 95% on day 7 was selected for further experiments. Fibroblasts were seeded into 24-well plates in DMEM/F12 medium (PanEco, Russia) supplemented with 10% FBS (Capricorn Scientific, Germany), 2 mM L-glutamine, and 1% penicillin-streptomycin (PanEco, Russia), and incubated at 37 °C in 5% CO<sub>a</sub> until they reached 60-70% confluence. The medium was then replaced with DMEM/F12 containing 1% FBS, and the inducers were added at the following final concentrations: 250 nM doxorubicin, 5 µM cisplatin, 10 µM bleomycin, and 5 µM etoposide. Cells were incubated under standard conditions for 24 hours, after which they were thoroughly washed and maintained for an additional 6 days in DMEM/F12 with 1% FBS, 2 mM L-glutamine, and 1% penicillin-streptomycin, with medium refreshed every three days. Control groups included cultures maintained in 10% FBS and in 1% FBS without any inducer. Subsequently, cells were processed for X-Gal staining, SPiDER-&Gal labeling, and staining with MitoTracker® and LysoTracker® dyes.

## Mitochondrial and Lysosomal Staining

Mitochondria were stained in 24-well plates (NEST Biotechnology, China) using the potential-sensitive fluorescent dye MitoTracker® Orange CMTMRos (Invitrogen, USA) at a final concentration of 0.4  $\mu \rm M$  in DMEM/F12 medium supplemented with 1% FBS. Cells were incubated with the dye for 30 minutes at 37 °C in a 5% CO $_2$  atmosphere. MitoTracker Orange readily diffuses across the plasma membranes of live cells and selectively accumulates in active mitochondria in a membrane potential–dependent manner.

Lysosomes were stained under identical conditions using the acidotropic fluorescent probe LysoTracker® Red DND-99 (Invitrogen, USA) at a concentration of 50 nM. In neutral extracellular environments, LysoTracker Red freely crosses cellular membranes. Upon entering acidic compartments such as lysosomes, its weakly basic moiety becomes protonated, which prevents its diffusion back across the lysosomal membrane. This leads to selective retention and bright fluorescent labeling of acidic organelles.

Following staining, cells were detached using 0.25% trypsin-EDTA and immediately subjected to flow cytometry analysis.

## Statistical Analysis

Flow cytometry data were processed using BD FACSDiva software (v9.0) and FlowJo (v10.8.1). At least 500 events per sample were analyzed, with an average of 2,500 events per sample. Statistical analyses were performed using GraphPad Prism 9.3.1. Normality of data distribution was assessed using the Shapiro-Wilk and Kolmogorov-Smirnov tests. For normally distributed data, results are presented as mean  $\pm$  standard deviation (Mean  $\pm$  SD); for non-normally distributed data, results are reported as median with interquartile range (Me  $\pm$  IQR). Multiple group comparisons were carried out using one-way analysis of variance (ANOVA), followed by Sidak's post hoc test for pairwise comparisons.

To comparatively evaluate the overall impact of the chemotherapeutic agents, we employed an integrative senescence induction index (IISI), which provides a composite assessment of the senescent phenotype by combining SA- $\beta$ -Gal activity with concomitant alterations in mitochondrial and lysosomal parameters.

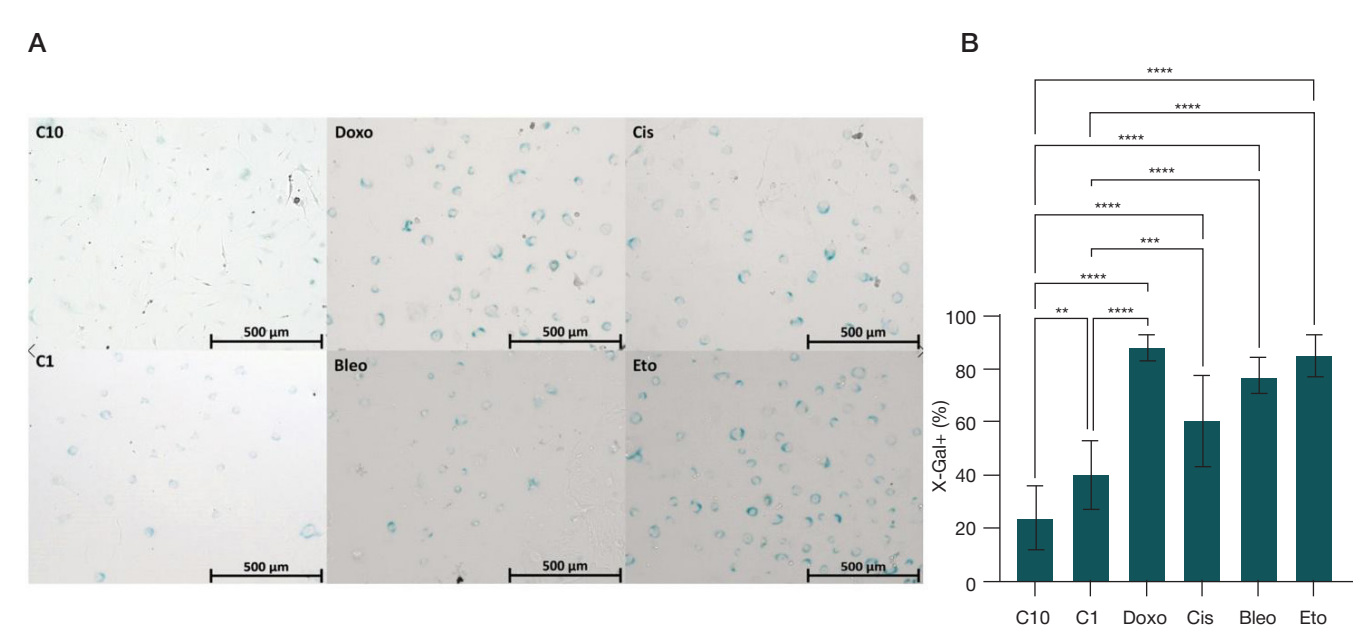


Fig. 1. A. Representative images of X-Gal chromogenic staining under different culture conditions. C10 — culture in 10% FBS; C1 — culture in 1% FBS; Doxo — doxorubicin; Cis — cisplatin; Bleo — bleomycin; Eto — etoposide. B. Comparative analysis of the proportion of SA-β-Gal-positive cells across experimental conditions (one-way ANOVA with Sidak's post hoc test; data pooled from nine microscopic fields across three independent wells per condition; Mean  $\pm$  SD; \*\* —  $\rho$  < 0.01, \*\*\* —  $\rho$  < 0.005, \*\*\* —  $\rho$  < 0.001)

#### **RESULTS**

Analysis of senescence induction in primary mouse dermal fibroblasts using the chromogenic substrate X-Gal revealed that all four tested agents – doxorubicin, cisplatin, bleomycin, and etoposide – significantly increased the proportion of senescent cells compared to the control group (Fig. 1).

Characteristic blue staining was predominantly localized in the perinuclear cytoplasm of fibroblasts and was uniformly observed across all inducer-treated groups (Fig. 1A). Notably, serum starvation alone also led to an increase in the proportion of SA- $\beta$ -Gal-positive cells (39  $\pm$  12%) compared to standard culture conditions with 10% FBS (23  $\pm$  11%). Nevertheless, in all groups treated with senescence-inducing agents, the fraction of SA- $\beta$ -Gal-positive cells was markedly higher, ranging from 60% to 87%. The highest level was observed with doxorubicin treatment, reaching 87.8  $\pm$  4.5% (Fig. 1B).

At the next stage, senescence induction was assessed in live cells using the fluorogenic substrate SPiDER- $\beta$ Gal and flow cytometry. The gating threshold for SA- $\beta$ -Gal-positive cells was established based on a negative control treated with bafilomycin A1 but without the addition of the SPiDER probe. The results obtained were consistent with those from X-Gal staining, and the distribution patterns of SA- $\beta$ -Gal-positive cells under the different inducers were highly comparable between the two independent detection methods (Fig. 2A, B).

Assessment of the mitochondrial compartment revealed intriguing alterations (Fig. 2C, D). Fluorescence intensity in the MitoTracker detection channel (561–585/15 nm) was relatively high under standard culture conditions (10% FBS), but unexpectedly increased further under serum starvation (1% FBS). In contrast, treatment with senescence-inducing agents led to a significant and expected decrease in fluorescence intensity, reflecting a loss of mitochondrial membrane potential. This reduction was most pronounced in cells treated with doxorubicin.

Alterations were also observed in the lysosomal compartment. Under normal culture conditions (10% FBS) and serum starvation (1% FBS), fluorescence intensity in the LysoTracker detection channel (561–610/20 nm) remained comparable.

However, upon treatment with senescence-inducing agents, a significant increase in lysosomal fluorescence was detected, indicating lysosomal hypertrophy. The most pronounced effects were observed with doxorubicin and etoposide (Fig. 2D, E).

To simultaneously evaluate the impact of each inducer across all three key parameters — the proportion of SA- $\beta$ -Gal-positive cells, the reduction in mitochondrial membrane potential, and the degree of lysosomal hypertrophy — we developed an Integrative Index of Senescence Induction (IISI):

$$IISI = \frac{\%SPiDER_{i}^{+}}{\%SPiDER_{C1}^{+}} \times \left(\frac{MFI_{c10}mito}{MFI_{mito}} + \frac{MFI_{lyso}}{MFI_{C10}lyso}\right)_{i}$$

where %SPiDER<sub>,+</sub> and %SPiDER<sub>C1</sub>+ represent the percentage of SA-β-Gal–positive cells under a specific senescence inducer and under serum starvation (1% FBS), respectively; MFI<sub>c10</sub> mito and MFImito denote the median fluorescence intensity (MFI) of MitoTracker in the control condition with 10% FBS and under senescence induction, respectively; MFI|yso and MFI<sub>C10</sub>|yso denote the MFI of LysoTracker under senescence induction and in the 10% FBS control, respectively.

The application of the IISI enabled us to determine that, under our experimental conditions, doxorubicin exerted the strongest overall effect across all three parameters compared to the other tested inducers (Fig. 3).

Thus, we performed a comparative analysis of alterations in the mitochondrial and lysosomal compartments in primary mouse fibroblasts in the context of chemotherapy-induced senescence, demonstrating that doxorubicin exerted the most pronounced effect among the tested agents. Nevertheless, it should be noted that the Integrative Index of Senescence Induction (IISI) serves as a tool for relative comparison within the framework of this study, and its absolute numerical value is not intended for standalone interpretation.

#### DISCUSSION

In the present study, using two independent senescence detection methods — chromogenic X-Gal staining and the fluorogenic substrate SPiDER — we confirmed that

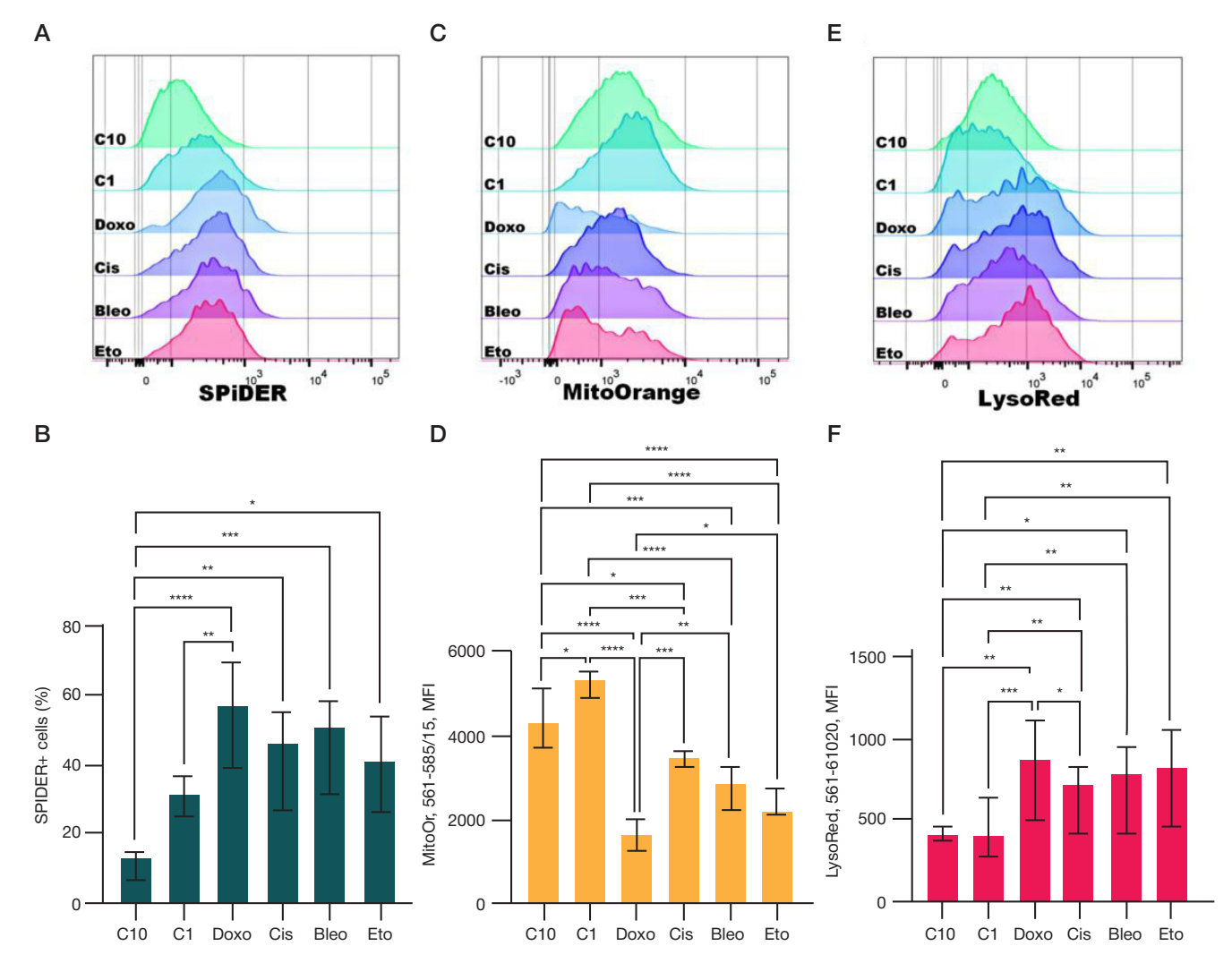


Fig. 2. The upper row shows representative histograms of SA-β-Gal–positive cells detected with SPiDER (A), mitochondrial staining with MitoTracker Orange (C), and lysosomal labeling with LysoTracker Red (E). Histograms correspond to control conditions (C10 — culture in 10% FBS; C1 — culture in 1% FBS) and treatment with senescence inducers (Doxo — doxorubicin; Cis — cisplatin; Bleo — bleomycin; Eto — etoposide). Each histogram represents pooled data from four biological replicates per condition — two independent fibroblast isolations (from two individual mice), each analyzed in duplicate. Overall, the histograms illustrate an increase in the proportion of SA-β-Gal–positive cells, a reduction in mitochondrial membrane potential, and lysosomal hypertrophy in response to senescence-inducing agents, consistent with the results of statistical analysis. The lower row presents the corresponding quantitative analyses: percentage of SA-β-Gal–positive cells assessed by SPiDER fluorescence (B); mitochondrial activity based on MitoTracker Orange signal intensity (D); and lysosomal compartment size evaluated via LysoTracker Red fluorescence (F). For each staining and experimental condition, the total sample size was n = 12 (six independent replicates per mouse, with fibroblasts derived from two mice). Replicates were processed on different days. Data are shown as median ± interquartile range (Me ± IQR); \* -p < 0.0.05, \*\*\* -p < 0.0.01, \*\*\*\* -p < 0.0.01, \*\*\*\*

doxorubicin, cisplatin, bleomycin, and etoposide significantly increase the proportion of SA- $\beta$ -Gal-positive cells, indicative of chemotherapy-induced senescence [26]. The most pronounced effect was observed with doxorubicin, which markedly elevated the fraction of X-Gal-positive cells (87.8  $\pm$  4.5%) and demonstrated the highest activity in the integrative assessment based on our newly developed Integrative Index of Senescence Induction (IISI).

Interestingly, serum starvation alone also led to an increase in SA- $\beta$ -Gal-positive cells. This observation aligns with the notion that reduced mitogenic stimulation and proliferative activity can elicit phenotypic features of aging even in the absence of exogenous damaging agents [27]. This effect is likely attributable to the depletion of antioxidant systems normally present in serum — such as albumin, glutathione, ascorbic acid, and tocopherols [28]. Under prolonged serum-free conditions, the antioxidant capacity of the medium diminishes, while basal mitochondrial respiration continues to generate reactive oxygen species (ROS) that cannot be effectively neutralized. This accumulation of ROS may induce genotoxic

stress and trigger the transition into a senescent state [28, 29]. Notably, serum starvation also resulted in a significant increase in fluorescence signal from the potential-sensitive mitochondrial dye MitoTracker Orange. This likely reflects an adaptive response to metabolic stress (due to reduced insulin levels in low-serum medium) through enhanced aerobic glycolysis [30, 31]. However, when senescence inducers were applied under the same low-serum conditions, a marked decrease in MitoTracker Orange signal was observed — especially with doxorubicin. This reduction is likely driven primarily by loss of mitochondrial membrane potential ( $\Delta \Psi m$ ), which outweighs any potential increase in mitochondrial mass. Such a state is characteristic of stable senescence, where a large pool of dysfunctional mitochondria fails to sustain adequate ATP production, forcing the cell to rely on anaerobic glycolysis for energy [32, 33]. This metabolic shift is associated with the secretion of metabolic intermediates — such as lactate, pyruvate, and alanine — into the extracellular environment, which neighboring tumor cells can exploit as alternative energy sources [34].

## ОРИГИНАЛЬНОЕ ИССЛЕДОВАНИЕ І ГЕРОНТОЛОГИЯ

Serum starvation in vitro, like other forms of metabolic stress and energy deficit, activates the transcription factor EB (TFEB) via AMPK activation and mTORC1 inhibition [35, 36]. TFEB activation promotes cellular adaptation by upregulating autophagy and lysosomal biogenesis, thereby recycling cellular components to supply energy and essential building blocks and maintain viability [37]. In our experiments, serum starvation did not significantly enhance LysoTracker Red signal, possibly due to efficient lysosomal turnover and biogenesis under these conditions [38, 39]. In contrast, all chemotherapeutic inducers caused a substantial increase in LysoTracker Red fluorescence, most likely reflecting significant lysosomal hypertrophy that outweighs any potential signal reduction due to lysosomal alkalinization (which would otherwise decrease accumulation of the acidotropic LysoTracker probe). Lysosomal enlargement is a hallmark of senescent cells, thought to compensate for impaired lysosomal function [40]. The strongest effect was again observed with doxorubicin. Together with the elevated proportion of SA-β-Gal-positive cells, this supports the concept that lysosomal accumulation is not merely a bystander phenomenon but a functional feature of the senescent state, reflecting the exhaustion of cellular adaptive reserves [41].

Doxorubicin exhibited the most robust effect across all evaluated parameters, surpassing the other agents. This is likely due to its multifaceted mechanism of action: DNA intercalation, topoisomerase II inhibition, ROS generation, and direct damage to mitochondrial DNA [22]. Consequently, doxorubicin emerged as the most potent senescence inducer in primary mouse dermal fibroblast cultures and demonstrated the most pronounced mitochondrial toxicity.

Modern oncology increasingly confronts the dual nature of many chemotherapeutic agents [42, 43]. While effectively halting tumor growth, these drugs may simultaneously initiate processes that promote recurrence, metastasis, and adverse side effects [44-46]. At the heart of this paradox appears to be the balance between direct cytotoxicity toward tumor cells and the induction of senescence — both within the tumor and in surrounding normal tissues [6, 45]. On one hand, therapyinduced senescence in the tumor microenvironment can support tumor cell survival by providing nutrients, promoting angiogenesis, and facilitating metastatic spread [5, 6]. On the other hand, senescence enforces a durable cell cycle arrest, and SASP-derived inflammatory factors can recruit immune cells, thereby enhancing immune-surveillance and potentially promoting clearance of senescent tumor cells [47-49]. Therefore, future in vitro and in vivo studies are needed to comprehensively evaluate not only the cytotoxic potential of anticancer agents but also their senogenic (senescence-inducing) and immunogenic profiles. Such integrated assessments will be crucial for optimizing therapeutic strategies that maximize tumor suppression while minimizing pro-tumorigenic and systemic side effects associated with therapy-induced senescence.

## CONCLUSIONS

In this study, we demonstrated that all tested chemotherapeutic agents — doxorubicin, cisplatin, bleomycin, and etoposide — effectively induce senescence in primary dermal fibroblasts isolated from C57BL/6 mice. This was confirmed by a significant increase in the proportion of SA-β-Gal–positive cells, consistently observed using both chromogenic X-Gal staining

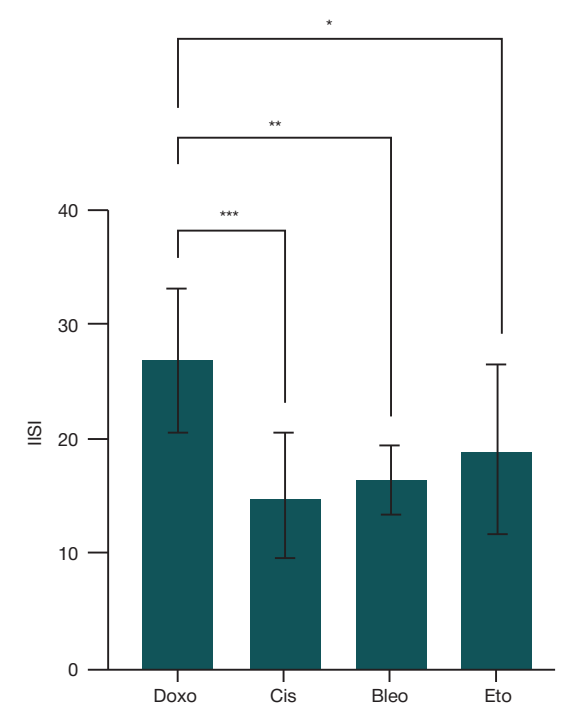


**Fig. 3.** Comparative analysis of the Integrative Index of Senescence Induction (IISI), which reflects the cumulative effect of each inducer across the three evaluated parameters: SA- $\beta$ -Gal positivity, mitochondrial membrane potential loss, and lysosomal hypertrophy. Doxo — doxorubicin; Cis — cisplatin; Bleo — bleomycin; Eto — etoposide. Data are presented as Mean  $\pm$  SD, n=8; \* — p<0.05, \*\* — p<0.01, \*\*\* — p<0.005

and the live-cell fluorogenic probe SPiDER-BGal. The most pronounced effect was elicited by doxorubicin, which induced a senescent phenotype in 87.5% of cells (as assessed by X-Gal staining). Serum starvation also increased the fraction of cells exhibiting senescence-like features, albeit to a considerably lesser extent than the pharmacological inducers. Concurrently with SA-β-Gal activation, we observed two hallmark features of the senescent state: a reduction in mitochondrial membrane potential and lysosomal hypertrophy. These alterations were most prominent following treatment with doxorubicin and etoposide. To enable a comprehensive comparison of the senescence-inducing efficacy of the tested compounds, we developed an Integrative Index of Senescence Induction (IISI), which combines three key parameters: the proportion of senescent cells, mitochondrial status, and lysosomal compartment integrity. According to this index, doxorubicin exhibited the strongest overall capacity to induce senescence across all evaluated metrics. These findings highlight substantial differences among commonly used chemotherapeutic agents in their ability to drive cellular senescence and identify doxorubicin as the most potent inducer in this experimental model.

Given that the tested agents elicited distinct senescence-associated phenotypes in fibroblasts, further investigation into their immunogenic profiles is warranted. Indeed, the immunomodulatory properties of chemotherapeutics — particularly their capacity to shape the tumor microenvironment via SASP-mediated immune cell recruitment or suppression — may be as therapeutically relevant as their direct cytotoxic effects. Understanding these nuances is essential for the rational design of immunologically informed cancer treatment strategies that balance tumor control with the mitigation of therapy-induced senescence—related complications.

#### References

- Aquino-Martinez R, Eckhardt BA, Rowsey JL, Fraser DG, Khosla S, Farr JN, Monroe DG. Senescent cells exacerbate chronic inflammation and contribute to periodontal disease progression in old mice. J Periodontol. 2021; 92 (10): 1483–95. DOI: 10.1002/JPER.20-0529. Epub 2021 Jan 6. PMID: 33341947; PMCID: PMC8281492.
- Tripathi U, Misra A, Tchkonia T, Kirkland JL. Impact of Senescent Cell Subtypes on Tissue Dysfunction and Repair: Importance and Research Questions. Mech Ageing Dev. 2021; 198: 111548. DOI: 10.1016/j.mad.2021.111548. Epub 2021 Aug 2. PMID: 34352325; PMCID: PMC8373827.
- Schosserer M, Grillari J, Breitenbach M. The Dual Role of Cellular Senescence in Developing Tumors and Their Response to Cancer Therapy. Front Oncol. 2017; 7: 278. DOI: 10.3389/fonc.2017.00278. PMID: 29218300; PMCID: PMC5703792.
- Ma L, Yu J, Fu Y, He X, Ge S, Jia R, et al. The dual role of cellular senescence in human tumor progression and therapy. MedComm (2020). 2024; 5 (9): e695. DOI: 10.1002/mco2.695. PMID: 39161800; PMCID: PMC11331035.
- Coppé JP, Kauser K, Campisi J, Beauséjour CM. Secretion of vascular endothelial growth factor by primary human fibroblasts at senescence. J Biol Chem. 2006; 281 (40): 29568–74. DOI: 10.1074/jbc.M603307200. Epub 2006 Jul 31. PMID: 16880208.
- Luo J, Sun T, Liu Z, Liu Y, Liu J, Wang S, et al. Persistent accumulation of therapy-induced senescent cells: an obstacle to long-term cancer treatment efficacy. Int J Oral Sci. 2025; 17 (1): 59. DOI: 10.1038/s41368-025-00380-w. PMID: 40750580; PMCID: PMC12317027.
- Kumari R, Jat P. Mechanisms of Cellular Senescence: Cell Cycle Arrest and Senescence Associated Secretory Phenotype. Front Cell Dev Biol. 2021; 9: 645593. DOI: 10.3389/fcell.2021.645593. PMID: 33855023; PMCID: PMC8039141.
- Sabbatinelli J, Prattichizzo F, Olivieri F, Procopio AD, Rippo MR, Giuliani A. Where Metabolism Meets Senescence: Focus on Endothelial Cells. Front Physiol. 2019; 10: 1523. DOI: 10.3389/fphys.2019.01523. PMID: 31920721; PMCID: PMC6930181.
- Aman Y, Schmauck-Medina T, Hansen M, Morimoto RI, Simon AK, Bjedov I, Palikaras K, Simonsen A, Johansen T, Tavernarakis N, Rubinsztein DC, Partridge L, Kroemer G, Labbadia J, Fang EF. Autophagy in healthy aging and disease. Nat Aging. 2021; 1 (8): 634–50. DOI: 10.1038/s43587-021-00098-4. Epub 2021 Aug 12. PMID: 34901876; PMCID: PMC8659158.
- Panfilova A, Zubareva T, Mironova E, Mazzoccoli G, Marasco MGP, Balazovskaia S, et al. Mitochondrial proteins as biomarkers of cellular senescence and age-associated diseases. Aging (Albany NY). 2025; 17. DOI: 10.18632/aging.206305. Epub ahead of print. PMID: 40856658.
- Chen W, Zhao H, Li Y. Mitochondrial dynamics in health and disease: mechanisms and potential targets. Signal Transduct Target Ther. 2023; 8 (1): 333. DOI: 10.1038/s41392-023-01547-9. PMID: 37669960; PMCID: PMC10480456.
- Murata H, Takamatsu H, Liu S, Kataoka K, Huh NH, Sakaguchi M. NRF2 Regulates PINK1 Expression under Oxidative Stress Conditions. PLoS One. 2015; 10 (11): e0142438. DOI: 10.1371/journal.pone.0142438. PMID: 26555609; PMCID: PMC4640816.
- Zlotorynski E. Defective mitochondria ignite the SASP. Nat Rev Mol Cell Biol. 2020; 21 (4): 179. DOI: 10.1038/s41580-020-0228-x. PMID: 32076133.
- Suski JM, Lebiedzinska M, Bonora M, Pinton P, Duszynski J, Wieckowski MR. Relation between mitochondrial membrane potential and ROS formation. Methods Mol Biol. 2012; 810: 183– 205. DOI: 10.1007/978-1-61779-382-0\_12. PMID: 22057568.
- Li W, Kawaguchi K, Tanaka S, He C, Maeshima Y, Suzuki E, Toi M. Cellular senescence triggers intracellular acidification and lysosomal pH alkalinized via ATP6AP2 attenuation in breast cancer cells. Commun Biol. 2023; 6 (1): 1147. DOI: 10.1038/s42003-023-05433-6. PMID: 37993606; PMCID: PMC10665353.
- Song Q, Meng B, Xu H, Mao Z. The emerging roles of vacuolar-type ATPase-dependent Lysosomal acidification in neurodegenerative diseases. Transl Neurodegener. 2020; 9 (1): 17. DOI:

- 10.1186/s40035-020-00196-0. PMID: 32393395; PMCID: PMC7212675.
- Chung CY, Shin HR, Berdan CA, Ford B, Ward CC, Olzmann JA, et al. Covalent targeting of the vacuolar H+-ATPase activates autophagy via mTORC1 inhibition. Nat Chem Biol. 2019; 15 (8): 776–85. DOI: 10.1038/s41589-019-0308-4. Epub 2019 Jul 8. PMID: 31285595; PMCID: PMC6641988.
- Omolekan TO, Chamcheu JC, Buerger C, Huang S. Pl3K/ AKT/mTOR Signaling Network in Human Health and Diseases. Cells. 2024; 13 (17): 1500. DOI: 10.3390/cells13171500. PMID: 39273070; PMCID: PMC11394329.
- Loo TM, Zhou X, Tanaka Y, Sugawara S, Yamauchi S, Kawasaki H, et al. Senescence-associated lysosomal dysfunction impairs cystine deprivation-induced lipid peroxidation and ferroptosis. Nat Commun. 2025; 16 (1): 6617. DOI: 10.1038/s41467-025-61894-9. PMID: 40731111; PMCID: PMC12307602.
- Kurz DJ, Decary S, Hong Y, Erusalimsky JD. Senescenceassociated (beta)-galactosidase reflects an increase in lysosomal mass during replicative ageing of human endothelial cells. J Cell Sci. 2000; 113 (Pt 20): 3613–22. DOI: 10.1242/jcs.113.20.3613. PMID: 11017877.
- Dimri GP, Lee X, Basile G, Acosta M, Scott G, Roskelley C, et al. A biomarker that identifies senescent human cells in culture and in aging skin in vivo. Proc Natl Acad Sci U S A. 1995; 92 (20): 9363–7. DOI: 10.1073/pnas.92.20.9363. PMID: 7568133; PMCID: PMC40985.
- Kciuk M, Gielecińska A, Mujwar S, Kołat D, Kałuzińska-Kołat Ż, Celik I, et al. Doxorubicin-An Agent with Multiple Mechanisms of Anticancer Activity. Cells. 2023; 12 (4): 659. DOI: 10.3390/cells12040659. PMID: 36831326; PMCID: PMC9954613.
- Dasari S, Tchounwou PB. Cisplatin in cancer therapy: molecular mechanisms of action. Eur J Pharmacol. 2014; 740: 364–78.
   DOI: 10.1016/j.ejphar.2014.07.025. Epub 2014 Jul 21. PMID: 25058905; PMCID: PMC4146684.
- Dorr RT. Bleomycin pharmacology: mechanism of action and resistance, and clinical pharmacokinetics. Semin Oncol. 1992; 19 (2 Suppl 5): 3–8. PMID: 1384141.
- Montecucco A, Zanetta F, Biamonti G. Molecular mechanisms of etoposide. EXCLI J. 2015; 14: 95–108. DOI: 10.17179/excli2015-561. PMID: 26600742; PMCID: PMC4652635.
- Lubberts S, Meijer C, Demaria M, Gietema JA. Early ageing after cytotoxic treatment for testicular cancer and cellular senescence: Time to act. Crit Rev Oncol Hematol. 2020; 151: 102963. DOI: 10.1016/j.critrevonc.2020.102963. Epub 2020 May 7. PMID: 32446180.
- Wiley CD, Campisi J. The metabolic roots of senescence: mechanisms and opportunities for intervention. Nat Metab. 2021;
   (10): 1290–301. DOI: 10.1038/s42255-021-00483-8. Epub 2021 Oct 18. PMID: 34663974; PMCID: PMC8889622.
- 28. Zhang Y, Xu YY, Sun WJ, Zhang MH, Zheng YF, Shen HM, et al. FBS or BSA Inhibits EGCG Induced Cell Death through Covalent Binding and the Reduction of Intracellular ROS Production. Biomed Res Int. 2016; 2016: 5013409. DOI: 10.1155/2016/5013409. Epub 2016 Oct 18. PMID: 27830147; PMCID: PMC5088332.
- Stival A, Silva A, Valadares M. Qualitative and quantitative evaluation of Fetal Bovine Serum composition: toward ethical and best quality in vitro science. NAM Journal. 2025. doi. org/10.1016/j.namjnl.2025.100047.
- Liu Y, Birsoy K. Metabolic sensing and control in mitochondria. Mol Cell. 2023; 83 (6): 877–89. DOI: 10.1016/j.molcel.2023.02.016. PMID: 36931256; PMCID: PMC10332353.
- 31. Choi EJ, Oh HT, Lee SH, Zhang CS, Li M, Kim SY, et al. Metabolic stress induces a double-positive feedback loop between AMPK and SQSTM1/p62 conferring dual activation of AMPK and NFE2L2/NRF2 to synergize antioxidant defense. Autophagy. 2024; 20 (11): 2490–510. DOI: 10.1080/15548627.2024.2374692. Epub 2024 Jul 10. PMID: 38953310; PMCID: PMC11572134.
- Fumagalli M, Rossiello F, Mondello C, d'Adda di Fagagna F. Stable cellular senescence is associated with persistent DDR activation. PLoS One. 2014; 9 (10): e110969. DOI: 10.1371/journal.pone.0110969. PMID: 25340529; PMCID: PMC4207795.

## ОРИГИНАЛЬНОЕ ИССЛЕДОВАНИЕ І ГЕРОНТОЛОГИЯ

- Ajoolabady A, Pratico D, Bahijri S, Eldakhakhny B, Tuomilehto J, Wu F, et al. Hallmarks and mechanisms of cellular senescence in aging and disease. Cell Death Discov. 2025; 11 (1): 364. DOI: 10.1038/s41420-025-02655-x. PMID: 40759632; PMCID: PMC12322153.
- 34. Dou X, Fu Q, Long Q, Liu S, Zou Y, Fu D, et al. PDK4-dependent hypercatabolism and lactate production of senescent cells promotes cancer malignancy. Nat Metab. 2023; 5 (11): 1887–910. DOI: 10.1038/s42255-023-00912-w. Epub 2023 Oct 30. Erratum in: Nat Metab. 2024; 6 (5): 980. DOI: 10.1038/s42255-024-01054-3. Erratum in: Nat Metab. 2024; 6 (7): 1416. DOI: 10.1038/s42255-024-01069-w. PMID: 37903887; PMCID: PMC10663165.
- Hardie DG, Ross FA, Hawley SA. AMPK: a nutrient and energy sensor that maintains energy homeostasis. Nat Rev Mol Cell Biol. 2012; 13 (4): 251–62. DOI: 10.1038/nrm3311. PMID: 22436748; PMCID: PMC5726489.
- Zhang S, Sheng H, Zhang X, Qi Q, Chan CB, Li L, et al. Cellular energy stress induces AMPK-mediated regulation of glioblastoma cell proliferation by PIKE-A phosphorylation. Cell Death Dis. 2019; 10 (3): 222. DOI: 10.1038/s41419-019-1452-1. Erratum in: Cell Death Dis. 2025; 16 (1): 447. DOI: 10.1038/s41419-025-07700-2. PMID: 30833542; PMCID: PMC6399291.
- 37. Shang L, Chen S, Du F, Li S, Zhao L, Wang X. Nutrient starvation elicits an acute autophagic response mediated by Ulk1 dephosphorylation and its subsequent dissociation from AMPK. Proc Natl Acad Sci U S A. 2011; 108 (12): 4788–93. DOI: 10.1073/pnas.1100844108. Epub 2011 Mar 7. PMID: 21383122; PMCID: PMC3064373.
- Lee C, Lamech L, Johns E, Overholtzer M. Selective Lysosome Membrane Turnover Is Induced by Nutrient Starvation. Dev Cell. 2020; 55 (3): 289–97.e4. DOI: 10.1016/j.devcel.2020.08.008. Epub 2020 Sep 10. PMID: 32916093; PMCID: PMC8337093.
- Ebner M, Puchkov D, López-Ortega O, Muthukottiappan P, Su Y, Schmied C, et al. Nutrient-regulated control of lysosome function by signaling lipid conversion. Cell. 2023; 186 (24): 5328–46.e26. DOI: 10.1016/j.cell.2023.09.027. Epub 2023 Oct 25. Erratum in: Cell. 2025; 188 (9): 2560. DOI: 10.1016/j.cell.2025.04.009. PMID: 37883971
- Hwang ES, Yoon G, Kang HT. A comparative analysis of the cell biology of senescence and aging. Cell Mol Life Sci. 2009; 66 (15): 2503–24. DOI: 10.1007/s00018-009-0034-2. Epub 2009 May 7. PMID: 19421842; PMCID: PMC11115533.

- Tan JX, Finkel T. Lysosomes in senescence and aging. EMBO Rep. 2023; 24 (11): e57265. DOI: 10.15252/embr.202357265. Epub 2023 Oct 9. PMID: 37811693; PMCID: PMC10626421.
- D'Alterio C, Scala S, Sozzi G, Roz L, Bertolini G. Paradoxical effects of chemotherapy on tumor relapse and metastasis promotion. Semin Cancer Biol. 2020; 60: 351–61. DOI: 10.1016/j.semcancer.2019.08.019. Epub 2019 Aug 24. PMID: 31454672.
- 43. Behranvand N, Nasri F, Zolfaghari Emameh R, Khani P, Hosseini A, Garssen J, Falak R. Chemotherapy: a double-edged sword in cancer treatment. Cancer Immunol Immunother. 2022; 71 (3): 507–26. DOI: 10.1007/s00262-021-03013-3. Epub 2021 Aug 5. Erratum in: Cancer Immunol Immunother. 2022; 71 (3): 527. DOI: 10.1007/s00262-021-03034-y. PMID: 34355266; PMCID: PMC10992618.
- 44. Middleton JD, Stover DG, Hai T. Chemotherapy-Exacerbated Breast Cancer Metastasis: A Paradox Explainable by Dysregulated Adaptive-Response. Int J Mol Sci. 2018; 19 (11): 3333. DOI: 10.3390/ijms19113333. PMID: 30373101; PMCID: PMC6274941.
- 45. Hwang HJ, Kang D, Shin J, Jung J, Ko S, Jung KH, et al. Therapy-induced senescent cancer cells contribute to cancer progression by promoting ribophorin 1-dependent PD-L1 upregulation. Nat Commun. 2025; 16 (1): 353. DOI: 10.1038/s41467-024-54132-1. PMID: 39753537; PMCID: PMC11699195.
- Guillon J, Petit C, Toutain B, Guette C, Lelièvre E, Coqueret O. Chemotherapy-induced senescence, an adaptive mechanism driving resistance and tumor heterogeneity. Cell Cycle. 2019; 18 (19): 2385–97. DOI: 10.1080/15384101.2019.1652047. Epub 2019 Aug 9. PMID: 31397193; PMCID: PMC6738909.
- 47. Jiao D, Zheng X, Du X, Wang D, Hu Z, Sun R, et al. Immunogenic senescence sensitizes lung cancer to LUNX-targeting therapy. Cancer Immunol Immunother. 2022; 71 (6): 1403–17. DOI: 10.1007/s00262-021-03077-1. Epub 2021 Oct 21. PMID: 34674012; PMCID: PMC9123058.
- Liu Y, Lomeli I, Kron SJ. Therapy-Induced Cellular Senescence: Potentiating Tumor Elimination or Driving Cancer Resistance and Recurrence? Cells. 2024; 13 (15): 1281. DOI: 10.3390/cells13151281. PMID: 39120312; PMCID: PMC11312217.
- Marin I, Boix O, Garcia-Garijo A, Sirois I, Caballe A, Zarzuela E, et al. Cellular Senescence Is Immunogenic and Promotes Antitumor Immunity. Cancer Discov. 2023; 13 (2): 410–31. DOI: 10.1158/2159-8290.CD-22-0523. PMID: 36302218; PMCID: PMC7614152.

## Литература

- Aquino-Martinez R, Eckhardt BA, Rowsey JL, Fraser DG, Khosla S, Farr JN, Monroe DG. Senescent cells exacerbate chronic inflammation and contribute to periodontal disease progression in old mice. J Periodontol. 2021; 92 (10): 1483–95. DOI: 10.1002/JPER.20-0529. Epub 2021 Jan 6. PMID: 33341947; PMCID: PMC8281492.
- Tripathi U, Misra A, Tchkonia T, Kirkland JL. Impact of Senescent Cell Subtypes on Tissue Dysfunction and Repair: Importance and Research Questions. Mech Ageing Dev. 2021; 198: 111548. DOI: 10.1016/j.mad.2021.111548. Epub 2021 Aug 2. PMID: 34352325; PMCID: PMC8373827.
- Schosserer M, Grillari J, Breitenbach M. The Dual Role of Cellular Senescence in Developing Tumors and Their Response to Cancer Therapy. Front Oncol. 2017; 7: 278. DOI: 10.3389/fonc.2017.00278. PMID: 29218300; PMCID: PMC5703792.
- Ma L, Yu J, Fu Y, He X, Ge S, Jia R, et al. The dual role of cellular senescence in human tumor progression and therapy. MedComm (2020). 2024; 5 (9): e695. DOI: 10.1002/mco2.695. PMID: 39161800; PMCID: PMC11331035.
- Coppé JP, Kauser K, Campisi J, Beauséjour CM. Secretion of vascular endothelial growth factor by primary human fibroblasts at senescence. J Biol Chem. 2006; 281 (40): 29568–74. DOI: 10.1074/jbc.M603307200. Epub 2006 Jul 31. PMID: 16880208.
- Luo J, Sun T, Liu Z, Liu Y, Liu J, Wang S, et al. Persistent accumulation of therapy-induced senescent cells: an obstacle to long-term cancer treatment efficacy. Int J Oral Sci. 2025; 17 (1): 59. DOI: 10.1038/s41368-025-00380-w. PMID: 40750580;

- PMCID: PMC12317027.
- Kumari R, Jat P. Mechanisms of Cellular Senescence: Cell Cycle Arrest and Senescence Associated Secretory Phenotype. Front Cell Dev Biol. 2021; 9: 645593. DOI: 10.3389/fcell.2021.645593. PMID: 33855023; PMCID: PMC8039141.
- Sabbatinelli J, Prattichizzo F, Olivieri F, Procopio AD, Rippo MR, Giuliani A. Where Metabolism Meets Senescence: Focus on Endothelial Cells. Front Physiol. 2019; 10: 1523. DOI: 10.3389/fphys.2019.01523. PMID: 31920721; PMCID: PMC6930181.
- Aman Y, Schmauck-Medina T, Hansen M, Morimoto RI, Simon AK, Bjedov I, Palikaras K, Simonsen A, Johansen T, Tavernarakis N, Rubinsztein DC, Partridge L, Kroemer G, Labbadia J, Fang EF. Autophagy in healthy aging and disease. Nat Aging. 2021; 1 (8): 634–50. DOI: 10.1038/s43587-021-00098-4. Epub 2021 Aug 12. PMID: 34901876; PMCID: PMC8659158.
- Panfilova A, Zubareva T, Mironova E, Mazzoccoli G, Marasco MGP, Balazovskaia S, et al. Mitochondrial proteins as biomarkers of cellular senescence and age-associated diseases. Aging (Albany NY). 2025; 17. DOI: 10.18632/aging.206305. Epub ahead of print. PMID: 40856658.
- Chen W, Zhao H, Li Y. Mitochondrial dynamics in health and disease: mechanisms and potential targets. Signal Transduct Target Ther. 2023; 8 (1): 333. DOI: 10.1038/s41392-023-01547-9. PMID: 37669960; PMCID: PMC10480456.
- Murata H, Takamatsu H, Liu S, Kataoka K, Huh NH, Sakaguchi M. NRF2 Regulates PINK1 Expression under Oxidative Stress Conditions. PLoS One. 2015; 10 (11): e0142438. DOI:

### ORIGINAL RESEARCH I GERONTOLOGY

- 10.1371/journal.pone.0142438. PMID: 26555609; PMCID: PMC4640816.
- Zlotorynski E. Defective mitochondria ignite the SASP. Nat Rev Mol Cell Biol. 2020; 21 (4): 179. DOI: 10.1038/s41580-020-0228-x. PMID: 32076133.
- Suski JM, Lebiedzinska M, Bonora M, Pinton P, Duszynski J, Wieckowski MR. Relation between mitochondrial membrane potential and ROS formation. Methods Mol Biol. 2012; 810: 183– 205. DOI: 10.1007/978-1-61779-382-0\_12. PMID: 22057568.
- Li W, Kawaguchi K, Tanaka S, He C, Maeshima Y, Suzuki E, Toi M. Cellular senescence triggers intracellular acidification and lysosomal pH alkalinized via ATP6AP2 attenuation in breast cancer cells. Commun Biol. 2023; 6 (1): 1147. DOI: 10.1038/s42003-023-05433-6. PMID: 37993606; PMCID: PMC10665353.
- Song Q, Meng B, Xu H, Mao Z. The emerging roles of vacuolar-type ATPase-dependent Lysosomal acidification in neurodegenerative diseases. Transl Neurodegener. 2020; 9 (1): 17. DOI: 10.1186/s40035-020-00196-0. PMID: 32393395; PMCID: PMC7212675.
- Chung CY, Shin HR, Berdan CA, Ford B, Ward CC, Olzmann JA, et al. Covalent targeting of the vacuolar H+-ATPase activates autophagy via mTORC1 inhibition. Nat Chem Biol. 2019; 15 (8): 776–85. DOI: 10.1038/s41589-019-0308-4. Epub 2019 Jul 8. PMID: 31285595; PMCID: PMC6641988.
- Omolekan TO, Chamcheu JC, Buerger C, Huang S. PI3K/ AKT/mTOR Signaling Network in Human Health and Diseases. Cells. 2024; 13 (17): 1500. DOI: 10.3390/cells13171500. PMID: 39273070; PMCID: PMC11394329.
- Loo TM, Zhou X, Tanaka Y, Sugawara S, Yamauchi S, Kawasaki H, et al. Senescence-associated lysosomal dysfunction impairs cystine deprivation-induced lipid peroxidation and ferroptosis. Nat Commun. 2025; 16 (1): 6617. DOI: 10.1038/s41467-025-61894-9. PMID: 40731111; PMCID: PMC12307602.
- Kurz DJ, Decary S, Hong Y, Erusalimsky JD. Senescenceassociated (beta)-galactosidase reflects an increase in lysosomal mass during replicative ageing of human endothelial cells. J Cell Sci. 2000; 113 (Pt 20): 3613–22. DOI: 10.1242/jcs.113.20.3613. PMID: 11017877.
- Dimri GP, Lee X, Basile G, Acosta M, Scott G, Roskelley C, et al. A biomarker that identifies senescent human cells in culture and in aging skin in vivo. Proc Natl Acad Sci U S A. 1995; 92 (20): 9363–7. DOI: 10.1073/pnas.92.20.9363. PMID: 7568133; PMCID: PMC40985.
- Kciuk M, Gielecińska A, Mujwar S, Kołat D, Kałuzińska-Kołat Ż, Celik I, et al. Doxorubicin-An Agent with Multiple Mechanisms of Anticancer Activity. Cells. 2023; 12 (4): 659. DOI: 10.3390/cells12040659. PMID: 36831326; PMCID: PMC9954613.
- Dasari S, Tchounwou PB. Cisplatin in cancer therapy: molecular mechanisms of action. Eur J Pharmacol. 2014; 740: 364–78.
   DOI: 10.1016/j.ejphar.2014.07.025. Epub 2014 Jul 21. PMID: 25058905; PMCID: PMC4146684.
- Dorr RT. Bleomycin pharmacology: mechanism of action and resistance, and clinical pharmacokinetics. Semin Oncol. 1992; 19 (2 Suppl 5): 3–8. PMID: 1384141.
- Montecucco A, Zanetta F, Biamonti G. Molecular mechanisms of etoposide. EXCLI J. 2015; 14: 95–108. DOI: 10.17179/excli2015-561. PMID: 26600742; PMCID: PMC4652635.
- Lubberts S, Meijer C, Demaria M, Gietema JA. Early ageing after cytotoxic treatment for testicular cancer and cellular senescence: Time to act. Crit Rev Oncol Hematol. 2020; 151: 102963. DOI: 10.1016/j.critrevonc.2020.102963. Epub 2020 May 7. PMID: 32446180.
- Wiley CD, Campisi J. The metabolic roots of senescence: mechanisms and opportunities for intervention. Nat Metab. 2021;
   (10): 1290–301. DOI: 10.1038/s42255-021-00483-8. Epub 2021 Oct 18. PMID: 34663974; PMCID: PMC8889622.
- 28. Zhang Y, Xu YY, Sun WJ, Zhang MH, Zheng YF, Shen HM, et al. FBS or BSA Inhibits EGCG Induced Cell Death through Covalent Binding and the Reduction of Intracellular ROS Production. Biomed Res Int. 2016; 2016: 5013409. DOI: 10.1155/2016/5013409. Epub 2016 Oct 18. PMID: 27830147; PMCID: PMC5088332.
- Stival A, Silva A, Valadares M. Qualitative and quantitative evaluation of Fetal Bovine Serum composition: toward ethical

- and best quality in vitro science. NAM Journal. 2025. doi. org/10.1016/j.namjnl.2025.100047.
- Liu Y, Birsoy K. Metabolic sensing and control in mitochondria. Mol Cell. 2023; 83 (6): 877–89. DOI: 10.1016/j.molcel.2023.02.016. PMID: 36931256; PMCID: PMC10332353.
- 31. Choi EJ, Oh HT, Lee SH, Zhang CS, Li M, Kim SY, et al. Metabolic stress induces a double-positive feedback loop between AMPK and SQSTM1/p62 conferring dual activation of AMPK and NFE2L2/NRF2 to synergize antioxidant defense. Autophagy. 2024; 20 (11): 2490–510. DOI: 10.1080/15548627.2024.2374692. Epub 2024 Jul 10. PMID: 38953310; PMCID: PMC11572134.
- Fumagalli M, Rossiello F, Mondello C, d'Adda di Fagagna F. Stable cellular senescence is associated with persistent DDR activation. PLoS One. 2014; 9 (10): e110969. DOI: 10.1371/journal.pone.0110969. PMID: 25340529: PMCID: PMC4207795.
- Ajoolabady A, Pratico D, Bahijri S, Eldakhakhny B, Tuomilehto J, Wu F, et al. Hallmarks and mechanisms of cellular senescence in aging and disease. Cell Death Discov. 2025; 11 (1): 364. DOI: 10.1038/s41420-025-02655-x. PMID: 40759632; PMCID: PMC12322153.
- 34. Dou X, Fu Q, Long Q, Liu S, Zou Y, Fu D, et al. PDK4-dependent hypercatabolism and lactate production of senescent cells promotes cancer malignancy. Nat Metab. 2023; 5 (11): 1887–910. DOI: 10.1038/s42255-023-00912-w. Epub 2023 Oct 30. Erratum in: Nat Metab. 2024; 6 (5): 980. DOI: 10.1038/s42255-024-01054-3. Erratum in: Nat Metab. 2024; 6 (7): 1416. DOI: 10.1038/s42255-024-01069-w. PMID: 37903887; PMCID: PMC10663165.
- Hardie DG, Ross FA, Hawley SA. AMPK: a nutrient and energy sensor that maintains energy homeostasis. Nat Rev Mol Cell Biol. 2012; 13 (4): 251–62. DOI: 10.1038/nrm3311. PMID: 22436748; PMCID: PMC5726489.
- Zhang S, Sheng H, Zhang X, Qi Q, Chan CB, Li L, et al. Cellular energy stress induces AMPK-mediated regulation of glioblastoma cell proliferation by PIKE-A phosphorylation. Cell Death Dis. 2019; 10 (3): 222. DOI: 10.1038/s41419-019-1452-1. Erratum in: Cell Death Dis. 2025; 16 (1): 447. DOI: 10.1038/s41419-025-07700-2. PMID: 30833542; PMCID: PMC6399291.
- 37. Shang L, Chen S, Du F, Li S, Zhao L, Wang X. Nutrient starvation elicits an acute autophagic response mediated by Ulk1 dephosphorylation and its subsequent dissociation from AMPK. Proc Natl Acad Sci U S A. 2011; 108 (12): 4788–93. DOI: 10.1073/pnas.1100844108. Epub 2011 Mar 7. PMID: 21383122; PMCID: PMC3064373.
- Lee C, Lamech L, Johns E, Overholtzer M. Selective Lysosome Membrane Turnover Is Induced by Nutrient Starvation. Dev Cell. 2020; 55 (3): 289–97.e4. DOI: 10.1016/j.devcel.2020.08.008. Epub 2020 Sep 10. PMID: 32916093; PMCID: PMC8337093.
- Ebner M, Puchkov D, López-Ortega O, Muthukottiappan P, Su Y, Schmied C, et al. Nutrient-regulated control of lysosome function by signaling lipid conversion. Cell. 2023; 186 (24): 5328–46.e26. DOI: 10.1016/j.cell.2023.09.027. Epub 2023 Oct 25. Erratum in: Cell. 2025; 188 (9): 2560. DOI: 10.1016/j.cell.2025.04.009. PMID: 37883971.
- Hwang ES, Yoon G, Kang HT. A comparative analysis of the cell biology of senescence and aging. Cell Mol Life Sci. 2009; 66 (15): 2503–24. DOI: 10.1007/s00018-009-0034-2. Epub 2009 May 7. PMID: 19421842; PMCID: PMC11115533.
- Tan JX, Finkel T. Lysosomes in senescence and aging. EMBO Rep. 2023; 24 (11): e57265. DOI: 10.15252/embr.202357265. Epub 2023 Oct 9. PMID: 37811693; PMCID: PMC10626421.
- D'Alterio C, Scala S, Sozzi G, Roz L, Bertolini G. Paradoxical effects of chemotherapy on tumor relapse and metastasis promotion. Semin Cancer Biol. 2020; 60: 351–61. DOI: 10.1016/j.semcancer.2019.08.019. Epub 2019 Aug 24. PMID: 31454672
- Behranvand N, Nasri F, Zolfaghari Emameh R, Khani P, Hosseini A, Garssen J, Falak R. Chemotherapy: a double-edged sword in cancer treatment. Cancer Immunol Immunother. 2022; 71 (3): 507–26. DOI: 10.1007/s00262-021-03013-3. Epub 2021 Aug 5. Erratum in: Cancer Immunol Immunother. 2022; 71 (3): 527. DOI: 10.1007/s00262-021-03034-y. PMID: 34355266; PMCID: PMC10992618.
- Middleton JD, Stover DG, Hai T. Chemotherapy-Exacerbated Breast Cancer Metastasis: A Paradox Explainable by Dysregulated

## ОРИГИНАЛЬНОЕ ИССЛЕДОВАНИЕ І ГЕРОНТОЛОГИЯ

- Adaptive-Response. Int J Mol Sci. 2018; 19 (11): 3333. DOI: 10.3390/ijms19113333. PMID: 30373101; PMCID: PMC6274941.
- 45. Hwang HJ, Kang D, Shin J, Jung J, Ko S, Jung KH, et al. Therapy-induced senescent cancer cells contribute to cancer progression by promoting ribophorin 1-dependent PD-L1 upregulation. Nat Commun. 2025; 16 (1): 353. DOI: 10.1038/s41467-024-54132-1. PMID: 39753537; PMCID: PMC11699195.
- Guillon J, Petit C, Toutain B, Guette C, Lelièvre E, Coqueret O. Chemotherapy-induced senescence, an adaptive mechanism driving resistance and tumor heterogeneity. Cell Cycle. 2019; 18 (19): 2385–97. DOI: 10.1080/15384101.2019.1652047. Epub 2019 Aug 9. PMID: 31397193; PMCID: PMC6738909.
- 47. Jiao D, Zheng X, Du X, Wang D, Hu Z, Sun R, et al. Immunogenic
- senescence sensitizes lung cancer to LUNX-targeting therapy. Cancer Immunol Immunother. 2022; 71 (6): 1403–17. DOI: 10.1007/s00262-021-03077-1. Epub 2021 Oct 21. PMID: 34674012; PMCID: PMC9123058.
- Liu Y, Lomeli I, Kron SJ. Therapy-Induced Cellular Senescence: Potentiating Tumor Elimination or Driving Cancer Resistance and Recurrence? Cells. 2024; 13 (15): 1281. DOI: 10.3390/cells13151281. PMID: 39120312; PMCID: PMC11312217.
- 49. Marin I, Boix O, Garcia-Garijo A, Sirois I, Caballe A, Zarzuela E, et al. Cellular Senescence Is Immunogenic and Promotes Antitumor Immunity. Cancer Discov. 2023; 13 (2): 410–31. DOI: 10.1158/2159-8290.CD-22-0523. PMID: 36302218; PMCID: PMC7614152.

# MORPHOLOGICAL, IMMUNOHISTOCHEMISTRY AND MOLECULAR ANALYSIS OF DIFFERENTIATED HIGH-GRADE CARCINOMA

Makhachev DR <sup>™</sup>, Bulanov DV, Shovkhalov MM, Bekmurziev BZ, Geroev IA, Netsvetova AM, Zhusupova AR, Gubich DS, Manovski AM Pirogov Russian National Research Medical University (Pirogov University), Moscow, Russia

High-grade non-anaplastic (HGFC-NA) thyroid tumors belong to a rare and aggressive category of neoplasms that occupy an intermediate position between differentiated and anaplastic carcinomas. There are high mortality rate and limited standard treatment options, which usually include surgical tumor removal with subsequent radioiodine treatment and levothyroxine suppression therapy. Targeted tyrosine kinase inhibitors are additionally considered in radioiodine-resistant forms, but the efficacy of those is limited. A clinical case of differentiated high-grade thyroid carcinoma (DHGTC) in a 62-year-old female patient post hemithyroidectomy is presented. Histological assessment, immunohistochemistry (TTF-1, PAX8, CK19, p53, Ki-67), and the key marker (*TERT*, *TP53*, *BRAF*) molecular testing methods were used. The tumor size was 3.4 × 2.8 × 2.5 cm; the tumor showed pronounced architectonic heterogeneity, focal necrosis, high mitotic activity — 8–10 mitoses per 10 fields of view at ×400 (corresponding to ≥ 5 per 2 mm²), and the Ki-67 proliferation index reached 35%. IHC was used to detect the TTF-1 and PAX8 expression, mutational p53 pattern of expression, suggesting the TP53 mutation. Molecular testing revealed no alteration of the *TERT* and *BRAF* genes. These characteristics made it possible to verify the diagnosis of DHGTC. A conclusion was drawn about the need for comprehensive morphological and molecular diagnosis of HGFC-NA tumors, since the mitotic activity quantitative parameters, Ki-67, and TERT/TP53 status determine the prognosis and the personalized therapy selection.

Keywords: thyroid carcinoma, high-grade non-anaplastic tumors, DHGTC, PDTC, Ki-67, TERT, TP53

Author contribution: FMakhachev DR, Bulanov DV, Shovkhalov MM, Bekmurziev BZ, Geroev IA — data analysis and interpretation, manuscript writing, editing; Netsvetova AM, Zhusupova AR — manuscript writing, editing; Gubich DS, Manovski AM — clinical data acquisition, editing.

Correspondence should be addressed: Dalgat R. Makhachev Akademika Volgina, 37, Moscow, 117437, Russia; dalgat2002@mail.ru

Received: 02.09.2025 Accepted: 15.09.2025 Published online: 24.09.2025

DOI: 10.24075/brsmu.2025.042

Copyright: © 2025 by the authors. Licensee: Pirogov University. This article is an open access article distributed under the terms and conditions of the Creative Commons Attribution (CC BY) license (https://creativecommons.org/licenses/by/4.0/).

## МОРФОЛОГИЧЕСКИЙ, ИММУНОГИСТОХИМИЧЕСКИЙ И МОЛЕКУЛЯРНЫЙ АНАЛИЗ ДИФФЕРЕНЦИРОВАННОЙ ВЫСОКОЗЛОКАЧЕСТВЕННОЙ КАРЦИНОМЫ

Д. Р. Махачев <sup>™</sup>, Д. В. Буланов, М. М. Шовхалов, Б. З. Бекмурзиев, И. А. Героев, А. М. Нецветова, А. Р. Жусупова, Д. С. Губич, А. М. Мановски Российский национальный исследовательский университет имени Н. И. Пирогова (Пироговский Университет), Москва, Россия

Высокозлокачественные неанапластические опухоли щитовидной железы (HGFC-NA) относятся к редкой и агрессивной категории новообразований, занимающих промежуточное положение между дифференцированными и анапластическими карциномами. Имеют место высокая смертность и ограниченные возможности стандартного лечения, которое обычно включает хирургическое удаление опухоли с последующей радиойодтерапией и супрессивной терапией левотироксином. При радиойодрезистентных формах дополнительно рассматривают таргетные тирозинкиназные ингибиторы, однако их эффективность ограничена. Представлен клинический случай дифференцированной высокозлокачественной карциномы (DHGTC) у пациентки 62 лет, перенесшей гемитиреоидэктомию. Использованы методы гистологического анализа, иммуногистохимии (TTF-1, PAX8, CK19, p53, Ki-67) и молекулярного тестирования ключевых маркеров (*TERT, TP53, BRAF*). Опухоль имела размеры 3,4 × 2,8 × 2,5 см, демонстрировала выраженную архитектоническую гетерогенность, очаговый некроз, высокую митотическую активность — 8–10 митозов на 10 полей зрения при ×400 (что соответствует ≥ 5 на 2 мм²), а индекс пролиферации Ki-67 достигал 35%. С помощью ИГХ выявлена экспрессия TTF-1 и PAX8, p53 с мутационным типом экспрессии, что указывает на мутацию TP53. Молекулярное исследование не показало изменения в генах *TERT* и *BRAF*. Эти признаки позволили верифицировать диагноз DHGTC. Сделан вывод о необходимости комплексной морфо-молекулярной диагностики HGFC-NA, поскольку количественные параметры митотической активности, Ki-67 и статус TERT/TP53 определяют прогноз и выбор персонализированной терапии.

Ключевые слова: рак щитовидной железы, высокозлокачественные неанапластические опухоли, DHGTC, PDTC, Ki-67, TERT, TP53

**Вклад авторов:** Д. Р. Махачев, Д. В. Буланов, М. М. Шовхалов, Б. З. Бекмурзиев, И. А. Героев — анализ и интерпретация данных, написание текста статьи, редактирование; Д. С. Губич, А. М. Мановски — сбор клинических данных, редактирование.

 Для корреспонденции: Далгат Рамазанович Махачев ул. Академика Волгина, д. 37, г. Москва, 117437, Россия; dalgat2002@mail.ru

Статья получена: 02.09.2025 Статья принята к печати: 15.09.2025 Опубликована онлайн: 24.09.2025

**DOI:** 10.24075/vrgmu.2025.042

Авторские права: © 2025 принадлежат авторам. Лицензиат: PHИMУ им. Н. И. Пирогова. Статья размещена в открытом доступе и распространяется на условиях лицензии Creative Commons Attribution (CC BY) (https://creativecommons.org/licenses/by/4.0/).

In recent years, the high-grade follicular cell-derived non-anaplastic (HGFC-NA) thyroid carcinomas attract attention of experts in endocrine disorders. According to the WHO classification (2022), this group is classified as a separate category combining aggressive neoplasms with the thyroid differentiation, high mitotic activity, necrotic foci, and poor prognosis. HGFC-NA tumors

occupy an intermediate position between differentiated and anaplastic carcinomas [1].

Two subtypes are distinguished in the structure of HGFC-NA tumors: poorly differentiated thyroid carcinoma (PDTC) and differentiated high-grade thyroid carcinoma (DHGTC). The PDTC diagnostic criteria fixed in the Turin Proposal (2006)

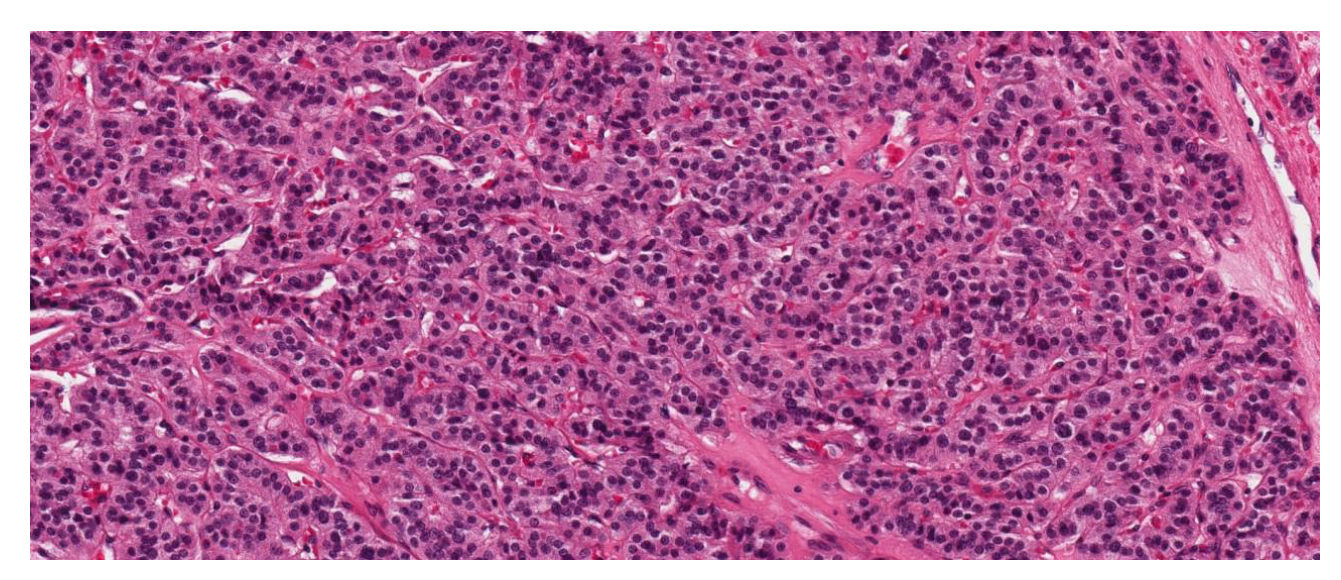


Fig. 1. Poorly differentiated thyroid carcinoma (PDTC) based on the Turin Proposal criteria. Solid/insular growth pattern with thin fibrovascular septa, highly dense small monomorphic cells with high nuclear/cytoplasmic ratio; no nuclear features typical for papillary thyroid carcinoma (H&E, ×200 magnification)

include solid, trabecular or insular growth pattern, absence of nuclear features of papillary carcinoma, and  $\geq 3$  mitoses per 2 mm<sup>2</sup> or necrotic foci [2] (Fig. 1).

It is important to distinguish the HGFC-NA tumors to clarify the diagnosis and choose the tactics that also includes targeted approaches. These tumors reflect a transitional biological range and require the comprehensive assessment of morphological, immunohistochemical, and molecular features. The HGFC-NA tumors are characterized by solid, trabecular, follicular, and sclerosing structures accompanied by cellular atypia, high Ki-67 index (> 20–30%), and the signs of neoangiogenesis [3–5].

Mutations in the *TERT* promoter, *TP53*  $\mu$  *BRAF* are considered to be the key molecular alterations. These are associated with the poor prognosis, radioiodine-resistance, and metastasis. DHGTC can have any morphological structure, including papillary or follicular, but it is diagnosed with  $\geq 5$  mitoses per 2 mm² and/or necrosis, regardless of differentiation [6, 7].

A clinical case of DHGTC with morphological assessment, immunohistochemistry, and molecular testing is provided below.

#### Clinical case

The female patient K. aged 62 years presented with complaints of the neck enlargement, moderate difficulty swallowing and hoarseness escalating within six months. She had a history of hyperthyroidism during therapy with antithyroid drugs and stage II hypertension. The patient had no family history of cancer. Examination revealed a dense mass sized up to 3.5 cm in the right lobe of the thyroid gland, which moved when swallowing.

#### Instrumental methods

Ultrasonography revealed a hypoechoic nodule sized 3.5 × 2.8 cm with uneven contours, hypervascularization, and microcalcifications. The mass TI-RADS score was 5. CT of the neck revealed no invasion of the surrounding tissues and regional lymph nodes. The fine-needle aspiration biopsy was classified as Bethesda V ("suspect for malignancy").

## Surgical treatment

The right-sided hemithyroidectomy was performed. There were no complications in the postoperative period.

#### Macroscopic examination

The tumor had a grey-white color, irregular lobular pattern, foci of necrosis and microcalcifications. Tumor size:  $3.4 \times 2.8 \times 2.5$  cm. The section showed alternating solid zones and areas of coagulative necrosis.

## Microscopic examination

The tumor showed pronounced architectonic heterogeneity: solid, trabecular, and pseudofollicular structures surrounded by thin fibrous septa. Cell nuclei were hyperchromic, roundoval, with moderate atypia and clearly visible nucleoli. Mitotic activity was high: 8–10 mitoses per 10 fields of view at ×400, which was above the diagnostic threshold for DHGTC. Furthermore, foci of coagulative necrosis and microvascular proliferation with signs of vascular invasion were revealed. There were no typical nuclear features of papillary carcinoma.

To demonstrate the differential diagnosis features, an example of anaplastic thyroid carcinoma (ATC) is provided. ATC can resemble high-grade tumors in terms of morphology, but it is distinguished by higher cellular pleomorphism, the presence of giant multinucleated cells, and a larger number of atypical mitoses (Fig. 2).

The combination of features identified is in this case typical for the solid/trabecular and pseudofollicular structure (Fig. 3A); foci of necrosis and high mitotic activity (Fig. 3B) make it possible to classify the tumor as a highly probable differentiated high-grade follicular thyroid carcinoma (DHGTC) belonging to the HGFC-NA group. Final verification required the use of additional histological assessment, extended immunohistochemistry (TTF-1, PAX8, CK19, p53, Ki-67), and molecular testing methods. The latter included assessment of mutations in the genes *TERT*, *TP53*, and *BRAF* using the NGS-panel method with confirmation by Sanger sequencing.

## Immunohistochemistry analysis

Tumor cells expressed TTF-1 and PAX8, which confirmed their origin in follicular cells. The Ki-67 index reached 35%. Galectin-3 expression and focal HBME-reaction were reported; no calcitonin and thyroglobulin were detected.

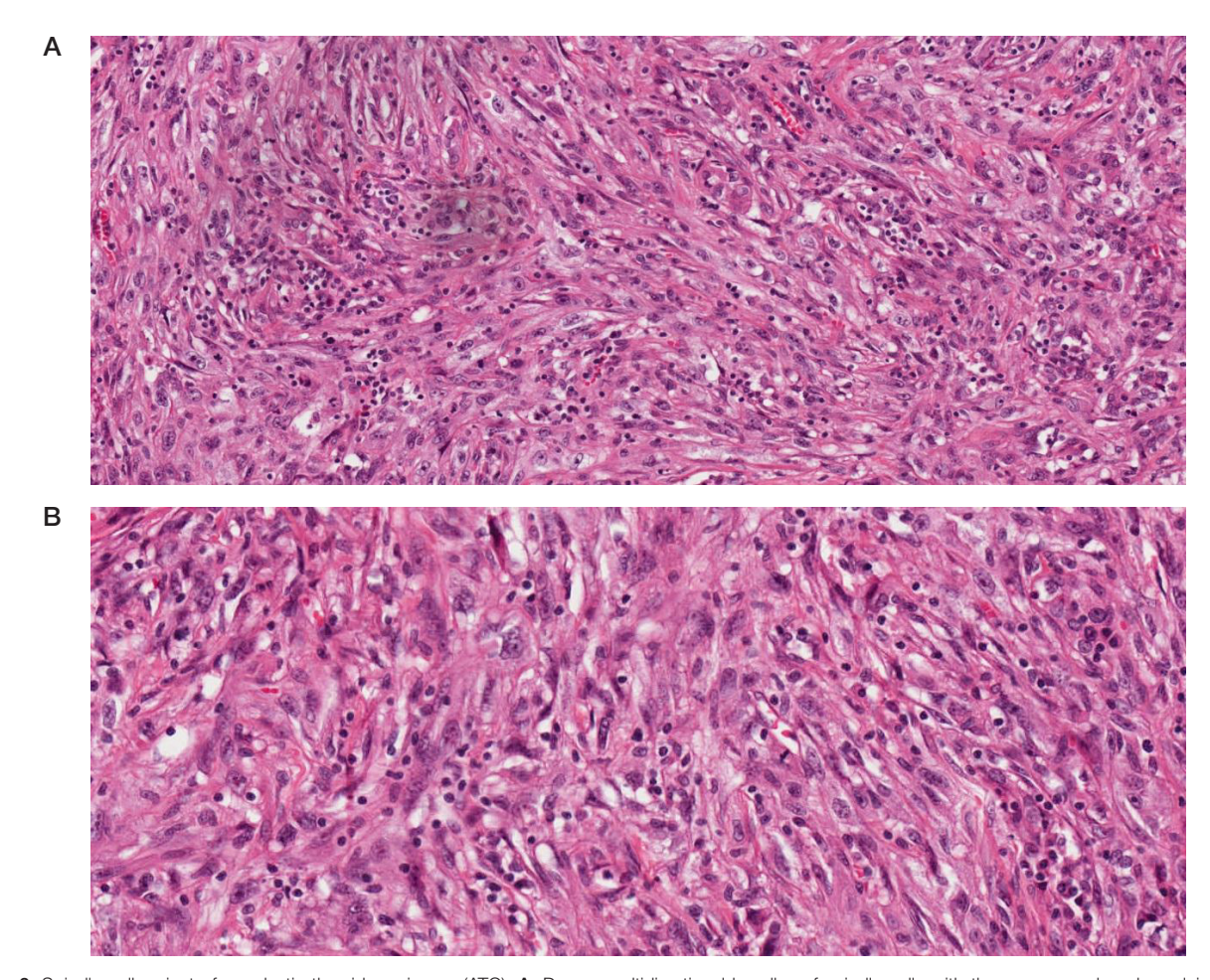


Fig. 2. Spindle cell variant of anaplastic thyroid carcinoma (ATC). A. Dense, multidirectional bundles of spindle cells with the pronounced nuclear pleiomorphism, coarsely granular chromatin (H&E, ×100 magnification). B. High cellularuty, multiple atypical mitoses, sporadic multinucleated tumor cells (H&E, ×400 magnification)

#### Molecular testing

The *TP53* mutation with the mutational p53 expression pattern was identified in the tumor, while no *TERT* and *BRAF V600E* mutations were reported. The profile in combination with morphology and immunohistochemistry assessment confirmed the diagnosis of DHGTC belonging to the HGFC-NA group.

### Clinical case discussion

The HGFC-NA tumors represent a recently distinguished category showing high diagnostic complexity. These occupy an intermediate position between differentiated and anaplastic carcinomas combining thyroid differentiation with aggressive biological behavior [8, 9].

The pronounced architectonic heterogeneity is the key feature of HGFC-NA tumors. Solid, trabecular, pseudofollicular, and sclerosing structures can be combined in the same tumor, which hampers the diagnosis, especially in small biopsies [10]. According to the WHO classification (2022), the decisive criteria are the presence of  $\geq$  5 mitoses per 2 mm², focal necrosis, and Ki-67 index > 20% with the preserved thyroid differentiation. In the case provided, the Ki-67 index reached 35%, and the *TP53* mutation identified suggested poor prognosis [11].

From a molecular perspective, HGFC-NA tumors are characterized by genomic instability. The most significant are mutations in the *TERT* promoter (35–40% of cases) associated with radioiodine resistance, *TP53* alterations (20–25%) reflecting genomic instability, and the less frequent *BRAF* 

V600E mutations that are found mainly in DHGTC, which can determine sensitivity to the MAPK cascade inhibitors [12].

In this case, molecular testing revealed the *TP53* mutation, the presence of which confirmed poor prognosis, while there were no *TERT* and *BRAF V600E* mutations. These findings are consistent with the literature data emphasizing that the presence of the combination of *TERT* and *TP53* mutations significantly worsens the prognosis, and an isolated *TP53* mutation also reflects high genomic instability. A negative test for *BRAF* precludes the possibility of using the MAPK cascade inhibitors, which emphasizes the need to search for other therapeutic targets.

For clinical practice it is important to distinguish PDTC and DHGTC, since the diagnostic criteria of those partially overlap. Comparative analysis of morphological, immunohistochemical, and molecular features is provided in Table 1.

From the prognostic point of view, the HGFC-NA tumors are characterized by aggressive course: the five-year survival rate is only 40–60%, it decreases considerably when there are *TERT* and *TP53* mutations. The main risk factors are high Ki-67 levels (>20–30%), micro- and macrovascular invasion, tumor extent at the time of diagnosis. Early detection of these features is of fundamental importance for personalized treatment selection, including targeted drugs, and patient enrollment in clinical trials [13–15].

A practical algorithm to diagnose PDTC and DHGTC can be presented as follows:

- 1. Morphological analysis: detection of the architectonic heterogeneity, necrosis, and mitotic activity.
  - 2. Quantitative criteria: the number of mitoses  $\geq$  3 per 2 mm<sup>2</sup>

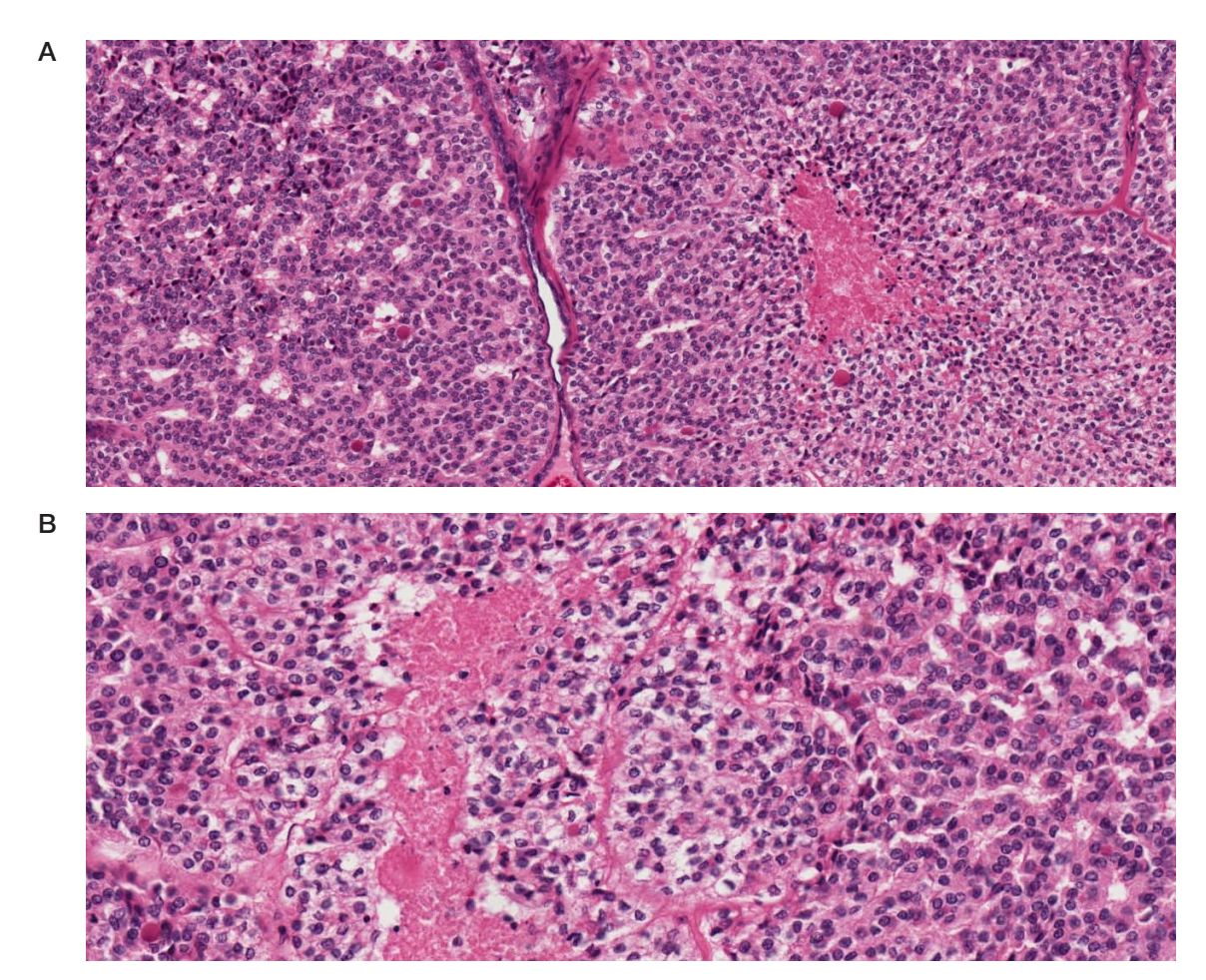


Fig. 3. Differentiated high-grade thyroid carcinoma (DHGTC). A. Solid/trabecular and alveolar areas with the zone of comedo/geographical necrosis (H&E, ×100 magnification). B. Pronounced increase in cytological atypia and proliferation; frequent mitoses (≥ 5 per 2 mm² when counted in the fields with the highest activity) (H&E, ×400 magnification)

suggests PDTC, the number of mitoses  $\geq$  5 suggests DHGTC.

- 3. Immunohistochemistry analysis: determination of the Ki-67, p53, TTF-1, PAX8 expression. The high Ki-67 index (>20–30%) and mutational p53 pattern are the signs of high tumor grade.
- 4. Molecular testing: determination of the *TERT*, *TP53*, *BRAF* mutations. The combination of those determines the prognosis and the targeted therapy options.
- 5. Data integration: the final classification is based on the combination of morphology, quantitative characteristics, and molecular profile.

Targeted therapy prospects

Identification of the *BRAF V600E* mutations opens the prospects for the use of MAPK cascade inhibitors (dabrafenib, trametinib). The use of appropriate targeted agents can be considered when the PI3K/AKT/mTOR pathway is activated. Participation in clinical trials of new drugs remains a promising area for patients with the combination of *TERT* and *TP53* mutations. Thus, the HGFC-NA tumor molecular profiling is not only of prognostic, but also of therapeutic value, since it allows one to select personalized treatment strategies.

Table. Comparison of morphological, immunohistochemical, and molecular features of poorly differentiated (PDTC) and differentiated high-grade tyroid carcinoma (DHGTC)

Criterion	PDTC	DHGTC
Architecture	Solid, trabecular, insular	Any: papillary, follicular, solid, etc.
Nuclear features of papillary carcinoma	Absent	May be present
Mitotic activity	≥ 3 mitoses per 2 mm²	≥ 5 mitoses per 2 mm²
Necrosis	Present (one of the diagnostic criteria)	May be present, strengthens the diagnosis
Turin Proposal criteria (2006)	Essential for making the diagnosis	Not used
Rate of TERT/TP53 mutations	May be present, more often TERT	Often TERT, TP53, sometimes BRAF
Ki-67	Frequently >10-20%	Usually >20%, often >30-40%
Prognosis	Poor, but slightly better, than for DHGTC	Poor, especially when there are TERT- and TP53- mutations
Is ruled out when there are	Nuclear features of papillary carcinoma	No clear exclusive features (quantitative criteria only)

#### CONCLUSION

High-grade non-anaplastic (HGFC-NA) thyroid tumors represent a rare and clinically significant category requiring a specific diagnostic approach. The case of differentiated high-grade carcinoma (DHGTC) provided showed the features typical for this group: morphological heterogeneity, focal necrosis, high mitotic activity, and the Ki-67 index above 30%, as well as the mutational p53 expression pattern with no *TERT* and *BRAF* alterations. The combination of morphological, immunohistochemichal, and molecular data made it possible to confirm the diagnosis and

estimate poor prognosis. This observation emphasizes the need for comprehensive assessment of HGFC-NA tumors involving mandatory consideration of the quantitative criteria (mitotic activity, Ki-67), as well as the *TERT* and *TP53* status. Disregard for these features can result in underestimation of the grade and selection of suboptimal treatment tactics. In the Russian context, the case presented demonstrates the importance of the molecular profiling introduction into routine practice of pathology diagnosis, which will make it possible to improve verification accuracy, enable timely detection of aggressive form and patient management strategy optimization.

#### References

- Rodrigo JP, Coca-Pelaz A, Agaimy A, Franchi A, Woolgar JA, Zafereo M, et al. Poorly differentiated thyroid carcinomas: conceptual controversy and clinical impact. Virchows Arch. 2024; 484 (2): 289– 304. Available from: https://doi.org/10.1007/s00428-024-03752-5.
- Cracolici V, Cipriani NA. High-grade non-anaplastic thyroid carcinomas of follicular cell origin: a review of poorly differentiated and high-grade differentiated carcinomas. Endocr Pathol. 2023; 34 (1): 29–45. Available from: https://doi.org/10.1007/s12022-023-09752-6.
- Resta IT, Montone KT, Livolsi VA. Differentiated high-grade thyroid carcinomas: diagnostic consideration and clinical features. Hum Pathol. 2024; 140: 1–9. Available from: https://doi.org/10.1016/j.humpath.2024.01.002.
- Duong MC, Nguyen LTT, Bhimani N, Thompson EK, Tufano RP, et al. Prognostic significance of key molecular markers in thyroid cancer: a systematic literature review and metaanalysis. Cancers (Basel). 2025; 17 (6): 939. Available from: https://doi.org/10.3390/cancers17060939.
- Thompson LDR. High-grade differentiated follicular cell-derived thyroid carcinoma versus poorly differentiated thyroid carcinoma: a clinicopathologic analysis of 41 cases. Endocr Pathol. 2023; 34 (1): 60–71. Available from: https://doi.org/10.1007/s12022-023-09770-4.
- Haq F, Bychkov A, Mete O, Kakudo K, Jung CK, et al. Identification of specific biomarkers for anaplastic thyroid carcinoma through spatial transcriptomic and immunohistochemical profiling. Endocr Pathol. 2025; 36 (1): 15–27. Available from: https://doi.org/10.1007/s12022-025-09858-z.
- Hernandez-Prera JC, Wenig BM. RAS-mutant follicular thyroid tumors: a continuous challenge for pathologists. Endocr Pathol. 2024; 35 (2): 98–110. Available from: https://doi.org/10.1007/s12022-024-09812-5.
- Chatterjee S, Mair M, Shaha AR, Paleri V, Sawhney R, et al. Current evidences in poorly differentiated thyroid carcinoma: a systematic review and subsection meta-analysis for clinical

- decision making. Endocrine. 2024; 79 (4): 680–96. Available from: https://doi.org/10.1007/s12020-024-03771-x.
- Yu HW, Jeong SI, Kim W, Choi JY, Ahn CH, et al. Incidence and clinicopathological features of differentiated high-grade thyroid carcinomas: an institutional experience. Endocr Pathol. 2023; 34 (2): 210–9. Available from: https://doi.org/10.1007/s12022-023-09778-w.
- Nkosi D, Crowe WE, Altman BJ, Oltvai ZN, Nikiforov YE. SATB2 is an emergent biomarker of anaplastic thyroid carcinoma: a series with comprehensive biomarker and molecular studies. Endocr Pathol. 2024; 35: 88–101. Available from: https://doi.org/10.1007/s12022-024-09833-0.
- Scholfield DW, Xu B, Levyn H, Eagan A, Shaha AR, et al. High-grade follicular cell-derived non-anaplastic thyroid carcinoma: correlating extent of invasion and mutation profile with oncologic outcome. Thyroid. 2025; 35 (2): 153–65. Available from: https://doi.org/10.1089/thy.2024.0499.
- Subbiah V, Kreitman RJ, Wainberg ZA, Cho JY, Schellens JHM, et al. Dabrafenib plus trametinib in BRAFV600E-mutated rare cancers: the phase 2 ROAR trial. Nat Med. 2023; 29 (5): 1103– 12. Available from: https://doi.org/10.1038/s41591-023-02321-8.
- 13. Hassan FA, Slone C, McDonald RJ, Dueber JC, Jha KK, et al. Folliculin (FLCN) in thyroid tumors: incidence, significance, and role as a driver gene and secondary alteration. Curr Oncol. 2025; 32 (4): 224. Available from: https://doi.org/10.3390/curroncol32040224.
- 14. Wang Y, Zhang L, Liu Z. Molecular classification of thyroid tumors and key molecular features to identify high-grade thyroid carcinomas. In: Faquin WC, Bongiovanni M, editors. Thyroid FNA cytology: differential diagnoses and pitfalls. Singapore: Springer, 2024; p. 239–248. Available from: https://doi.org/10.1007/978-981-99-6782-7\_21.
- 15. Tan G, Jin B, Qian X, Li Y, Zhao H, et al. TERT promoter mutations contribute to adverse clinical outcomes and poor prognosis in radioiodine-refractory differentiated thyroid cancer. Sci Rep. 2024; 14: 75087. Available from: https://doi.org/10.1038/s41598-024-75087-9.

## Литература

- Rodrigo JP, Coca-Pelaz A, Agaimy A, Franchi A, Woolgar JA, Zafereo M, et al. Poorly differentiated thyroid carcinomas: conceptual controversy and clinical impact. Virchows Arch. 2024; 484 (2): 289– 304. Available from: https://doi.org/10.1007/s00428-024-03752-5.
- Cracolici V, Cipriani NA. High-grade non-anaplastic thyroid carcinomas of follicular cell origin: a review of poorly differentiated and high-grade differentiated carcinomas. Endocr Pathol. 2023; 34 (1): 29–45. Available from: https://doi.org/10.1007/s12022-023-09752-6.
- Resta IT, Montone KT, Livolsi VA. Differentiated high-grade thyroid carcinomas: diagnostic consideration and clinical features. Hum Pathol. 2024; 140: 1–9. Available from: https://doi.org/10.1016/j.humpath.2024.01.002.
- Duong MC, Nguyen LTT, Bhimani N, Thompson EK, Tufano RP, et al. Prognostic significance of key molecular markers in thyroid cancer: a systematic literature review and metaanalysis. Cancers (Basel). 2025; 17 (6): 939. Available from: https://doi.org/10.3390/cancers17060939.
- Thompson LDR. High-grade differentiated follicular cell-derived thyroid carcinoma versus poorly differentiated thyroid carcinoma:

- a clinicopathologic analysis of 41 cases. Endocr Pathol. 2023; 34 (1): 60–71. Available from: https://doi.org/10.1007/s12022-023-09770-4.
- Haq F, Bychkov A, Mete O, Kakudo K, Jung CK, et al. Identification of specific biomarkers for anaplastic thyroid carcinoma through spatial transcriptomic and immunohistochemical profiling. Endocr Pathol. 2025; 36 (1): 15–27. Available from: https://doi.org/10.1007/s12022-025-09858-z.
- Hernandez-Prera JC, Wenig BM. RAS-mutant follicular thyroid tumors: a continuous challenge for pathologists. Endocr Pathol. 2024; 35 (2): 98–110. Available from: https://doi.org/10.1007/s12022-024-09812-5.
- Chatterjee S, Mair M, Shaha AR, Paleri V, Sawhney R, et al. Current evidences in poorly differentiated thyroid carcinoma: a systematic review and subsection meta-analysis for clinical decision making. Endocrine. 2024; 79 (4): 680–96. Available from: https://doi.org/10.1007/s12020-024-03771-x.
- Yu HW, Jeong SI, Kim W, Choi JY, Ahn CH, et al. Incidence and clinicopathological features of differentiated high-grade thyroid carcinomas: an institutional experience. Endocr Pathol. 2023; 34 (2): 210–9. Available from: https://doi.org/10.1007/s12022-023-09778-w.

## КЛИНИЧЕСКИЙ СЛУЧАЙ І ЭНДОКРИНОЛОГИЯ

- Nkosi D, Crowe WE, Altman BJ, Oltvai ZN, Nikiforov YE. SATB2 is an emergent biomarker of anaplastic thyroid carcinoma: a series with comprehensive biomarker and molecular studies. Endocr Pathol. 2024; 35: 88–101. Available from: https://doi.org/10.1007/s12022-024-09833-0.
- Scholfield DW, Xu B, Levyn H, Eagan A, Shaha AR, et al. High-grade follicular cell-derived non-anaplastic thyroid carcinoma: correlating extent of invasion and mutation profile with oncologic outcome. Thyroid. 2025; 35 (2): 153–65. Available from: https://doi.org/10.1089/thy.2024.0499.
- Subbiah V, Kreitman RJ, Wainberg ZA, Cho JY, Schellens JHM, et al. Dabrafenib plus trametinib in BRAFV600E-mutated rare cancers: the phase 2 ROAR trial. Nat Med. 2023; 29 (5): 1103– 12. Available from: https://doi.org/10.1038/s41591-023-02321-8.
- 13. Hassan FA, Slone C, McDonald RJ, Dueber JC, Jha KK, et al. Folliculin (FLCN) in thyroid tumors: incidence, significance, and role as a driver gene and secondary alteration. Curr Oncol. 2025; 32 (4): 224. Available from: https://doi.org/10.3390/curroncol32040224.
- 14. Wang Y, Zhang L, Liu Z. Molecular classification of thyroid tumors and key molecular features to identify high-grade thyroid carcinomas. In: Faquin WC, Bongiovanni M, editors. Thyroid FNA cytology: differential diagnoses and pitfalls. Singapore: Springer, 2024; p. 239–248. Available from: https://doi.org/10.1007/978-981-99-6782-7\_21.
- Tan G, Jin B, Qian X, Li Y, Zhao H, et al. TERT promoter mutations contribute to adverse clinical outcomes and poor prognosis in radioiodine-refractory differentiated thyroid cancer. Sci Rep. 2024; 14: 75087. Available from: https://doi.org/10.1038/s41598-024-75087-9.

## ORIGINAL RESEARCH | ENDOCRINOLOGY

### REVIVAL OF RADIOIMMUNOASSAY FOR DETERMINATION OF INSULIN AUTOANTIBODIES

Timofeev AV<sup>1</sup>, Galimov RR<sup>1</sup>, Kolesnikova EA<sup>1</sup>, Artyuhov AS<sup>1</sup>, Skoblov YuS<sup>2</sup>, Taktarov SV<sup>3</sup>

- <sup>1</sup> Russian Children's Clinical Hospital (RCCH) Pirogov Russian National Research Medical University, Moscow, Russia
- <sup>2</sup> Shemyakin-Ovchinnikov Institute of Bioorganic Chemistry, Moscow, Russia
- <sup>3</sup> Russian University of Medicine of the Ministry of Health of the Russian Federation, Moscow, Russia

Insulin autoantibodies (IAA) represent the major serological marker of type 1 diabetes mellitus (T1D), the disease resulting from autoimmune damage to β-cells in the pancreatic islets. Testing for IAA is used in early and differential diagnosis of T1D, as well as to perform screening for this disorder. The best foreign diagnostic labs perform IAA tests using different radioimmunoassay (RIA) formats. The RIA performance characteristics, i. e. diagnostic sensitivity (DSe), diagnostic specificity (DSp), and diagnostic accuracy (DA), are on average equal to 44%, 100%, and 81%, respectively. Unfortunately, in Russia RIA has not been used to determine IAA for a long time. All Russian labs use the enzyme-linked immunoassay (ELISA)-based test systems for this purpose. DSe, DSp, and DA of ELISA systems are on average 24%, 87%, and 62%, respectively, i.e. considerably lower compared to RIA systems. Our study aimed to reproduce IAA RIA in the diagnostic lab of the RCCH. The method is based on IAA competitive binding to insulin and <sup>125</sup>I-labeled insulin. Serum samples from patients with new onset T1D and patients without diabetes were tested for IAA. DSe, DSp, and DA were 43%, 100%, and 73%, respectively. Thus, performance characteristics of the reproduced IAA RIA are close to those of RIAs used in foreign labs and are significantly superior to the characteristics of ELISA-based tests.

Keywords: insulin autoantibodies, type 1 diabetes mellitus, radioimmunoassay, diagnostic sensitivity, diagnostic specificity, diagnostic accuracy

**Author contribution:** Timofeev AV — study concept, analysis of the results, manuscript editing; Galimov RR — selection and preparation of serum samples, RIA; Kolesnikova EA — manuscript writing; Artyuhov AS — statistical processing of the RIA results; Skoblov YuS — labeling of insulin with radioactive iodine, measuring the sample radioactivity with a gamma counter; Taktarov SV — preparation of serum samples, RIA.

Compliance with ethical standards: the study was conducted in accordance with the principles of the Declaration of Helsinki (1964) and further amendments.

Correspondence should be addressed: Alexei V. Timofeev Leninsky prospect, 117, korp. 2, Moscow, 119571, Russia; alvaltim@gmail.com

Received: 16.09.2025 Accepted: 16.10.2025 Published online: 26.10.2025

DOI: 10.24075/brsmu.2025.049

Copyright: © 2025 by the authors. Licensee: Pirogov University. This article is an open access article distributed under the terms and conditions of the Creative Commons Attribution (CC BY) license (https://creativecommons.org/licenses/by/4.0/).

## РЕАНИМАЦИЯ РАДИОИММУНОЛОГИЧЕСКОГО МЕТОДА ОПРЕДЕЛЕНИЯ АУТОАНТИТЕЛ К ИНСУЛИНУ

А. В. Тимофеев<sup>1 М</sup>, Р. Р. Галимов<sup>1</sup>, Е. А. Колесникова<sup>1</sup>, А. С. Артюхов<sup>1</sup>, Ю. С. Скоблов<sup>2</sup>, С. В. Тактаров<sup>3</sup>

- <sup>1</sup> Российская детская клиническая больница (РДКБ) филиал Российского национального исследовательского медицинского университета имени Н. И. Пирогова, Москва, Россия
- <sup>2</sup> Институт биоорганической химии имени М. М. Шемякина и Ю. А. Овчинникова, Москва, Россия
- <sup>3</sup> Российский университет медицины Министерства здравоохранения Российской Федерации, Москва, Россия

Аутоантитела к инсулину (insulin autoantibodies, IAA) — один из главных серологических маркеров сахарного диабета 1-го типа (СД1) — заболевания, обусловленного аутоиммунным разрушением β-клеток в островках поджелудочной железы. Тестирование на IAA используют в ранней и дифференциальной диагностике СД1 и при скрининге на это заболевание. Лучшие зарубежные клинико-диагностические лаборатории (КДЛ) тестируют IAA с помощью разных вариантов радиоиммунологического анализа (РИА). Операционные параметры РИА — диагностическая чувствительность (ДЧ), диагностическая специфичность (ДС) и диагностическая точность (ДТ) — в среднем составляют, соответственно, 44%, 100% и 81%. К сожалению, в России РИА уже давно не применяют для определения IAA. Все российские КДЛ с этой целью используют тест-системы, основанные на иммуноферментном анализе (ИФА). У этих тест-систем ДЧ, ДС и ДТ в среднем составляют, соответственно, 24%, 87% и 62%, т. е. существенно ниже, чем у тест-систем РИА. Целью нашей работы было воспроизвести метод РИА IAA в КДЛ РДКБ. Метод основан на конкурентном связывании IAA с инсулином и инсулином, меченным 125 I. Тестировали IAA в образцах сывороток пациентов с впервые выявленным СД1 и пациентов без этого заболевания. ДЧ, ДС и ДТ составили, соответственно, 43%, 100% и 73%. Таким образом, операционные параметры воспроизведенного нами метода РИА IAA приближаются к параметрам методов РИА, применяемых в зарубежных КДЛ, и существенно превосходят параметры метода ИФА.

**Ключевые слова:** аутоантитела к инсулину, сахарный диабет 1-го типа, радиоиммунологический анализ, диагностическая чувствительность, диагностическая специфичность, диагностическая точность

Вклад авторов: А. В. Тимофеев — идея исследования, анализ результатов, редактирование рукописи; Р. Р. Галимов — подбор и подготовка образцов сывороток, выполнение РИА; Е. А. Колесникова — подготовка текста рукописи; А. С. Артюхов — статистическая обработка результатов РИА; Ю. С. Скоблов — мечение инсулина радиоактивным йодом, измерение радиоактивности проб на счетчике участиц; С. В. Тактаров — подготовка образцов сывороток, выполнение РИА.

Соблюдение этических стандартов: исследование проведено в соответствии с принципами Хельсинкской декларации (1964 г.) и ее дальнейшими поправками.

Для корреспонденции: Алексей Валентинович Тимофеев Ленинский проспект, д. 117, корп. 2, г. Москва, 119571, Россия; alvaltim@gmail.com

Статья получена: 16.09.2025 Статья принята к печати: 16.10.2025 Опубликована онлайн: 26.10.2025

DOI: 10.24075/vrgmu.2025.049

Авторские права: © 2025 принадлежат авторам. Лицензиат: РНИМУ им. Н. И. Пирогова. Статья размещена в открытом доступе и распространяется на условиях лицензии Creative Commons Attribution (CC BY) (https://creativecommons.org/licenses/by/4.0/).

## ОРИГИНАЛЬНОЕ ИССЛЕДОВАНИЕ І ЭНДОКРИНОЛОГИЯ

Type 1 diabetes mellitus (T1D) results from the autoimmune damage to  $\beta$ -cells in the pancreatic islets. Destruction of  $\beta$ -cells leads to insulin deficiency and, consequently, to hyperglycemia and other severe metabolic disorders. All T1D patients need lifelong insulin therapy. T1D affects mostly children and adolescents. There is a hereditary risk of T1D: close relatives of patients have approximately 40 times higher risk of the disease [1].

T1D is characterized by latent preclinical stage (PS), in which the gradual  $\beta\text{-cell}$  destruction takes place [2]. PS lasts months to years and ends when the population of  $\beta\text{-cells}$  is reduced by 70–80%. At this moment absolute insulin deficiency, hyperglycemia, and its symptoms emerge: the T1D onset occurs and the clinical stage of the disease begins. Approximately 50% of patients develop an acute T1D complication at the onset: diabetic ketoacidosis leading to severe neurocognitive disorders and eventually to death. The delayed insulin prescription is the main cause of ketoacidosis.

The idea that T1D is an autoimmune disease had erased by early 1980s. By that time it had been shown that the majority of T1D patients carry serum autoantibodies (autoAB) binding islet cell structures on the cryostat sections of the pancreas [3]. Such autoAb were named islet cell antibodies (ICA). It was clear that ICA bind to some cytoplasmic antigens of  $\beta$ -cells, the potential autoimmune response targets. The most likely candidate for such antigens seemed to be insulin, the main product of  $\beta$ -cells. This hypothesis was confirmed in 1983 by the group of the US researchers led by Jerry Palmer [4]. Palmer and his colleagues found IAA in patients with the new-onset T1D never treated by insulin, and in some healthy relatives of T1D patients by RIA.

Later, autoABs against other  $\beta$ -cell antigens were discovered, specifically the glutamic acid decarboxylase antibodies (GADA), islet antigen-2 antibodies (IA-2A), and zinc transporter 8 antibodies (ZnT8A) [5]. AutoABs do not play any essential role in destruction of  $\beta$ -cells, but serve its highly specific laboratory markers.

Testing for autoABs is used for:

- early diagnosis of T1D in the PS;
- confirmation of the T1D diagnosis when the clinical picture is confusing;
- differential diagnosis between T1D and other DM types and variants:
- screening for the T1D PS in persons at risk (for example, among the first-degree relatives) and in the population.

The latter task is of special importance for two reasons. First, the detection of the  $\beta$ -cell destruction markers suggests high probability of T1D onset and allows the patients and their parents to get ready. It also allows physicians to timely prescribe insulin therapy and prevent ketoacidosis and its sequelae. Second, screening reveals the patients having indications for drug prevention of T1D involving the use of the drug suppressing the anti- $\beta$ -cell immune response, for example teplizumab [6].

Table 1. Operational parameters of various IAA tests based on the IASP data [7]

The screening programs have been conducted for many years in European countries, the USA, Canada, Australia, and Israel [7], and in the end of 2024 such a program was launched in Russia, in the Endocrinology Research Center [8]. The tests for autoABs represent the main screening tool, and the central place is occupied by the test for IAA, since this autoAB emerges as early as in the beginning of the PS and serves as the earliest indicator of the anti- $\beta$ -cell immune response [9].

Various methods are used for IAA testing in different labs. The most common ones are RIA, LIPS (Luciferase Immunoprecipitation System) assay; electrochemiluminescence (ECL) analysis; ELISA and CLIA (chemiluminescent immunoassay). Performance characteristics of these methods, diagnostic sensitivity (DSe), diagnostic specificity (DSp), and diagnostic accuracy (DA), differ considerably. Comparative assessment of different IAA tests is periodically conducted as part of the international Islet Autoantibody Standardization Program (IASP) [10]. The participating labs receive the sets of sera from patients with new-onset T1D and from healthy blood donors; each lab performs testing of all sera for IAA by its own method. The results of two IASP rounds conducted in 2018 and 2020 are provided in Table 1.

As can be seen, RIA yields the best DSe and DSp, along with the maximum DA; LIPS assay ranks second in DA, ELISA ranks fourth, and CLIA shows no DA (AUC < 0.5). The ELISA and CLIA unsatisfactory characteristics are explained by the fact that in these methods an antigen (insulin) is absorbed on the solid phase (plastic or magnetic particles), which leads to disruption of its conformation and shielding of antigenic determinants.

Unfortunately, absolutely all Russian labs use the commercially available ELISA systems for IAA testing. The operating parameters of those are even worse than that of ELISA systems represented in the IASP. For example, in the widely used Orgentec Anti-Insulin kit (Orgentec Diagnostika GmbH, REF ORG520, Germany) DSe = 4%, DSp = 95.6%, DA = 50%, i.e. its results are of no clinical significance [11]. Recently, the Maglumi IAA CLIA system (Shenzhen New Industries Biomedical Engineering Co., Ltd; China) became available on the Russian market, but the system user manual contains no data on its performance characteristics [12].

Thus, in our country there is a need to develop and introduce reliable, informative test system for IAA determination. In this regard, the Russian Children's Clinical Hospital diagnostic lab attempted to reproduce classical RIA IAA.

## **METHODS**

## Study overview

Serum samples from the patients with the maximum and minimum likelihood of being IAA carriers, i.e. patients with

Method	DSe, %		DSp, %		AUC		DA, %		
	Me	IQR	Me	IQR	Me	IQR	Me	IQR	N <sub>CDL</sub>
RIA	44.0	20–56	100.0	99–100	0.811	0.73-0.835	81.1	73–83.5	13
LIPS	46.0	40–51	98.9	97–99	0.804	0.784-0.842	80.4	78.4–84.2	11
ECL	53.0	16–58	97.2	92–99	0.774	0.606-0.824	77.4	60.6–82.4	10
ELISA*	24.0	24–30	87.3	83–90	0.624	0.616-0.629	62.4	61.6–62.9	6
CLIA	11.0	9–14	66.1	56–76	0.254	0.243-0.265	25.4	24.3-26.5	2

Note: AUC — area under receiver operating curve; N<sub>LAB</sub> — number of participating labs; Me — median; IQR — interquartile range.\* — all labs used home-made test systems (commercially available systems were not used).

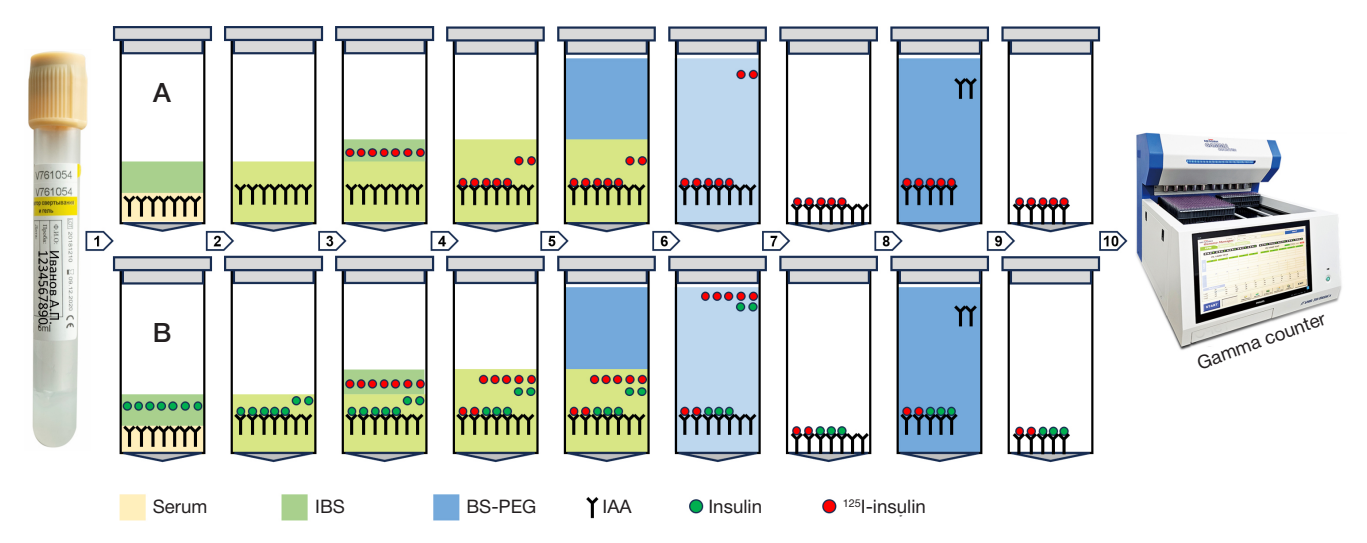


Fig. 1. RIA IAA procedure 1. Serum samples (75 µL) were poured into two series of 1.7 mL Eppendorf conical tubes (Costar 3207, Corning). A total of 75 µL of the 0.23M incubation buffer solution (IBS), pH 7.4 with the following composition were added to each A series tube: NaH,PO, (Sigma-Aldrich, REF S-0751) 0.014M; Na, HPO, (Panreac, REF 141677) 0.067M; NaCl (Sigma-Aldrich, REF S-9625) 0.15M; bovine serum albumin (CDH, REF TC1546) 0.05%; Twin-20 (Panreac, RÉF 162312) 0.05%. A total of 75 µL of the IBS with the recombinant human insulin (Insulin Reference Standard, Eli Lilly, USA) at a concentration of 9 × 10<sup>-3</sup> U/mL were added to each B series tube. 2. Test tubes of both series were vortexed with a vortex mixer and incubated for 30 min on the Ha ELMI-ST3 orbital shaker (Elmi, Latvia) with the platform rotation speed 250 rpm at room temperature. IAA bound to insulin during incubation. 3. A total of 100 µL of IBS with the recombinant human insulin labeled with the 125l (125l-insulin) at a concentration of 7.5 × 10<sup>-6</sup> U/mL were added to each tube of both series. Furthermore, 100 µL of IBS with the 125I-insulin were added to each of two tubes to calculate total radioactivity. The 125I-insulin preparation was produced in the Institute of Bioorganic Chemistry by monoiodination of insulin based on tyrosine A14 using chloramine-T as an oxidizing agent, purified by gel filtration of the column with Sephadex G-15. Iodination involved the use of sodium iodide (1251) (ISOTOPE, RF). Finally, we obtained a stabilized 1251-insulin preparation with the following radiochemical characteristics: total activity — 352 kBq, specific activity — 58 TBq/mmol, radiochemical purity — 92%. 4. All the test tubes were sealed and incubated for 7 days in a refrigerator at +4 °C. During incubation the serum IAA bound to insulin and 125I-insulin, and the equilibrium between IAA binding with the labeled and non-labeled ligands established. 5. A total of 500 µL of the buffer solution (pH 8.6) containing polyethyleneglycol (BS-PEG) with the following composition added to all tubes, except those for total activity calculation: Tris 0.05M (Sigma-Aldrich REF 7-9 Tris base T13,78); PEG-8000 (Polyethylenglycol 8000 BioChemica AppliChem REF A2204.0500) 14%. BS-PEG was previously cooled to 0 °C. 6, 7. The tubes were vortexed with a vortex mixer and centriguged in the Beckman G-2-21 centrifuge at 2000 g for 30 min at +4 °C. The supernatant was removed with an aspirator. As a result, a precipitate was obtained containing the IAA complexes with the labeled and unlabeled insulin, as well as IAA that did not bind to insulin. 8, 9. A total of 1000 µL of BS-PEG with the 11% PEG-8000 previously cooled to 0 °C were added to all tubes, except those for TR calculation. The tubes were vortexed with a vortex mixer and centriqueed in the Beckman G-2-21 centrifuge at 2000 g for 30 min at +4 °C. The supernatant was removed with an aspirator. As a result, a precipitate was obtained containing the IAA complexes with the labeled and unlabeled insulin. 10. Radioactivity was measured in all the tubes (including those for total activity calculation) with the Wizard y-spectrometer (PerkinElmer, USA) at a measuring time of 1 min

new-onset T1D (T1D group) and patients having no such disorder (group C, control), were tested for IAA. The study was conducted in January—February 2024 in the Russian Children's Clinical Hospital and Institute of Bioorganic Chemistry.

## Description of patient groups

T1D group (n = 21)

M: F = 8: 13 (38%: 62%); age 1.1–17.9 years (median age 10.1 years, 95% confidence interval for the median 4.2–12.1 years).
Inclusion criteria: age 0–18 years; diagnosis "type 1 diabetes mellitus, new-onset" (ICD-10 E10.1 or E10.9); T1D duration from the date of the diagnosis to the date of blood sample collection ≤ 3 months; presence of at least two

autoAB types out of the following: ICA, GADA, IA-2A, ZnT8A.

Group C (n = 19)

M: F=12: 7 (63%: 37%); age 2.5–46.9 years (median age 13.3 years, 95% confidence interval for the median 10.2–16.6 years).

Inclusion criteria for the group: any age, any sex; the patient is generally healthy (ICD-10 Z00) or diagnosed with one of the follwing: type 2 diabetes mellitus (ICD-10 E11), other specified diabetes mellitus forms, including various monogenic DM forms (ICD-10 E13, E13.9), obesity (ICD-10 E66), unspecified DM (ICD-10 E14, E14.9), Cushing syndrome (ICD-10 E24), pituitary-dependent Cushing's disease (ICD-10 E24.0), Turner syndrome (ICD-10 Q96); patient was never diagnosed with T1D; patient never received insulin injections; no GADA, IA-2A, ZnT8A in the patient's serum.

### IAA testing method

Competitive radioimmunoassay (RIA) by J.Palmer, et al. was reproduced [4]. The details of the RIA procedures are provided in Fig. 1.

## Calculation of IAA concentration

Stages of calculating the IAA concentration:

- for each serum sample radioactivity (RA), counts per minute (cpm) was registered in the test tube without unlabeled insulin (RAA) and in the tube with unlabeled insulin (RA<sub>a</sub>);
- an average total RA (TRA) for two test tubes was calculated. It was equal to 5000 cpm;
- for each serum sample the  $^{125}\text{l-insulin}$  binding percent (BP) in the test tube without unlabeled insulin (BP $_{\text{A}})$  and in the tube with unlabeled insulin (BP $_{\text{B}})$  was calculated using the formulas: BP $_{\text{A}}$  = RA $_{\text{A}}$ : TR $_{\text{A}}$  and BP $_{\text{B}}$  = RA $_{\text{B}}$ : TR $_{\text{A}}$ ;
- for each serum sample the difference between the binding percentage values (D, delta) was calculated:  $D = BP_A BP_B$ ;
- for each serum sample the IAA concentration  $(\mathrm{C}_{\mathrm{IAA}})$  was calculated:

 $C_{IAA} = (D \times 10,000) : 100 (nU/mL).$ 

## Methods for statistical processing of the results and calculation of the test performance characteristics

To detect outliers in the T1D group and group C, the left-tailed and right-tailed Grubbs's tests were used, respectively. The method by

## ОРИГИНАЛЬНОЕ ИССЛЕДОВАНИЕ І ЭНДОКРИНОЛОГИЯ

Table 2. Results of measuring  $\mathbf{C}_{\text{\tiny IAA}}$  in serum samples

	T1D group					Group C					
Nº	N₂ Patient				N∘		T				
	Sex	Age	Diagnosis (ICD-10)	CIAA, nU/mL		Sex	Age	Diagnosis (ICD-10)	CIAA, nU/mL		
1	m	7.9	n-oT1D (E10.1)	29	22	m	42.0	Healthy (Z00)	6		
2	f	14.0	n-oT1D (E10.1)	11	23	m	46.9	MGD MODY2 (E13)	37		
3	m	10.1	n-oT1D (E10.1)	102	24	m	40.9	T2D (E11)	15		
4	m	4.0	n-oT1D (E10.1)	17	25	m	15.5	T2D (E11)	6		
5	f	12.3	n-oT1D (E10.1)	471	26	m	7.6	Healthy (Z00)	24		
6	f	3.0	n-oT1D (E10.1)	20	27	f	7.0	Healthy (Z00)	10		
7	f	5.2	n-oT1D (E10.1)	24	28	f	10.6	T2D (E11)	172		
8	m	13.7	n-oT1D (E10.1)	164	29	f	27.7	UDM (E14)	24		
9	f	12.2	n-oT1D (E10.1)	17	30	m	15.4	Healthy (Z00)	29		
10	f	4.1	n-oT1D (E10.1)	193	31	f	15.1	T2D (E11. E66)	33		
11	m	11.0	n-oT1D (E10.1)	58	32	m	11.8	Healthy (Z00)	12		
12	m	13.8	n-oT1D (E10.1)	25	33	m	16.8	UDM (E14)	15		
13	m	12.0	n-oT1D (E10.1)	1	34	m	2.5	DMster (E13.9)	17		
14	f	11.3	n-oT1D (E10.1)	19	35	f	16.5	T2D (E11. Q96.3)	22		
15	f	3.4	n-oT1D (E10.1)	16	36	f	13.3	Obesity(E66)	9		
16	f	11.7	n-oT1D (E10.1)	41	37	m	2.8	DMster (E13.9)	20		
17	f	8.0	n-oT1D (E10.1)	21	38	m	10.6	DMster (E13.9)	45		
18	m	2.6	n-oT1D (E10.1)	256	39	m	8.8	Healthy (Z00)	14		
19	f	17.9	n-oT1D (E10.1)	1047	40	f	12.8	T2D (E11. E24.0)	31		
20	f	4.2	n-oT1D (E10.1)	83							
21	f	1.1	n-oT1D (E10.1)	73							

Note: Ne — ordinal number of the serum sample; NOT1D — new-onset type 1 diabetes mellitus; MGD MODY2 — monogenic diabetes mellitus, MODY2 variant (mutation in the hexokinase gene); T2D — type 2 diabetes mellitus; UDM — diabetes mellitus unspecified; DMster — diabetes mellitus caused by taking glucocorticosteroids. The result classified as an outlier is highlighted in red

DeLong et al. was used to plot the operating characteristic curve [13], and the T1D prevalence was considered to be 0.123% [14]. DSe, DSp, and DA were calculated based on the AUC. The MedCalc medical statistical software was used for calculations [15].

### **RESULTS**

The  $C_{\text{IAA}}$  measurement results are provided in Table 2.

One result (of the serum sample No. 28) was classified as an outlier. Thus, statistical analysis included the results of  $C_{\rm IAA}$  measurement in 21 serum samples of the T1D group and 18 serum samples of group C. In the T1D group, the  $C_{\rm IAA}$  values varied between 1 and 1047 nU/mL, in group C these varied between 6 and 45 nU/mL. When plotting the test operating characteristic curve, the MedCalc software automatically selected the  $C_{\rm IAA}$  value exceeding 45 nU/mL as a test positivity criterion (presence of IAA in the serum sample). DSe, DSp, and DA of the test calculated based on the AUC using the above criterion were 42.9%, 100%, and 72.8% with the 95% confidence intervals 21.8–66%, 81.5–100%, and 56.1–85.7%, respectively (Fig. 2).

## DISCUSSION

According to IASP data, the median DSe, DSp, and DA of various RIA IAA methods are 44%, 100%, and 81.1 respectively (Table 1). DSe of our method (42.9%) is very close to the median DSe of the IASP RIA, and DSp matches the median IASP DSp,

but does not fall into its interquartile range. However, DA of our method (72.8%) turned out to be significantly lower compared to the IASP RIA DA and did not fall into its interquartile range.

We explain discrepancy between the result of our RIA method and the RIA results obtained in other IASP labs (the lower DA of our method) by two factors:

- very small number of individuals in both groups;
- the incubation buffer solution (IBS) used by J. Palmer, et al. [4] contained bovine  $\gamma\text{-globulin}$  in a concentration of 0.025% that blocked nonspecific insulin binding with the non-IAA immunoglobulins in the serum samples. There was no such reagent in our IBS.

It should be noted that the performance characteristics of our IAA testing methods turned out to be better than that of the ELISA and CLIA methods represented in IASP, and were significantly superior to performance characteristics of the abovementioned Orgentec Anti-Insulin test system popular in Russian labs.

### CONCLUSIONS

Ultimately, we regard our results as successful, since the performance characteristics of our method turned out to be much better than that of the ELISA and CLIA methods. We believe that after appropriate adjustment our RIA IAA test can be used for scientific purposes and in clinical practice. Unfortunately, it is currently impossible to use this method in the diagnostic lab of the Russian Children's Clinical Hospital

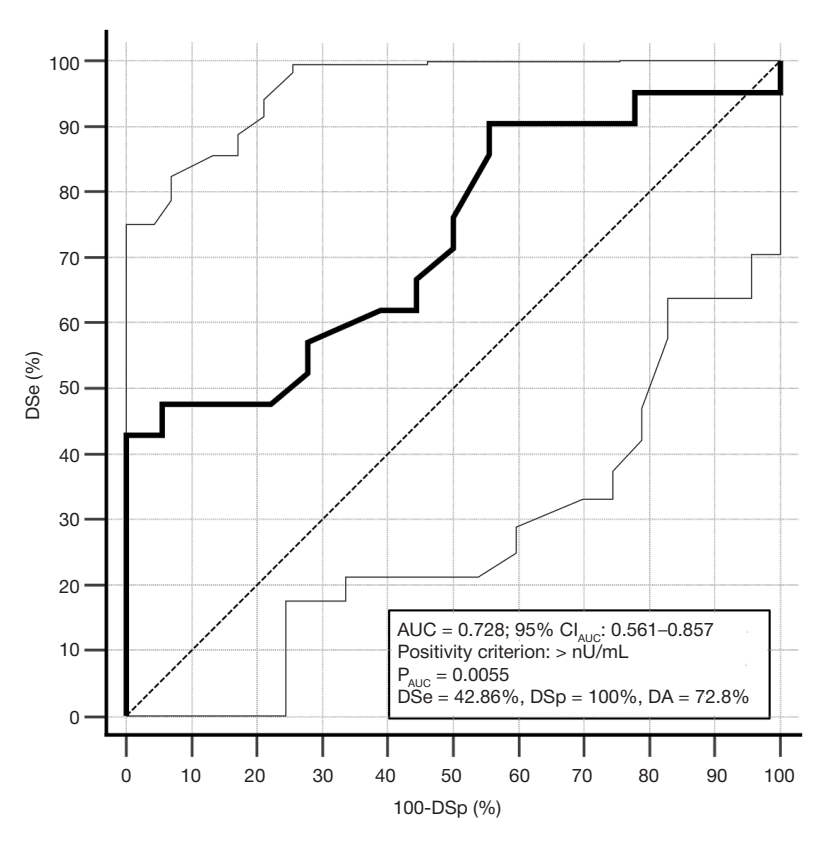


Fig. 2. Receiver Operating Curve of the IAA test. Dashed curve — the line bounding the AUC of 0.5. Solid curve — the test receiver operating characteristic curve. Dotted curves — borders of the 95% confidence interval (95%Cl<sub>AUC</sub>) for the operating characteristic curve. P<sub>AUC</sub> — probability of significance of the null hypothesis about the lack of difference between AUC 0.5 and AUC of the test

due to two factors: lack of the gamma counter; lack of facilities for radionuclide handling licensed by Rospotrebnadzor and Roszdravnadzor. However, we hope that over time we will

manage to tune RIA IAA the Russian diabetologic science and practice are in need of in the Russian Children's Clinical Hospital, branch of the Pirogov University.

## References

- Ziegler AG, Nepom GT. Prediction and Pathogenesis in Type 1 Diabetes. Immunity. 2010; 32 (4): 468–78. PubMed PMID: 20412757. DOI:10.1016/j.immuni.2010.03.018.
- Obshchestvennaya organizaciya Rossijskaya associaciya endokrinologov. Saharnyj diabet 1 tipa u detej. Klinicheskie rekomendacii. 2025. Dostupno po ssylke: https://edu. endocrincentr.ru/sites/default/files/recommendation\_pdf/ kr287\_3.pdf. Data obrashcheniya 08.10.2025. Russian.
- Bottazzo GF, Florin-Christensen A, Doniach D. Islet-cell antibodies in diabetes mellitus with autoimmune polyendocrine deficiencies. Lancet. 1974; 7892 (2): 1279–83. PubMed PMID: 29061712. DOI: 10.1016/S0140-6736(74)90140-8.
- Palmer JP, Asplin CM, Clemons P, Lyen K, Tatpati O, Raghu PK et al. Insulin antibodies in insulin-dependent diabetics before insulin treatment. Science. 1983; 222 (4630): 1337–9. PubMed PMID: 6362005. DOI: 10.1126/science.6362005.
- Kawasaki E. Anti-Islet Autoantibodies in Type 1 Diabetes. Int J Mol Sci. 2023; 24 (12): 10012. PubMed PMID 37373160. DOI: 10.3390/iims241210012.
- Herold KC, Bundy BN, Long SA, Bluestone JA, DiMeglio LA, Dufort MJ, et al. An anti-CD3 antibody, teplizumab, in relatives at risk for type 1 diabetes. N Engl J Med. 2019; 381 (7): 603–13. PubMed PMID: 31180194. DOI: 10.1056/NEJMoa1902226.
- Phillip M, Achenbach P, Addala A, Albanese-O'Neill A, Battelino T, et al. Consensus guidance for monitoring individuals with islet autoantibody-positive pre-stage 3 type 1 diabetes. Diabetologia. 2024; 67 (9): 1731–59. PubMed PMID: 38910151. DOI: 10.1007/s00125-024-06205-5.
- 8. GNC RF FGBU «NMIC endokrinologii im. akademika I.I. Dedova».

- Priglashenie k uchastiyu v issledovanii po skriningu saharnogo diabeta 1 tipa. Dostupno po ssylke: https://www.endocrincentr.ru/sites/default/files/all/issledovanie\_po\_skriningu\_saharnogo\_diabeta\_1\_tipa/priglashenie\_dlya\_uchastiya\_v\_skrininge.pdf?language=en. (Data obrashcheniya 08.10.2025.) Russian.
- Yu L, Rewers M, Gianani R, Kawasaki E, Zhang Y, Verge C et al. Antiislet autoantibodies usually develop sequentially rather than simultaneously. J Clin Endocrinol Metab. 1996; 81 (12): 4264–7. PubMed PMID: 8954025. DOI: 10.1210/jcem.81.12.8954025.
- Marzinotto I, Pittman DL, Williams AJK, Long AE, Achenbach P, Schlosser M, et al. Islet Autoantibody Standardization Program: interlaboratory comparison of insulin autoantibody assay performance in 2018 and 2020 workshops. Diabetologia. 2024; 66 (5): 897–912. PubMed PMID: 36759247, DOI: 10.1007/s00125-023-05877-9.
- 11. Timofeev AV, Gorst KA, Uvarov VYu, Pronina EA, Vitebskaya AV, Popovich AV, i dr. Diagnosticheskaya cennost' primenyayushchihsya v Rossii metodov issledovaniya antitel k antigenam β-kletok. Klassicheskij immunoflyuorescentnyj metod opredeleniya antitel k ostrovkovym kletkam, radioimmunnyj metod opredeleniya antitel k glutamatdekarboksilaze i immunofermentnye metody opredeleniya antitel k tirozinfosfataze i insulinu. Saharnyj diabet. 2016; 19 (4): 331–40. DOI: /10.14341/DM8032. Russian.
- Shenzhen New Industries Biomedical Engineering Co., Ltd. MAGLUMI IAA (CLIA) Instruction for Use. Available from: https://hoachatxetnghiem.com.vn/en/downloads/snibe-maglumi-iaa-clia.pdf. (Last accession 07.10.2025.)
- DeLong ER, DeLong DM, Clarke-Pearson DL. Comparing the areas under two or more correlated receiver operating characteristic curves: a nonparametric approach. Biometrics.

## ОРИГИНАЛЬНОЕ ИССЛЕДОВАНИЕ І ЭНДОКРИНОЛОГИЯ

- 1988; 44 (3): 837-45. PubMed PMID 3203132.
- 14. Dedov II, Shestakova MV, Vikulova OK, Zheleznyakova AV, Isakov MA, Sazonova DV, i dr. Saharnyj diabet v Rossijskoj Federacii: dinamika epidemiologicheskih pokazatelej po dannym
- Federal'nogo registra saharnogo diabeta za period 2010-2022 gg. Saharnyjdiabet. 2023; 26(2): 104-23. DOI: 10.14341/DM13035. Russian.
- MedCalc® Statistical Software version 23.3.7 (MedCalc Software Ltd, Ostend, Belgium; https://www.medcalc.org; 2025).

#### Литература

- Ziegler AG, Nepom GT. Prediction and Pathogenesis in Type 1 Diabetes. Immunity. 2010; 32 (4): 468–78. PubMed PMID: 20412757. DOI:10.1016/j.immuni.2010.03.018.
- Общественная организация Российская ассоциация эндокринологов. Сахарный диабет 1 типа у детей. Клинические рекомендации. 2025. Доступно по ссылке: https://edu.endocrincentr.ru/sites/default/files/recommendation\_ pdf/kr287\_3.pdf. Дата обращения 08.10.2025.
- Bottazzo GF, Florin-Christensen A, Doniach D. Islet-cell antibodies in diabetes mellitus with autoimmune polyendocrine deficiencies. Lancet. 1974; 7892 (2): 1279–83. PubMed PMID: 29061712. DOI: 10.1016/S0140-6736(74)90140-8.
- Palmer JP, Asplin CM, Clemons P, Lyen K, Tatpati O, Raghu PK et al. Insulin antibodies in insulin-dependent diabetics before insulin treatment. Science. 1983; 222 (4630): 1337–9. PubMed PMID: 6362005. DOI: 10.1126/science.6362005.
- Kawasaki E. Anti-Islet Autoantibodies in Type 1 Diabetes. Int J Mol Sci. 2023; 24 (12): 10012. PubMed PMID 37373160. DOI: 10.3390/ijms241210012.
- Herold KC, Bundy BN, Long SA, Bluestone JA, DiMeglio LA, Dufort MJ, et al. An anti-CD3 antibody, teplizumab, in relatives at risk for type 1 diabetes. N Engl J Med. 2019; 381 (7): 603–13. PubMed PMID: 31180194. DOI: 10.1056/NEJMoa1902226.
- Phillip M, Achenbach P, Addala A, Albanese-O'Neill A, Battelino T, et al. Consensus guidance for monitoring individuals with islet autoantibody-positive pre-stage 3 type 1 diabetes. Diabetologia. 2024; 67 (9): 1731–59. PubMed PMID: 38910151. DOI: 10.1007/s00125-024-06205-5.
- 8. ГНЦ РФ ФГБУ «НМИЦ эндокринологии им. академика И.И. Дедова». Приглашение к участию в исследовании по скринингу сахарного диабета 1 типа. Доступно по ссылке: https://www.endocrincentr.ru/ sites/default/ files/all/issledovanie\_po\_skriningu\_saharnogo\_diabeta\_1\_tipa/priglashenie\_dlya\_uchastiya\_v\_skrininge.pdf?language=en. Дата обращения 08.10.2025.

- Yu L, Rewers M, Gianani R, Kawasaki E, Zhang Y, Verge C et al. Antiislet autoantibodies usually develop sequentially rather than simultaneously. J Clin Endocrinol Metab. 1996; 81 (12): 4264–7. PubMed PMID: 8954025. DOI: 10.1210/jcem.81.12.8954025.
- Marzinotto I, Pittman DL, Williams AJK, Long AE, Achenbach P, Schlosser M, et al. Islet Autoantibody Standardization Program: interlaboratory comparison of insulin autoantibody assay performance in 2018 and 2020 workshops. Diabetologia. 2024; 66 (5): 897–912. PubMed PMID: 36759247. DOI: 10.1007/s00125-023-05877-9.
- 11. Тимофеев А. В., Горст К. А., Уваров В. Ю., Пронина Е. А., Витебская А. В., Попович А. В. и др. Диагностическая ценность применяющихся в России методов исследования антител к антигенам β-клеток. Классический иммунофлюоресцентный метод определения антител к островковым клеткам, радиоиммунный метод определения антител к глутаматдекарбоксилазе и иммуноферментные методы определения антител к тирозинфосфатазе и инсулину. Сахарный диабет. 2016; 19 (4): 331–40. DOI: /10.14341/DM8032.
- Shenzhen New Industries Biomedical Engineering Co., Ltd. MAGLUMI IAA (CLIA) Instruction for Use. Available from: https://hoachatxetnghiem.com.vn/en/downloads/snibe-maglumi-iaa-clia.pdf. (Last accession 07.10.2025.)
- DeLong ER, DeLong DM, Clarke-Pearson DL. Comparing the areas under two or more correlated receiver operating characteristic curves: a nonparametric approach. Biometrics. 1988; 44 (3): 837–45. PubMed PMID 3203132.
- 14. Дедов И. И., Шестакова М. В., Викулова О. К., Железнякова А. В., Исаков М. А., Сазонова Д. В. и др. Сахарный диабет в Российской Федерации: динамика эпидемиологических показателей по данным Федерального регистра сахарного диабета за период 2010–2022 гг. Сахарный диабет. 2023; 26 (2): 104–23. DOI: 10.14341/DM13035.
- MedCalc® Statistical Software version 23.3.7 (MedCalc Software Ltd, Ostend, Belgium; https://www.medcalc.org; 2025).

# PROSPECTS OF FINDING PATHOLOGICALLY BASED THERAPIES FOR EPILEPSY ASSOCIATED WITH BRAIN GLIOMA

Ashkhatsava TI¹, Kalinin VA<sup>2™</sup>, Yakunina AV<sup>2</sup>, Poverennova IE<sup>2</sup>

- <sup>1</sup> Federal Center of Brain Research and Neurotechnologies of the Federal Medical Biological Agency, Moscow, Russia
- <sup>2</sup> Samara State Medical University, Samara, Russia

In recent decades, scientific research on tumor-associated epilepsy has increasingly focused on the study of the biochemical and molecular mechanisms of the brain tumor and peritumoral tissues, opening up new and unprecedented perspectives in understanding the glioma-associated epilepsy pathogenesis and treatment. Evidence suggests that neurons play a central role in tumor growth and cancer cells, in turn, can reconfigure the nervous system and its functions. Extracellular glutamate levels in the tissue around the glioma are up to 100 times higher than those in the healthy brain, as detected. At the same time, the available data support the idea that the excitatory neurotransmitter glutamate is the most significant mediator of the seizures related to glioma. The article reports some aspects of the cerebral glioma pathogenesis. The authors believe that modern antiepileptic drugs can affect the neoplastic process course. A number of antiepileptic drugs having the antitumor potential are presented.

Keywords: tumor-associated epilepsy, glioma, primary brain tumors, neurooncology, antiepileptic drugs

Author contribution: Ashkhatsava TI — data collection and systematization; Kalinin VA, Yakunina AV — data analysis, manuscript writing; Poverennova IE — manuscript editing.

Correspondence should be addressed: Vladimir A. Kalinin

Chapaevskaya, 89, Samara, 89443099, Russia; v.a.kalinin@samsmu.ru

Received: 18.09.2025 Accepted: 06.10.2025 Published online: 27.10.2025

DOI: 10.24075/brsmu.2025.051

Copyright: © 2025 by the authors. Licensee: Pirogov University. This article is an open access article distributed under the terms and conditions of the Creative Commons Attribution (CC BY) license (https://creativecommons.org/licenses/by/4.0/).

# ПЕРСПЕКТИВЫ ПОИСКА ПАТОГЕНЕТИЧЕСКИ ОБОСНОВАННОЙ ТЕРАПИИ ЭПИЛЕПСИИ, АССОЦИИРОВАННОЙ С ГЛИОМОЙ ГОЛОВНОГО МОЗГА

Т. И. Ашхацава¹, В. А. Калинин²⊠, А. В. Якунина², И. Е. Повереннова²

- <sup>1</sup> Федеральный центр мозга и нейротехнологий. Москва. Россия
- <sup>2</sup> Самарский государственный медицинский университет, Самара, Россия

В последние десятилетия научные исследования глиальных опухолей головного мозга в большей степени сосредоточены на изучении биохимических и молекулярных механизмов как в самой опухолевой, так и в перитуморальной ткани, что открывает новые и беспрецедентные перспективы в понимании патогенеза и терапии эпилепсии, ассоциированной с глиомами. Данные свидетельствуют о том, что нейроны играют центральную роль в росте опухоли и, в свою очередь, раковые клетки могут изменять конфигурацию нервной системы и ее функций. В ткани, окружающей глиому, выявляются уровни внеклеточного глутамата до 100 раз выше, чем в здоровом мозге. В то же время существующие данные подтверждают концепцию о том, что возбуждающий нейромедиатор глутамат является важнейшим медиатором припадков, связанных с глиомой. В статье описаны некоторые аспекты патогенеза глиомы головного мозга. По мнению авторов, современные противоэпилептические препараты могут влиять на течение опухолевого процесса. Представлен ряд противоэпилептических препаратов, имеющих противоопухолевый потенциал.

Ключевые слова: опухоль-ассоциированная эпилепсия, глиома, первичные опухоли головного мозга, нейроонкология, противоэпилептические препараты

**Вклад авторов:** Т. И. Ашхацава — сбор материала, систематизация данных; В. А. Калинин, А. А. Якунина — анализ данных, написание статьи; И. Е. Повереннова — редакторование статьи.

Для корреспонденции: Владимир Анатольевич Калинин

ул. Чапаевская, д. 89, г. Самара, 89443099, Россия; v.a.kalinin@samsmu.ru

Статья получена: 18.09.2025 Статья принята к печати: 06.10.2025 Опубликована онлайн: 27.10.2025

DOI: 10.24075/vrgmu.2025.051

Авторские права: © 2025 принадлежат авторам. Лицензиат: РНИМУ им. Н. И. Пирогова. Статья размещена в открытом доступе и распространяется на условиях лицензии Creative Commons Attribution (CC BY) (https://creativecommons.org/licenses/by/4.0/).

According to the 2017 ILAE Classification of the Epilepsies, the brain tumor-associated epilepsy is a structural focal epilepsy that is diagnosed in 10-15% of epilepsy cases. Back in 1947, in the fifth edition of Diseases of the Nervous System, John Eastman Wilson mentioned that generalized seizures may be the first symptom of an intracranial tumor, noting the fact of a later onset of tumor-associated epilepsy in contrast to idiopathic epilepsy. In 2003, K. Luiken and his colleagues from the University of Bonn proposed calling this group "long-term epilepsy-associated tumors" (LEATs) [1]. The group includes glioneuronal tumors and some astrocytomas, more often of low malignancy.

The most common tumors of the central nervous system are glioblastomas (grade IV gliomas according to the WHO

classification). The average age of disease onset is 64 years, and the overall five-year survival rate is 6.8% — one of the worst across the entire range of cancers. With low-grade gliomas, 70-90% of patients suffer from epileptic seizures when the tumor is detected, whereas with glioblastoma, seizures are less common (up to 60%) [2].

# Pathogenetic processes underlying the development of gliomas and tumor-associated epilepsy

According to recent data, neurons play a central role in tumor growth, and pathological cells, in turn, can change the configuration of the nervous system and its functions. There

is evidence of the formation of functional synapses between neurons and glioma cells [3].

Epileptogenesis in peritumoral tissue is a multifactorial process. Glioblastomas and tumor-associated epilepsies have common pathophysiological mechanisms that underpin both tumor progression and the persistence of epileptic seizures. One of the main pathological vehicles is the aberrant transmission of glutamate signals in the tumor tissue and its microenvironment. The levels of extracellular glutamate registered in the tissue surrounding the glioma were found to be up to 100 times higher than those peculiar to the healthy brain. On the one hand, a high level of glutamate stimulates the proliferation and invasion of glioma cells, and on the other hand, it can lead to epileptic seizures, excitotoxicity and, consequently, boost the volume of the tumor and the area it occupies [4].

In the past decade, the cystine/glutamate antiporter (SLC7A11, or xCT) has been recognized as an important factor in various processes of tumor progression: it is the main transporter of cystine into the cell, exchanging it for glutamate, which subsequently promotes the synthesis of glutathione needed to protect cells from oxidative stress. [5].

Another mechanism that increases the amount of glutamate is expression of the BCAT1 gene, which encodes the cytosolic form of the branched chain amino acid transaminase enzyme. The level of BCAT1 expression is an important prognostic factor for glioma patients, since it is associated with the malignant progression of wild-type IDH1 gliomas [6]. Thus, BCAT1 is a promising target for the treatment of primary glioblastoma and gliomas.

There is evidence that a growing amount of glutamate in peritumoral tissue increases the risk of tumor necrosis; it is an important prognostic factor supporting an unfavorable outcome. The excitatory effect of glutamate is realized through the activation of three main types of ionotropic receptors and several classes of metabotropic receptors associated with G proteins. Ionotropic receptors are those interacting with N-methyl-D-aspartic acid (NMDA),  $\alpha$ -amino-3-hydroxy-5-methyl-4-isoxazolpropionic acid (AMPA), and kainic acid (KA) [7]. The permeability of AMPA receptors to  $\text{Ca}^{2+}$  is determined by the presence or absence of the GluR2 subunit in the receptor complex.

The analysis of the drug resistance of glioblastomas also revealed epigenetic modifications, in particular DNA methylation, which determines the progression of the tumor. MicroRNAs, a non-coding class of RNA, play a significant role in this process. MicroRNAs with both pro-oncogenic and protective effects were identified, as well as epigenetic modifications of microRNAs that can alter their expression in glioblastoma through methylation. Clarifying the form of epilepsy by examining specific microRNAs in blood plasma, especially in clinically complex cases, can help select the most effective antiepileptic therapy [8].

Thus, it is obvious that there are common mechanisms of pathogenesis of peritumoral changes and generation of epileptic seizures, and the described processes become cascading, mutually reinforcing and accelerating each other. Disrupting or slowing down the pathological processes will not only solve the problem of epileptic seizures but also allow controlling the growth of the tumor.

## Search for antiepileptic drugs with potential antitumor effects

Currently, it can be said that drugs that alter the mechanisms behind an epileptic seizure can highly likely affect tumor aggression, too. Thus, timely antiepileptic therapy improves the survival of glioblastoma patients. In light of the hypothesis that glutamate released from glioma cells can not only activate surrounding neurons (causing epileptic seizures and triggering excitotoxicity processes) but also boost the progression of glioma, the preferred drugs for patients with partial and generalized seizures should be those with antiglutamate action [9].

Perampanel used for epilepsy in patients with IDH1-wild type and MGMT-unmethylated glioblastoma stopped seizures and supported survival for 18 months [10].

An in-depth and comprehensive review of various aspects of epileptogenesis in cerebral glioblastoma cases gives basis for the selection of drugs. While there have not been developed specific recommendations addressing the choice of an anticonvulsant for tumor-associated epilepsy, the identification of compounds with antitumor effect *in vitro* is a persistent subject of interest. Numerous preclinical studies have shown that levetiracetam can enhance the glioblastoma response to temozolomide [11]. Brivaracetam, with its molecule similar in structure to that of levetiracetam, should produce the same effect. Moreover, brivaracetam's action can be more pronounced, since this drug is better tolerated than levetiracetam.

From our point of view, brivaracetam and lacosamide, the latest antiepileptic medicines, show promise in treatment of tumor-associated epilepsy. The authors hypothesized that they hinder the release of glutamate not only from neurons but also from astroglia [12]. Lacosamide inhibits histone deacetylase, suggesting an antitumor effect that requires further investigation. Indeed, the respective mechanism has been considered as blocking the cell cycle in glioma cells, possibly by activating miR-195-5p microRNA. The researchers have also suggested that by modulating other microRNA modifications (miR-107), lacosamide can inhibit cell growth, enhance apoptosis, and block cell migration and invasion. A great advantage of this drug is the possibility to administer is parenterally in equivalent doses.

Currently, one of the most promising combinations of antiepileptic drugs in cases of epilepsy associated with cerebral gliomas may be that of levetiracetam and lacosamide. It can effectively control epileptic seizures and mixes well with adjuvant radiochemotherapy, which mitigates the risk of adverse events stemming from the treatment of the underlying disease. However, the encouraging results from in vitro studies that looked into the effect of levetiracetam and lacosamide on glioblastoma were not fully confirmed in in vivo studies, which yielded mixed results regarding patient survival [13].

#### CONCLUSION

The analysis of literature shows that the problem of the pathogenesis of tumor-associated epilepsy is a matter of interest for many researchers. The related modern concepts revolve around both biochemical disorders in the peritumoral zone as a result of blastomatous growth, and the kindling effect associated with impaired neural migration [14]. However, there is a number of specific issues related to the diagnosis and therapy of the disease that have not been studied sufficiently. The problems of early diagnosis of primary brain tumors remain relevant. The subjects requiring attention in the first place are clinical diagnosing, the study of the semiology of the attack, which allow formulating indications, designing a neuroimaging techniques application algorithm, and suggesting histology and classification of the degree of tumor anaplasia. Currently, neuroimaging algorithms are becoming more complex in parallel with the development of technology [15]. There is no single strategy for choosing antiepileptic drugs against a tumorassociated epilepsy. Meanwhile, clarifying the mechanisms of epileptogenesis is a prerequisite both for the development of therapeutically effective antiepileptic drugs and for improving strategies for the comprehensive treatment of tumor-associated epilepsy. Excessive activity of glutamate and its receptors boosts the growth of glioma itself and promotes apoptosis and epileptic activity in the peritumoral region. The foci of epilepsy activity and glioma can affect each other. There is probably a pathological vicious circle in which tumor growth provokes epileptic seizures, and excessive neural activity can stimulate tumor progression. The combination of antiepileptic drugs with different mechanisms of action will improve the prognosis and the quality of life of patients with brain tumor-associated epilepsy [16]. Perampanel, a selective, non-

competitive AMPA antagonist, may be one of the drugs of choice for additional therapy of the related epileptic seizures [16]. Other new antiepileptic drugs, such as lacosamide and brivaracetam, can probably affect both the quality of life of patients and their survival (given in pathogenetically justified combinations). The use of antiepileptic drugs that induce microsomal liver enzymes of the P450 system should be avoided, since sch action may reduce the effectiveness of chemotherapy. In addition, the use of inhibitors of the P450 system may increase the risk of adverse events caused by chemotherapeutic drugs. Clarification of the patterns of epileptogenesis is required both for the development of effective anticonvulsants and for the improvement of strategies designed for complex treatment of tumors associated with epilepsy.

#### References

- SLuyken C, Blümcke I, Fimmers R, Urbach H, Elger C, Wiestler O, et al. 2003. The spectrum of longterm epilepsy-associated tumors: long-term seizure and tumor outcome and neurosurgical aspects. Epilepsia. 2003; 44: 822–30.
- Lange F, Hornschemeyer J, Kirschstein T.Glutamatergic Mechanisms in Glioblastoma and Tumor-Associated Epilepsy. Cells. 2021; 10 (5): 1226. Available from: https://doi.org/10.3390/cells10051226.
- Venkataramani V, Tanev DI, Strahle C, et al. Glutamatergic synaptic input to glioma cells drives brain tumour progression. Nature. 2019; 573 (7775): 532–38. Available from: https://doi. org/10.1038/s41586-019-1564-x.
- Yuen TI, Morokoff AP, Bjorksten A, et al. Glutamate is associated with a higher risk of seizures in patients with gliomas. Neurology. 2012; 79 (9): 883–9. Available from: https://doi.org/10.1212/ WNL.0b013e318266fa89.
- Lo M, Wang YZ, Gout PW. The x(c)-cystine/glutamate antiporter: a potential target for therapy of cancer and other diseases. J Cell Physiol. 2008; 215 (3): 593–602. Available from: https://doi. org/10.1002/jcp.21366.
- Yi L, Fan X, Li J, et al. Enrichment of branched chain amino acid transaminase 1 correlates with multiple biological processes and contributes to poor survival of IDH1 wild-type gliomas. Aging (Albany NY). 2021; 13 (3): 3645–60. Available from: https://doi. org/10.18632/aging.202328.
- Traynelis SF, Wollmuth LP, McBain CJ, et al. Glutamate receptor ion channels: structure, regulation, and function. Pharmacol Rev. 2010; 62 (3): 405–96. Available from: https://doi.org/10.1124/pr.109.002451.
- Timechko EE, Lysova KD, Yakimov AM, Paramonova AI, Vasilieva AA, Kantimirova EA, et al. Circulating microRNAs as Biomarkers of Various Forms of Epilepsy. Med Sci. 2025; 13: 7. Available from: https://doi.org/10.3390/medsci13010007.
- Pina-Garza JE, Rosenfeld W, Saeki K, et al. Efficacy and safety of adjunctive perampanel in adolescent patients with epilepsy: Post hoc analysis of six randomized studies. Epilepsy Behav. 2020; 104: 106876. Available from: https://doi.org/10.1016/j.

- yebeh.2019.106876.
- Rosche J, Piek J, Hildebrandt G, Grossmann A, Kirschstein T, Benecke R. Perampanel in der Behandlung eines Patienten mit Glioblastoma multiforme ohne IHD-1-Mutation und ohne MGMT-Promotor-Methylierung. Fortschr Neurol Psychiatr. 2015; 83 (5): 286–9. Available from: https://doi.org/10.1055/s-0034-1399459.
- 11. Roh TH, Moon JH, Park HH, et al. Association between survival and levetiracetam use in glioblastoma patients treated with temozolomide chemoradiotherapy. Sci Rep. 2020; 10 (1): 10783. Available from: https://doi.org/10.1038/s41598-020-67697-w.
- Fukuyama K, Ueda Y, Okada M. Effects of Carbamazepine, Lacosamide and Zonisamide on Gliotransmitter Release Associated with Activated Astroglial Hemichannels. Pharmaceuticals (Basel). 2020; 13 (6): 117. Available from: https://doi.org/10.3390/ph13060117.
- 13. Bianconi A, Koumantakis E, Gatto A, Zeppa P, Saaid A, Nico E, et al. Effects of Levetiracetam and Lacosamide on survival and seizure control in IDH-wild type glioblastoma during temozolomide plus radiation adjuvant therapy. Brain and Spine. 2024; 4: 102732. Available from: https://doi.org/10.1016/j.bas.2023.102732.
- 14. Vasilenko AV, Ulitin AYu, Ablaev NR, Dikonenko MV, Mansurov AS, SHajhov M. M. Epilepsiya u bol'nyh s gliomami: mekhanizmy, lechenie i vliyanie protivosudorozhnoj terapii. Rossijskij zhurnal personalizirovannoj mediciny. 2023; 3 (3): 38–47. DOI: 10.18705/2782-3806-2023-3-3-38-47. Russian.
- 15. Kopachev DN, SHishkina LV, SHkatova AM, Golovteev AL, Troickij AA, Grinenko OA, i dr. Glionejronal'nye opuholi, associirovannye s epilepsiej. ZHurnal nevrologii i psihiatrii im. S. S. Korsakova. 2022; 122 (4): 127–34. Dostupno po ssylke: https://doi.org/10.17116/jnevro2022122041127. Russian.
- Lebedeva AV, Burd SG, Vlasov PN, Ermolenko NA, ZHidkova IA, Zyryanov SK, i dr. Lechenie epilepsii, associirovannoj s pervichnymi i metastaticheskimi opuholyami golovnogo mozga. Epilepsiya i paroksizmal'nye sostoyaniya. 2021; 13 (3): 286–304. Dostupno po ssylke: https://doi.org/10.17749/2077-8333/epi.par.con.2021.099. Russian.

## Литература

- SLuyken C, Blümcke I, Fimmers R, Urbach H, Elger C, Wiestler O, et al. 2003. The spectrum of longterm epilepsy-associated tumors: long-term seizure and tumor outcome and neurosurgical aspects. Epilepsia. 2003; 44: 822–30.
- Lange F, Hornschemeyer J, Kirschstein T.Glutamatergic Mechanisms in Glioblastoma and Tumor-Associated Epilepsy. Cells. 2021; 10 (5): 1226. Available from: https://doi.org/10.3390/cells10051226.
- Venkataramani V, Tanev DI, Strahle C, et al. Glutamatergic synaptic input to glioma cells drives brain tumour progression. Nature. 2019; 573 (7775): 532–38. Available from: https://doi. org/10.1038/s41586-019-1564-x.
- Yuen TI, Morokoff AP, Bjorksten A, et al. Glutamate is associated with a higher risk of seizures in patients with gliomas. Neurology.

- 2012; 79 (9): 883–9. Available from: https://doi.org/10.1212/WNL.0b013e318266fa89.
- Lo M, Wang YZ, Gout PW. The x(c)-cystine/glutamate antiporter: a potential target for therapy of cancer and other diseases. J Cell Physiol. 2008; 215 (3): 593–602. Available from: https://doi. org/10.1002/jcp.21366.
- Yi L, Fan X, Li J, et al. Enrichment of branched chain amino acid transaminase 1 correlates with multiple biological processes and contributes to poor survival of IDH1 wild-type gliomas. Aging (Albany NY). 2021; 13 (3): 3645–60. Available from: https://doi. org/10.18632/aging.202328.
- Traynelis SF, Wollmuth LP, McBain CJ, et al. Glutamate receptor ion channels: structure, regulation, and function. Pharmacol Rev.

## МНЕНИЕ I НЕЙРООНКОЛОГИЯ

- 2010; 62 (3): 405–96. Available from: https://doi.org/10.1124/pr.109.002451.
- 8. Timechko EE, Lysova KD, Yakimov AM, Paramonova AI, Vasilieva AA, Kantimirova EA, et al. Circulating microRNAs as Biomarkers of Various Forms of Epilepsy. Med Sci. 2025; 13: 7. Available from: https://doi.org/10.3390/medsci13010007.
- Pina-Garza JE, Rosenfeld W, Saeki K, et al. Efficacy and safety of adjunctive perampanel in adolescent patients with epilepsy: Post hoc analysis of six randomized studies. Epilepsy Behav. 2020; 104: 106876. Available from: https://doi.org/10.1016/j. yebeh.2019.106876.
- Rosche J, Piek J, Hildebrandt G, Grossmann A, Kirschstein T, Benecke R. Perampanel in der Behandlung eines Patienten mit Glioblastoma multiforme ohne IHD-1-Mutation und ohne MGMT-Promotor-Methylierung. Fortschr Neurol Psychiatr. 2015; 83 (5): 286–9. Available from: https://doi.org/10.1055/s-0034-1399459.
- 11. Roh TH, Moon JH, Park HH, et al. Association between survival and levetiracetam use in glioblastoma patients treated with temozolomide chemoradiotherapy. Sci Rep. 2020; 10 (1): 10783. Available from: https://doi.org/10.1038/s41598-020-67697-w.
- Fukuyama K, Ueda Y, Okada M. Effects of Carbamazepine, Lacosamide and Zonisamide on Gliotransmitter Release Associated with Activated Astroglial Hemichannels. Pharmaceuticals (Basel). 2020;

- 13 (6): 117. Available from: https://doi.org/10.3390/ph13060117.
- 13. Bianconi A, Koumantakis E, Gatto A, Zeppa P, Saaid A, Nico E, et al. Effects of Levetiracetam and Lacosamide on survival and seizure control in IDH-wild type glioblastoma during temozolomide plus radiation adjuvant therapy. Brain and Spine. 2024; 4: 102732. Available from: https://doi.org/10.1016/j.bas.2023.102732.
- 14. Василенко А. В., Улитин А. Ю., Аблаев Н. Р., Диконенко М. В., Мансуров А. С., Шайхов М. М. Эпилепсия у больных с глиомами: механизмы, лечение и влияние противосудорожной терапии. Российский журнал персонализированной медицины. 2023; 3 (3): 38–47. DOI: 10.18705/2782-3806-2023-3-3-38-47.
- Копачев Д. Н., Шишкина Л. В., Шкатова А. М., Головтеев А. Л., Троицкий А. А., Гриненко О. А., и др. Глионейрональные опухоли, ассоциированные с эпилепсией. Журнал неврологии и психиатрии им. С. С. Корсакова. 2022; 122 (4): 127–34. Доступно по ссылке: https://doi.org/10.17116/ jnevro2022122041127.
- Лебедева А. В., Бурд С. Г., Власов П. Н., Ермоленко Н. А., Жидкова И. А., Зырянов С. К., и др. Лечение эпилепсии, ассоциированной с первичными и метастатическими опухолями головного мозга. Эпилепсия и пароксизмальные состояния. 2021; 13 (3): 286–304. Доступно по ссылке: https://doi.org/10.17749/2077-8333/epi.par.con.2021.099.

### TRANSCRIPTOMIC FEATURES OF FAP+ CELLS ACROSS MOLECULAR SUBTYPES OF BREAST CANCER

Kalinchuk AYu, Patskan IA, Stadelman MM, Grigorieva ES <sup>™</sup>, Tashireva LA

Tomsk National Research Medical Center, Russian Academy of Sciences, Tomsk, Russia

Understanding subtype-specific variability of functional programs in FAP+ tumor-associated fibroblasts (TAFs) is fundamental for developing effective therapeutic strategies targeting stromal components. The aim of this study was to identify subtype-specific signaling pathways, markers, and molecular features of FAP+ TAFs. Using spatial transcriptomic analysis, we demonstrated that FAP+ TAFs in luminal breast cancer exhibit a phenotype characterized by extracellular matrix organization (GO:0030198, FDR q-value = 0.0307) and expression of genes associated with metastasis (*COL10A1*, *MMP13*, *CXCL14*, *TSPAN8*). In contrast, FAP+ TAFs in triple-negative breast cancer display a pronounced immunomodulatory phenotype with overexpression of immunosuppressive genes (*CD36*, *PLA2G2A*, *CHI3L1*) and enrichment of immune response-related pathways (immune response (GO:0006955, FDR q-value = 7.85e-17), inflammatory response (GO:0006954, FDR q-value = 2.79e-11), regulation of cytokine production (GO:0001817, FDR q-value = 3.39e-10)). We also identified subtype-specific gene signatures related to radioresistance: luminal A and B subtypes showed activation of DNA repair pathways (*IGF1R*, *ERBB3*, *CRIP1*), while triple-negative tumors demonstrated enrichment of epithelial-mesenchymal transition and stemness markers (*ZEB2*, *NOTCH4*, *FOXM1*). These findings emphasize that FAP+ fibroblasts are not a homogeneous population but functionally specialize depending on tumor subtype — acting as stromal architects in luminal breast cancer and as regulators of immune response in triple-negative breast cancer.

Keywords: breast cancer, tumor microenvironment, fibroblasts, spatial transcriptomics

Funding: this work was supported by the Russian Science Foundation (grant No. 25-65-00021).

**Author contribution:** Kalinchuk AYu — writing and formatting; Patskan IA — bioinformatic analysis; Shtadelman MM — data collection and analysis; Grigoryeva ES — interpretation of results; Tashireva LA — interpretation of results, concept development. All authors participated in the final editing of the article.

Compliance with ethical standards: The study was approved by the Ethics Committee of the Tomsk National Research Medical Center of Oncology (Protocol No. 3 dated August 25, 2020). The work was conducted in accordance with the principles of the Helsinki Declaration (1964) and its amendments (1975 and 1983). All patients provided written informed consent to participate in the study.

Correspondence should be addressed: Evgeniya S. Grigoryeva

Koperativny Lane, str. 7, Tomsk, 634009, Russia; grigoryeva.es@gmail.com

Received: 10.09.2025 Accepted: 08.10.2025 Published online: 16.10.2025

DOI: 10.24075/brsmu.2025.046

Copyright: © 2025 by the authors. Licensee: Pirogov University. This article is an open access article distributed under the terms and conditions of the Creative Commons Attribution (CC BY) license (https://creativecommons.org/licenses/by/4.0/).

# ОСОБЕННОСТИ ТРАНСКРИПТОМНОГО ПРОФИЛЯ FAP+-КЛЕТОК В ОПУХОЛЯХ МОЛОЧНОЙ ЖЕЛЕЗЫ РАЗЛИЧНЫХ МОЛЕКУЛЯРНО-БИОЛОГИЧЕСКИХ ПОДТИПОВ

А. Ю. Калинчук, И. А. Пацкан, М. М. Штадельман, Е. С. Григорьева 🖾, Л. А. Таширева

Томский национальный исследовательский медицинский центр Российской академии наук, Томск, Россия

Понимание подтип-специфичной вариабельности функциональных программ FAP+ опухоль-ассоциированных фибробластов (ОАФ) является фундаментальным для разработки эффективных терапевтических стратегий, нацеленных на стромальные мишени. Целью работы было идентифицировать подтип-специфичные сигнальные пути, маркеры и молекулярные особенности FAP+ ОАФ. Исследовали образцы тканей, полученные от 15 пациенток с раком молочной железы (РМЖ). С помощью пространственного транскриптомного анализа продемонстрировано, что FAP+ ОАФ при люминальном РМЖ проявляют фенотип, характеризующийся организацией внеклеточного матрикса (GO:0030198, FDR q-value = 0,0307) и экспрессией генов, ассоциированных с метастазированием (*COL10A1*, *MMP13*, *CXCL14*, *TSPAN8*). В отличие от этого, FAP+ ОАФ при тройном негативном раке демонстрируют выраженный иммуномодуляторный фенотип со сверхэкспрессией генов иммуносупрессии (*CD36*, *PLA2G2A*, *CHI3L1*) и обогащением сигнальных путей иммунного ответа (иммунный ответ (GO:0006955, FDR q-value = 7,85e-17), ответ на воспальние (GO:0006954, FDR q-value = 2,79e-11), регуляция продукции цитокинов (GO:0001817, FDR q-value = 3,39e-10)). Идентифицированы также подтипспецифичные сигнатуры генов радиорезистентности: люминальные A- и Б-подтипы, показана активация путей репарации ДНК (*IGF1R*, *ERBB3*, *CRIP1*), в то время как тройные негативные опухоли демонстрируют обогащение маркеров эпителиально-мезенхимального перехода и стволовости (*ZEB2*, *NOTCH4*, *FOXM1*). Эти данные подчеркивают, что FAP+-фибробласты не являются однородной популяцией, а функционально специализируются в зависимости от подтипа опухоли, выступая в качестве архитекторов стромы при люминальном раке и регуляторов иммунного ответа при тройном негативном РМЖ.

Ключевые слова: рак молочной железы, опухолевое микроокружение, фибробласты, пространственная транскриптомика

Финансирование: работа выполнена при поддержке Российского научного фонда (грант № 25-65-00021).

**Вклад авторов:** А. Ю. Калинчук — написание и оформление статьи; И. А. Пацкан — биоинформатический анализ; М. М. Штадельман — сбор и анализ данных; Е. С. Григорьева — интерпретация полученных данных; Л. А. Таширева — интерпретация полученных данных, разработка концепции. Все авторы участвовали в финальном редактировании статьи.

Соблюдение этических стандартов: исследование одобрено этическим комитетом НИИ онкологии Томского НИМЦ (Протокол № 3 от 25 августа 2020 г.). Работа выполнена в соответствии с принципами Хельсинкской декларации (1964 г.) и ее поправками (1975 и 1983 гг.). Все пациентки предоставили письменное информированное согласие на участие в исследовании.

Для корреспонденции: Евгения Сергеевна Григорьева

Переулок Кооперативный, д. 7, г. Томск, 634009, Россия; grigoryeva.es@gmail.com

Статья получена: 10.09.2025 Статья принята к печати: 08.10.2025 Опубликована онлайн: 16.10.2025

DOI: 10.24075/vrgmu.2025.046

Авторские права: © 2025 принадлежат авторам. **Лицензиат:** PHИMУ им. Н.И. Пирогова. Статья размещена в открытом доступе и распространяется на условиях лицензии Creative Commons Attribution (CC BY) (https://creativecommons.org/licenses/by/4.0/).

## ОРИГИНАЛЬНОЕ ИССЛЕДОВАНИЕ І ОНКОЛОГИЯ

The heterogeneity of breast cancer (BC) is determined not only by the diversity of tumor cells, but also by the complex cellular composition of the tumor microenvironment [1]. One of the key cell types in the tumor microenvironment are cancer-associated fibroblasts (CAFs), which actively contribute to oncogenesis through multiple mechanisms: extracellular matrix remodeling [2], immunosuppression mediated via physical barrier formation against immunocompetent cells [3], and secretion of proinflammatory cytokines and growth factors that directly promote tumor cell proliferation and angiogenesis [4, 5].

Among the various subpopulations of CAFs, fibroblasts expressing fibroblast activation protein alpha (FAP) are of particular interest due to their critical role in carcinogenesis. In certain carcinomas, elevated FAP expression serves as a universal marker of aggressive tumor stroma and is consistently associated with poor clinical prognosis [6]. However, in breast cancer its significance is controversial. As is well established, the molecular subtype of breast cancer holds significant prognostic value, due in part to the distinct tumor microenvironment characteristics associated with each subtype. Studies utilizing FAP inhibitor conjugated with Technetium-99m ([99mTc]TciFAP) single-photon emission computed tomography (SPECT) have demonstrated that FAP expression significantly correlates with specific molecular subtypes. For instance, Vallejo-Armenta et al. reported a strong positive correlation between radiotracer accumulation in the primary tumor and molecular subtypes. Notably, the authors demonstrated that HER2-enriched and luminal B HER2-positive subtypes exhibited the highest radiotracer uptake ratios, suggesting a more pronounced FAP expression within the stroma of these particularly aggressive breast cancer phenotypes [7]. The association of FAP expression with clinical parameters is further supported by the work of Tchou et al., who confirmed its localization within the tumor stroma and documented heterogeneity depending on various tumor characteristics. However, in their study, differences in the proportion of FAP-expressing cells across molecular subtypes did not reach statistical significance [8]. Another study suggests that certain subsets of CAFs enriched in FAP expression are associated with a subtype of triple-negative breast cancer [9]. Subsequent studies confirmed that fibroblasts in breast cancer represent a heterogeneous population. Croizer H. et al. demonstrated that the luminal A subtype is characterized by numerous clusters containing CAFs that secrete cytokines, including TGFβ, as well as CAFs associated with the extracellular matrix. In contrast, the luminal B, HER2-enriched, and triplenegative subtypes exhibited clusters enriched with CAFs linked to wound healing processes [10]. The study by Kashyap et al. showed that in luminal breast cancer, higher levels of FAP were associated with distant recurrence [11]. Nevertheless, to date, there are no direct data comparing the transcriptomic profiles of FAP+ cells across breast cancer subtypes. At the same time, a key question remains open regarding the extent to which the transcriptomic landscape — and consequently, the functional program — of FAP $^{\scriptscriptstyle +}$  cells varies among the main molecular subtypes of breast cancer. Understanding these subtypespecific differences is critically important for the development of new therapeutic strategies.

Currently, therapy targeting FAP represents one of the most promising directions in oncology. The high and specific expression of FAP on stromal cells within tumors, combined with its almost complete absence in healthy tissues, makes this protein an ideal target for the development of highly selective agents. Various therapeutic modalities targeting FAP are actively being developed and are undergoing clinical trials, including Chimeric Antigen Receptor T-cells (CAR-T

cells), bispecific antibodies, antibody-drug conjugates (ADCs), and radiopharmaceuticals delivering cytotoxic agents directly to the tumor stroma [6]. The success of these innovative approaches directly depends on a deep understanding of the target biology. The heterogeneity of FAP+ cells among breast cancer subtypes may lead to variable drug efficacy, highlighting the need for their stratification. In this study, we conducted a comparative analysis of the transcriptomic profiles of FAP+ cells associated with luminal and triple-negative breast cancer subtypes. Our goal was to identify subtype-specific signaling pathways, markers, and molecular characteristics of this cell population. The obtained data not only deepen the understanding of stromal biology in breast cancer but also have direct translational relevance, providing a rationale for the development and optimization of subtype-specific targeted therapies directed at FAP+ cells.

#### **METHODS**

#### **Patients**

The study included samples from 15 female patients diagnosed with luminal A/B (n=7) and triple-negative (n=8) breast cancer. Inclusion criteria: morphologically confirmed luminal A/B (n=7) and triple negative (n=8) breast cancer. The exclusion criterion was HER2-positive subtypes. Spatial transcriptomic analysis was performed on formalin-fixed, paraffin-embedded (FFPE) tissue sections obtained during trypan-biopsy or surgical intervention before treatment. Detailed descriptions of histological sample preparation, library construction, and sequencing using the 10X Visium platform can be found in the original articles [12, 13]. The sequencing data of breast cancer tissue sections used in this publication are available under GEO series accession number GSE242311.

## **Bioinformatic Data Analysis**

The initial processing of raw data in FASTQ format was performed using Space Ranger v1.3 software (10x Genomics, Pleasanton, CA, USA) with default parameters. Alignment of FASTQ files was carried out against the human reference genome (GRCh38). Aggregation of tissue sections for manual annotation was conducted using the "spaceranger aggr" function. Manual annotation of the sections was performed using Loupe Browser v8.1.2 software (10x Genomics, Pleasanton, CA, USA) and involved identification of spots with FAP expression levels greater than 3, analyzed separately for luminal and triple-negative patients (Fig. 1).

Each selected spot was evaluated by a pathologist to confirm the presence of fibroblasts. Spots lacking fibroblasts were manually excluded from the cluster. Differential gene expression analysis between annotated clusters was conducted using the built-in tools of Loupe Browser v8.1.2 (10x Genomics, Pleasanton, CA, USA). Genes with |log fold change (LFC)| > 0.58 and adjusted p-values (FDR) < 0.05 were considered differentially expressed. To visualize the annotated cell clusters in reduced-dimensional space, the t-SNE (t-Distributed Stochastic Neighbor Embedding) method was applied using Loupe Browser's built-in tools. Functional pathway enrichment analysis was performed using the STRING online resource [14], based on the Gene Ontology database [15], employing lists of differentially expressed genes ranked by expression level and corrected p-values (FDR q-value) obtained from the differential expression analysis. Biological processes with FDR q-value < 0.05 were considered significant. Further analysis was carried out

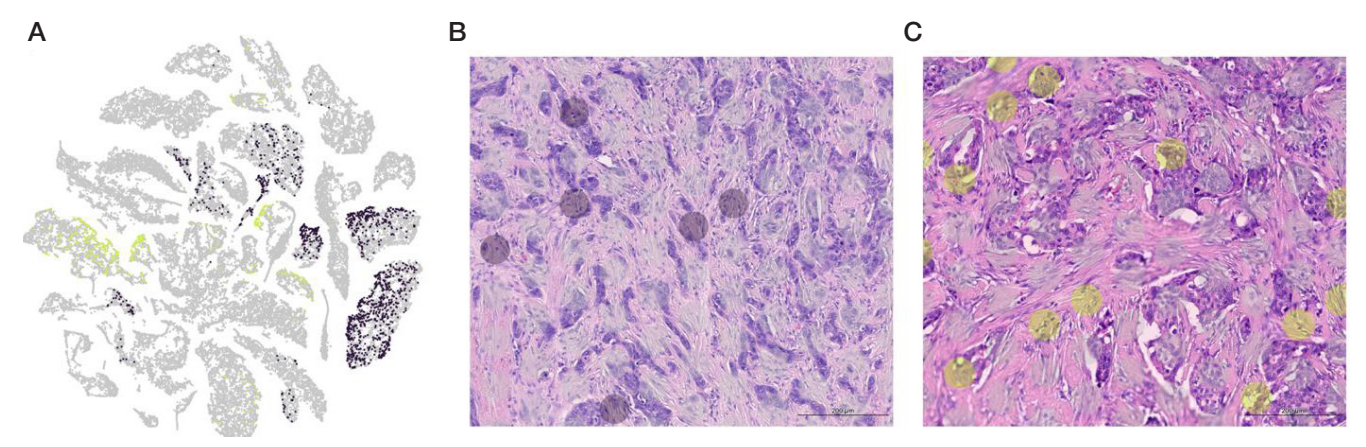


Fig. 1. A. Clusters of FAP+ cells in luminal (blue) and triple-negative (yellow) breast cancer patients obtained by combining data in Space Ranger v1.3 software.

B. Tissue section of a luminal breast tumor with identified FAP+ spots. C. Tissue section of a triple-negative breast tumor with identified FAP+ spots.

in the R environment (https://www.R-project.org/) using the Seurat package (v5.0.0) [16]. Each of the 15 samples was converted into a Seurat object via the "Load10X\_spatial" command and subsequently merged into a single object using the "merge" function. Preprocessing included filtering spots with parameters "nCount\_Spatial" > 500 and "nFeature\_Spatial" > 200. Manual annotation results exported from Loupe Browser v8.1.2 as tables were incorporated into the metadata section of each respective sample.

To generate averaged transcriptomic profiles from the annotated FAP-positive spots for each sample, the "AggregateExpression" function from the Seurat package (v5.0.0) was used with parameters slot = "counts", normalization.method = "LogNormalize", and scale.factor = 10,000. As a result, 15 transcriptomic profiles were obtained, each representing the averaged expression levels across all spots of the corresponding sample. These profiles were normalized using a scaling factor of 10,000 and subjected to logarithmic transformation. For visualization of fibroblast and radioresistance gene signature expression in the studied samples, heatmaps were created in the R environment (https://www.R-project.org/) using the packages pheatmap (v1.0.13) [17], RColorBrewer (v1.1-3) [18], and dplyr (vX.X.X) [19]. The heatmap visualization included a step of Z-score standardization of the target gene expression matrix by rows (genes). Spatial transcriptomic analysis was conducted on formalin-fixed, paraffin-embedded (FFPE) tissue sections obtained during surgery.

## **RESULTS**

## Biological processes enriched in FAP+ regions of luminal and triple-negative breast cancer

To understand the differences in biological processes between the two clusters of luminal and triple-negative tumors, we performed pathway enrichment analysis to identify enriched molecular processes in the transcriptomic data. The most significant pathways were identified from Gene Ontology datasets (Fig. 2).

The conducted study identified key biological processes activated in FAP+ regions of patients with luminal and triple-negative breast cancer. FAP+ spots in luminal breast cancer patients were characterized by activation of morphogenesis (GO:0009887, FDR q-value = 0,00058), tissue development (GO:0009888, FDR q-value = 0,0013), and extracellular matrix organization processes (GO:0030198, FDR q-value = 0,0307), whereas in triple-negative breast cancer patients, immune

signaling pathways predominated, including immune response (GO:0006955, FDR q-value = 7,85e<sup>-17</sup>), inflammatory response (GO:0006954, FDR q-value = 2,79e<sup>-11</sup>), cytokine production regulation (GO:0001817, FDR q-value = 3,39e<sup>-10</sup>), as well as angiogenesis (GO:0001525, FDR q-value = 7,83e<sup>-08</sup>).

### Fibroblast- specific markers in FAP+ tumor regions

Next, we selected fibroblast-specific, highly expressed, and significantly enriched genes in the two groups of breast cancer patients. These genes were annotated as functionally important in cancer development (Fig. 3).

In luminal breast tumors, the list of DEGs included ASPN, COL10A1, COL2A1, OMD, DCN, MMP13, SERPINA1/SERPINA3, PLAT, LRRC15, CXCL14, and TSPAN8, whereas in triple-negative tumors, the genes comprised MMP7, COL4A1, COL4A2, COL15A1, ENG, TGM2, SLC11A1, CHI3L1, PLA2G2A, FDCSP, and CD36.

## Gene signatures associated with resistance to radiotherapy

An important question regarding the characteristics of FAP+cells is their radiosensitivity or resistance, as FAP represents a promising target for radionuclide therapy. In this regard, we selected among the overexpressed genes those that are pathogenetically associated with radioresistance according to the literature data, in two groups of breast cancer patients (Fig. 4).

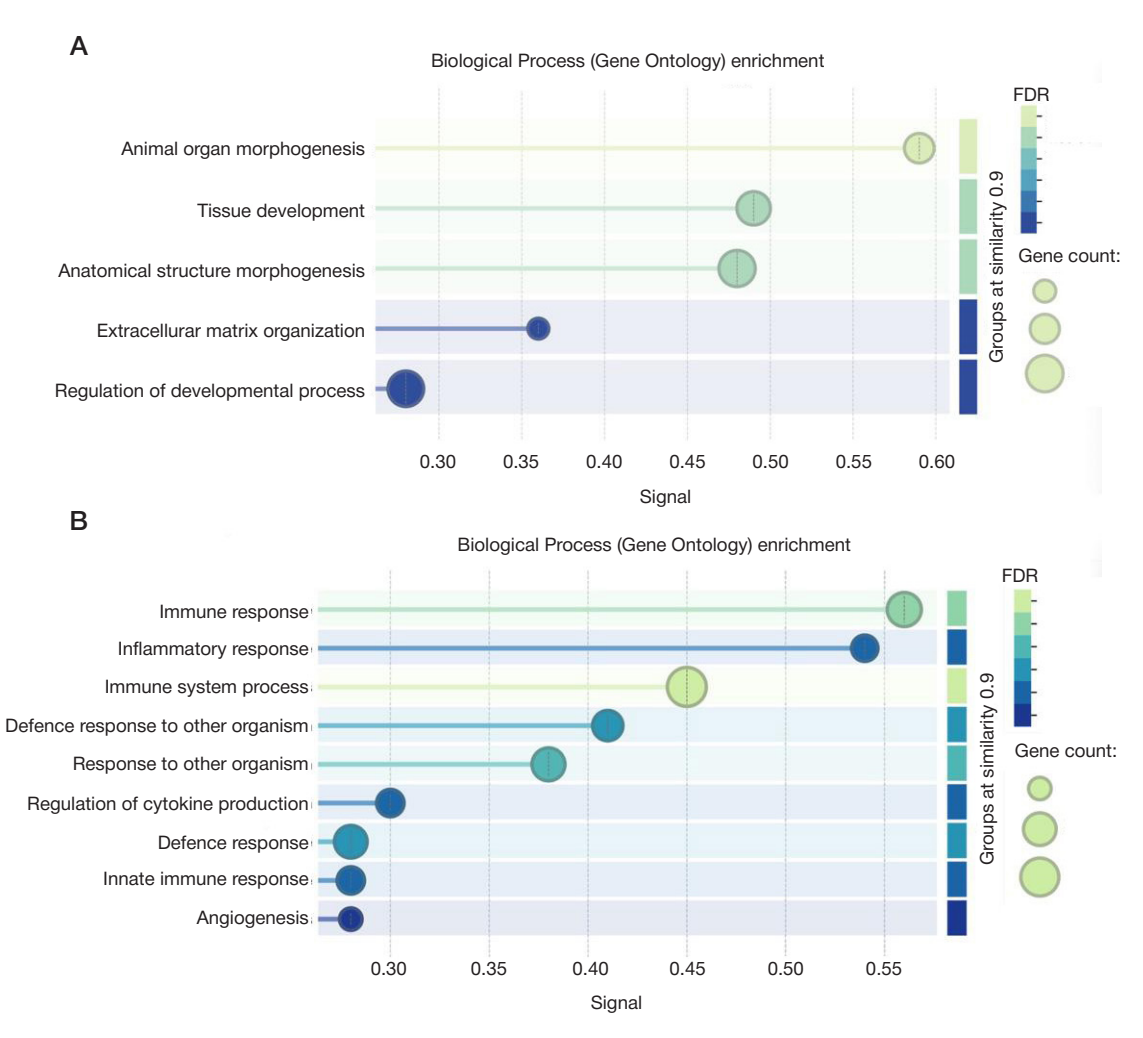
In luminal breast cancer, the expression of genes *IGF1R*, *ERBB3*, *GREB1*, *XBP1*, *SERPINA1/SERPINA3*, *TIMP3*, *FASN*, *IL6ST*, *BCAM*, and *CRIP1* was observed. Meanwhile, in triplenegative tumors, the overexpressed genes included *CD36*, *CX3CL1*, *A2M*, *MYBL2*, *NOTCH4*, *S100A8/S100A9*, *TGM2*, *UBE2C*, *FOXM1*, and *ZEB2*.

#### DISCUSSION

The conducted analysis revealed fundamental differences in the biological functions of FAP+ cells within the microenvironment of luminal and triple-negative breast cancer subtypes. These findings not only highlight the heterogeneity of the tumor stroma but also hold significant implications for the development of personalized therapeutic strategies, particularly for targeted therapy utilizing FAP as a target.

A key finding of our study is the clear distinction in the role of stromal FAP+ cells depending on the molecular subtype of the tumor. In luminal breast cancer, FAP+ cells exhibit pronounced activity in morphogenesis, tissue development, and extracellular matrix organization processes, with no

## ОРИГИНАЛЬНОЕ ИССЛЕДОВАНИЕ І ОНКОЛОГИЯ



 $\textbf{Fig. 2.} \ \ \textbf{Significant signaling pathways activated in FAP} \ \ \textbf{regions of luminal (A)} \ \ \textbf{and triple-negative (B)} \ \ \textbf{breast tumors}$ 

signs of inflammatory response. This is consistent with the identified fibroblast marker genes, such as *COL10A1*, *COL2A1*, *MMP13*, *CXCL14*, and *TSPAN8*. In particular, the high expression of *MMP13* in FAP+ cells indicates active matrix remodeling [20]. Among the identified genes, it is important to highlight those associated with chemoresistance in breast cancer. For instance, the expression of *CXCL14* is a distinctive feature of fibroblasts that enhance metastasis and promote chemoresistance [21] according to mechanistic studies, as is TSPAN8, which is expressed by myofibroblasts [22]. Such a stromal niche likely provides structural support to the tumor, promotes its progression and therapy resistance, creating a dense desmoplastic microenvironment.

In triple-negative breast cancer, FAP+ cells, on the contrary, display a pronounced immunomodulatory and proinflammatory phenotype. Enrichment of signaling pathways related to immune response and cytokine regulation, as well as the overexpression of genes CHI3L1, CD36, and PLA2G2A, indicate active interaction with immune cells in the microenvironment. It is known that CD36+ fibroblasts possess a potent immunosuppressive effect [23] by suppressing macrophage activity, whereas PLA2G2A+ fibroblasts inhibit the effects of CD8+ cytotoxic lymphocytes [24]. It has been shown that fibroblasts can secrete CHI3L1, leading to increased IL8 production and stimulation of angiogenesis [25]. All of this may contribute to the formation of an immunosuppressive microenvironment, tumor evasion from immune surveillance, and the maintenance of chronic inflammation. Thus, the obtained data indicate significant differences in the molecular

signatures of tumor-associated fibroblasts of tumors of different molecular biological subtypes.

Understanding the radiosensitivity of FAP+ cells is critical for the development of FAP-targeted radionuclide therapies. Our data revealed potential bases for the operation of distinct radioresistance mechanisms in the two subtypes. In the luminal subtype, the identified genes indicate activation of survival and repair pathways. IGF1R and ERBB3 are well-known receptor tyrosine kinases mediating radioresistance in malignancies [26, 27]. It has been shown that the gene *SERPINA1* is associated with radioresistance in lung cancer [28], whereas inhibition of *FASN* improves radiotherapy outcomes in breast cancer [29]. Another gene, *CRIP1*, can interact with BRCA2, enhancing DNA repair during chemotherapy [30]. This suggests that radioresistance in this subtype may be mediated through enhanced DNA repair.

In triple-negative breast cancer, the radioresistance gene signature is broader and is associated with epithelial-mesenchymal transition (EMT) and stemness. ZEB2 and NOTCH4 are key inducers of EMT, which is linked to therapy resistance [31, 32, 33]. FOXM1 and UBE2C regulate the cell cycle and mitosis, contributing to the rapid recovery of the tumor cell population [34, 35]. Moreover, enhanced DNA repair dependent on FoxO3a/FoxM1 may play a key role in the survival of fibroblasts resistant to cell death following irradiation [36]. TGM2 gene is also associated with radioresistance [37]. This suggests that in triple-negative breast cancer, resistance may be associated with the presence of a population of stem-like tumor cells exhibiting mesenchymal characteristics.

#### Fibroblast Signature (Pseudobulk)

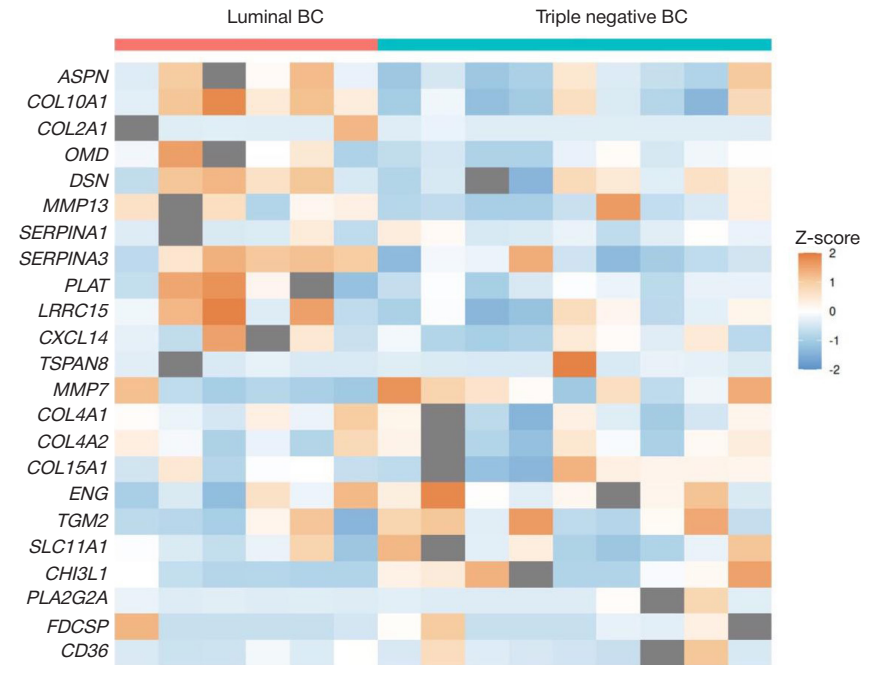


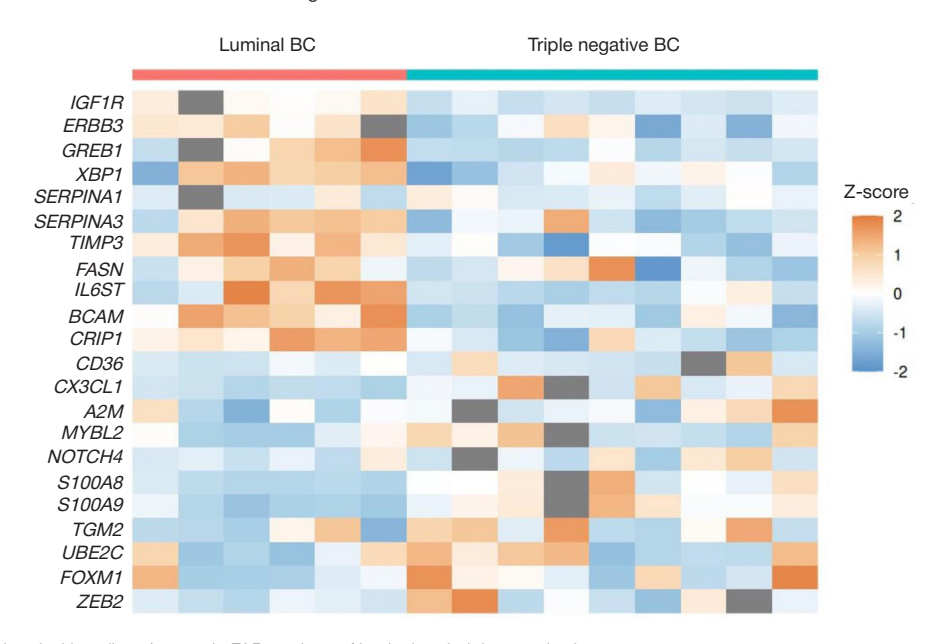
Fig. 3. Fibroblast-specific genes in FAP+ regions of luminal and triple-negative breast tumors

Our study demonstrates that FAP+ fibroblasts are not a homogeneous population but functionally adapt to the molecular subtype specificity. In luminal breast cancer, they act as architects of the stroma, whereas in triple-negative breast cancer, they function as immune regulators and promoters of angiogenesis. The identification of distinct gene sets associated with radioresistance suggests that resistance cases may occur during FAP-targeted radionuclide therapy, warranting the proactive development of strategies to overcome it.

#### **CONCLUSIONS**

The study enabled the identification of highly specific transcriptomic profiles of FAP+ stroma of luminal and triple-negative breast tumors, clearly reflecting the biology of molecular subtypes of breast cancer. The obtained data emphasize the necessity of considering the tumor's molecular subtype when developing stroma-targeted therapies and open new avenues for creating personalized combination treatments aimed at specific resistance mechanisms within the tumor microenvironment.

#### Radioresistance Signature



 $\textbf{Fig. 4.} \ \textbf{Genes associated with radioresistance in FAP}^+ \ \textbf{regions of luminal and triple-negative breast tumors}$ 

#### References

- Soongsathitanon J, Jamjuntra P, Sumransub N, Yangngam S, de la Fuente M, Landskron G, et al. Crosstalk between tumor-infiltrating immune cells and cancer-associated fibroblasts in tumor growth and immunosuppression of breast cancer. J Immunol Res. 2021; 2021: 8840066. DOI: 10.1155/2021/8840066.
- Ohlund D, Elyada E, Tuveson D. Fibroblast heterogeneity in the cancer wound. J Exp Med. 2014; 211 (8): 1503–23. DOI: 10.1084/jem.20140692.
- 3. Liu T, Zhou L, Li D, Andl T, Zhang Y. Cancer-associated fibroblasts build and secure the tumor microenvironment. Front Cell Dev Biol. 2019; 7: 60. DOI: 10.3389/fcell.2019.00060.
- Ershaid N, Sharon Y, Doron H, Raz Y, Shani O, Cohen N, et al. Nlrp3 inflammasome in fibroblasts links tissue damage with inflammation in breast cancer progression and metastasis. Nat Commun. 2019; 10 (1): 4375. DOI: 10.1038/s41467-019-12370-8.
- Suh J, Kim DH, Lee YH, Jang JH, Surh YJ. Fibroblast growth factor-2, derived from cancer-associated fibroblasts, stimulates growth and progression of human breast cancer cells via Fgfr1 signaling. Mol Carcinog. 2020; 59 (9): 1028–40. DOI: 10.1002/mc.23233.
- Fitzgerald AA, Weiner LM. The role of fibroblast activation protein in health and malignancy. Cancer Metastasis Rev. 2020; 39 (3): 783–803. DOI: 10.1007/s10555-020-09909-3.
- Vallejo-Armenta P, Ferro-Flores G, Santos-Cuevas C, García-Pérez FO, Casanova-Triviño P, Sandoval-Bonilla B, et al. [99mTc] Tc-iFAP/SPECT tumor stroma imaging: acquisition and analysis of clinical images in six different cancer entities. Pharmaceuticals (Basel). 2022;15(6):729. DOI: 10.3390/ph15060729.
- Tchou J, Zhang PJ, Bi Y, Satija C, Marjumdar R, Stephen TL, et al. Fibroblast activation protein expression by stromal cells and tumorassociated macrophages in human breast cancer. Hum Pathol. 2013; 44 (11): 2549–57. DOI: 10.1016/j.humpath.2013.06.016.
- Mohammed Ali DA, Salah H. Immunohistochemical study of fibroblast activation protein and α-smooth muscle actin expression and distribution in triple negative breast cancer. Int J Cancer Biomed Res. 2020; 4 (1): 27–34. DOI: 10.21608/jcbr.2020.26388.1020.
- Croizer H, Mhaidly R, Kieffer Y, et al. Deciphering the spatial landscape and plasticity of immunosuppressive fibroblasts in breast cancer. Nat Commun. 2024; 15: 2806. DOI: 10.1038/s41467-024-47068-z.
- 11. Bonneau C, Eliès A, Kieffer Y, Bourachot B, Ladoire S, Pelon F, et al. A subset of activated fibroblasts is associated with distant relapse in early luminal breast cancer. Breast Cancer Res. 2020; 22 (1): 76. DOI: 10.1186/s13058-020-01311-9.
- Tashireva L, Grigoryeva E, Alifanov V, lamshchikov P, Zavyalova M, Perelmuter V, et al. Spatial Heterogeneity of Integrins and Their Ligands in Primary Breast Tumors. Discov Med. 2023; 35 (178): 910–20. DOI: 10.24976/Discov.Med.202335178.86.
- Tashireva LA, Kalinchuk AY, Gerashchenko TS, Menyailo M, Khozyainova A, Denisov EV, Perelmuter VM, et al. Spatial Profile of Tumor Microenvironment in PD-L1-Negative and PD-L1-Positive Triple-Negative Breast Cancer. Int J Mol Sci. 2023; 24 (2): 1433. DOI: 10.3390/ijms24021433.
- 14. Szklarczyk D, Kirsch R, Koutrouli M, Nastou K, Mehryary F, Hachilif R, et al. The STRING database in 2023: protein-protein association networks and functional enrichment analyses for any sequenced genome of interest. Nucleic Acids Res. 2023; 51 (D1): D638–D646. DOI: 10.1093/nar/gkac1000.
- The Gene Ontology Consortium, et al. The Gene Ontology knowledgebase in 2023. Genetics. 2023; 224 (1): iyad031. DOI: 10.1093/genetics/iyad031.
- Hao Y, Stuart T, Kowalski MH, et al. Dictionary learning for integrative, multimodal and scalable single-cell analysis. Nat Biotechnol. 2024; 42 (2): 293–304. DOI: 10.1038/s41587-023-01767-y.
- Kolde R, et al. pheatmap: Pretty Heatmaps. R package version 1.0.13.
   2025. Available from: https://CRAN.R-project.org/package=pheatmap.
- Neuwirth E, et al. RColorBrewer: ColorBrewer Palettes. R package version 1.1-3. 2022. Available from: https://CRAN.R-project.org/ package=RColorBrewer.
- Wickham H, François R, Henry L, Müller K, Vaughan D, et al. dplyr: A Grammar of Data Manipulation. R package version 1.1.4. 2025. Available from: https://dplyr.tidyverse.org.

- Sun X, Hu X. Unveiling matrix metalloproteinase 13's dynamic role in breast cancer: a link to physical changes and prognostic modulation. Int J Mol Sci. 2025; 26 (7): 3083. DOI: 10.3390/ijms26073083.
- 21. Xu W, Yang H, Xu K, Zhu A, Hall SRR, Jia Y, et al. Transitional CXCL14+ cancer-associated fibroblasts enhance tumour metastasis and confer resistance to EGFR-TKIs, revealing therapeutic vulnerability to filgotinib in lung adenocarcinoma. Clin Transl Med. 2025; 15 (4): e70281. DOI: 10.1002/ctm2.70281.
- 22. Fan G, Yu B, Tang L, Zhu R, Chen J, Zhu Y, et al. TSPAN8+ myofibroblastic cancer-associated fibroblasts promote chemoresistance in patients with breast cancer. Sci Transl Med. 2024; 16 (741): eadj5705. DOI: 10.1126/scitranslmed.adj5705.
- 23. Zhu GQ, Tang Z, Huang R, et al. CD36+ cancer-associated fibroblasts provide immunosuppressive microenvironment for hepatocellular carcinoma via secretion of macrophage migration inhibitory factor. Cell Discov. 2023; 9: 25. DOI: 10.1038/s41421-023-00529-z.
- 24. Ge W, Yue M, Lin R, Zhou T, Xu H, Wang Y, et al. PLA2G2A+ cancer-associated fibroblasts mediate pancreatic cancer immune escape via impeding antitumor immune response of CD8+ cytotoxic T cells. Cancer Lett. 2023; 558: 216095. DOI: 10.1016/j.canlet.2023.216095.
- 25. Watanabe K, Shiga K, Maeda A, Harata S, Yanagita T, Suzuki T, et al. Chitinase 3-like 1 secreted from cancer-associated fibroblasts promotes tumor angiogenesis via interleukin-8 secretion in colorectal cancer. Int J Oncol. 2022; 60 (1): 3. DOI: 10.3892/ijo.2021.5293.
- Simpson AD, Soo YWJ, Rieunier G, et al. Type 1 IGF receptor associates with adverse outcome and cellular radioresistance in paediatric high-grade glioma. Br J Cancer. 2020; 122: 624–9. DOI: 10.1038/s41416-019-0677-1.
- Chen Y, Lu A, Hu Z, Li J, Lu J. ERBB3 targeting: a promising approach to overcoming cancer therapeutic resistance. Cancer Lett. 2024; 599: 217146. DOI: 10.1016/j.canlet.2024.217146.
- Huang W, Ding X. Serum biomarkers analyzed by LC-MS/MS as predictors for short outcome of non-small cell lung cancer patients treated with chemoradiotherapy. Neoplasma. 2013; 60: 11–18.
- 29. Chen CI, Kuo DY, Chuang HY. FASN inhibition shows the potential for enhancing radiotherapy outcomes by targeting glycolysis, AKT, and ERK pathways in breast cancer. Int J Radiat Biol. 2025; 101 (3): 292–303. DOI: 10.1080/09553002.2024.2446585.
- Sun H, Zhou R, Zheng Y, et al. CRIP1 cooperates with BRCA2 to drive the nuclear enrichment of RAD51 and to facilitate homologous repair upon DNA damage induced by chemotherapy. Oncogene. 2021; 40: 5342–55. DOI: 10.1038/s41388-021-01932-0.
- Sánchez-Tilló E, Siles L, de Barrios O, Cuatrecasas M, Vaquero EC, Castells A, et al. Expanding roles of ZEB factors in tumorigenesis and tumor progression. Am J Cancer Res. 2011; 1 (7): 897–912
- Vandamme N, Denecker G, Bruneel K, et al. The EMT transcription factor ZEB2 promotes proliferation of primary and metastatic melanoma while suppressing an invasive, mesenchymallike phenotype. Cancer Res. 2020; 80 (14): 2983–95. DOI: 10.1158/0008-5472.CAN-19-2373.
- 33. Yahyanejad S, Theys J, Vooijs M. Targeting Notch to overcome radiation resistance. Oncotarget. 2016;7(7):7610-28. DOI: 10.18632/oncotarget.6714.
- Xiu G, Sui X, Wang Y, Zhang Z. FOXM1 regulates radiosensitivity of lung cancer cell partly by upregulating KIF20A. Eur J Pharmacol. 2018; 833: 79–85. DOI: 10.1016/j.ejphar.2018.04.021.
- 35. Zhao M, Li J, Wang R, Mi L, Gu Y, Chen R, et al. Ubiquitination-binding enzyme 2C is associated with cancer development and prognosis and is a potential therapeutic target. Onco Targets Ther. 2024; 17: 1159–71. DOI: 10.2147/OTT.S485053.
- Im J, Lawrence J, Seelig D, et al. FoxM1-dependent RAD51 and BRCA2 signaling protects idiopathic pulmonary fibrosis fibroblasts from radiation-induced cell death. Cell Death Dis. 2018; 9: 584. DOI: 10.1038/s41419-018-0652-4.
- 37. Sun C, Du Z, Yang W, Wang Q. Transglutaminase 2 nuclear localization enhances glioblastoma radiation resistance. Discov Oncol. 2025; 16 (1): 952. DOI: 10.1007/s12672-025-02599-9.

#### Литература

- Soongsathitanon J, Jamjuntra P, Sumransub N, Yangngam S, de la Fuente M, Landskron G, et al. Crosstalk between tumor-infiltrating immune cells and cancer-associated fibroblasts in tumor growth and immunosuppression of breast cancer. J Immunol Res. 2021; 2021: 8840066. DOI: 10.1155/2021/8840066.
- Ohlund D, Elyada E, Tuveson D. Fibroblast heterogeneity in the cancer wound. J Exp Med. 2014; 211 (8): 1503–23. DOI: 10.1084/iem.20140692.
- 3. Liu T, Zhou L, Li D, Andl T, Zhang Y. Cancer-associated fibroblasts build and secure the tumor microenvironment. Front Cell Dev Biol. 2019; 7: 60. DOI: 10.3389/fcell.2019.00060.
- Ershaid N, Sharon Y, Doron H, Raz Y, Shani O, Cohen N, et al. Nlrp3 inflammasome in fibroblasts links tissue damage with inflammation in breast cancer progression and metastasis. Nat Commun. 2019; 10 (1): 4375. DOI: 10.1038/s41467-019-12370-8.
- Suh J, Kim DH, Lee YH, Jang JH, Surh YJ. Fibroblast growth factor-2, derived from cancer-associated fibroblasts, stimulates growth and progression of human breast cancer cells via Fgfr1 signaling. Mol Carcinog. 2020; 59 (9): 1028–40. DOI: 10.1002/mc.23233.
- Fitzgerald AA, Weiner LM. The role of fibroblast activation protein in health and malignancy. Cancer Metastasis Rev. 2020; 39 (3): 783–803. DOI: 10.1007/s10555-020-09909-3.
- Vallejo-Armenta P, Ferro-Flores G, Santos-Cuevas C, García-Pérez FO, Casanova-Triviño P, Sandoval-Bonilla B, et al. [99mTc] Tc-iFAP/SPECT tumor stroma imaging: acquisition and analysis of clinical images in six different cancer entities. Pharmaceuticals (Basel). 2022;15(6):729. DOI: 10.3390/ph15060729.
- Tchou J, Zhang PJ, Bi Y, Satija C, Marjumdar R, Stephen TL, et al. Fibroblast activation protein expression by stromal cells and tumorassociated macrophages in human breast cancer. Hum Pathol. 2013; 44 (11): 2549–57. DOI: 10.1016/j.humpath.2013.06.016.
- Mohammed Ali DA, Salah H. Immunohistochemical study of fibroblast activation protein and α-smooth muscle actin expression and distribution in triple negative breast cancer. Int J Cancer Biomed Res. 2020; 4 (1): 27–34. DOI: 10.21608/jcbr.2020.26388.1020.
- Croizer H, Mhaidly R, Kieffer Y, et al. Deciphering the spatial landscape and plasticity of immunosuppressive fibroblasts in breast cancer. Nat Commun. 2024; 15: 2806. DOI: 10.1038/s41467-024-47068-z.
- Bonneau C, Eliès A, Kieffer Y, Bourachot B, Ladoire S, Pelon F, et al. A subset of activated fibroblasts is associated with distant relapse in early luminal breast cancer. Breast Cancer Res. 2020; 22 (1): 76. DOI: 10.1186/s13058-020-01311-9.
- Tashireva L, Grigoryeva E, Alifanov V, lamshchikov P, Zavyalova M, Perelmuter V, et al. Spatial Heterogeneity of Integrins and Their Ligands in Primary Breast Tumors. Discov Med. 2023; 35 (178): 910–20. DOI: 10.24976/Discov.Med.202335178.86.
- Tashireva LA, Kalinchuk AY, Gerashchenko TS, Menyailo M, Khozyainova A, Denisov EV, Perelmuter VM, et al. Spatial Profile of Tumor Microenvironment in PD-L1-Negative and PD-L1-Positive Triple-Negative Breast Cancer. Int J Mol Sci. 2023; 24 (2): 1433. DOI: 10.3390/ijms24021433.
- 14. Szklarczyk D, Kirsch R, Koutrouli M, Nastou K, Mehryary F, Hachilif R, et al. The STRING database in 2023: protein-protein association networks and functional enrichment analyses for any sequenced genome of interest. Nucleic Acids Res. 2023; 51 (D1): D638–D646. DOI: 10.1093/nar/gkac1000.
- The Gene Ontology Consortium, et al. The Gene Ontology knowledgebase in 2023. Genetics. 2023; 224 (1): iyad031. DOI: 10.1093/genetics/iyad031.
- Hao Y, Stuart T, Kowalski MH, et al. Dictionary learning for integrative, multimodal and scalable single-cell analysis. Nat Biotechnol. 2024; 42 (2): 293–304. DOI: 10.1038/s41587-023-01767-y.
- Kolde R, et al. pheatmap: Pretty Heatmaps. R package version 1.0.13.
   2025. Available from: https://CRAN.R-project.org/package=pheatmap.
- Neuwirth E, et al. RColorBrewer: ColorBrewer Palettes. R package version 1.1-3. 2022. Available from: https://CRAN.R-project.org/ package=RColorBrewer.
- Wickham H, François R, Henry L, Müller K, Vaughan D, et al. dplyr: A Grammar of Data Manipulation. R package version 1.1.4. 2025. Available from: https://dplyr.tidyverse.org.

- Sun X, Hu X. Unveiling matrix metalloproteinase 13's dynamic role in breast cancer: a link to physical changes and prognostic modulation. Int J Mol Sci. 2025; 26 (7): 3083. DOI: 10.3390/ijms26073083.
- 21. Xu W, Yang H, Xu K, Zhu A, Hall SRR, Jia Y, et al. Transitional CXCL14+ cancer-associated fibroblasts enhance tumour metastasis and confer resistance to EGFR-TKls, revealing therapeutic vulnerability to filgotinib in lung adenocarcinoma. Clin Transl Med. 2025; 15 (4): e70281. DOI: 10.1002/ctm2.70281.
- 22. Fan G, Yu B, Tang L, Zhu R, Chen J, Zhu Y, et al. TSPAN8+ myofibroblastic cancer-associated fibroblasts promote chemoresistance in patients with breast cancer. Sci Transl Med. 2024; 16 (741): eadj5705. DOI: 10.1126/scitranslmed.adj5705.
- 23. Zhu GQ, Tang Z, Huang R, et al. CD36+ cancer-associated fibroblasts provide immunosuppressive microenvironment for hepatocellular carcinoma via secretion of macrophage migration inhibitory factor. Cell Discov. 2023; 9: 25. DOI: 10.1038/s41421-023-00529-z.
- 24. Ge W, Yue M, Lin R, Zhou T, Xu H, Wang Y, et al. PLA2G2A+ cancer-associated fibroblasts mediate pancreatic cancer immune escape via impeding antitumor immune response of CD8+ cytotoxic T cells. Cancer Lett. 2023; 558: 216095. DOI: 10.1016/j.canlet.2023.216095.
- 25. Watanabe K, Shiga K, Maeda A, Harata S, Yanagita T, Suzuki T, et al. Chitinase 3-like 1 secreted from cancer-associated fibroblasts promotes tumor angiogenesis via interleukin-8 secretion in colorectal cancer. Int J Oncol. 2022; 60 (1): 3. DOI: 10.3892/ijo.2021.5293.
- Simpson AD, Soo YWJ, Rieunier G, et al. Type 1 IGF receptor associates with adverse outcome and cellular radioresistance in paediatric high-grade glioma. Br J Cancer. 2020; 122: 624–9. DOI: 10.1038/s41416-019-0677-1.
- 27. Chen Y, Lu A, Hu Z, Li J, Lu J. ERBB3 targeting: a promising approach to overcoming cancer therapeutic resistance. Cancer Lett. 2024; 599: 217146. DOI: 10.1016/j.canlet.2024.217146.
- Huang W, Ding X. Serum biomarkers analyzed by LC-MS/MS as predictors for short outcome of non-small cell lung cancer patients treated with chemoradiotherapy. Neoplasma. 2013; 60: 11–18.
- 29. Chen CI, Kuo DY, Chuang HY. FASN inhibition shows the potential for enhancing radiotherapy outcomes by targeting glycolysis, AKT, and ERK pathways in breast cancer. Int J Radiat Biol. 2025; 101 (3): 292–303. DOI: 10.1080/09553002.2024.2446585.
- Sun H, Zhou R, Zheng Y, et al. CRIP1 cooperates with BRCA2 to drive the nuclear enrichment of RAD51 and to facilitate homologous repair upon DNA damage induced by chemotherapy. Oncogene. 2021; 40: 5342–55. DOI: 10.1038/s41388-021-01932-0.
- Sánchez-Tilló E, Siles L, de Barrios O, Cuatrecasas M, Vaquero EC, Castells A, et al. Expanding roles of ZEB factors in tumorigenesis and tumor progression. Am J Cancer Res. 2011; 1 (7): 897–912.
- Vandamme N, Denecker G, Bruneel K, et al. The EMT transcription factor ZEB2 promotes proliferation of primary and metastatic melanoma while suppressing an invasive, mesenchymallike phenotype. Cancer Res. 2020; 80 (14): 2983–95. DOI: 10.1158/0008-5472.CAN-19-2373.
- 33. Yahyanejad S, Theys J, Vooijs M. Targeting Notch to overcome radiation resistance. Oncotarget. 2016;7(7):7610-28. DOI: 10.18632/oncotarget.6714.
- Xiu G, Sui X, Wang Y, Zhang Z. FOXM1 regulates radiosensitivity of lung cancer cell partly by upregulating KIF20A. Eur J Pharmacol. 2018; 833: 79–85. DOI: 10.1016/j.ejphar.2018.04.021.
- 35. Zhao M, Li J, Wang R, Mi L, Gu Y, Chen R, et al. Ubiquitination-binding enzyme 2C is associated with cancer development and prognosis and is a potential therapeutic target. Onco Targets Ther. 2024; 17: 1159–71. DOI: 10.2147/OTT.S485053.
- 36. Im J, Lawrence J, Seelig D, et al. FoxM1-dependent RAD51 and BRCA2 signaling protects idiopathic pulmonary fibrosis fibroblasts from radiation-induced cell death. Cell Death Dis. 2018; 9: 584. DOI: 10.1038/s41419-018-0652-4.
- Sun C, Du Z, Yang W, Wang Q. Transglutaminase 2 nuclear localization enhances glioblastoma radiation resistance. Discov Oncol. 2025; 16 (1): 952. DOI: 10.1007/s12672-025-02599-9.

# OPTIMIZATION OF HUMAN B CELL CULTURE CONDITIONS FOR EXPANSION OF ACTIVATED OR DIFFERENTIATED B CELLS

Sokolova SR, Grigorova IL™

Pirogov Russian National Research Medical University, Moscow, Russia

In vitro B cell cutures are important for fundamental and translational research and can be used to study antigenic specificity of B and T cells, as well as to produce monoclonal antibodies and other biopharmaceuticals. That is why the development of an optimal protocol for culturing of activated B cells, antibody-secreting cells (ASCs), and germinal center (GC) B cells in vitro remains an important task. The study aimed to find the conditions ensuring the following: high B cell expansion and survival rates, ASC accumulation, GC B cell production and accumulation. For that the CD27<sup>-</sup> and/or CD27<sup>+</sup> B cells from human peripheral blood were cultured in the presence of the feeder 3T3-hCD40L line, various combinations of cytokines (IL21, IL4, BAFF), human serum components or under the control conditions throughout 7 days. Flow cytometry analysis of B cell cultures showed that the combined presence of CD40L and IL21 was essential for achieving high B cell expansion, survival, and differentiation with the production of the CD27<sup>high</sup>CD38<sup>high</sup> ASCs and CD95<sup>high</sup>Bcl-6<sup>+</sup> GC-like B cells. The highest expansion was observed in the cultures of CD27<sup>-</sup> naïve cells in the presence of human serum components. The IL4 supplementation moderately increased the share of GC-like B cells. The maximum ASC accumulation was observed in the cultures of CD27<sup>+</sup> memory B cells. The approach developed made it possible to find the optimal conditions for in vitro B cell culturing and clearly demonstrated the impact of both individual IL-21, IL-4, BAFF cytokines and their combinations on the B cell cultures of various subpopulations.

Keywords: B cells, antibody-secreting cells (ASCs), germinal center (GC) B cells, human lymphocytes cultures in vitro, 3T3-hCD40L

Funding: the study was supported by the Russian Science Foundation (grant No. 24-15-00545).

Acknowledgements: the authors express their gratitude to E. Zakatina for assistance in manuscript editing.

**Author contribution:** Grigorova IL — study design, concept of the article, editing, approval of the final version of the article; Sokolova SR — experimental procedure, processing of the results, manuscript writing.

Compliance with ethical standards: the study was approved by the Ethics Committee of the Pirogov Russian National Research Medical University (protocol No. 240 date 23 May 2024). All subjects signed the informed consent for participation in the study.

Correspondence should be addressed: Irina L. Grigorova Ostrovityanova, 1, Moscow, 117997, Russia; grig76@gmail.com

 $\textbf{Received:}\ 26.09.2025\ \textbf{Accepted:}\ 10.10.2025\ \textbf{Published online:}\ 30.10.2025$ 

DOI: 10.24075/brsmu.2025.053

Copyright: © 2025 by the authors. Licensee: Pirogov University. This article is an open access article distributed under the terms and conditions of the Creative Commons Attribution (CC BY) license (https://creativecommons.org/licenses/by/4.0/).

# ОПТИМИЗАЦИЯ УСЛОВИЙ КУЛЬТИВИРОВАНИЯ В-КЛЕТОК ЧЕЛОВЕКА ДЛЯ ЭКСПАНСИИ АКТИВИРОВАННЫХ ИЛИ ДИФФЕРЕНЦИРОВАННЫХ В-КЛЕТОК

С. Р. Соколова, И. Л. Григорова 🖾

Российский национальный исследовательский медицинский университет имени Н. И. Пирогова, Москва, Россия

Культуры В-клеток *in vitro* имеют важное значение для фундаментальной и прикладной науки: они могут быть использованы для изучения антигенной специфичности В- и Т-клеток, а также для получения моноклональных антител и других биопрепаратов. Поэтому создание оптимальных протоколов культивирования активированных В-клеток, антитело-секретирующих клеток (АСК) и В-клеток герминативных центров (ГЦ) *in vitro* остается актуальной задачей. Целю работы было подобрать условия, обеспечивающие: высокий уровень экспансии и выживаемости В-клеток, накопление АСК, образование и накопление В-клеток ГЦ. Для этого В-клетки CD27- и/или CD27- из периферической крови человека культивировали в присутствии фидерной линии 3Т3-hCD40L, различных комбинаций цитокинов (IL21, IL4, BAFF), компонентов человеческой сыворотки или в контрольных условиях в течение 7 дней. Цитофлуориметрический анализ В-клеточных культур показал, что совместное присутствие CD40L и IL21 необходимо для достижения высокой экспансии, выживаемости и дифференцировки В-клеток с образованием CD27<sup>high</sup>CD38<sup>high</sup> АСК и CD95<sup>high</sup>BcI-6+ ГЦ-подобных клеток. Наибольшая экспансия наблюдалась в культурах из CD27- наивных клеток в присутствии компонентов человеческой сыворотки, добавление IL4 умеренно повышало долю ГЦ-подобных клеток. Максимальное накопление АСК наблюдалось в культурах из CD27+В-клетки памяти. Разработанный подход позволил подобрать оптимальные условия для культивирования В-клеток *in vitro*, а также наглядно продемонстрировал влияние как отдельных цитокинов IL-21, IL-4, BAFF, так и их комбинаций на В-клеточные культуры из различных субпопуляций.

Ключевые слова: В-клетки, антитело-секретирующие клетки, АСК, В-клетки герминативных центров, ГЦ, культуры лимфоцитов человека in vitro, 3T3-CD40L

Финансирование: исследование выполнено при финансовой поддержке Российского научного фонда (грант № 24-15-00545).

Благодарности: авторы благодарны Е. Закатиной за помощь в редактировании статьи.

**Вклад авторов:** И. Л. Григорова — дизайн исследования, концепция статьи, редактирование, утверждение конечного варианта статьи; С. Р. Соколова — постановка экспериментов, обработка результатов, написание текста.

Соблюдение этических стандартов: исследование одобрено этическим комитетом РНИМУ имени Н. И. Пирогова (протокол № 240 от 23 мая 2024 г.). Все участники подписали добровольное информированное согласие на участие в исследовании.

Для корреспонденции: Ирина Леонидовна Григорова ул. Островитянова, д. 1, г. Москва, 117997, Россия; grig76@gmail.com

Статья получена: 26.09.2025 Статья принята к печати: 10.10.2025 Опубликована онлайн: 30.10.2025

DOI: 10.24075/vrgmu.2025.053

Авторские права: © 2025 принадлежат авторам. Лицензиат: РНИМУ им. Н. И. Пирогова. Статья размещена в открытом доступе и распространяется на условиях лицензии Creative Commons Attribution (CC BY) (https://creativecommons.org/licenses/by/4.0/).

B cells and the antibodies they produce provide an effective immune response to pathogens and vaccines. Through antigendependent differentiation, naive B cells differentiate to antibody-secreting cells (ASCs) and memory cells [1]. In addition to providing a humoral immune response, B cells can function as antigen-presenting cells (APCs) [2]. Upon binding of antigen to B cell receptor (BCR), the complex is internalized by B cells and the processed peptides are then presented on their surface in a complex with MHCII for subsequent interaction with CD4+T helper (Th) cells [3]. Key signals to B cells from cellular cooperation with Th cells include CD40-CD40L interaction as well as secreted cytokines IL-21 and IL-4 [4]. Upon acquisition of T cell help B cells undergo proliferation and differentiate either into short-lived ASCs or germinal center (GC) B cells (a fate driven by master transcription factor BCL6) [5, 6].

The unique properties of B cells make the *in vitro* cell cultivation critical for various applications such as obtaining APCs for analyzing antigen-specific T-cell responses as well as ASCs for antibody production [7, 8], and creating cell models for studying lymphomas [9]. Numerous studies have investigated how CD40L, T-cell cytokines and microenvironment factors such as BAFF influence B-cell cultures to promote proliferation, class switching, and antibody-secreting cell (ASC) formation [10–12]. However, studies on *in vitro* BCL6+ GC B cell formation from human B cells are still limited. The aim of the work was to find optimal conditions to expand B cells and to efficiently turn them into antibody-secreting cells (ASCs) or germinal center (GC) cells *in vitro*.

In our study, we analyzed human peripheral blood naive B cells and CD27 $^{+}$  memory B cells cultured with T-cell signals (CD40L, IL-21, IL-4), BAFF, and additional medium components. We also assessed B-cell expansion, and accumulation of ASC and BCL6 $^{+}$  B cells.

**METHODS** 

## pcDNA-hCD40LG Plasmid Design

Human CD40LG gene sequence (NM\_000074.3) was obtained using polymerase chain reaction (PCR) from total cDNA of human peripheral blood mononuclear cells (MC) using forward 5'-ATATGGATCCGCCACCATGATCGAAACATACAACCA-3' and reverse 5'-ATATGAATTCACACTGTTCAGAGTTTGAGT AAGCC-3' primers. The primer sequences included BamHI and EcoRI restriction sites at their 5' and 3' ends of CD40LG gene, respectively, as well as Kozak sequence (GCCACCATG) at the 5' end of the gene. After digestion of PCR product and pcDNA3.1+ vector (Thermo Fisher Scientific, USA, Cat. No. V79020) using restriction endonucleases BamHI-HF and EcoRI-HF (New England Biolabs, USA, Cat. Nos. R3136 and R3101), they were ligated using the Quick Ligation™ Kit (New England Biolabs, USA, Cat. No. M2200) and transformed into E. coli (strain NEB Stable, New England Biolabs, USA, Cat. No. C3040H). The plasmid was purified and isolated using the Plasmid Miniprep 2.0 kit (Evrogen, Russia, Cat. No. BC221) for further transfection.

## Generation of a Mouse Fibroblast Feeder Line Expressing Human CD40L (3T3-hCD40L)

3T3-hCD40L feeder line was generated from NIH 3T3 mouse fibroblast cell line from the cell culture collection of the D. I. Ivanovsky Institute of Virology. NIH 3T3 cells were cultured in DMEM (PanEco, Russia, Cat. No. C415p) supplemented with 10% fetal bovine serum (FBS, STEMCELL Technologies, Canada,

Cat. No. 06472) and 1× penicillin/streptomycin antibiotic mixture (PanEco, Russia, Cat. No. A065p). Cells were passaged every 3-4 days. To generate NIH 3T3 clones stably expressing hCD40L, cells were transfected with pcDNA-hCD40LG plasmid using Lipofectamine® 3000 reagent (Thermo Fisher Scientific, USA, Cat. No. L3000015) according to manufacturer's instructions, followed by clone selection in DMEM medium supplemented with geneticin G418 (0.5 mg/ml; Thermo Fisher Scientific, USA, Cat. No. 10131027). Monoclonal cell lines were generated by limiting dilutions. CD40L expression was assessed by flow cytometry using anti-CD154-FITC antibodies (1:20; clone TRAP1, BD Bioscience, USA, Cat. No. 561721). The monoclonal cell line with the highest CD40L expression level was used in the study (Fig. 1A).

## Isolation of Mononuclear Cells (MC) from the Peripheral Blood of Healthy Donors

The study was conducted in accordance with the 2013 Declaration of Helsinki. Patient exclusion criteria were (a) infectious diseases in the acute or recovering stage; (b) autoimmune or chronic diseases. Peripheral blood from healthy donors was collected in vacuum tubes containing K3EDTA as anticoagulant. A total of four independent, unrelated donors, aged 21 to 65 years (median 39 years), participated in the study. The male to female ratio was 1:1. MCs were isolated on a Ficoll gradient (PanEco, Russia, Cat. No. P050E) in accordance with the protocol [13]. The obtained cells were stored in cooled cell sorting buffer (0.5% FBS in Dulbecco's phosphate buffered saline (DPBS)). Cells were counted using a CytoSMART Cell Counter (Corning, USA) using trypan blue. Cell viability was > 95%.

## B cell Staining for Flow Cytometry Analysis (FACS)

B cell analysis was performed by flow cytometry using antibodies to the cell surface markers CD19, CD27, CD38, CD95 (Fas) as well as the intracellular transcription factor BCL6. Cells were stained and stored at 4 °C. For sorting of all B cells (CD3-CD19+CD20+), 20 × 106 MCs were preincubated in blocking solution with addition of 10 µg/ml Human Fc-block (clone K112-91, BD Biosciences, USA, cat. no. 564220) for 10 min on ice, after which they were stained with a mixture of antibodies anti-CD3-R718 (1:100, clone SK7; BD Biosciences, USA, cat. no. 751978), anti-CD19-BV510 (1: 100, clone SJ25C1; BD Biosciences, USA, cat. no. 562947), anti-CD20-FITC (1:20, clone L27; BD Biosciences, USA, cat. 347673) MCs were incubated for 30 min on ice in the dark. To sort CD3-CD19+CD20+CD27- naive B cells and CD3-CD19+CD20+CD27+ memory B cells, MCs were additionally stained with anti-CD27-PerCP-Cy5.5 (1:50, clone M-T271; BioLegend, USA, cat. no. 356408). After the staining, the cells were resuspended in sorting buffer. To assess the phenotype of B cell cultures on day 7, the supernatant with B cells was collected from the wells without subsequent trypsinization. The selected cells were resuspended in a blocking buffer and then stained with the following antibody mixture: anti-CD19-BV510 (1:100), anti-CD27-PerCP-Cy5.5 (1:50), anti-CD38-APC-R700 (1:50, clone HIT2; BD Biosciences, USA, cat. no. 564979), anti-CD95-PE (1:100, clone DX2; BioLegend, USA, cat. no. 305608).

Prior to flow cytometry analysis, the cells were stained with Helix NP Blue at a concentration of 25 nM (Biolegend, USA, cat. no. 425305) to exclude dead cells. Intracellular staining of cells was performed using the True-Nuclear™ Transcription Factor Buffer Set (BioLegend, USA, cat. No. 424401) and anti-BCL-6-AlexaFluor488 antibodies (1:20, clone: K112-91;

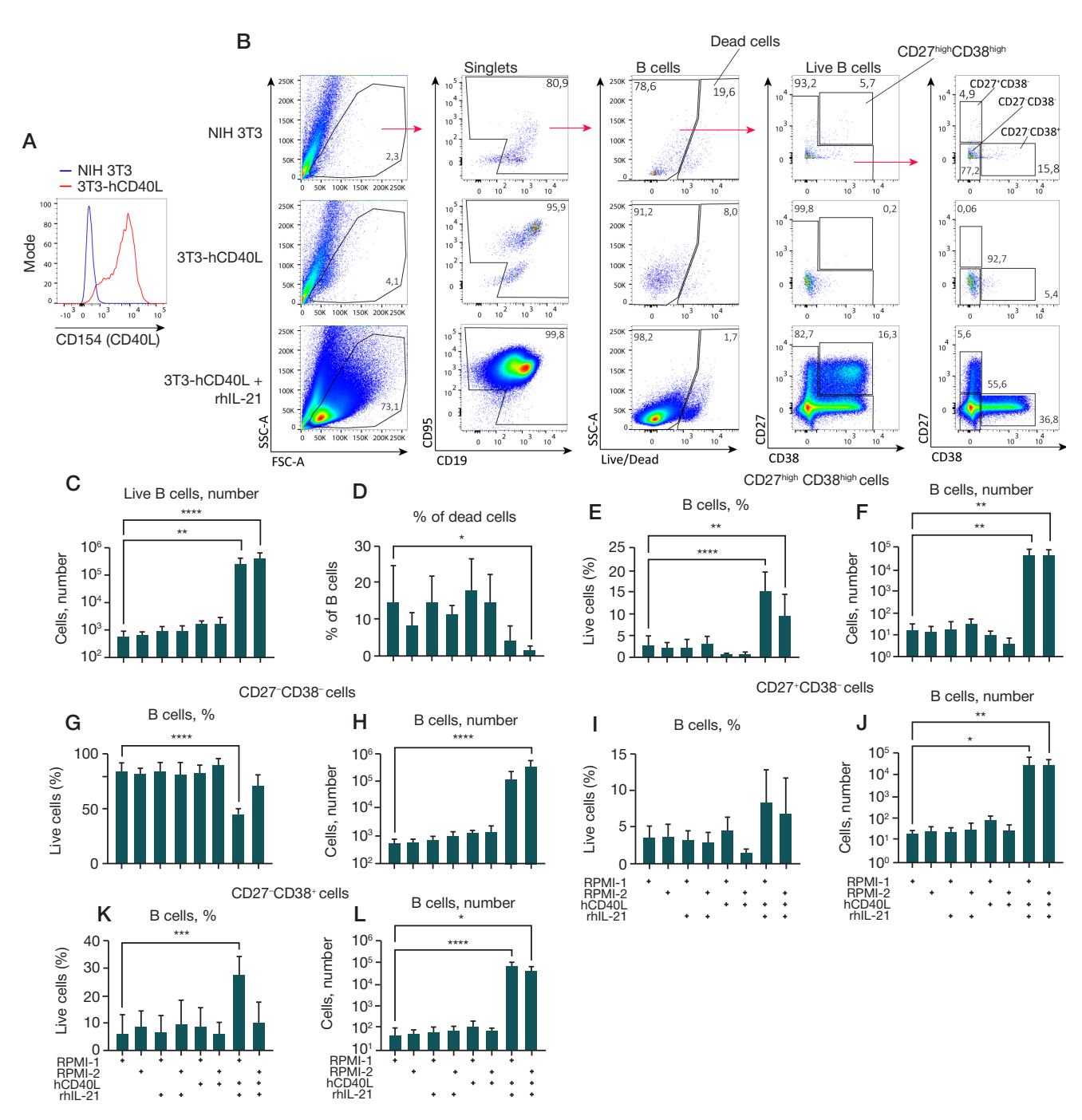


Fig. 1. Analysis of effect of a feeder line expressing rhCD40L, cytokine IL-21, and culture medium composition on the growth of B cell culture. The feeder line 3T3-hCD40L was obtained by transfecting the NIH 3T3 mouse fibroblast line with the pcDNA3.1-hCD40L plasmid to obtain a cell line stably expressing the transgene and subsequent selection of a monoclone with the highest level of hCD40L.  $1.5 \times 10^4$  (CD19 $^{\circ}$  B cells obtained as a result of fluorescence sorting from human peripheral blood PBMCs were cultured on the feeder line 3T3-hCD40L with/without the addition of rhIL-21 (50 ng/ml) in two different culture media compositions (RPMI-1 and RPMI-2) for 7 days. Comparison was performed relative to B cells cultured in the presence of the untransfected NIH 3T3 feeder line. B cell cultures were analyzed by flow cytometry. A. Histogram of the distribution of the hCD40L (CD154) expression level on the surface of 3T3-hCD40L feeder cells (marked with a *red line*) compared with control untransfected NIH 3T3 fibroblasts (marked with a *blue line*). B. Representative graphs of the cytometric analysis. The gating strategy is indicated by arrows. C, D. The number of live B cells (C) and the percentage of dead B cells (D) in the cultures. E-L. Quantitative analysis of the percentage of live B cells and the total number of live B cells phenotypically divided by surface expression of CD27 and CD38 into CD27<sup>high</sup> CD38<sup>high</sup> — plasma cells and plasmablasts (E, F), CD27-CD38-G, H), CD27-CD38-B cells (K, L). The data is presented as the mean  $\pm$  standard deviation (SD) for four independent experiments (n = 4), each experiment was performed in duplicate. Statistical analysis was performed by one-way analysis of variance (ANOVA) with Dunnett's correction for multiple comparisons, \*, \*\*\*, \*\*\*\*\*\* —  $p \le 0.05$ ; 0.001; 0.0001; 0.0001, respectively

BD Biosciences, USA, cat. No. 561524) for 12 h. The following subpopulations were identified using cytometric analysis of cultures: CD19+CD27highCD38high (defined as ASC), CD19+CD38-CD27-, CD19+CD38-CD27-, CD19+CD38-CD27-B cells, CD19+CD95high B cells (corresponding to activated B cells), CD19+CD95highBCL6+B cells (defined as GC B cells). B-cell sorting and flow cytometry (FACS) analysis of B-cell cultures were performed on a BD FACSAria™ III cell sorter

using FACSDiva™ software. FlowJo version 10.8.1 was used for data processing.

## Co-cultivation of B cells with Feeder Cells

3T3-hCD40L fibroblasts and control non-transfected cells were inactivated in DMEM with mitomycin C (5  $\mu$ g/ml; Sigma Aldrich, USA, cat. no. 50-07-7) for 2 h, washed with DPBS (PanEco,

## ОРИГИНАЛЬНОЕ ИССЛЕДОВАНИЕ І МОЛЕКУЛЯРНАЯ БИОЛОГИЯ

Table 1. Experimental design for optimizing CD19+CD20+ B cell culture conditions

3T3	3T3-hCD40L	3T3	3T3-hCD40L	3T3	3T3-hCD40L	3T3	3T3-hCD40L	
RPMI-1		RPMI-2		RPMI-1		RPMI-2		
	-	-		+ IL-21				

Table 2. Experimental design for studying cultures of CD20+CD27- naive B cells and CD20+CD27+ memory B cells

3T3-hCD40L										
	RPMI-2 + IL21									
	CD19-CD	20-CD27-		CD19 <sup>-</sup> CD20 <sup>-</sup> CD27 <sup>+</sup>						
_	+IL-4	-	+IL-4	-	+IL-4	-	+IL-4			
-	-	+BAFF	+BAFF	-	-	+BAFF	+BAFF			

Russia, cat. no. P060E) at least 3 times, and plated onto a sixwell plate (Wuxi NEST, cat. no. 703002) at a density of 3 × 105 cells/well. The following day,  $1.5 \times 10^4$  sorted CD19-CD20- B cells were added. Cultivation was performed in the following media: RPMI-1 based on RPMI-1640 (PanEco, Russia, cat. no. C330p) with the inclusion of 10% FBS, 1× sodium pyruvate (PanEco, Russia, cat. no. F023), 1× GlutaMAX™ (Thermo Fisher Scientific, USA, cat. no. 35050061), 1× antibiotic mixture and RPMI-2 based on the richRPMI (BioinnLabs, cat. no. bn-3A3R), containing human transferrin, insulin, albumin, as well as glutathione and additional microelements and vitamins, with the inclusion of 10% FBS,  $1 \times \text{GlutaMAX}^{\text{TM}}$ ,  $1 \times \text{antibiotics}$ . Recombinant human IL-21 (rhIL-21, SCI-store, cat. #PSG260) was added to the media at a concentration of 50 ng/ml. CD20-CD27- and CD20-CD27- B cells were cultured in RPMI-2 supplemented with IL-21 ± IL-4 (SCI-store, cat. #PSG040, 10 ng/ml) and  $\pm$  BAFF (BioLegend, cat. #559604, 100 ng/ml). Cultivation was carried out for 7 days with medium replacement on day 3 and day 5. The experimental schemes for culturing all CD19-CD20- B cells, as well as CD19-CD20-CD27- naive and CD19-CD20-CD27+ memory B cells under the test and control conditions are presented in Tables 1 and 2.

### Statistical Analysis

For the independent experiments described in the study, we used MCs from the blood of four genetically unrelated adult donors. Statistical analysis was performed using GraphPad Prism version 9.5.1 (GraphPad Software Inc, USA). The statistical methods are specified in the figure legends. Statistically insignificant differences between groups are not indicated on the graphs. Outliers are not excluded from the analysis.

## **RESULTS**

In the first stage of the study, we determined how the presence of CD40L, the cytokine IL-21, or specialized additives in the cell medium impacts B-cell survival and expansion as well as the formation of ASCs and germinal center B-cells (Fig. 1, 2). A transgenic NIH 3T3 murine fibroblast cell line stably expressing hCD40L (3T3-hCD40L) was generated for long-term co-culture of B cells with human CD40L (hCD40L) (Fig. 1A).

B cells (CD19+CD20+) were obtained from human peripheral blood MCs by fluorescence sorting (with a population purity of > 99%).  $1.5 \times 10^4$  B cells were cultured for 7 days in a sixwell plate in the presence of 3T3-hCD40L feeders or control untransfected 3T3 cells. Two media were used for cultivation: standard RPMI-1640 supplemented with 10% fetal bovine serum, sodium pyruvate, and glutamine (designated as RPMI-1) or the same medium enriched with human serum supplements including recombinant insulin, transferrin, lipid-rich

albumin, glutathione as well as additional trace elements and vitamins (RPMI-2). IL-21 was added at a concentration of 50 ng/ml (Table 1).

Flow cytometry analysis of the resulting B-cell cultures (Fig. 1B) showed that the combined action of hCD40L and IL-21 resulted in the highest level of B-cell expansion (Fig. 1C) and increased B-cell survival, especially when supplemented with recombinant proteins from human serum (Fig. 1D).

Cultures with hCD40L and IL-21 also showed the highest accumulation of CD27<sup>high</sup>CD38<sup>high</sup> ASC (Fig. 1E, F), an increase in the number (but not percentage) of CD27<sup>-</sup>CD38<sup>-</sup> B cells (Fig. 1G, H), and accumulation of CD27<sup>+</sup> and CD38<sup>+</sup> B cells (Fig. 1 I-L), with the percentage of CD27<sup>-</sup>CD38<sup>+</sup> B cells being significantly higher when cultured in RPMI-1 (Fig. 1K).

GC B cells are characterized by increased surface expression of CD95 (Fas) and the presence of the intracellular transcription factor BCL6 [5]. CD95 expression also increases on activated B cells [15]. Based on this, we assessed CD95 expression on the surface of B cells in culture as a marker of cellular activation (Fig. 2A).

Based on the data analysis, up to 97% of B cells in the culture increased their surface expression of CD95 in the presence of 3T3-hCD40L-cells (Fig. 2A-C) while the addition of IL-21 did not significantly affect the percentage of CD95<sup>high</sup> B cells (Fig. 2B). Moreover, up to 80% of all CD95<sup>high</sup> B cells had the CD27-CD38-phenotype (Fig. 2D, E). The number of CD27+CD38-CD95<sup>high</sup> and CD27-CD38+CD95<sup>high</sup> B cells in cultures increased with the combined addition of hCD40L and IL-21 (Fig. 2G, I) while their proportion did not change (Fig. 2F, H).

To assess the accumulation of CD95<sup>high</sup> BCL6<sup>+</sup> (GC-like) B cells, we fixed surface-stained B cells with further intracellular staining with antibodies to BCL6 (Fig. 2J). Quantitative analysis revealed a low representation of this B cell subpopulation in the cultures (< 2%) (Fig. 2K). The most noticeable accumulation of GC-like B cells was observed in the RPMI-2 culture supplemented with 3T3-hCD40L feeders and IL21 (Fig. 2L). In the RPMI-2 medium, more than 50% of GC-like B cells had the CD27-CD38- phenotype which is significantly higher than in cultures with RPMI-1 (Fig. 2M, N). CD27+CD38-CD95<sup>high</sup> BCL6+ B cells were equally abundant in cultures with RPMI-1 and RPMI-2 (Fig. 2O, P) while the proportion of CD27-CD38+GC-like B cells was significantly increased in cultures with RPMI-1 (Fig. 2Q, R).

Thus, co-cultivation of B cells with 3T3-hCD40L feeders and IL-21 allows for the greatest expansion and survival of B cells. Under these conditions, on day 7 of culture in RPMI-1, approximately 15% of living cells were ASCs and 0.2% were GC-like B cells, with 10% and 0.4% for RPMI-2, respectively. RPMI-2 was chosen for further work as it was compositionally richer for B cells.

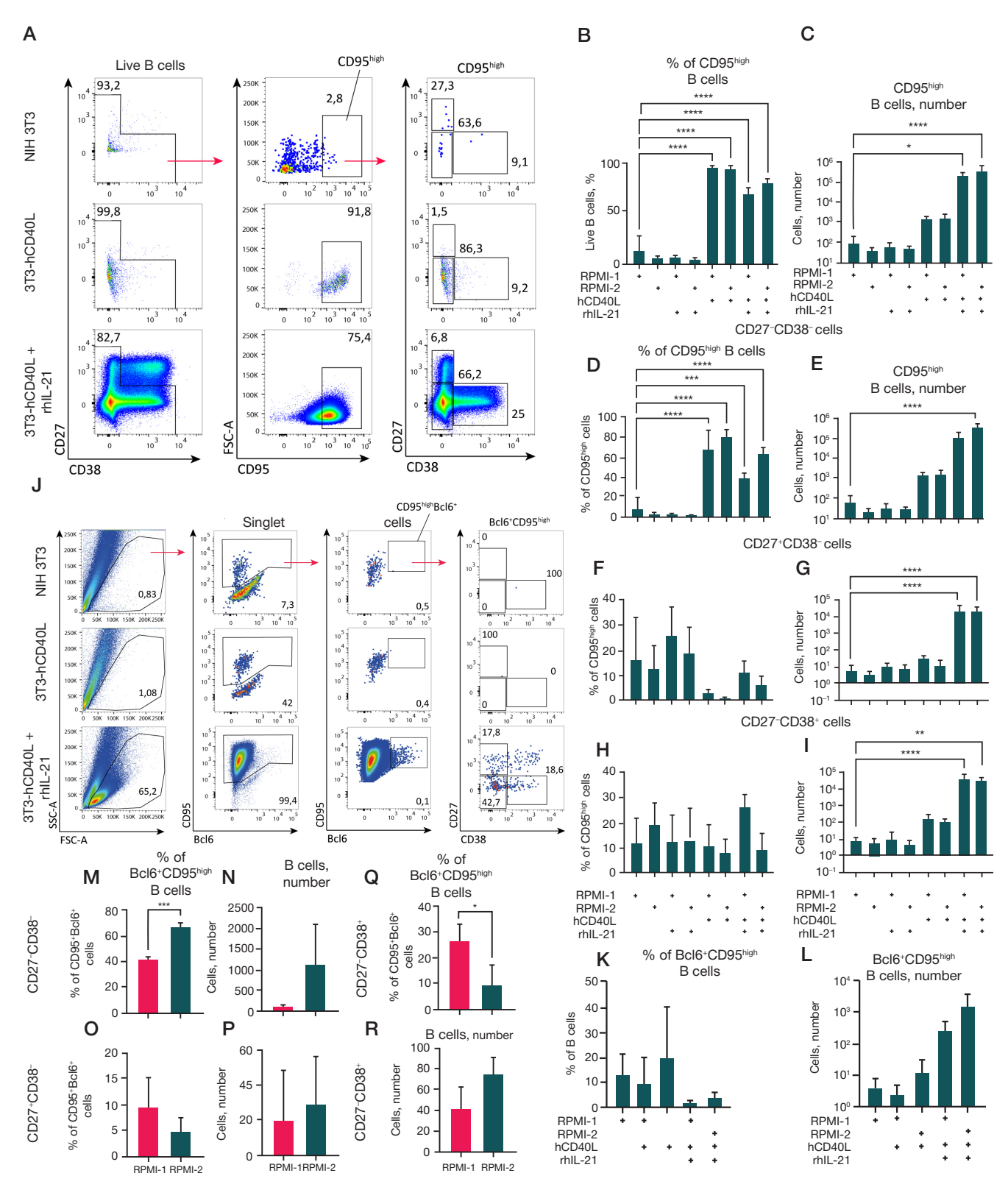


Fig. 2. Analysis of the effect of CD40L, IL-21, and cell culture medium composition on the surface expression of CD95 and intracellular expression of the transcription factor BCL6 in B-cell cultures. A-I. Analysis of the surface expression of CD95 and co-expression of CD27 and CD38 on B cells in cultures (excluding CD27<sup>high</sup> CD38<sup>high</sup> — plasma cells). Representative graphs of flow cytometry analysis. The gating strategy is indicated by arrows (A). Quantitative analysis of the percentage of (B) and absolute number (C) of CD95<sup>high</sup> -B cells in cultures. Quantitative analysis of the percentage of B cells and the absolute number of live CD95<sup>high</sup> -B cells or CD27<sup>+</sup>CD38<sup>+</sup> (P, E), CD27<sup>+</sup>CD38<sup>+</sup> (F, G), and CD27<sup>+</sup>CD38<sup>+</sup> (H, I) B cells. J-R. B cells cultured in the presence of NIH 3T3 feeder line expressing hCD40L with or without rhIL-21 (50 ng/ml) in RPMI-1 or RPMI-2 were fixed and permeabilized for staining of the intracellular transcription factor BCL6. Comparison was made relative to B cells cultured in the presence of the untransfected NIH 3T3 line. Representative graphs of flow cytometry analysis of fixed B cells from the cultures. The gating strategy is indicated by arrows (J). Quantitative analysis of the BCL6<sup>+</sup>CD95<sup>high</sup> -B cells percentage (K) and absolute number (L) of the total number of B cells. Quantitative analysis of the percentage and absolute number of CD27<sup>+</sup>CD38<sup>+</sup> (M, N), CD27<sup>+</sup>CD38<sup>+</sup> (O, P) and CD27<sup>+</sup>CD38<sup>+</sup> (Q, R) BCL6<sup>+</sup>CD95<sup>high</sup> B cells. The graphs present the data as the mean ± standard deviation (SD) for lindependent experiments (n = 4), each experiment was performed in duplicate. Statistical analysis of CD95<sup>high</sup> B cell (K, L) subpopulations was performed by unpaired T-test. \*, \*\*, \*\*\*, \*\*\*\* —  $p \le 0.05$ ; 0.001; 0.0001; 0.0001 respectively

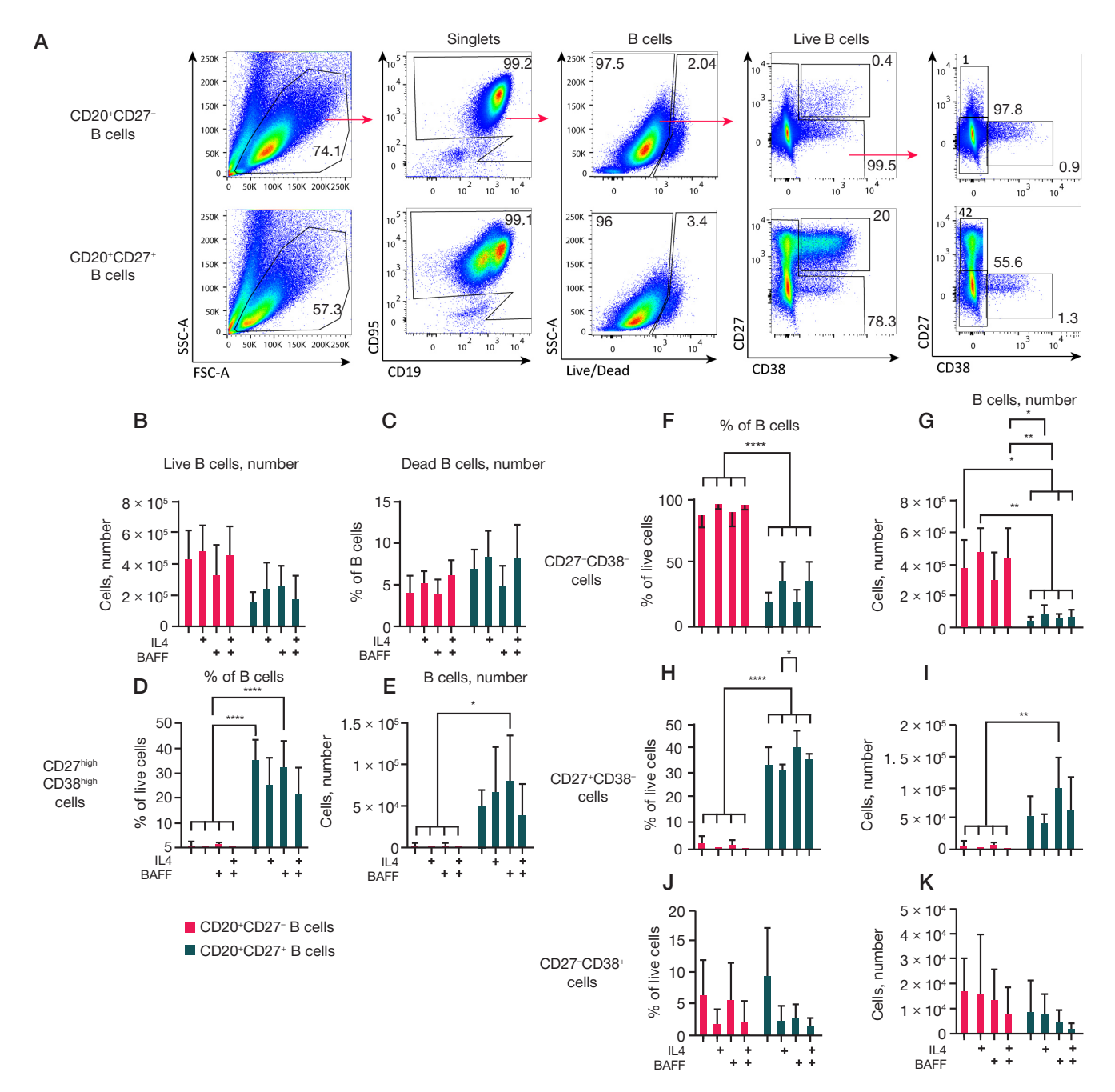


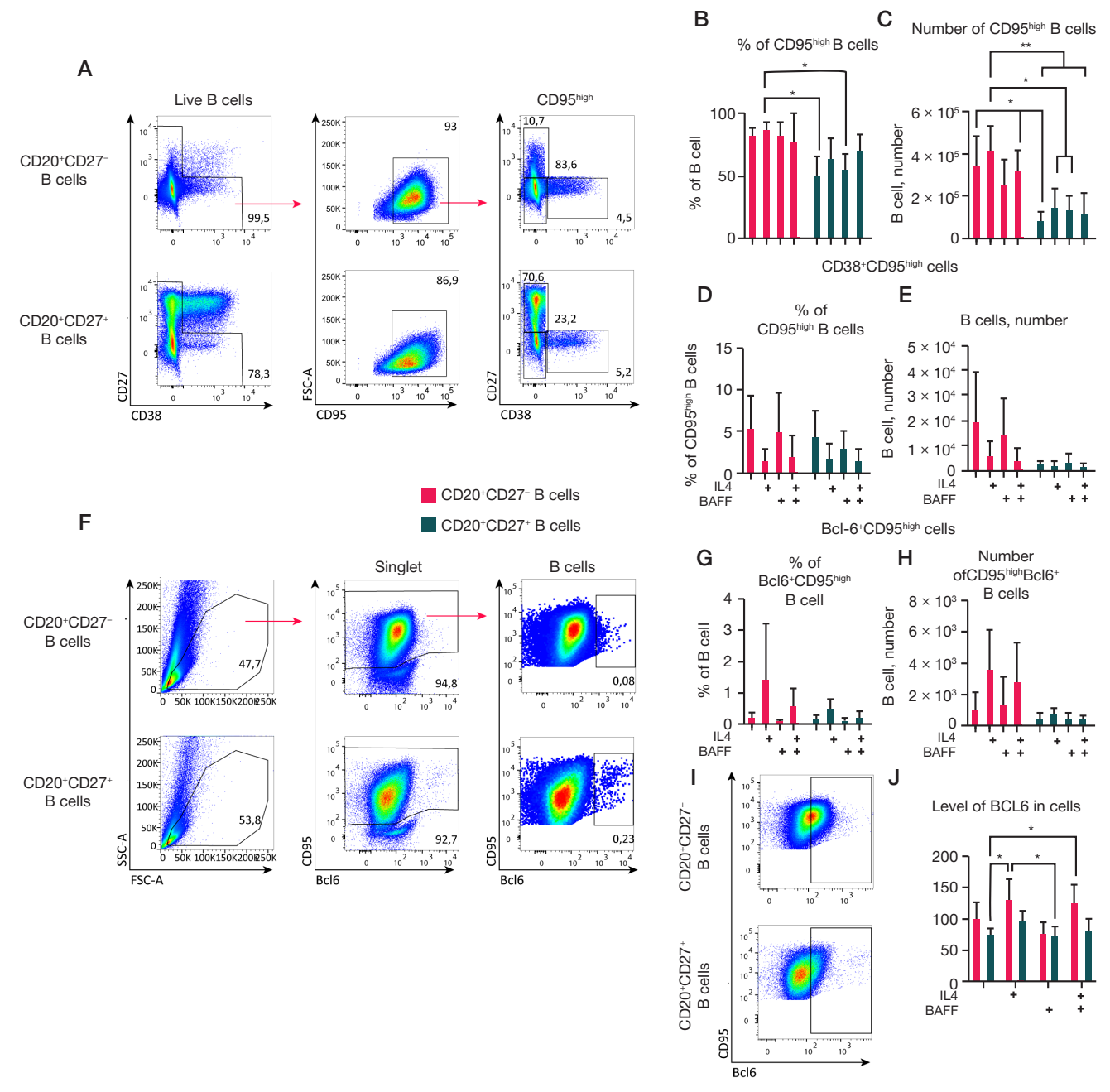
Fig. 3. Analysis of the effect of different cytokine compositions on CD27<sup>-</sup> and CD27<sup>+</sup> memory B cell cultures. Predominantly naive B cells (CD19<sup>+</sup>CD20<sup>+</sup>CD27<sup>-</sup>) and memory B cells (CD19<sup>+</sup>CD20<sup>+</sup>CD27<sup>-</sup>) obtained from blood PBMC by FACS, at a concentration of 1.5 × 10<sup>4</sup> were cultured on 3T3 feeder cells expressing hCD40L in RPMI-2 culture medium in the presence of rhIL-21 (50 ng/ml), with or without the addition of rhIL-4 (10 ng/ml) and rhBAFF (100 ng/ml) cytokines for 7 days. Cell cultures were analyzed by flow cytometry. **A.** Representative graphs of flow cytometry analysis. Arrows indicate the gating strategy. The number of live B cells (**B**) and the percentage of dead B cells (**C**) in cultures. Quantitative analysis of the percentage of live B cells and the absolute number of CD27<sup>high</sup>CD38<sup>high</sup> — plasma cells and plasmablasts (**D**, **E**), CD27<sup>-</sup>CD38<sup>-</sup> (**F**, **G**), CD27<sup>-</sup>CD38<sup>-</sup> (**H**, **I**), and CD27<sup>-</sup>CD38<sup>-</sup> (**J**, **K**) B cells. The graphs present the data as the mean ± standard deviation (SD) for four independent experiments (n = 4), each experiment was performed in duplicate. Statistical analysis was performed by two-way analysis of variance (ANOVA) with Tukey's test for multiple comparisons, \*, \*\*, \*\*\*, \*\*\*\*, \*\*\*\*, \*\*\*\*, \*\*\*\*, \*\*\*\*, \*\*\*\*, \*\*\*\*, \*\*\*\*, \*\*\*\*, \*\*\*\*, \*\*\*\*, \*\*\*\*, \*\*\*\*, \*\*\*\*, \*\*\*\*, \*\*\*\*, \*\*\*\*\*, \*\*\*\*,

In the next series of experiments, we investigated the effect of different cytokine compositions (IL-4, BAFF) on cell cultures of CD20+CD27- B cells which were predominantly naive B cells, and CD20+CD27+ memory B cells. Individual B cell subpopulations were obtained from peripheral blood MCs by fluorescence sorting (with a population purity of > 95%). 1.5 × 10<sup>4</sup> B cells were cultured in RPMI-2 medium in the presence of 3T3 hCD40L cells supplemented with IL-21 (50 ng/ml) and the cytokines IL-4 (10 ng/ml) and/or BAFF (100 ng/ml) (Table 2).

Flow cytometric analysis of cell cultures on day 7 (Fig. 3A) showed that various cytokine compositions had no significant effect on B-cell expansion or survival (Fig. 3B, C). For all

cytokine combinations, a trend toward increased expansion and a decreased proportion of dead B cells was observed in cultures of CD27<sup>-</sup> naive B cells compared with CD27<sup>+</sup> memory B cells.

Importantly, cultures of CD27+ memory B cells showed a significant accumulation of CD27highCD38high ASC (20–35% of all B cells) (Fig. 3D, E). In the cultures of predominantly naive CD27-B cells, the proportion of ASC was less than 2% (Fig. 3D, E) while the proportion of CD27-CD38-B cells (Fig. 3F, G) was significantly higher compared to the cultures of CD27+B cells. CD27+CD38-B cells were abundant in memory B cell cultures, and CD27-CD38+B cells were present in all cases



without significant differences (Fig. 3H–K). Regardless of the starting population, adding IL-4 decreased the proportion of ASC, CD27+CD38-, and CD27-CD38+ cells (Fig. 3D, E, H–K).

Regardless of the conditions and starting cells, the majority of cells had CD95<sup>high</sup> phenotype. Moreover, the proportion and number of CD95<sup>high</sup> B cells were slightly increased in CD27<sup>-</sup>naive B cell cultures (Fig. 4A-C). Notably, a trend toward a decrease in the CD27<sup>-</sup>CD38<sup>+</sup>CD95<sup>high</sup> B cell subpopulation was observed in the presence of IL4 under all other tested conditions (Fig. 4D, E).

Analysis of the number and proportion of CD95<sup>high</sup>BCL6<sup>+</sup> B cells (Fig. 4F) in cultures from CD27<sup>-</sup> and CD27<sup>+</sup> B cells revealed no statistically significant differences (Fig. 4G, H). However, the addition of IL-4 was shown to increase the proportion of GC-like B cells (especially in the case of CD27<sup>-</sup> B cells). Notably, a trend toward increased BCL6 levels in CD27<sup>-</sup> B-cell cultures compared to CD27<sup>+</sup> B-cells was observed under all tested conditions except the addition of BAFF without IL-4 (Fig. 4I, J).

When cultured in RPMI-2 medium with 3T3-hCD40L feeders and IL-21, a significantly greater expansion of the naive

CD27<sup>-</sup> B-cell cultures with minimal ASC accumulation was observed as compared to the CD27<sup>+</sup> memory B-cell cultures where ASC reached 30%. No statistically significant differences in the accumulation of GC-like B-cells were detected. The addition of BAFF had no significant effect on B-cell cultures while IL-4 caused a slight decrease in the proportion of ASC and an increase in GC-like B-cells, especially in CD27<sup>-</sup> B-cell cultures.

#### DISCUSSION

In vitro cultivation of human B cells is of fundamental importance for solving a wide range of biotechnological problems, in particular, obtaining ASCs for antibody production, using B cells as antigen-presenting cells for T cell activation, and testing transgenic immunotherapy products [16]. Although there are numerous studies on B cell cultivation conditions [11–13], developing effective protocols for specific applications still remains important.

The aim of this study was to find an optimal combinations of conditions for (a) efficient B cell expansion in cell culture; (b) maximal accumulation of ASC population; (c) BCL6-expressing B cells similar to GC B cells. We comprehensively explored the impact of baseline B-cell status based on CD27 marker (CD27<sup>-</sup> and CD27<sup>+</sup> subsets), a combination of proteins and supplements replacing human serum, the cytokine BAFF that is critical for B-cell survival, and also the stimuli that mimic T-cell support (CD40L, IL-21, IL-4), on the efficiency of cell culture protocols.

## Expansion and Maintenance of Activated B-Cell Viability

Cytometric analysis of B-cell cultures on day 7 of co-culture demonstrated that the highest expansion and survival rates were achieved using a transgenic feeder line expressing human hCD40L in combination with the cytokine IL-21. These data are consistent with previously described results [17, 18]. At the same time, the addition of IL-4 and BAFF cytokines to the culture at concentrations of 10 and 100 ng/ml, respectively, did not have a statistically significant effect on cell proliferation or viability.

Optimization of the cell culture medium composition showed that adding recombinant human insulin, transferrin, and albumin into a base medium containing 10% FBS resulted in the greatest reduction in percentage of dead cells.

Based on the comparative analysis, cultures initiated from CD27<sup>-</sup> B cells were, on average, 1.5 times more abundant than cultures derived from CD27<sup>+</sup> cells and also exhibited a lower percentage of cell death as has been previously described [19].

Thus, it is advisable to use CD27<sup>-</sup> cells as the initial population for optimal expansion and maintenance of activated B cells viability *in vitro*. The most effective protocol involves co-cultivation with feeder cells expressing hCD40L in a medium enriched with IL-21, supplemented with a combination of serum proteins (including insulin, transferrin, and albumin).

## Accumulation of ASC in B-cell Cultures

The next task was to determine the cell culture conditions that promote accumulation of CD27<sup>high</sup>CD38<sup>high</sup> ASC in B-cell cultures. It was shown that in the presence of both hCD40L and IL-21, CD27<sup>high</sup>CD38<sup>high</sup> cells accumulated in the cultures reaching 10-15% of the total cell pool. This is consistent with the previously published results [20, 21, 22]. The addition of recombinant serum proteins to the culture medium resulted in

a decrease in the proportion of ASC in the cultures. Significant accumulation of CD27<sup>high</sup>CD38<sup>high</sup> B cells was observed in the cultures of memory CD27<sup>+</sup> B cells (20–35% of all living cells), consistently with previous studies [21, 23] and the rapid recruitment of memory B cells to the ASC response upon repeated exposure to antigen and T-cell help [24]. In contrast to the memory B cell cultures, in the cultures from predominantly naive CD27<sup>-</sup> B cells the proportion and number of ASC were significantly reduced (1–2% of the total cell number).

It was also demonstrated that in the presence of the cytokine BAFF, the number of CD27<sup>high</sup>CD38<sup>high</sup> and CD27<sup>+</sup>CD38<sup>-</sup> B cells in the cultures of CD27<sup>+</sup> B cells was maximal, consistent with other data available [25, 26]. Conversely, upon the addition of IL-4, abundance and proportion of ASC and CD27<sup>+</sup>CD38<sup>-</sup> cells tended to decrease while the proportion of CD27<sup>-</sup>CD38<sup>-</sup> B cells tended to increase.

Our findings suggest that for ASC abundance in B cell culture, it is preferable to use CD27+ memory B cells in combination with hCD40L and IL-21, along with the addition of BAFF. It should be noted that the analysis was performed without considering the levels of ASC antibody secretion which can vary significantly depending on the level of ASC maturation and multiple additional factors, and requires separate studies to optimize antibody production in cell cultures.

### Accumulation of GC B Cells in Cell Cultures

As mentioned earlier, the signal through the BCR as well as the Th cell "help" in the form of CD40L and IL-21 secretion induces the appearance of GC B cells. A key marker of GC B cells is the expression of BCL6 transcription factor [5]. Phenotypic analysis of lymphocytes from human secondary lymphoid organs identified CD95<sup>high</sup>BCL6+CD38+CD27+/- B cells as GC B cells [27]. In our study, we were able to identify GC-like B cells in cultures by a combination of the surface marker CD95 and the intracellular transcription factor BCL6.

Accumulation of CD95<sup>high</sup>BCL6<sup>+</sup> B cells occurred in cultures with hCD40L and IL-21, consistently with *in vivo* studies [28]. The initial cell populations of CD27<sup>-</sup> and CD27<sup>+</sup> B cells did not significantly affect the proportion and number of CD95<sup>high</sup>BCL6<sup>+</sup> in the final B cell cultures. However, in cultures from CD27<sup>-</sup> B cells, BCL6 level tended to increase. The addition of recombinant serum proteins and IL4 contributed to an increase in the proportion of GC-like B cells and a decrease in ASC. This is consistent with the results of studies suggesting that the combined action of IL-21 and IL-4 secreted by Th increases and stabilizes BCL6 expression in activated B cells [29], promoting their differentiation into GC B cells [5]. Moreover, BCL6 is an antagonist of the transcription factor Blimp-1 and inhibits further differentiation of B cells into ASC [24].

Thus, we were able to demonstrate that culturing B cells in the presence of hCD40L and IL-21 also allows for the formation of GC-like B cells to be observed through increased BCL6 expression. Moreover, a slightly higher accumulation of GC-like B cells was observed in a culture of CD27- naive B cells when IL-4 and human serum substitutes were included in the medium.

However, it should be noted that none of the components used in this study resulted in the accumulation of more than 1% GC-like B cells. GC B cells are highly sensitive to apoptosis in the absence of support from Th and specialized cells — follicular dendritic cells (FDCs) [30]. It was shown that FDC-based cell lines is likely to be preferable for culturing GC B cells [10]. Based on our data and the results of previous studies, we suggest that maintaining GC B-cell cultures *in vitro* requires

## ORIGINAL RESEARCH I MOLECULAR BIOLOGY

using more complex co-cultivation systems with the inclusion of FDC-like B-cell lines.

#### **CONCLUSIONS**

The study helped to identify optimal conditions for the effective expansion of B cells from human peripheral blood *in vitro* as well as for obtaining ASC-enriched cell culture. The presence of hCD40L-expressing feeder cells and IL-21 in the cultures was shown to be necessary for both proliferation and survival as well as for B cell differentiation *in vitro*. For optimal B cell culture

expansion, it is preferable to use CD27<sup>-</sup> naive B cells and a medium supplemented with a combination of human serum proteins (including insulin, transferrin, and albumin). Meanwhile, using CD27<sup>+</sup> memory B cells and adding BAFF to medium are preferable for making ASC more abundant. In this study, we were able to assess the accumulation of CD95<sup>high</sup>BCL6<sup>+</sup> GC-like B cells. However, the combination of conditions used was insufficient to significantly increase the abundance of GC-like B cells in cultures. Presumably, the generation of GC-like B cell culture from peripheral blood B cells may require using FDC-like feeder cells and additional soluble factors.

#### References

- Elsner RA, Shlomchik MJ. Germinal Center and Extrafollicular B Cell Responses in Vaccination, Immunity, and Autoimmunity. Immunity. 2020; 53 (6): 1136–50.
- Ghosh D, Jiang W, Mukhopadhyay D, Mellins ED. New insights into B cells as antigen presenting cells. Current Opinion in Immunology. 2021; 70: 129–37.
- Rastogi I, Jeon D, Moseman JE, Muralidhar A, Potluri HK, McNeel DG. Role of B cells as antigen presenting cells. Front Immunol. 2022; 13: 954936
- Shulman Z, Gitlin AD, Weinstein JS, Lainez B, Esplugues E, Flavell RA, et al. Dynamic signaling by T follicular helper cells during germinal center B cell selection. Science. 2014; 345 (6200): 1058–62.
- Ye BH, Cattoretti G, Shen Q, Zhang J, Hawe N, Waard R de, et al. The BCL-6 proto-oncogene controls germinal-centre formation and Th2-type inflammation. Nat Genet. 1997; 16 (2): 161–70.
- Duy C, Yu JJ, Nahar R, Swaminathan S, Kweon SM, Polo JM, et al. BCL6 is critical for the development of a diverse primary B cell repertoire. J Exp Med. 2010; 207 (6): 1209–21.
- Wong R, Bhattacharya D. Basics of memory Bcell responses: lessons from and for the real world. Immunology. 2019; 156 (2): 120.
- 8. Pedrioli A, Oxenius A. Single B cell technologies for monoclonal antibody discovery. Trends Immunol. 2021; 42 (12): 1143–58.
- Arpin C, Déchanet J, Kooten CV, Merville P, Grouard G, Brière F, et al. Generation of Memory B Cells and Plasma Cells in Vitro. Science.1995; 268: 720–2.
- Caeser R, Di Re M, Krupka JA, Gao J, Lara-Chica M, Dias JML, et al. Genetic modification of primary human B cells to model highgrade lymphoma. Nat Commun. 2019; 10 (1): 4543.
- Rovsing AB, Green K, Jensen L, Nielsen IH, Mikkelsen JG, Degn SE. Multiparametric Optimization of Human Primary B-Cell Cultures Using Design of Experiments. Scand J Immunol. 2025; 102 (2): e70043.
- Avery DT, Kalled SL, Ellyard JI, Ambrose C, Bixler SA, Thien M, et al. BAFF selectively enhances the survival of plasmablasts generated from human memory B cells. J Clin Invest. 2003; 112 (2): 286–97.
- Avery DT, Kalled SL, Ellyard JI, Ambrose C, Bixler SA, Thien M, et al. BAFF selectively enhances the survival of plasmablasts generated from human memory B cells. J Clin Invest. 2004; 113 (7): 1069.
- Butov KR, Osipova EY, Mikhalkin NB, Trubina NM, P anteleev MA, Machlus KR. In vitro megakaryocyte culture from human bone marrow aspirates as a research and diagnostic tool. Platelets. 2021; 32 (7): 928–35.
- Schattner EJ, Elkon KB, Yoo DH, Tumang J, Krammer PH, Crow MK, Friedman SM. CD40 ligation induces Apo-1/Fas expression on human B lymphocytes and facilitates apoptosis through the Apo-1/Fas pathway. J Exp Med. 1995; 182 (5): 1557–65. DOI: 10.1084/jem.182.5.1557.
- Verstegen NJ, Pollastro S, Unger PPA, Marsman C, Elias G, Jorritsma T, et al. Single-cell analysis reveals dynamics of human B cell differentiation and identifies novel B and antibody-secreting cell intermediates. eLife. 2023; 12: e83578.

- Good KL, Bryant VL, Tangye SG. Kinetics of Human B Cell Behavior and Amplification of Proliferative Responses following Stimulation with IL-21. J Immunol. 2006; 177 (8): 5236–47.
- Byazrova MG Astahova EA, Spiridonova AB, Vasileva YuV, Prilipov AG, Filatov AV. Stimulyaciya V-limfocitov cheloveka in vitro s pomoshch'yu IL-21/CD40L i ih harakteristika. Immunologiya. 2020; 41 (6): 501–10. Russian.
- Fecteau JF, Néron S. CD40 stimulation of human peripheral B lymphocytes: distinct response from naive and memory cells. J Immunol. 2003; 171 (9): 4621–9.
- Ding BB, Bi E, Chen H, Yu JJ, Ye BH. IL-21 and CD40L Synergistically Promote Plasma Cell Differentiation through Upregulation of Blimp-1 in Human B Cells. J Immunol. 2013; 190 (4): 1827–36.
- Ettinger R, Sims GP, Fairhurst AM, Robbins R, da Silva YS, Spolski R, et al. IL-21 induces differentiation of human naive and memory B cells into antibody-secreting plasma cells. J Immunol. 2005; 175 (12): 7867–79.
- Unger PA, Verstegen NJM, Marsman C, Jorritsma T, Rispens T, Ten Brinke A, van Ham SM. Minimalistic In Vitro Culture to Drive Human Naive B Cell Differentiation into Antibody-Secreting Cells. Cells. 2021; 10 (5): 1183.
- Deenick EK, Avery DT, Chan A, Berglund LJ, Ives ML, Moens L, et al. Naive and memory human B cells have distinct requirements for STAT3 activation to differentiate into antibody-secreting plasma cells. Journal of Experimental Medicine. 2013; 210 (12): 2739–53.
- 24. Ise W, Kurosaki T. Plasma cell differentiation during the germinal center reaction. Immunol Rev. 2019; 288 (1): 64–74.
- Robinson MJ, Pitt C, Brodie EJ, Valk AM, O'Donnell K, Nitschke L, et al. BAFF, IL-4 and IL-21 separably program germinal centerlike phenotype acquisition, BCL6 expression, proliferation and survival of CD40L-activated B cells in vitro. Immunol Cell Biol. 2019; 97 (9): 826–39.
- Avery DT, Kalled SL, Ellyard JI, Ambrose C, Bixler SA, Thien M, et al. BAFF selectively enhances the survival of plasmablasts generated from human memory B cells. J Clin Invest. 2003; 112 (2): 286–97.
- 27. Bohnhorst JØ, Bjørgan MB, Thoen JE, Natvig JB, Thompson KM. Bm1-Bm5 classification of peripheral blood B cells reveals circulating germinal center founder cells in healthy individuals and disturbance in the B cell subpopulations in patients with primary Sjögren's syndrome. J Immunol. 2001; 167 (7): 3610–8.
- Linterman MA, Beaton L, Yu D, Ramiscal RR, Srivastava M, Hogan JJ, et al. IL-21 acts directly on B cells to regulate Bcl-6 expression and germinal center responses. J Exp Med. 2010; 207 (2): 353–63.
- Chevrier S, Kratina T, Emslie D, Tarlinton DM, Corcoran LM. IL4 and IL21 cooperate to induce the high Bcl6 protein level required for germinal center formation. Immunol Cell Biol. 2017; 95 (10): 925–32.
- Krimpenfort LT, Degn SE, Heesters BA. The follicular dendritic cell: At the germinal center of autoimmunity? Cell Reports. 2024; 43 (3): 113869.

## ОРИГИНАЛЬНОЕ ИССЛЕДОВАНИЕ І МОЛЕКУЛЯРНАЯ БИОЛОГИЯ

#### Литература

- Elsner RA, Shlomchik MJ. Germinal Center and Extrafollicular B Cell Responses in Vaccination, Immunity, and Autoimmunity. Immunity. 2020; 53 (6): 1136–50.
- Ghosh D, Jiang W, Mukhopadhyay D, Mellins ED. New insights into B cells as antigen presenting cells. Current Opinion in Immunology. 2021; 70: 129–37.
- Rastogi I, Jeon D, Moseman JE, Muralidhar A, Potluri HK, McNeel DG. Role of B cells as antigen presenting cells. Front Immunol. 2022; 13: 954936.
- Shulman Z, Gitlin AD, Weinstein JS, Lainez B, Esplugues E, Flavell RA, et al. Dynamic signaling by T follicular helper cells during germinal center B cell selection. Science. 2014; 345 (6200): 1058–62.
- Ye BH, Cattoretti G, Shen Q, Zhang J, Hawe N, Waard R de, et al. The BCL-6 proto-oncogene controls germinal-centre formation and Th2-type inflammation. Nat Genet. 1997; 16 (2): 161–70.
- Duy C, Yu JJ, Nahar R, Swaminathan S, Kweon SM, Polo JM, et al. BCL6 is critical for the development of a diverse primary B cell repertoire. J Exp Med. 2010; 207 (6): 1209–21.
- 7. Wong R, Bhattacharya D. Basics of memory Bcell responses: lessons from and for the real world. Immunology. 2019; 156 (2): 120.
- Pedrioli A, Oxenius A. Single B cell technologies for monoclonal antibody discovery. Trends Immunol. 2021; 42 (12): 1143–58.
- Arpin C, Déchanet J, Kooten CV, Merville P, Grouard G, Brière F, et al. Generation of Memory B Cells and Plasma Cells in Vitro. Science.1995; 268: 720–2.
- Caeser R, Di Re M, Krupka JA, Gao J, Lara-Chica M, Dias JML, et al. Genetic modification of primary human B cells to model highgrade lymphoma. Nat Commun. 2019; 10 (1): 4543.
- Rovsing AB, Green K, Jensen L, Nielsen IH, Mikkelsen JG, Degn SE. Multiparametric Optimization of Human Primary B-Cell Cultures Using Design of Experiments. Scand J Immunol. 2025; 102 (2): e70043.
- Avery DT, Kalled SL, Ellyard JI, Ambrose C, Bixler SA, Thien M, et al. BAFF selectively enhances the survival of plasmablasts generated from human memory B cells. J Clin Invest. 2003; 112 (2): 286–97.
- Avery DT, Kalled SL, Ellyard JI, Ambrose C, Bixler SA, Thien M, et al. BAFF selectively enhances the survival of plasmablasts generated from human memory B cells. J Clin Invest. 2004; 113 (7): 1069.
- 14. Butov KR, Osipova EY, Mikhalkin NB, Trubina NM, P anteleev MA, Machlus KR. In vitro megakaryocyte culture from human bone marrow aspirates as a research and diagnostic tool. Platelets. 2021; 32 (7): 928–35.
- Schattner EJ, Elkon KB, Yoo DH, Tumang J, Krammer PH, Crow MK, Friedman SM. CD40 ligation induces Apo-1/Fas expression on human B lymphocytes and facilitates apoptosis through the Apo-1/Fas pathway. J Exp Med. 1995; 182 (5): 1557–65. DOI: 10.1084/jem.182.5.1557.
- Verstegen NJ, Pollastro S, Unger PPA, Marsman C, Elias G, Jorritsma T, et al. Single-cell analysis reveals dynamics of human B cell differentiation and identifies novel B and antibody-secreting cell intermediates. eLife. 2023; 12: e83578.

- Good KL, Bryant VL, Tangye SG. Kinetics of Human B Cell Behavior and Amplification of Proliferative Responses following Stimulation with IL-21. J Immunol. 2006; 177 (8): 5236–47.
- Бязрова М. Г, Астахова Е. А., Спиридонова А. Б., Васильева Ю. В., Прилипов А. Г, Филатов А. В. Стимуляция В-лимфоцитов человека in vitro с помощью ИЛ-21/CD40L и их характеристика. Иммунология. 2020; 41 (6): 501–10.
- Fecteau JF, Néron S. CD40 stimulation of human peripheral B lymphocytes: distinct response from naive and memory cells. J Immunol. 2003; 171 (9): 4621–9.
- Ding BB, Bi E, Chen H, Yu JJ, Ye BH. IL-21 and CD40L Synergistically Promote Plasma Cell Differentiation through Upregulation of Blimp-1 in Human B Cells. J Immunol. 2013; 190 (4): 1827–36.
- Ettinger R, Sims GP, Fairhurst AM, Robbins R, da Silva YS, Spolski R, et al. IL-21 induces differentiation of human naive and memory B cells into antibody-secreting plasma cells. J Immunol. 2005; 175 (12): 7867–79.
- Unger PA, Verstegen NJM, Marsman C, Jorritsma T, Rispens T, Ten Brinke A, van Ham SM. Minimalistic In Vitro Culture to Drive Human Naive B Cell Differentiation into Antibody-Secreting Cells. Cells. 2021; 10 (5): 1183.
- 23. Deenick EK, Avery DT, Chan A, Berglund LJ, Ives ML, Moens L, et al. Naive and memory human B cells have distinct requirements for STAT3 activation to differentiate into antibody-secreting plasma cells. Journal of Experimental Medicine. 2013; 210 (12): 2739–53.
- 24. Ise W, Kurosaki T. Plasma cell differentiation during the germinal center reaction. Immunol Rev. 2019; 288 (1): 64–74.
- Robinson MJ, Pitt C, Brodie EJ, Valk AM, O'Donnell K, Nitschke L, et al. BAFF, IL-4 and IL-21 separably program germinal center-like phenotype acquisition, BCL6 expression, proliferation and survival of CD40L-activated B cells in vitro. Immunol Cell Biol. 2019; 97 (9): 826–39.
- Avery DT, Kalled SL, Ellyard JI, Ambrose C, Bixler SA, Thien M, et al. BAFF selectively enhances the survival of plasmablasts generated from human memory B cells. J Clin Invest. 2003; 112 (2): 286–97
- 27. Bohnhorst Jø, Bjørgan MB, Thoen JE, Natvig JB, Thompson KM. Bm1-Bm5 classification of peripheral blood B cells reveals circulating germinal center founder cells in healthy individuals and disturbance in the B cell subpopulations in patients with primary Sjögren's syndrome. J Immunol. 2001; 167 (7): 3610–8.
- Linterman MA, Beaton L, Yu D, Ramiscal RR, Srivastava M, Hogan JJ, et al. IL-21 acts directly on B cells to regulate Bcl-6 expression and germinal center responses. J Exp Med. 2010; 207 (2): 353–63.
- Chevrier S, Kratina T, Emslie D, Tarlinton DM, Corcoran LM. IL4 and IL21 cooperate to induce the high Bcl6 protein level required for germinal center formation. Immunol Cell Biol. 2017; 95 (10): 925–32.
- Krimpenfort LT, Degn SE, Heesters BA. The follicular dendritic cell: At the germinal center of autoimmunity? Cell Reports. 2024; 43 (3): 113869.

### COMPARATIVE ANALYSIS OF METALLIC ENDOVASCULAR COIL FRAME DESIGNS

Chepeleva EV<sup>1</sup>, Kozyr KV<sup>1</sup>, Borodin VP<sup>1</sup>, Khakhalkin W<sup>1</sup>, Vladimirov SV<sup>1</sup>, Makhmudov MA<sup>1</sup>, Badoian AG<sup>1</sup>, Baranov AA<sup>1</sup>, Krestyaninov OV<sup>1,2</sup>

- <sup>1</sup> Meshalkin National Medical Research Center, Novosibirsk, Russia
- <sup>2</sup> Novosibirsk State Medical University, Novosibirsk, Russia

Currently the development of the production of domestic medical devices is of special importance in the context of ensuring the healthcare system sustainability. Leveraging international experience in developing embolic coils, while considering the capabilities of Russian production, will enable the creation of devices that meet global standarts. The study aimed to conduct systematic evaluation of six endovascular coil models from leading foreign manufacturers and perform comprehensive assessment of the design features of the metal coil frames, including analysis of geometrical dimensions, materials used, and engineering solutions. Based on our findings and a comparison with clinical and experimental literature data we determined the optimal parameters for creating the coil prototype: the wire diameter 0.07–0.12 mm, coil-core type interlock mechanism, and atraumatic polymer tip. These solutions ensure the optimal combination of performance characteristics and manufacturability. The findings provide the basis for the development of domestic analogues meeting the today's clinical requirements, considering the available production capacity.

Keywords: endovascular coils, vascular embolization, vascular surgery, shape memory materials, production technologies

Funding: the study was conducted as part of the Russian Science Foundation project No. 25-15-00480.

Author contribution: Chepeleva EV — data analysis, manuscript writing and editing; Kozyr KV, Borodin VP — experimental procedure, data analysis, visualization of findings; Khakhalkin VV — study concept and design, data analysis; Vladimirov SV — experimental procedure, data analysis, visualization of findings; Makhmudov MA, Badoian AG, Baranov AA — technical support, data validation, graphics design; Krestyaninov OV — general research management, coordinating work, editing and approval of the final version of the manuscript.

Correspondence should be addressed: Elena V. Chepeleva

Rechkunovskaya, 15, Novosibirsk, 630055, Russia; e\_chepeleva@meshalkin.ru

Received: 15.09.2025 Accepted: 30.09.2025 Published online: 23.10.2025

DOI: 10.24075/brsmu.2025.048

Copyright: © 2025 by the authors. Licensee: Pirogov University. This article is an open access article distributed under the terms and conditions of the Creative Commons Attribution (CC BY) license (https://creativecommons.org/licenses/by/4.0/).

# СРАВНИТЕЛЬНЫЙ АНАЛИЗ КОНСТРУКЦИЙ МЕТАЛЛИЧЕСКИХ КАРКАСОВ ЭНДОВАСКУЛЯРНЫХ СПИРАЛЕЙ

Е. В. Чепелева¹ <sup>⊠</sup>, К. В. Козырь¹, В. П. Бородин¹, В. В. Хахалкин¹, С. В. Владимиров¹, М. А. Махмудов¹, А. Г. Бадоян¹, А. А. Баранов¹, О. В. Крестьянинов¹.²

В современных условиях развитие отечественного производства медицинских изделий приобретает особое значение в контексте обеспечения устойчивости системы здравоохранения. Использование международного опыта при разработке эмболизационных спиралей с учетом возможностей российских производств позволит создать изделия, соответствующие мировым стандартам. Целью работы было провести систематический анализ шести моделей эндоваскулярных спиралей ведущих зарубежных производителей и комплексное изучение конструктивных особенностей металлических каркасов спирали, включая оценку геометрических параметров, используемых материалов и технических решений. По результатам исследования и их сопоставления с клиническими и экспериментальными литературными данными определены оптимальные параметры для создания прототипа спирали: диаметр проволоки 0,07–0,12 мм, замковый механизм типа «спираль-сердечник» и полимерный атравматический кончик. Данные решения обеспечивают оптимальное сочетание эксплуатационных характеристик и техноогичности изготовления. Полученные результаты формируют основу для разработки отечественных аналогов, соответствующих современным клиническим требованиям, с учетом имеющихся производственных возможностей

Ключевые слова: эндоваскулярные спирали, эмболизация сосудов, сосудистая хирургия, материалы с памятью формы, технологии производства

Финансирование: исследование выполнено в рамках проекта Российского Научного Фонда № 25-15-00480.

Вклад авторов: Е. В. Чепелева — анализ данных, написание и редактирование текста статьи; К. В. Козырь, В. П. Бородин — проведение экспериментов, анализ данных, визуализация результатов; В. В. Хахалкин — концепция и дизайн исследования, анализ данных; С. В. Владимиров — проведение экспериментов, анализ данных, визуализация результатов; М. А. Махмудов, А. Г. Бадоян, А. А. Баранов — техническая поддержка, валидация данных, подготовка графических материалов; О. В. Крестьянинов — общее руководство исследованием, координация работы, редактирование и утверждение финальной версии текста.

🔀 Для корреспонденции: Елена Васильевна Чепелева

ул. Речкуновская, д. 15, г. Новосибирск, 630055, Россия; e\_chepeleva@meshalkin.ru

Статья получена: 15.09.2025 Статья принята к печати: 30.09.2025 Опубликована онлайн: 23.10.2025

DOI: 10.24075/vrgmu.2025.048

Авторские права: © 2025 принадлежат авторам. **Лицензиат:** РНИМУ им. Н. И. Пирогова. Статья размещена в открытом доступе и распространяется на условиях лицензии Creative Commons Attribution (CC BY) (https://creativecommons.org/licenses/by/4.0/).

<sup>1</sup> Национальный медицинский исследовательский центр имени Е. Н. Мешалкина, Новосибирск, Россия

 $<sup>^{2}</sup>$  Новосибирский государственный медицинский университет, Новосибирск, Россия

## ОРИГИНАЛЬНОЕ ИССЛЕДОВАНИЕ І СОСУДИСТАЯ ХИРУРГИЯ

The dependence on imported endovascular coils for embolization is a major challenge for the public health system of the Russian Federation. Hundreds of thousands embolization surgical procedures due to vascular disorders are performed annually all over the world, and all the products used for this purpose in Russia are manufactured by foreign companies. In 2020, global sales of coils were about 1.14 billion of US dollars, in 2021 these reached 1.175 billion of US dollars, and the rate still demonstrates a steady upward trend [1]. Under conditions of import dependence there is a need for import substitution, and the analysis of world experience should be conducted to create versatile structures with optimal biotech properties.

Despite their common function, endovascular coils for vascular embolization vary considerably according to materials, geometry, and dimensions, but any coil represents a metal frame maid of the wire twisted into a primary coil [2]. The key requirements for the coils are as follows: high biocompatibility, controlled thrombogenicity, optimal radial stiffness and flexibility, as well as the ability to restore the 3D structure after implantation [3]. Polymer fibers or a hydrogel coating are often applied to the surface in order to enhance thrombogenicity, and the secondary coil configuration varies depending on the target blood vessel anatomy [4, 5]. The coils cause irreversible embolization, ensuring complete blood vessel occlusion due to thrombus formation [6]. Such an effect is achieved in one of three ways: mechanical obturation of the blood vessel lumen resulting in the considerably reduced blood flow; development of a thrombogenic frame contributing to platelet aggregation and stable blood clot formation; controlled damage to the blood vessel wall stimulating the release of endogenous procoagulant factors. Thrombotic occlusion usually occurs within five minutes after installation, despite the fact that temporal parameters may vary depending on the device type, blood vessel diameter, and baseline hemodynamics in the area embolized [6, 7].

Modern research in the field of vascular embolization demonstrates considerable progress in coil development, especially in the context of improving the materials and technologies for production of those. The key materials to produce endovascular coils include platinum alloys, nickel titanium (nitinol), stainless steel, and the magnesium and zincbased biodegradable alloys [2, 8]. Despite high cost, platinum alloys are widely used in clinical practice due to exceptional radiopacity ensuring accurate imaging during the intervention, optimal flexibility making it possible to adapt to the complex blood vessel anatomy, and high biocompatibility minimizing the risk of immune reactions [9]. Nitinol possessing superelasticity and shape memory effect makes it possible to restore initial configuration of the coil after delivery, which is especially important when treating complex aneurysms [10]. The stainless steel coils show radiopacity, but are inferior to other alloys (for example, to platinum ones). Stiffness of those resulting from high strength can hamper tight installation into the blood vessel. Therefore, the stainless steel coils are used mostly for occlusion of large diameter blood vessels [11, 12]. Biodegradable alloys represent a promising avenue in endovascular technology. Their capability of the controlled resorption after performing the therapeutic function makes it possible to minimize the risk of delayed complications and avoid re-interventions. Furthermore, ensuring safety via monitoring the magnesium and zinc ion levels in biological tissues remains an important aspect of the use of such materials [13].

In parallel with the research in the field of materials science, the endovascular coil evolution is related to optimization of the coil structural parameters. Modifications of the recent years were focused on improving the detachment mechanisms, increasing

the coil length (up to 50-60 cm), introducing flexible materials and innovative coatings that enhance thrombogenesis. The diverse morphology of the next-generation devices covers the spectrum between classic 2D configurations and 3D structures topographically adapted to the aneurysmal sac anatomy [4]. Introduction of nanocoatings (Target Nano, Axium EX) and 3D-printed constructs (Target 3D, Micrusframe) ensures effective filling of both small complex aneurisms and large cavities. Special focus is on biocompatible coatings: polyglycolic/polylactic acid microfilaments and hydrophilic acrylic copolymers, which minimize inflammatory responses [14-16]. It is assumed that the combination of additive technologies with bioactive coatings will make it possible to personalize selection of coiling systems considering the aneurism size, localization, and morphology, thereby increasing the endovascular intervention safety and efficacy.

The development of domestic endovascular coils requires a complex approach based on the analysis of relevant advances in materials science and engineering solutions. It is important to adapt world experience considering the specifics of the national industrial infrastructure and regulatory framework. This enables creation of competitive medical technologies compliant with international standards and meeting the demands of the domestic public health system. The systematic review of the key parameters of modern foreign endovascular coils, i.e. geometry, materials, frame features, and production technologies, will make it possible to identify the model design solutions typical for different manufacturers. It is assumed that comparison will reveal the dominant trends in the product key element design and make it possible to classify the coils based on the technological and structural characteristics. Understanding the relationship between materials, geometry, and production technologies will provide the basis for shaping the new criteria relevant for the development of innovative devices.

The study aimed to assess the dimensions, materials, and structural features of metal frames of the endovascular coils available on the market. The research objectives were as follows:

To conduct a systematic review of the range of endovascular coils in terms of geometric parameters (diameter, length, shape).

To perform microscopic analysis of the structural elements of the metal coil frames.

To characterize the methods to produce the key coil frame elements (atraumatic tip, main part and interlock).

To investigate the feature of the polymeric fiber attachment inside the frame and the effect of polymeric fibers on the structure.

## METHODS

The following endovascular coils were studied:

- Manufacturer COOK MEDICAL LLC (USA), model Nester G52754.
- 2. Manufacturer COOK MEDICAL LLC (USA), model MReye Flipper G20235.
- 3. Manufacturer MicroVention, Inc (USA), model Terumo AZUR 18 45-480810.
- 4. Manufacturer Boston Scientific Corporation (USA), model Interlock Spiral 2D M00136155.
- 5. Manufacturer Boston Scientific Corporation (USA), model Interlock Spiral -35 M001363700.
- Manufacturer PFM Medical GmbH (Germany), model Nit-Occlud PDA 145044V1.

The coil dimensions and design features were assessed using the NORGAU NVMIII-2010D video measuring system (Norgau Russland LLC, Russia).

## ORIGINAL RESEARCH I VASCULAR SURGERY

Table. Endovascular coil characteristics. Values are presented as M  $\pm$  SD, where M is the mean; SD is the standard deviation; the 95% confidence interval for each mean is provided in parentheses.

Mnufacturer	Model	Coil wire material	Wire diameter, mm	Coil diameter, mm	Atraumatic tip type	Interlock mechanism type	Polymer fiber attachment
COOK MEDICAL LLC (USA)	Nester G52754	Platinum	0.125 ± 0.003 (0.116-0.134)	0.537 ± 0.004 (0.526–0.548)	Spherical, melted	Coil-coil (screw-type connection)	Between the coil turns due to friction
COOK MEDICAL LLC (USA)	MReye Flipper G20235	Inconel®	0.172 ± 0.003 (0.163–0.181)	0.777 ± 0.007 (0.760-0.794)	Spherical, brazed	Coil-coil (screw-type connection)	Between the coil t urns due to friction
MicroVention, Inc (USA)	Terumo AZUR 18 45-480810	Platinum	0.072 ± 0.005 (0.059-0.085)	0.302 ± 0.004 (0.291–0.313)	Nibbled, covered with polymer glue	Detachment by electrical current	Hydrophilic polymer in the form of a sheath
Boston Scientific Corporation (USA)	Interlock Spiral 2D M00136155	Platinum	0.079 ± 0.003 (0.070-0.088)	0.306 ± 0.004 (0.295–0.317)	Spherical, brazed	Milled interlock	Between the coil turns due to friction
Boston Scientific Corporation (USA)	Interlock Spiral -35 M001363700	Platinum	0.176 ± 0.005 (0.163–0.189)	0.526 ± 0.005 (0.513–0.539)	Spherical, brazed (the diameter is larger than the coil thickness)	Groove-groove milled interlock	Between the coil turns due to friction
PFM Medical GmbH	Nit-Occlud PDA 145044V1	Titanium nickelide	0.243 ± 0.003 (0.234-0.252)	0.763 ± 0.005 (0.750-0.776)	Spherical, brazed	Coil-core (semi-helicoidal connection)	No

The coil samples were positioned freely on the microscope stage without applying mechanical tension in order to avoid deformation. To ensure the contrast and measurement accuracy, we used the annular reflection light source allowing for clearly visualize the contours of the structural elements. Measurement was performed using the INSPEC software (Micro-Vu, USA). The procedure included manual selection of the contour with the subsequent use of the Distance tool to determine the key geometric parameters: external coil diameter (based on the spiral extreme points) and wire thickness (three measurement repeats per parameter). Statistical processing of the results was performed using the Student's t-test in Statistica 10.0 (StatSoft, USA). The data provided in the Table

are presented as M  $\pm$  SD, where M is the mean; SD is the standard deviation.

### **RESULTS**

In terms of structure all the studied coils represent the spirals made of wire 0.07–0.25 mm in diameter (Table).

The Nester G52754 coil (COOK MEDICAL LLC) (Fig. 1) made of platinum consists of three elements: the atraumatic tip, the main coil with an increment equivalent to the wire diameter, and the interlock part. The interlock is achieved through screwing the spiral of the proximal coil part (about 2.2 mm long) onto the distal part of the delivery system. The

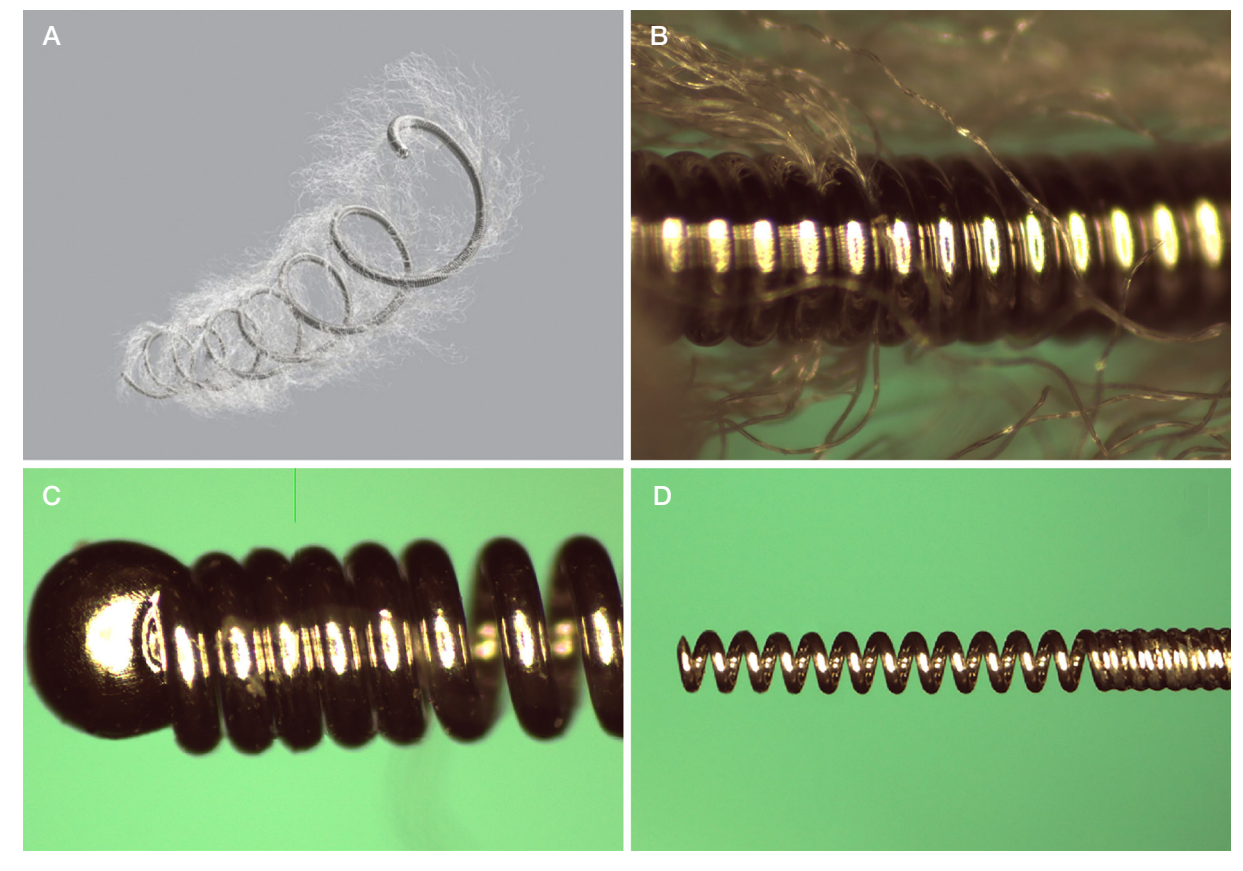


Fig. 1. Nester endovascular coil manufactured by COOK MEDICAL LLC: general view (A); fiber attachment (B); atraumatic tip (C); interlock part (D)

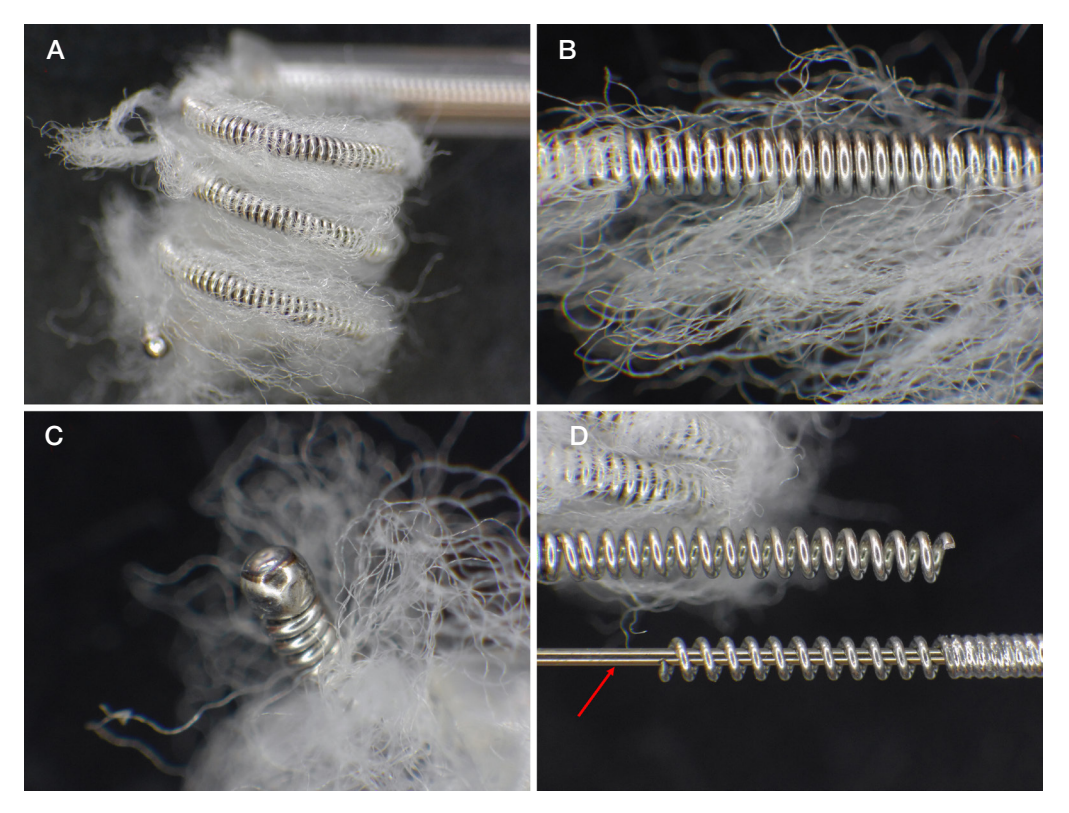


Fig. 2. MReye Flipper endovascular coil manufactured by COOK MEDICAL LLC: general view (A); fiber attachment (B); atraumatic tip (C); interlock parts of the coil and delivery system, delivery system rod (red arrow) (D)

atraumatic tip is shaped by the reflow method. The interlock coil is attached to the main one by brazing. The polymer fibers are held between the spirals by friction.

The MReye Flipper G20235 coil (COOK MEDICAL LLC) (Fig. 2) is structurally similar to Nester, but made of the Inconel® alloy belonging to the family of the nickel-chromium heatresistant alloys. Besides the material, the coil differs from Nester in geometric dimensions, it is also made of the larger diameter wire.

The Terumo AZUR 18 45-480810 coil (MicroVention, Inc.) (Fig. 3) belonging to the hydrogel coil family is made of platinum,

the atraumatic tip is made of a polymer, and the main structural feature of the product is the Electric Detachment System (EDS) for smooth and predictable detachment of the coil from the delivery system. For realization of the EDS, the delivery system comprising two electrical conductors running throughout is connected to the handle (not presented in the figure) having a built-in galvanic power source and an activation button. After pushing the button the electrolysis process is launched, through which the low-voltage electric current dissolves the interlock pin in about 20 s, releasing the coil.

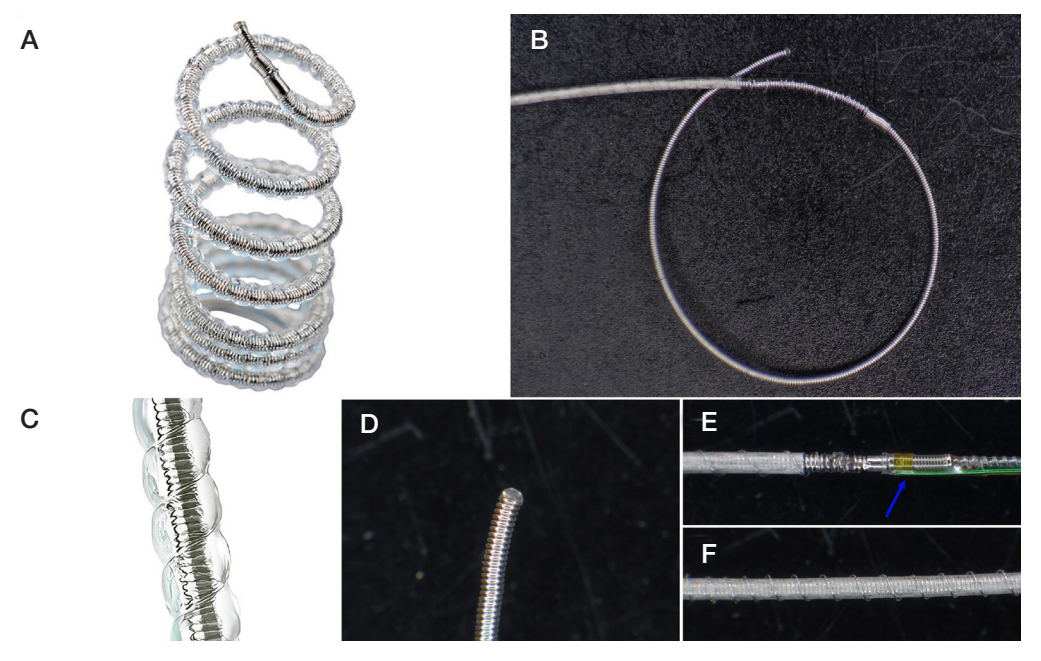


Fig. 3. Terumo AZUR 18 endovascular coil manufactured by MicroVention, Inc.: general view (A); distal part of the coil, in which the margin, where the hydrogel sheath begins, is pointed with the red arrow (B); activated hydrogel sheath (C); atraumatic tip (D); thermoelectric coil detachment system (blue \*) (E); hydrogel sheath (F)

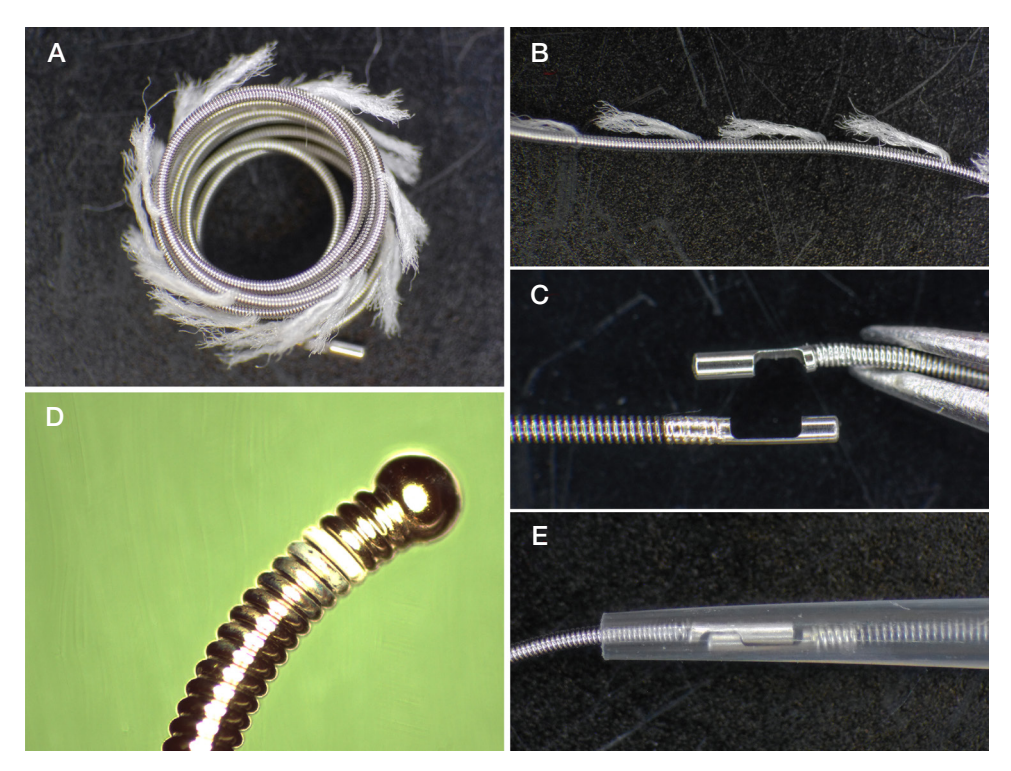


Fig. 4. Interlock Spiral 2D endovascular coil manufactured by Boston Scientific Corporation: general view (A); fiber attachment (B); interlock parts of coil and delivery system (C); atraumatic tip (D); interlocked coil and delivery system (E)

The Interlock Spiral 2D M00136155 coil (Boston Scientific Corporation) (Fig. 4) has much in common with the Nester and Flipper, but it is equipped with the groove-to-groove interlock mechanism held in engagement by the catheter tube of the delivery system. The interlock element (diameter 0.2 mm) is connected to the main coil by brazing. The polymer fibers are bundled together and evenly distributed between the spirals throughout the coil length. The atraumatic tip is made by brazing the platinum ball or reflow of the distal coil end.

The Interlock Spiral-35 M001363700 coil (Boston Scientific Corporation) (Fig. 5) is structurally identical to the previous model, but after the release from the delivery system the coil is not twisted into spirals, but is distributed in space in a chaotic manner. The polymer filaments, that are also bundled together, are longer than that of the Interlock Spiral 2D. The spherical atraumatic tip (0.8 mm) is produced by the reflow method. The interlock mechanism is tightly inserted in the coil without any traces of the glue or brazing, it is held by friction.

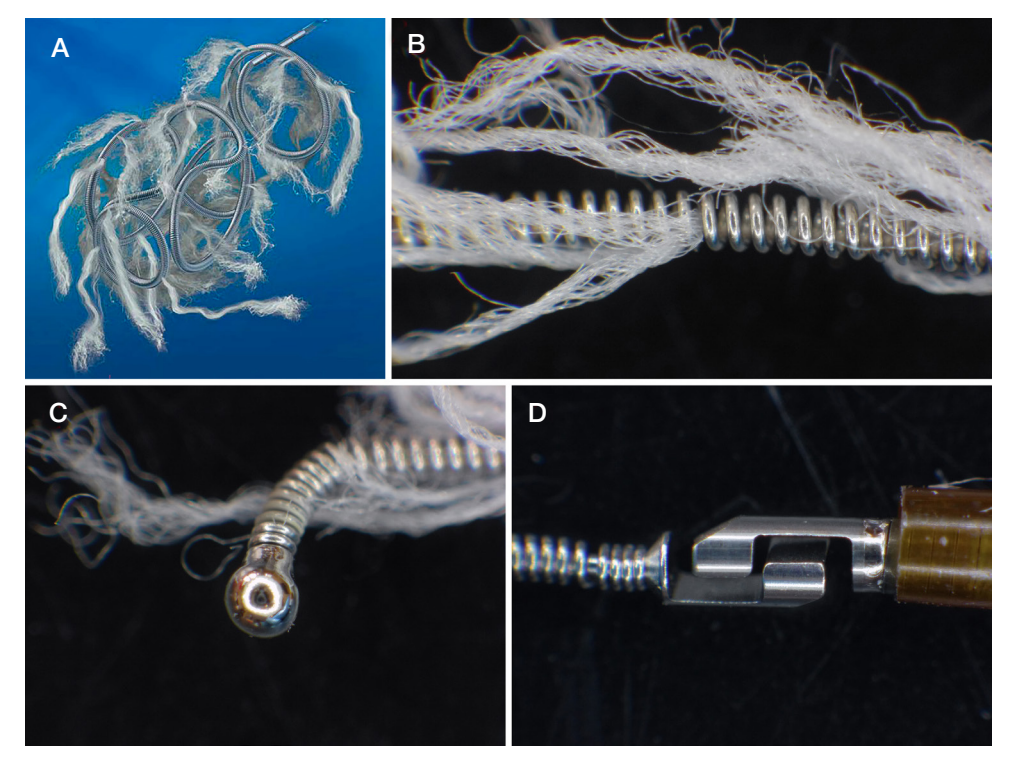


Fig. 5. Interlock Spiral - 35 endovascular coil manufactured by Boston Scientific Corporation: general view (A); fiber attachment (B); atraumatic tip (C); interlock part of the coil (D)

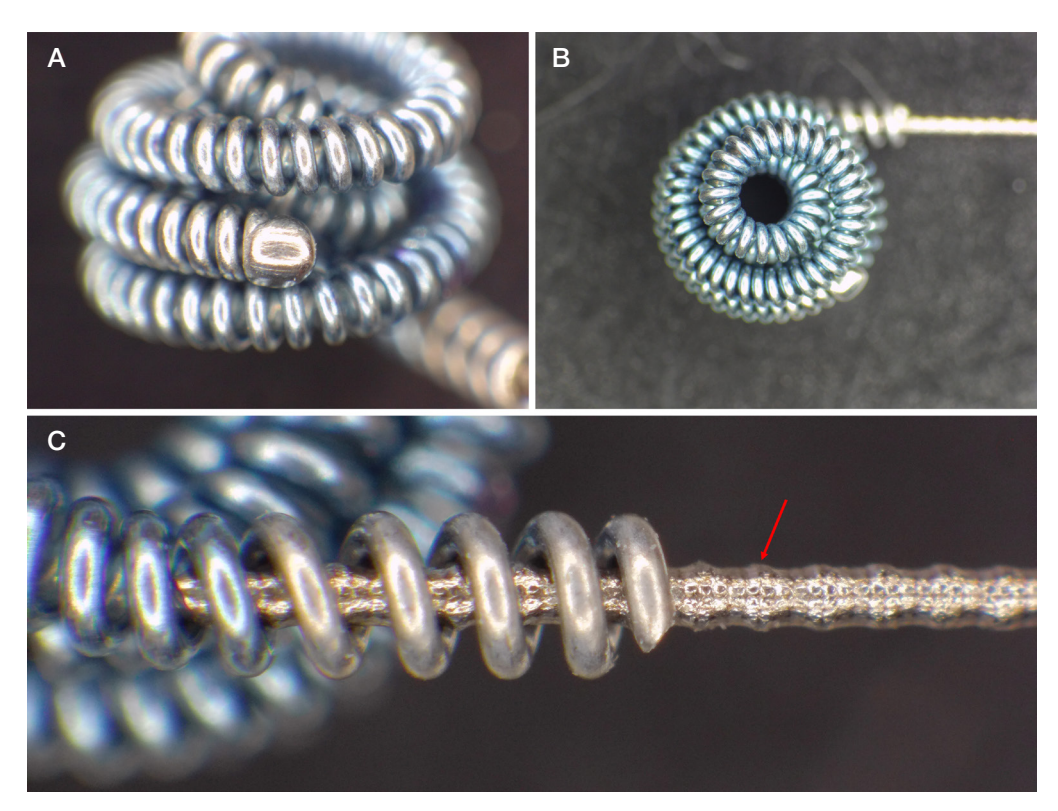


Fig. 6. Nit-Occlud PDA endovascular coil manufactured by PFM Medical GMBH: atraumatic tip (A); general view (B); interlock part, in which the screw notches on the delivery system rod for connection to the coil are pointed with the red arrow (C)

The Nit-Occlud PDA 145044V1 (PFM Medical GmbH) (Fig. 6) is the only coil considered that is made of titanium nickelide. After the release from the delivery system it is twisted into a tight stiff secondary coil. There are no polymer filaments. The interlock mechanism is realized through winding the turns of the coil onto the notches on the delivery system rod.

#### **DISCUSSION**

When developing sophisticated items, such as endovascular coils, the design team has to choose affordable materials and seek to maximize the structure simplicity and minimize the number of technological operations. This makes it possible to reduce the cost, waste, and the number of intermediate control stages.

The source wire diameter is the main factor determining the coil stiffness being the major selection criterion in endovascular surgery. With the emergence of soft, super-soft, and ultra-soft models, physicians now have an alternative to conventional stiff coils. Since soft coils are easier to insert in the affected area, practical understanding of their mechanical properties can help an endovascular surgeon select a certain coil [17]. Therefore, the coils made of the source wire 0.07 mm in diameter are considerably easier to install in the affected area compared to the coils made of the wire with the maximum diameter of 0.25 mm.

The presence of the atraumatic tip is an essential characteristic of the coil manufactured. The main complication of endovascular coiling is the risk of coil migration. The anchor coil technique is one of the key techniques reducing such risk [18]. The use of the coils with atraumatic tips allows the surgeon to minimize the risk of vascular wall perforation and endothelial damage, thereby increasing the intervention safety and contributing to its higher efficacy via reduction of the rate of intraoperative and postoperative complications.

The occlusion capability is likely to be the most important feature of any coil. The coiling technology is developed in order

to improve the occlusion efficacy by adding various elements or changing the coil parameters that are usually aimed to improve thrombogenicity or packing tightness. Some earlier generation coils, such as Nester и Tornado (Cook Medical, Bloomington, Indiana), representing the pushed platinum coils made of platinum and nichrome, have the nylon bibers contributing to occlusion through stimulation of formation of the thrombus filling the space between the coil turns [19]. This technique was also realized in the detachable coils, for example in Concerto (Medtronic) [20]. Another approach is designing the coils so soft that these behave as a liquid metal, effectively filling the target space. An example are the Ruby family coils (Penumbra Inc, Alameda, California) [21]. Other products, such as AZUR CX Hydrocoil (Terumo Medical), have a hydrogel coating that expands after the delivery, filling the space between the turns [22]. The hydrogel starts expanding in 3 min and achieves the maximum width by 20 min. That is why the complete target vessel occlusion may need time. One of the papers presents the mid-term results of the use of the coils with the hydrogel and fibrous coating for arterial embolization in the animal experiment. In a month after the procedure the arteries embolized with the hydrogel-coated coils were 100% occluded. In 4 months the results were 80% [23]. Thus, coils with the hydrogel coating show a stable occlusion effect in the medium term.

The analysis of the coils reviewed has shown that the Flipper and Nester models have the simplest design in terms of production. Elements of the frames of these coils are made of different alloys, the glue is not used in the construct, and the processing tools are publicly available. At the same time, platinum is an expensive and not always freely accessible material. The melted tip production may require specialized laser equipment. Relative simplicity of the design of the above coils does not lower high efficacy and safety of the use of such devices for treatment of a broad spectrum of vascular disorders, mostly arteriovenous malformations and iatrogenic vascular complications. The analysis of the results of the retrospective

cohort study including 102 cases of endovascular embolization with the Nester and Flipper occlusion coils has shown that the technical success rate was 100%. The clinical efficacy determined as achieving the target blood vessel occlusion and symptom regression was reported in 98% of patients. In terms of safety, the intervention profile was beneficial: no severe adverse events associated with the device migration, mechanical destruction or periprocedural complications were reported [24].

The weak point of the Terumo AZUR coil is the interlock mechanism activated by the electric current. Such a detachment principle has indisputable advantages when used in the neurointerventional procedures characterized by low blood flow rate. Such a design requires the development of the complex expensive electronic handle of the delivery system and the set of conductive elements. At the same time, when working inside peripheral blood vessels, the use of the coils equipped with the electrolytic detachment mechanism considerably limits the possibility of the implant postoperative maneuvering and positioning. Furthermore, the benefits of this technological solution remain unclear. The hydrophilic self-expanding sheath requires expertise and experience with such materials, as well as fixation with additional wire. At the same time, the use of the polymer atraumatic tip is a simple technological process that can provide the basis for the development of new coils.

The Interlock Spiral coils by Boston Scientific Corporation stand out due to the use of long sparsely arranged fibers for embolization, which simplifies the production process. However, the interlock mechanism is designed as two reciprocal cylindrical brackets, for the manufacture of which the expensive metalworking equipment is necessary, and high processing accuracy and the lack of sharp edges are critically important due to small size, to avoid damage to vessel walls after implantation.

In the Nit-Occlud coil PFM Medical GmbH refused to use polymer fibers, ensuring embolization due to the tightly twisted construct made of the elastic nitinol alloy. Nitinol produced by many companies is not subject to State control. The nitinol molding methods are well understood and realized using the affordable equipment. Simplicity of the interlock mechanism requiring no additional parts is one more benefit of such design.

It is important to develop a prototype based on the analysis of foreign analogues. However, the possibility of the endovascular coil import substitution is associated with a number of interrelated aspects requiring a comprehensive assessment. The analysis of the current situation on the Russian medical devices market demonstrates a steady upward trend in the share of domestic products [25]. According to the Consolidated Strategy on the Development of the Manufacturing Industry until 2030 and for the period up to 2035, in 2022, 26.8% of medical devices in the total market volume were of Russian origin, and it is planned to achieve the value of 36% by the year 2030, which is in line with

the strategic goals of ensuring technological sovereignty in the critically important industries [26].

The institutional support by the State implemented through the subsidy, preferential loan, and tax preference mechanisms is the key factor of the domestic production development [25, 27]. These measures create economic incentives for localization of production, which is confirmed by the dynamics of the growth in the number of Russian enterprises in the field of medical devices and equipment [28]. However, the industry's technological readiness for production of endovascular coils is limited due to structural problems [26, 29]. The main barrier is the lack of full-cycle production, including the dependence on the imported substrates and specialized equipment for precision processing of materials. One more factor is the need for the products to comply with the ISO 13485 international standards and EEU requirements, determining the need for the quality control system modernization. It is worth noting a considerable financial barrier for bringing medical products to the Russian market. As of October 2023, the costs of registering one product in the Russian Federation reach 1.5-7 million rubles, and the time spent on issuing a registration certificate can be 3-18 months [28]. The prospects for overcoming the above barriers are associated with the implementation of the cluster approach involving integration of the scientific research institutions, production facilities, and clinical sites. Creation of competence centers in the field of biocompatible materials and additive technologies, which will make it possible to reduce dependency on the imported components, seems to be a priority [26, 30].

Thus, despite the existing technological and economic barriers, import substitution of endovascular coils in Russia has great potential. The key condition of success is the possibility of the shift from prototype development to serial production, which requires a systematic State support and extrabudgetary fund-raising.

## CONCLUSIONS

Comparative analysis of the embolic coils produced by foreign manufacturers of medical equipment shows the dramatically different technical approaches to designing the devices similar in their purpose and effect. The alloys based on platinum, titanium nickelide and nickel-chromium alloy are used as the materials for coils. It is preferred that a polymer atraumatic tip and the "coil-core" interlock mechanism, along with the small diameter (in the range of 0.07–0.12 mm) nitinol wire as a material, are used to ensure the required biotechnical characteristics of the structure of the universal coil prototype. To determine the coil optimal shape and dimensions, it is planned to continue the study of their mechanical properties and polymer fibers used. The shift from prototype development to serial production of domestic embolic coils is possible, but it requires the creation of an appropriate technological base and significant investment costs.

## References

- Henkes H, Klisch J, Lylyk P. Will coiling survive through the next decade?
   J Clin Med. 2022; 11 (11): 3230. DOI: 10.3390/jcm11113230.
- Yueqi Z, Hongbo Z, Yiran Z, Huayin W, Liming W, Gen Z, et al. Endovascular metal devices for the treatment of cerebrovascular diseases. Adv Mater. 2018; 30 (52): e1805452. DOI: 10.1002/adma.201805452.
- Qiu MY, Suskin CB, Becerra-Garcia JJ, Roberts SH, Rucker DG, Zayed MA, et al. Quantification of the flexural rigidity of endovascular surgical devices using three-point bending tests.
- Res Sq. 2023. Preprint. DOI: 10.21203/rs.3.rs-3736325/v1.
- Campos JK, Lien BV, Wang AS, Lin L. Advances in endovascular aneurysm management: coiling and adjunctive devices. Stroke Vasc Neurol. 2020; 5 (1): 1–8. DOI: 10.1136/svn-2019-000303.
- Oka S, Kohno S, Arizono S, Onishi Y, Fumimoto M, Yoshida A, et al. Enhancing precision in vascular embolization: evaluating the effectiveness of the intentional early detachment technique with detachable coils in complex cases. CVIR Endovasc. 2024; 7 (1): 40. DOI: 10.1186/s42155-024-00453-7.

## ОРИГИНАЛЬНОЕ ИССЛЕДОВАНИЕ І СОСУДИСТАЯ ХИРУРГИЯ

- Xiao N, Lewandowski RJ. Embolic agents: coils. Semin Intervent Radiol. 2022; 39 (1): 113–118. DOI: 10.1055/s-0041-1740939.
- 7. Yuki I, Lee D, Murayama Y. Thrombus organization and healing in an experimental aneurysm model. Part II. The effect of various types of bioactive bioabsorbable polymeric coils. J Neurosurg. 2007; 107 (1): 109–120. DOI: 10.3171/JNS-07/07/0109.
- White JB, Ken CG, Cloft HJ, Kallmes DF. Coils in a nutshell: a review of coil physical properties. AJNR Am J Neuroradiol. 2008; 29 (7): 1242–6. DOI: 10.3174/ajnr.A1067.
- Cowley A, Woodward B. A healthy future: platinum in medical applications. Platin Met Rev. 2011; 55 (2): 98–107.
- Kónya A, Maxin M, Wright KC. New embolization coil containing a nitinol wire core: preliminary in vitro and in vivo experiences. J Vasc Interv Radiol. 2001; 12 (7): 869–77. DOI: 10.1016/S1051-0443(07)61513-9.
- Kobeiter H, Lapeyre M, Becquemin JP, et al. Percutaneous coil embolization of postcatheterization arterial femoral pseudoaneurysms. J Vasc Surg. 2002; 36 (1): 127–31. DOI: 10.1067/mva.2002.124372.
- Yoshioka H, Kuroda C, Hori S, et al. Splenic embolization for hypersplenism using steel coils. AJR Am J Roentgenol. 1985; 144 (6): 1269–74. DOI: 10.2214/ajr.144.6.1269.
- Oliver AA, Sikora-Jasinska M, Demir AG, Guillory RJ 2nd. Recent advances and directions in the development of bioresorbable metallic cardiovascular stents: insights from recent human and in vivo studies. Acta Biomater. 2021; 127: 1–23. DOI: 10.1016/j.actbio.2021.03.058.
- Waldau B, Fargen KM, Mack WJ, Wilson NM, Khaldi A, Hoh BL, et al. Axium MicroFX coil for the Completing Endovascular Aneurysm Surgery Study (ACCESS). Interv Neuroradiol. 2012; 18 (2): 200–7. DOI: 10.1177/159101991201800213.
- 75. Fargen KM, Blackburn S, Deshaies EM, Carpenter JS, Jabbour P, Mack WJ, et al. Final results of the multicenter, prospective Axium MicroFX for Endovascular Repair of IntraCranial Aneurysm Study (AMERICA). J Neurointerv Surg. 2015; 7 (1): 40–43. DOI: 10.1136/neurintsurg-2013-011049.
- Abi-Aad KR, Aoun RJN, Rahme RJ, Ward JD, Kniss J, Kwasny MJ, et al. New generation hydrogel endovascular aneurysm treatment trial (HEAT): a study protocol for a multicenter randomized controlled trial. Neuroradiology. 2018; 60 (10): 1075–84. DOI: 10.1007/s00234-018-2074-5.
- White JB, Ken CG, Cloft HJ, Kallmes DF. Coils in a nutshell: a review of coil physical properties. AJNR Am J Neuroradiol. 2008; 29 (7): 1242–6. DOI: 10.3174/ajnr.A1067. PMID: 18417605; PMCID: PMC8119172.
- Kanemaru K, Ezura M, Nishiyama Y, Yagi T, Yoshioka H, Fukumoto Y, et al. Anchor coil technique for arteriovenous fistula embolization. A technical note. Interv Neuroradiol. 2014; 20 (3): 283–6. DOI: 10.15274/INR-2014-10054. PMID: 24976089;

- PMCID: PMC4178771.
- Liebig T, Henkes H, Fischer S, Weber W, Miloslavski E, Mariushi W, et al. Fibered electrolytically detachable platinum coils used for the endovascular treatment of intracranial aneurysms. Interv Neuroradiol. 2004; 10 (1): 5–26. DOI: 10.1177/159101990401000101.
- Girdhar G, Read M, Sohn J, Shah C, Shrivastava S. In vitro thrombogenicity assessment of polymer filament modified and native platinum embolic coils. J Neurol Sci. 2014; 339 (1–2): 97– 101. DOI: 10.1016/j.jns.2014.01.030.
- Patel PJ, Arko FR 3rd. Ruby® coil and POD® system: a coil platform for fast and easy embolization. Endovasc Today. 2018; 17: 22–9.
- Ferral H. Hydrogel-coated coils: product description and clinical applications. Semin Intervent Radiol. 2015; 32 (4): 343–8. DOI: 10.1055/s-0035-1564809.
- Fohlen A, Namur J, Ghegediban H, Laurent A, Wassef M, Pelage JP. Midterm Recanalization after Arterial Embolization Using Hydrogel-Coated Coils versus Fibered Coils in an Animal Model. J Vasc Interv Radiol. 2019; 30 (6): 940–8. DOI: 10.1016/j. ivir.2018.05.005. PMID: 30174160.
- 24. Hochreiter-Hufford A, Gatz J, Griggs AM, Schoch RD, Birmingham KM, Frederick C, et al. Real-world data to support post-market safety and performance of embolization coils: evidence generation from a medical device manufacturer and data institute partnership. BMC Med Inform Decis Mak. 2024; 24: 263. DOI: 10.1186/s12911-024-02659-0.
- Makarenko ED. Mekhanizmy prodvizheniya rossijskogo medicinskogo oborudovaniya na vnutrennem rynke. Finansovye rynki i banki. 2024;
   (3): 24–29. DOI: 10.24412/2658-3917-2024-3-24-29. Russian.
- 26. Rasporyazhenie Pravitel'stva Rossijskoj Federacii ot 06.06.2020 № 1512-r «Ob utverzhdenii Svodnoj strategii razvitiya obrabatyvayushchej promyshlennosti Rossijskoj Federacii do 2024 goda i na period do 2035 goda» (v red. ot 09.09.2023 № 2436-r, 07.11.2023 № 3113-r, 21.10.2024 № 2963-r). Russian.
- Abdikeev NM. Realizaciya planov po importozameshcheniyu v vysokotekhnologichnyh otraslyah otechestvennoj promyshlennosti v usloviyah vneshnih sankcij. Nauchnye trudy Vol'nogo ekonomicheskogo obshchestva Rossii. 2022; (3): 202–14. Russian.
- Hodos DV, Mushenko RD. Perspektivy razvitiya rynka professional'nogo oborudovaniya v usloviyah transformacii sfery medicinskih uslug v RF. EV. 2024; 1 (36): 92–100. DOI: 10.36807/2411-7269-2024-1-36-92-100. Russian.
- 29. Nahod VI, Krivenko AN, Butkova TV. Implantiruemye medicinskie izdeliya: obzor rynka. Zdorov'e megapolisa. 2024; 4 (1): 209–16. DOI: 10.47619/2713-2617.zm.2024.v.5i4p1. Russian.
- Ershova EYu. Additivnye tekhnologii kak osnova narashchivaniya potenciala nacional'noj innovacionnoj sistemy. Vestnik Akademii znanij. 2025; 4 (69): 212–6. Russian.

#### Литература

- Henkes H, Klisch J, Lylyk P. Will coiling survive through the next decade?
   J Clin Med. 2022; 11 (11): 3230. DOI: 10.3390/jcm11113230.
- Yueqi Z, Hongbo Z, Yiran Z, Huayin W, Liming W, Gen Z, et al. Endovascular metal devices for the treatment of cerebrovascular diseases. Adv Mater. 2018; 30 (52): e1805452. DOI: 10.1002/adma.201805452.
- Qiu MY, Suskin CB, Becerra-Garcia JJ, Roberts SH, Rucker DG, Zayed MA, et al. Quantification of the flexural rigidity of endovascular surgical devices using three-point bending tests. Res Sq. 2023. Preprint. DOI: 10.21203/rs.3.rs-3736325/v1.
- Campos JK, Lien BV, Wang AS, Lin L. Advances in endovascular aneurysm management: coiling and adjunctive devices. Stroke Vasc Neurol. 2020; 5 (1): 1–8. DOI: 10.1136/svn-2019-000303.
- Oka S, Kohno S, Arizono S, Onishi Y, Fumimoto M, Yoshida A, et al. Enhancing precision in vascular embolization: evaluating the effectiveness of the intentional early detachment technique with detachable coils in complex cases. CVIR Endovasc. 2024; 7 (1): 40. DOI: 10.1186/s42155-024-00453-7.
- Xiao N, Lewandowski RJ. Embolic agents: coils. Semin Intervent Radiol. 2022; 39 (1): 113–118. DOI: 10.1055/s-0041-1740939.

- 7. Yuki I, Lee D, Murayama Y. Thrombus organization and healing in an experimental aneurysm model. Part II. The effect of various types of bioactive bioabsorbable polymeric coils. J Neurosurg. 2007; 107 (1): 109–120. DOI: 10.3171/JNS-07/07/0109.
- White JB, Ken CG, Cloft HJ, Kallmes DF. Coils in a nutshell: a review of coil physical properties. AJNR Am J Neuroradiol. 2008; 29 (7): 1242–6. DOI: 10.3174/ajnr.A1067.
- 9. Cowley A, Woodward B. A healthy future: platinum in medical applications. Platin Met Rev. 2011; 55 (2): 98–107.
- Kónya A, Maxin M, Wright KC. New embolization coil containing a nitinol wire core: preliminary in vitro and in vivo experiences. J Vasc Interv Radiol. 2001; 12 (7): 869–77. DOI: 10.1016/S1051-0443(07)61513-9.
- Kobeiter H, Lapeyre M, Becquemin JP, et al. Percutaneous coil embolization of postcatheterization arterial femoral pseudoaneurysms. J Vasc Surg. 2002; 36 (1): 127–31. DOI: 10.1067/mva.2002.124372.
- Yoshioka H, Kuroda C, Hori S, et al. Splenic embolization for hypersplenism using steel coils. AJR Am J Roentgenol. 1985; 144 (6): 1269–74. DOI: 10.2214/ajr.144.6.1269.
- 3. Oliver AA, Sikora-Jasinska M, Demir AG, Guillory RJ 2nd.

## ORIGINAL RESEARCH I VASCULAR SURGERY

- Recent advances and directions in the development of bioresorbable metallic cardiovascular stents: insights from recent human and in vivo studies. Acta Biomater. 2021; 127: 1–23. DOI: 10.1016/j.actbio.2021.03.058.
- Waldau B, Fargen KM, Mack WJ, Wilson NM, Khaldi A, Hoh BL, et al. Axium MicroFX coil for the Completing Endovascular Aneurysm Surgery Study (ACCESS). Interv Neuroradiol. 2012; 18 (2): 200–7. DOI: 10.1177/159101991201800213.
- 15. Fargen KM, Blackburn S, Deshaies EM, Carpenter JS, Jabbour P, Mack WJ, et al. Final results of the multicenter, prospective Axium MicroFX for Endovascular Repair of IntraCranial Aneurysm Study (AMERICA). J Neurointerv Surg. 2015; 7 (1): 40–43. DOI: 10.1136/neurintsurg-2013-011049.
- Abi-Aad KR, Aoun RJN, Rahme RJ, Ward JD, Kniss J, Kwasny MJ, et al. New generation hydrogel endovascular aneurysm treatment trial (HEAT): a study protocol for a multicenter randomized controlled trial. Neuroradiology. 2018; 60 (10): 1075–84. DOI: 10.1007/s00234-018-2074-5.
- White JB, Ken CG, Cloft HJ, Kallmes DF. Coils in a nutshell: a review of coil physical properties. AJNR Am J Neuroradiol. 2008; 29 (7): 1242–6. DOI: 10.3174/ajnr.A1067. PMID: 18417605; PMCID: PMC8119172.
- Kanemaru K, Ezura M, Nishiyama Y, Yagi T, Yoshioka H, Fukumoto Y, et al. Anchor coil technique for arteriovenous fistula embolization. A technical note. Interv Neuroradiol. 2014; 20 (3): 283–6. DOI: 10.15274/INR-2014-10054. PMID: 24976089; PMCID: PMC4178771.
- Liebig T, Henkes H, Fischer S, Weber W, Miloslavski E, Mariushi W, et al. Fibered electrolytically detachable platinum coils used for the endovascular treatment of intracranial aneurysms. Interv Neuroradiol. 2004; 10 (1): 5–26. DOI: 10.1177/159101990401000101.
- Girdhar G, Read M, Sohn J, Shah C, Shrivastava S. In vitro thrombogenicity assessment of polymer filament modified and native platinum embolic coils. J Neurol Sci. 2014; 339 (1–2): 97– 101. DOI: 10.1016/j.jns.2014.01.030.
- Patel PJ, Arko FR 3rd. Ruby<sup>®</sup> coil and POD<sup>®</sup> system: a coil platform for fast and easy embolization. Endovasc Today. 2018; 17: 22–9

- Ferral H. Hydrogel-coated coils: product description and clinical applications. Semin Intervent Radiol. 2015; 32 (4): 343–8. DOI: 10.1055/s-0035-1564809.
- Fohlen A, Namur J, Ghegediban H, Laurent A, Wassef M, Pelage JP. Midterm Recanalization after Arterial Embolization Using Hydrogel-Coated Coils versus Fibered Coils in an Animal Model. J Vasc Interv Radiol. 2019; 30 (6): 940–8. DOI: 10.1016/j. ivir.2018.05.005. PMID: 30174160.
- 24. Hochreiter-Hufford A, Gatz J, Griggs AM, Schoch RD, Birmingham KM, Frederick C, et al. Real-world data to support post-market safety and performance of embolization coils: evidence generation from a medical device manufacturer and data institute partnership. BMC Med Inform Decis Mak. 2024; 24: 263. DOI: 10.1186/s12911-024-02659-0.
- 25. Макаренко Е. Д. Механизмы продвижения российского медицинского оборудования на внутреннем рынке. Финансовые рынки и банки. 2024; (3): 24–29. DOI: 10.24412/2658-3917-2024-3-24-29.
- 26. Распоряжение Правительства Российской Федерации от 06.06.2020 № 1512-р «Об утверждении Сводной стратегии развития обрабатывающей промышленности Российской Федерации до 2024 года и на период до 2035 года» (в ред. от 09.09.2023 № 2436-р, 07.11.2023 № 3113-р, 21.10.2024 № 2963-р).
- Абдикеев Н. М. Реализация планов по импортозамещению в высокотехнологичных отраслях отечественной промышленности в условиях внешних санкций. Научные труды Вольного экономического общества России. 2022; (3): 202–14.
- Ходос Д. В., Мушенко Р. Д. Перспективы развития рынка профессионального оборудования в условиях трансформации сферы медицинских услуг в РФ. ЭВ. 2024; 1 (36): 92–100. DOI: 10.36807/2411-7269-2024-1-36-92-100.
- Наход В. И., Кривенко А. Н., Буткова Т. В. Имплантируемые медицинские изделия: обзор рынка. Здоровье мегаполиса. 2024; 4 (1): 209–16. DOI: 10.47619/2713-2617.zm.2024.v.5i4p1.
- 30. Ершова Е. Ю. Аддитивные технологии как основа наращивания потенциала национальной инновационной системы. Вестник Академии знаний. 2025; 4 (69): 212–6.

## CYTOCOMPATIBILITY OF PRESSURELESS SINTERED POROUS B4C-CERAMICS ASSESSED IN VITRO

Chepeleva EV™, Kozyr KV, Vaver AA, Khakhalkin VV

Institute of Experimental Biology and Medicine, Meshalkin National Medical Research Center, Novosibirsk, Russia

The materials used to restore bone defets have a number of systemic limitations. The metal implants showing high mechanical strength have an insufficient osseointegration capability, while ceramic and polymer materials have better biocompatibility, but do not meet the requirements of mechanical reliability in the zones of considerable load. In this regard, the study of new classes of materials combining the strength characteristics with the osseogenic potential seems to be a promising area. The study aimed to assess cytocompatibility of the boron carbide (B<sub>4</sub>C)-based porous ceramic material to confirm the possibility of its use for bone defect replacement. The B<sub>4</sub>C semi-finished products were manufactured by pressureless sintering at 1900–2100 °C; ultrastructure of the resulting sample surface was examined by atomic force and scanning electron microscopy. Citotoxicity of the B<sub>4</sub>C samples was estimated by an indirect method relative to human mesenchymal stem cells. The following cell survival rates were reported: 102.1% (24 h) and 99.1% (72 h) for the samples autoclaved; 110.0% (24 h) and 94.4% (72 h) for those treated with ethylene oxide. No significant intergroup differences were revealed (Mann–Whitney U-test). The findings allow us to consider B<sub>4</sub>C ceramics as a promising solution for bone grafting. However, further research is required to assess its clinical potential, including the development of sterilization protocols for larger and complex-shaped samples.

Keywords: boron carbide, bone implants, ceramics, sterilization, biocompatibility

Funding: the study was supported by the Russian Science Foundation grant (project No. 25-25-00187).

Author contribution: Chepeleva EV, Khakhalkin VV — study concept and design; Chepeleva EV, Kozyr KV, Vaver AA, Khakhalkin VV — experimental procedure and data processing; Chepeleva EV — manuscript writing; Kozyr KV, Vaver AA, Khakhalkin VV — manuscript editing.

Correspondence should be addressed: Elena V. Chepeleva

Rechkunovskaya, 15, Novosibirsk, 630055, Russia; e\_chepeleva@meshalkin.ru, amareza@mail.ru

Received: 10.09.2025 Accepted: 28.09.2025 Published online: 12.10.2025

DOI: 10.24075/brsmu.2025.044

Copyright: © 2025 by the authors. Licensee: Pirogov University. This article is an open access article distributed under the terms and conditions of the Creative Commons Attribution (CC BY) license (https://creativecommons.org/licenses/by/4.0/).

# ЦИТОСОВМЕСТИМОСТЬ СВОБОДНОСПЕЧЕННОЙ ПОРИСТОЙ В $_{\scriptscriptstyle 4}$ С-КЕРАМИКИ ПРИ ИССЛЕДОВАНИИ *IN VITRO*

Е. В. Чепелева <sup>™</sup>, К. В. Козырь, А. А. Вавер, В. В. Хахалкин

Институт экспериментальной биологии и медицины, Национальный медицинский исследовательский центр имени Е. Н. Мешалкина, Новосибирск, Россия

Материалы, применяемые при восстановлении костных дефектов, имеют ряд системных ограничений. Металлические импланты, демонстрируя высокую механическую прочность, обладают недостаточной остеоинтеграционной способностью, в то время как керамические и полимерные материалы имеют лучшую биосовместимость, но не удовлетворяют требованиям по механической надежности в зонах значительной нагрузки. В этой связи перспективным направлением представляется исследование новых классов материалов, сочетающих прочностные характеристики с остеогенным потенциалом. Цель исследования — оценить цитосовместимость пористого керамического материала на основе карбида бора (B<sub>4</sub>C) для подтверждения возможности его использования при замещении костных дефектов. Заготовки B<sub>4</sub>C изготавливали методом свободного спекания при 1900–2100 °C, исследование ультраструктуры поверхности полученных образцов проводили методами атомно-силовой и сканирующей электронной микроскопии. Цитотоксичность образцов В<sub>4</sub>C оценивали непрямым методом по отношению к мезенхимальным стволовым клеткам человека. Получены следующие показатели выживаемости клеток: для образцов после автоклавирования — 102,1% (24 ч) и 99,1% (72 ч); после обработки этиленоксидом — 110,0% (24 ч) и 94,4% (72 ч). Статистически значимых различий между группами не выявлено (*U*-критерий Манна–Уитни). Полученные результаты позволяют рассматривать В<sub>4</sub>C-керамику как перспективное решение для костной пластики, однако для оценки ее клинического потенциала требуются дальнейшие исследования, включая разработку протоколов стерилизации для образцов большего размера и сложной формы.

Ключевые слова: карбид бора, костные импланты, керамика, стерилизация, биосовместимость

Финансирование: исследование выполнено за счет гранта Российского научного фонда (проект № 25-25-00187).

**Вклад авторов:** Е. В. Чепелева, В. В. Хахалкин — концепция и дизайн исследования; Е. В. Чепелева, К. В. Козырь, А. А. Вавер, В. В. Хахалкин — проведение экспериментов и обработка данных; Е. В. Чепелева — написание статьи; К. В. Козырь, А. А. Вавер, В. В. Хахалкин — редактирование статьи.

Для корреспонденции: Елена Васильевна Чепелева

ул. Речкуновская, 15, г. Новосибирск, 630055, Россия; e\_chepeleva@meshalkin.ru, amareza@mail.ru

Статья получена: 10.09.2025 Статья принята к печати: 28.09.2025 Опубликована онлайн: 12.10.2025

DOI: 10.24075/vrgmu.2025.044

Авторские права: © 2025 принадлежат авторам. Лицензиат: РНИМУ им. Н. И. Пирогова. Статья размещена в открытом доступе и распространяется на условиях лицензии Creative Commons Attribution (CC BY) (https://creativecommons.org/licenses/by/4.0/).

## ОРИГИНАЛЬНОЕ ИССЛЕДОВАНИЕ І ТРАВМАТОЛОГИЯ

The today's traumatology and orthopedics face the challenge of reconstructing the large bone defects resulting from injuries, tumor resection or degenerative disorders [1]. The key approach to treatment of bone defects is the use of implantable materials for replacement. An ideal bone grafting material must be biocompatible, it must ensure osteoconduction (the process, when the bone replacement material serves as a structural matrix for osteoblast migration and proliferation), osteoinduction (the process, though which mesenchymal stem cells and osteoprogenitor cells are activated to differentiate in the osteogenic direction), as well as preserve the structural and mechanical properties of the regenerated bone [2]. There is currently no universal approach to bone grafting, and selection of the optimal material should be based on the specific clinical situation, defect size, and functional requirements. The range of materials widely used for bone defect replacement includes polymer matrices, bioceramics, and structural metal alloys; bone autografts and allografts are used in certain clinical situations [2–4]. The analysis of the effectiveness of available solutions shows systemic limitations that vary depending on the material class (Table 1) [3-11].

Today, the approaches to bone tissue restoration are focused on overcoming the current limitations through the development of fundamentally new solutions, among which several key directions can be distinguished. Tissue engineering allowing one to produce biomimetic structures by combining biocompatible matrices, progenitor cells, and bioactive molecules for targeted stimulation of osteogenesis is one of the most promising [4, 12–14]. A significant potential arises from the use of additive technologies (3D printing, selective laser melting), ensuring fabrication of implants having the complex architecture, controllable porosity and showing full compliance with the defect anatomy, which is impossible when using conventional methods [3, 15, 16].

Boron carbide is conventionally used as a structural material due to high hardness (up to 48.5 GPa), relatively low density (~2.52 g/cm³), and chemically inert nature [17]. The properties of  $B_4^{}$ C as an independent implantable material are currently poorly understood, and the scarse research is focused mainly on its role as an auxiliary component (modifying additives, protective coatings).

The study aimed to assess biocompatibility of the boron carbide-based ceramic samples by assessing their cytotoxic effects on mesenchymal stem cells.

### **METHODS**

The boron carbide semi-finished products were fabricated using the proprietary technology (patent No. RU 2 836 825 C1) [18]. During the technological process the source boron carbide powder (UNICHIM & EP, Russia) together with the adhesive agent was loaded into the XLB-3 atomizer dryer (Oriental Development Limited, China) for 1 h. Then the moulding powder was pressed using the SOROKIN 7.50 hydropneumatic press (Lekht, Russia) by cold pressing in order to produce a semifinished product, from which parts of appropriate shape were fabricated by mechanical processing. To remove the adhesive agent, the moulded part was put in the EKPS-50 muffle furnace (Smolensk SKTB-SPU, Russia). Then the semi-finished product was placed in the HP W 250 hot pressing device (FCT Systeme GmbH, Russia), in which pressureless sintering occured at at temperature of 1900-2100 °C in 14 phases involving heating, interim passage, and evacuating. The source semi-finished products were cut into samples sized 5  $\times$  5  $\times$  30 mm using the diamond blades and cleaned of the dust formed during cutting in the CD-4830 ultrasonic bath (Codyson, China) in the ethanol medium, then triple washed with distilled water for 40 min. Samples of the same size made of the BT 1-00 titanium (TNMK, Russia) were used as a reference material.

The structure of the surface of boron carbide-based samples was examined using the KYKY-EM6900LV scanning

**Table 1.** Comparative analysis of the major classes of materials for bone grafting [3–11]

Material class	Examples	Benefits	Limitations
		Biomaterials	
Bone tissue	Autograft	No risk of rejection, osteoconductivity, osteoinductivity	Limited material volume, additional surgical intervention and the associated risk of complications
	Allograft	No material volume limitation, osteoconductivity, osteoinductivity	Risk of immune rejection, risk of viral ot bacterial infection transmission, additional steps required for processing
Natural polymers	Proteins (collagen, fibrin, gelatin); polysaccharides (hyaluronic acid, chondroitin sulfate, alginate, chitosan)	Biocompatibility, biodegradability	Low mechanical strength, natural impurities, variability of properties
Natural minerals	Corals	Biocompatibility	Limited availability, slow resorption
	Sy	nthetic materials	
Metals	Titanium and alloys, tantalum, stainless steel, magnesium and alloys	High mechanical strength and wear resistance, biocompatibility	Low biodegradability, risk of toxicity due to release of metal ions, low resistance to cyclic loads
Bioceramics	Bioinert (ceramic aluminum oxide); biodegradable (hydroxyapatite, β-tricalcium phosphate, bioglass)	Biocompatibility, structural similarity to bone tissue, osteoconductivity/ osteoinductivity (depending on the structure and composition)	Brittleness, low bending and torsional strength, difficulty controlling the resorption rate
Polymers	Biodegradable (polycaprolactone, polylactic acid, polyglycolic acid)	Biodegradability, biocompatibility, versatility	Low mechanical strength, risk of inflammation due to degradation products
	Non-biodegradable (polyethylene, polyurethane)	Biocompatibility, versatility	
Composite materials	Hydroxyapatite-collagen matrices, calcium phosphate coatings on metals	Combination of mechanical properties and biocompatibility	Production complexity, high cost, possible structure heterogeneity

electron microscope (KYKY Technology Co., Ltd., China) at an accelerating voltage of 20 kV and electron beam amperage of 120  $\mu A$ . The sample surface topography was assessed with the NTEGRA II atomic microscopy system (NT-MDT Spectrum Instruments, Russia) in the semi-contact mode using the HA\_FM A silicon ultra-sharp cantilever (NT-MDT Spectrum Instruments, Russia) at the scan frequency of 0.7 Hz. The Nova-Px software (NT-MDT Spectrum Instruments, Russia) was used to produce the 3D topographic images.

Two methods widely used in laboratory and clinical practice were chosen for sample sterilization: physical (autoclaving) and chemical (ethylene oxide) ones. Before using in the experiment, a half of boron carbide samples and titanium samples were sterilized in an autoclave (Youjoy BES-12L-B-LED, China) at a temperature of 121 °C, pressure of 1.1 atm. for 45 min. The remaining samples were subjected to ethylene oxide sterilization in the Steri-Vac 5XL gas sterilizer/aerator (3M, USA) with the ethylene oxide concentration of 750 mg/L, temperature in the chamber 37°C, 70% humidity for 3 h. Aeration was carried out at the sterilization temperature for at least 8 h.

Cytotoxicity of samples was estimated by an indirect method involving assessment viability of the MSC-DP-1 human mesenchymal stem cells, MSCs (the shared research facility "Vertebrate Cell Culture Collection", Institute of Cytology RAS), in the extract obtained by incubation of the test samples in the DMEM/F12 culture medium (Servicebio, China) at 37 °C in the humid atmosphere with 5% CO $_{\rm 2}$  throughout 72 h in accordance with GOST ISO 10993-12-2023 [19]. Since MSCs are osteoblast progenitors that play a key role in bone tissue regeneration, the use of these makes it possible to estimate the extent, to which the test material would be compatible with the target biological medium *in vivo*.

The MSC-DP-1 cells were cultured in the DMEM/F12 medium (Servicebio, China) supplemented with 10% fetal calf serum (PanEco, Russia), 100 U/mL penicillin (Thermo Fisher Scientific, USA), 100 U/mL streptomycin (Thermo Fisher Scientific, USA), and 2 mmol/L L- glutamine (PanEco, Russia) at 37 °C in the humid atmosphere with 5% CO<sub>2</sub>. To assess cytotoxicity of the extracts, the cells were sown on the flat bottom 96-well culture plates, 2 × 10<sup>4</sup> cells per 200 µL of medium in each well, and incubated throughout 24 h. Then the medium was replaced with 200 µL of the extract. After incubation in extracts at 37 °C in the humid atmosphere with 5% CO<sub>2</sub> under standard conditions throughout 24 and 72 h, cell viability was measured using the EZcount™ XTT Cell Assay Kit for cell proliferation assessment (HiMedia Labs, India). Optical density of the well content was measured at the wavelength of 450 nm and reference wavelength of 690 nm using the Stat Fax-2100 microplate photometer (Awareness Technology, Inc., USA). The cells cultured in the DMEM/F12 complete medium were used as a control. The number of repetitions per group was 5. Cell viability was calculated as a ratio between optical density in experimental groups and the control group (A):

Cell viability = 
$$(A_{experimental group}/A_{control}) \times 100\%$$
.

The sample was considered non-toxic when the cell viability index was greater than 70% (GOST ISO 10993-5-2023) [20].

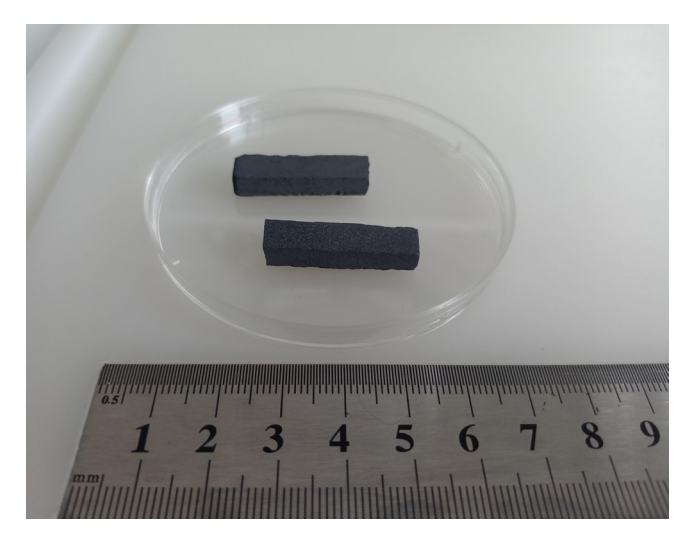


Fig. 1. Overall appearance of the  $\mathrm{B_4C}$  ceramics samples produced by pressureless sintering

Statistical data processing was performed using the Statistica 10.0 software (StatSoft, USA). The data distribution was tested for normality using the Shapiro–Wilk test. The Mann–Whitney U-test was used to identify intergroup differences. The study results are presented as Me (25%; 75%), where Me is the median, and interquartile range represents the values of the  $25^{\text{th}}$  and  $75^{\text{th}}$  percentiles. Bonferroni correction was applied to adjust for multiple comparisons; after adjustment the significance level was as follows:  $\alpha=0.0125$ ; the intergroup differences were considered significant at p<0.0125.

### **RESULTS**

The overall appearance of the boron carbide-based porous ceramic samples sized  $5 \times 5 \times 30$  mm is presented in Fig. 1. The material main technical characteristics are provided in Table 2.

Microphotographs of the surface of the sintered boron carbide-based samples show a typical polycrystalline structure with the pronounced granular organization, the average granule size is 40 µm (Fig. 2). The granules that are located tightly, without significant gaps, are mostly of angular morphology with rounded margins. The margins have a complex configuration, including twin structures and areas of incomplete fusion. The surface has a highly porous structure of the interconnected pores that are mostly roundish or oval with the average size of 30 µm. The analysis of interconnections between pores revealed the branched channels and chains forming the interpore communication system. The distribution of pores in the material volume is relatively even, with local clusters and the zones of increased porosity. The pore walls have a smooth surface with microroughness and partial fusion of adjacent structures.

Topographic analysis of the test sample structure demonstrates complex morphology of the relief showing the pronounced mucrostructure heterogeneity; the root-mean-square roughness of the samples is 0.203  $\pm$  0.037  $\mu m$ , the elevational gradient is 1.563  $\pm$  0.607  $\mu m$  (Fig. 3). On the surface

 $\textbf{Table 2.} \ \ \textbf{Characteristics of the B}_{4}\textbf{C ceramics samples produced by pressureless sintering [18]}$ 

Technical characteristics	Value	
Raw material particle size	3 µm	
Density	1.8 g/cm <sup>3</sup>	
Bending strength	250-300 Mpa	
Open porosity of the semi-finished product	50–60 %	

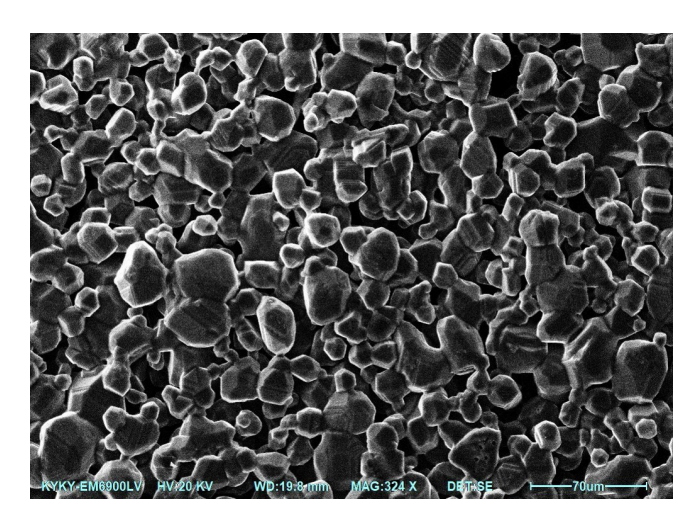


Fig. 2. Microstructure of the surface of the  $\rm B_4^{}C$  ceramics produced by pressureless sintering. Scale bar — 70  $\mu m$ 

the elements can be seen represented by both submicron-sized elevations and shallow depressions of various configurations. Uneven distribution of the altitude characteristics with formation of local hilly structures and the areas of increased roughness is reported.

When assessing viability of the MSCs cultured with the boron carbide sample-derived extracts, no toxic effects were revealed in both experimental and comparison groups (Fig. 4). The semi-finished products made of the BT 1-00 titanium were used as negative controls, which confirmed the method reproducibility and compliance of the biological response in the test system with the specified requirements. No effect of the sterilization method on the cell viability was also reported (Fig. 4).

### DISCUSSION

The findings showing the lack of significant cytotoxic effects of moulded boron carbide on the MSCs are consistent with the data of previous studies focused on the material biocompatibility. However, in these studies boron carbide was tested as a powder or single particles. It was earlier shown that the B,C nanoparticles produced by solvothermal synthesis

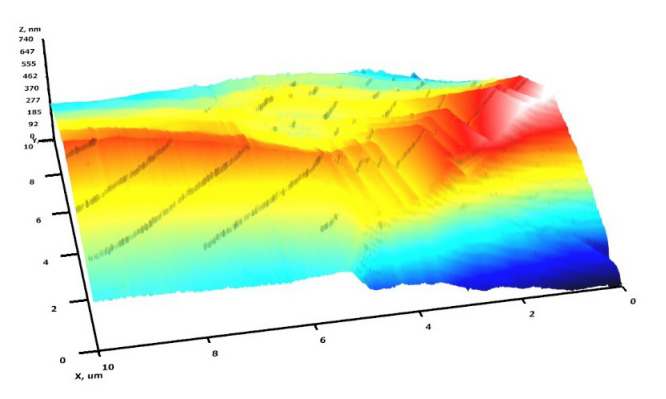


Fig. 3. AFM image of the relief of the surface of the  $B_4C$  ceramics produced by pressureless sintering. Field size  $10\times10~\mu m$ . Scale of the Z axis:  $0-0.74~\mu m$ 

have no toxic effect on the HeLa (cervical cancer) and HEK-293 (human embryonic kidney) cells in the concentrations of 100–800 µg/L [21]. Biocompatibility of amorphous boron carbide powder when contacting both somatic (Hs680 fibroblasts) and immune (RAW 264.7 macrophages) cells was also reported [22]. The lack of significant differences in cell viability between groups subjected to autoclaving and ethylene oxide sterilization suggests stability of the  $\rm B_4C$  sample properties and tolerance of samples to sorption of toxic compounds during processing. It should be noted that in this study small boron carbide samples (5  $\times$  5  $\times$  30 mm) were used. In the future, further research may be required to select the conditions for sterilization of the larger and/or more complex-shaped samples, since the material porous structure can hinder diffusion of the sterilizing agents and contribute to accumulation of condensate in deep zones.

Currently, the vast majority of papers in the field of the boron carbide medical use are focused on using the  $B_4C$  nanoparticles as the highly effective carriers for targeted boron-10 isotope delivery within the framework of the boron neutron capture therapy of malignant neoplasms [23]. In contrast to the extensively studied therapeutic use, the issues related to the use of  $B_4C$  as a biocompatible material for implants are poorly undestood. The use of  $B_4C$  as an additive when making porous ceramic matrices of aluminum oxide results in improvement of their mechanical properties and cytocompatibility [24], but the

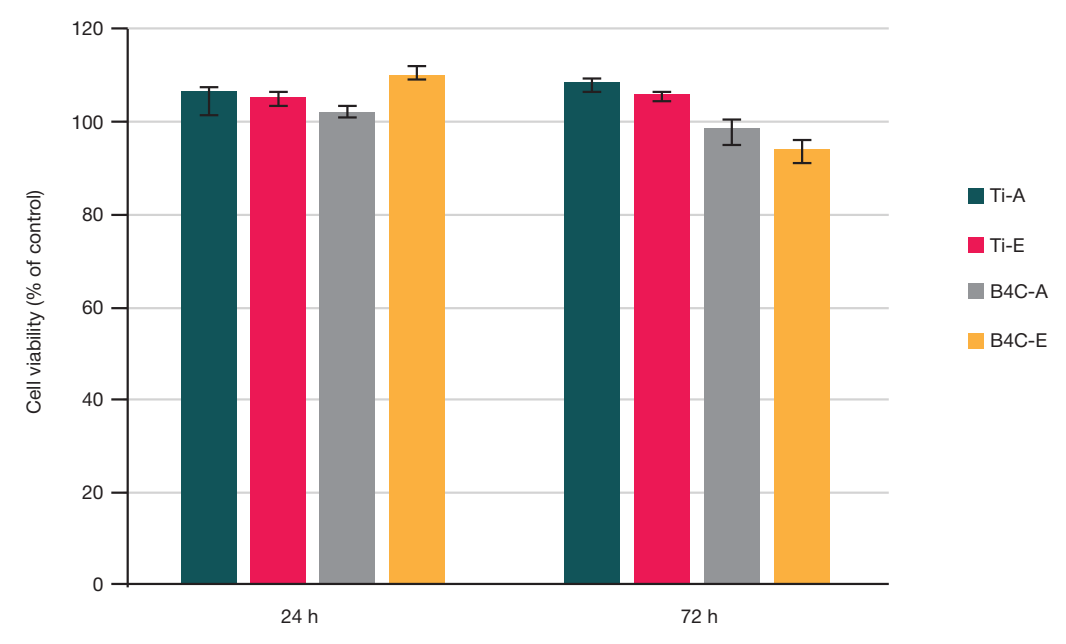


Fig. 4. Viability of the MSC-DP-1 mesenchymal stem cells after culturing for 24 and 72 h with the extracts obtained from the boron carbide (B<sub>4</sub>C) and titanium (Ti) samples sterilized by autoclaving (A) or with ethylene oxide (E). Me (25%; 75%), Mann-Whitney U-test

detailed mechanisms underlying these effects require further investigation.

When constructing porous ceramic matrices for bone replacement, the main task is to optimize their architecture that must ensure both mechanical stability and the conditions contributing to effective diffusion of nutrients and oxygen [25]. Based on the results of a number of studies, the optimal percentage of porosity is within the limits of 40-90% [3]. A fundamental contradiction emerges: on the one hand, the material porosity contributes to adhesion, proliferation, and differentiation of MSCs into osteoblasts, but on the other hand high porosity limits mechanical strength, which results in the need to search for the compromise between these parameters [6]. As for the dense matrix made of hydroxyapatite, the most common ceramic-based alloplastic material, the bending strength limits are within 38-250 MPa; as for the porous matrix, the bending strength limit depending on the pore shape and concentration is 2-11 MPa, which is considerably lower compared to that of the bone tissue (135-193 MPa) [26]. Despite the fact that there numerous methods to modify the calcium phosphate ceramics, this material is still inferior to the bone tissue in flexibility, elasticity, and strength. Due to brittleness, such implants are not used to restore the bones that bear a significant load [6]. In such cases (for example, when manufacturing the components of the hip joint endoprosthesis), the class A ceramic aluminum oxide (Al<sub>2</sub>O<sub>3</sub>) can be used as an alternative material [27]. The boron carbidebased porous ceramics can theoretically be used for implants as an alternative to the ceramic aluminum oxide-based materials in order to reduce the load on the joint, since it has lower density (approximately 1.8 g/cm³), which is comparable with the cortical bone tissue density, while the density of the aluminum oxide-based ceramics is 3.94 g/cm³ [6]. It should be noted that the ceramic aluminum oxide bending strength is higher than that of the sintered boron carbide-based ceramics (500 MPa and 250-300 MPa, respectively). One technological solution to improve the porous B<sub>4</sub>C matrix strength can be the aluminum impregnation accomplished through application of metal powder on the matrix and repeated sintering at the temperature above the aluminum melting point (above 660 °C). The ceramic composite produced in this way has a specific gravity of 2.2-2.6 g/cm<sup>3</sup> and the bending strength of at least 600 MPa [18].

The pore geometry and the material surface roughness are additional factors affecting adhesion and cell proliferation in the implantation site [28]. The pore complex spatial organization not only increases the area for cell adhesion, but produces mechanical stimuli for cell differentiation. The surface roughness, in turn, contributes to adhesion of the extracellular matrix proteins via integrin receptors, and the surface hydrophilicity associated with microrelief ensures the optimal wettability, thereby contributing to the nutrient diffusion and cell migration [29]. It has been shown that osteoblast adhesion and proliferation on the hydroxyapatite surfaces increase with increasing surface roughness from 0.733  $\pm$  0.203 to 4.680  $\pm$ 0.433 µm [30]. In this study we did not assess cell adhesion and proliferation on the surface of the boron carbide-based ceramics to determine the optimal material processing method; further research is planned.

### **CONCLUSIONS**

The study conducted has shown cytocompatibility of the ceramic samples made of boron carbide by pressureless sintering, which makes this material a promising candidate to be used for medical implants. However, the study limitations associated with small sample size require validation in further experiments involving large or complex-structured semi-finished products. In clinical practice, the material developed can be used to produce personalized implants for replacement of bone tissue defects in maxillofacial surgery and orthoperdics, especially in the cases requiring the combination of mechanical strength and bone tissue integration capacity. It is reasonable to use the B<sub>4</sub>C ceramics as a component of the combined constructs for arthroplasty, in which its low density makes it possible to reduce the total endoprosthesis weight. To improve the boron carbidebased porous matrix strength, it is a far-reaching approach to produce composite materials by impregnation of semi-finished products with molten metals. Further directions of assessing the B<sub>4</sub>C ceramics biocompatibility include estimation of the effect of miscrostructure (particle size, porosity) on the surface adhesive properties and osteogenic activity in vitro, study of the material long-term stability under physiological conditions, as well as investigation of the stress-corrosion behavior with the cyclic load mimicking the natural biomechanics, which is especially important for joint replacement.

### References

- Hoveidaei AH, Ghaseminejad-Raeini A, Esmaeili S, Sharafi A, Ghaderi A, Pirahesh K, et al. Effectiveness of synthetic versus autologous bone grafts in foot and ankle surgery: a systematic review and meta-analysis. BMC Musculoskelet Disord. 2024; 25 (1): 539.
- Vaiani L, Boccaccio A, Uva AE, Palumbo G, Piccininni A, Guglielmi P, et al. Ceramic materials for biomedical applications: an overview on properties and fabrication processes. J Funct Biomater. 2023; 14 (3): 146.
- Bilyalov AR, Minasov BSH, Yakupov RR, Akbashev VN, Rafikova GA, Bikmeev AT, i dr. Ispol'zovanie keramicheskoj 3D-pechati dlya zadach tkanevoj inzhenerii: obzor. Politravma. 2023; (1): 89–109. DOI: 10.24412/1819-1495-2023-1-89-109. Russian.
- Vlasova TI, Arsenteva EV, Hudajberenova GD, Polyakova DI. Sovremennyj vzglyad na ispol'zovanie kostnyh zamenitelej i vozmozhnost' usileniya ih osteogennosti kletochnymi tekhnologiyami. Medicinskij vestnik Bashkortostana. 2020; 15 (2): 53–58. Russian.
- 5. Arif U, Haider S, Haider A, Khan N, Alghyamah AA, Jamila N,

- et al. Biocompatible polymers and their potential biomedical applications: a review. Curr Pharm Des. 2019; 25 (34): 3608–19. DOI: 10.2174/1381612825999191011105148.
- Muhametov UF, Lyulin SV, Borzunov DYu, Gareev IF, Bejlerli OA, Yang G, i dr. Alloplasticheskie i implantacionnye materialy dlya kostnoj plastiki: obzor literatury. Kreativnaya hirurgiya i onkologiya. 2021; 11 (4): 343–53. DOI: 10.24060/2076-3093-2021-11-4-343-353. Russian.
- Popov AA, Kirsanova VA, Sviridova IK, Akhmedova SA, Filyushin MM, Sergeeva NS. Osteo-replacement properties of scleractinium coral aquaculture skeleton (experimental study). Russ J Transplantol Artif Organs. 2019; 21 (3): 121–6. DOI: 10.15825/1995-1191-2019-3-121-126.
- Brett E, Flacco J, Blackshear C, Longaker MT, Wan DC. Biomimetics of bone implants: the regenerative road. Biores Open Access. 2017; 6 (1): 1–6. DOI: 10.1089/biores.2016.0044.
- Smirnov IV, Smirnova PV, Teterina AYU, Kalita VI, Komlev VS. Formirovanie bioaktivnyh keramicheskih pokrytij na titanovyh implantatah. Geny i kletki. 2022; 17 (3): 215. Russian.
- 10. Poprygina TD, Ponomareva NI, Gordeev SK, Samodaj VG.

## ОРИГИНАЛЬНОЕ ИССЛЕДОВАНИЕ І ТРАВМАТОЛОГИЯ

- Impregnirovanie uglerodnyh nanostrukturnyh implantatov (UNI) kostnym gidroksiapatitom. Prikladnye informacionnye aspekty mediciny. 2022; 25 (1): 51–7. DOI: 10.18499/2070-9277-2022-25-1-51-57. Russian.
- Pankratov AS, Fadeeva IS, Yurasova YuB, Grinin VM, CHerkesov IV, Korshunov VV, i dr. Osteoinduktivnyj potencial chastichno demineralizovannogo kostnogo matriksa i vozmozhnosti ego ispol'zovaniya v klinicheskoj praktike. Vestnik RAMN. 2022; 77 (2): 143–51. Russian.
- 12. Liu J, Yang L, Liu K, Gao F. Hydrogel scaffolds in bone regeneration: their promising roles in angiogenesis. Front Bioeng Biotechnol. 2023; 11: 1217874. DOI: 10.3389/fbioe.2023.1217874.
- Cichoń E, Guzik M. Bacterial-derived polyhydroxyalkanoate/ bioceramic composites in clinical practice: state of the art and future perspectives. ACS Biomater Sci Eng. 2025; 11 (8): 4653–70.
- Fan D, Liu Y, Wang Y, Wang Q, Guo H, Cai Y, et al. 3D printing of bone and cartilage with polymer materials. Front Pharmacol. 2022; 13: 1044726.
- 15. Marchenko ES, Gordienko II, Kozulin AA, Bajgonakova GA, Borisov SA, Garin AS, i dr. Issledovanie biosovmestimosti poristyh 3D-TiNi implantatov v usloviyah *in vivo*. Sibirskij zhurnal klinicheskoj i eksperimental'noj mediciny. 2024; 39 (1): 184–93. DOI: 10.29001/2073-8552-2024-39-1-184-193. Russian.
- Crovace AM, Lacitignola L, Forleo DM, Staffieri F, Francioso E, Di Meo A, et al. 3D biomimetic porous titanium (Ti6Al4V ELI) scaffolds for large bone critical defect reconstruction: an experimental study in sheep. Animals (Basel). 2020; 10 (8): 1389.
- 17. Martynov RS, Pak AYa, Volokitin OG, Nikitin DS, Larionov KB, Povalyaev PV, i dr. Sintez poroshka karbida bora bezvakuumnym elektrodugovym metodom i poluchenie ob"emnoj keramiki metodom iskrovogo plazmennogo spekaniya. Vestnik Permskogo nacional'nogo issledovatel'skogo politekhnicheskogo universiteta. Mashinostroenie, materialovedenie. 2023; 25 (3): 65–76. DOI: 10.15593/2224-9877/2023.3.07. Russian.
- Hahalkin W, avtor. Sposob polucheniya legkogo keramicheskogo kompozita. Patent RF № RU2836825C1. 24.03.2025. Russian.
- 19. GOST ISO 10993-12-2023. Izdeliya medicinskie. Ocenka biologicheskogo dejstviya medicinskih izdelij. CHast' 12. Otbor i podgotovka obrazcov dlya provedeniya issledovanij: mezhgosudarstvennyj standart: vveden 2024-06-01. Mezhgosudarstvennyj sovet po standartizacii, metrologii i sertifikacii. Moskva: Standartinform, 2023. Russian.
- GOST ISO 10993-5-2023. Izdeliya medicinskie. Ocenka biologicheskogo dejstviya medicinskih izdelij. CHast' 5. Issledovaniya

- na citotoksichnost' metodami *in vitro*: mezhgosudarstvennyj standart: vveden v dejstvie 01.06.2024. Mezhgosudarstvennyj sovet po standartizacii, metrologii i sertifikacii. Moskva: Standartinform, 2023. Russian.
- Singh P, Kaur G, Singh K, Kaur M, Kumar M, Meena R, et al. Nanostructured boron carbide (B4C): A bio-compatible and recyclable photo-catalyst for efficient wastewater treatment. Materialia. 2018; 1: 258–64.
- Stodolak-Zych E, Gubernat A, Ścisłowska-Czarnecka A, Chadzińska M, Zych L, Zientara D, et al. The influence of surface chemical composition of particles of boron carbide powders on their biological properties. Appl Surf Sci. 2022; 582: 152380.
- Wróblewska A, Szermer-Olearnik B, Szczygieł A, Węgierek-Ciura K, Mierzejewska J, Kozień D, et al. Macrophages as carriers of boron carbide nanoparticles dedicated to boron neutron capture therapy. J Nanobiotechnol. 2024; 22 (1): 183.
- Öksüz KE. Macro-porous aluminum oxide-boron carbide ceramics for hard tissue applications. Recep Tayyip Erdoğan Üniv Fen Mühendis Bilim Derg. 2023; 4 (2): 65–75.
- Boccaccio A, Fiorentino M, Uva AE, Laghetti LN, Monno G. Rhombicuboctahedron unit cell based scaffolds for bone regeneration: geometry optimization with a mechanobiologydriven algorithm. Mater Sci Eng C Mater Biol Appl. 2018; 83: 51–66. DOI: 10.1016/j.msec.2017.09.004.
- 26. CHuprunov KO. Razrabotka metoda polucheniya nanostrukturnyh sfericheskih poroshkovyh materialov na osnove gidroksilapatita s reguliruemymi fazovym sostavom i pokazatelyami dispersnosti [dissertaciya]. M., 2022. Russian.
- Nekisheva AA, Abdulazizov BD, Peshekhodko DI. Obzor materialov dlya izgotovleniya endoprotezov tazobedrennogo sustava. Medicina. Sociologiya. Filosofiya. Prikladnye issledovaniya. 2020; 6: 48–54. Russian.
- Marques A, Miranda G, Silva F, Pinto P, Carvalho Ö. Review on current limits and potentialities of technologies for biomedical ceramic scaffolds production. J Biomed Mater Res B Appl Biomater. 2021; 109 (3): 377–93. DOI: 10.1002/jbm.b.34706.
- Cai S, Wu C, Yang W, Liang W, Yu H, Liu L. Recent advance in surface modification for regulating cell adhesion and behaviors. Nanotechnol Rev. 2020; 9 (1): 971–89. DOI: 10.1515/ntrev-2020-0076.
- Deligianni DD, Katsala ND, Koutsoukos PG, Missirlis YF. Effect of surface roughness of hydroxyapatite on human bone marrow cell adhesion, proliferation, differentiation and detachment strength. Biomaterials. 2001; 22 (1): 87–96. DOI: 10.1016/S0142-9612(00)00174-5.

### Литература

- Hoveidaei AH, Ghaseminejad-Raeini A, Esmaeili S, Sharafi A, Ghaderi A, Pirahesh K, et al. Effectiveness of synthetic versus autologous bone grafts in foot and ankle surgery: a systematic review and meta-analysis. BMC Musculoskelet Disord. 2024; 25 (1): 539.
- Vaiani L, Boccaccio A, Uva AE, Palumbo G, Piccininni A, Guglielmi P, et al. Ceramic materials for biomedical applications: an overview on properties and fabrication processes. J Funct Biomater. 2023; 14 (3): 146.
- Билялов А. Р., Минасов Б. Ш., Якупов Р. Р., Акбашев В. Н., Рафикова Г. А., Бикмеев А. Т., и др. Использование керамической 3D-печати для задач тканевой инженерии: обзор. Политравма. 2023; (1): 89–109. DOI: 10.24412/1819-1495-2023-1-89-109.
- Власова Т. И., Арсентьева Е. В., Худайберенова Г. Д., Полякова Д. И. Современный взгляд на использование костных заменителей и возможность усиления их остеогенности клеточными технологиями. Медицинский вестник Башкортостана. 2020; 15 (2): 53–58.
- Arif U, Haider S, Haider A, Khan N, Alghyamah AA, Jamila N, et al. Biocompatible polymers and their potential biomedical applications: a review. Curr Pharm Des. 2019; 25 (34): 3608–19. DOI: 10.2174/1381612825999191011105148.
- 6. Мухаметов У. Ф., Люлин С. В., Борзунов Д. Ю., Гареев И. Ф., Бейлерли О. А., Yang G., и др. Аллопластические и

- имплантационные материалы для костной пластики: обзор литературы. Креативная хирургия и онкология. 2021; 11 (4): 343–53. DOI: 10.24060/2076-3093-2021-11-4-343-353.
- Popov AA, Kirsanova VA, Sviridova IK, Akhmedova SA, Filyushin MM, Sergeeva NS. Osteo-replacement properties of scleractinium coral aquaculture skeleton (experimental study). Russ J Transplantol Artif Organs. 2019; 21 (3): 121–6. DOI: 10.15825/1995-1191-2019-3-121-126.
- Brett E, Flacco J, Blackshear C, Longaker MT, Wan DC. Biomimetics of bone implants: the regenerative road. Biores Open Access. 2017; 6 (1): 1–6. DOI: 10.1089/biores.2016.0044.
- 9. Смирнов И. В., Смирнова П. В., Тетерина А. Ю., Калита В. И., Комлев В. С. Формирование биоактивных керамических покрытий на титановых имплантатах. Гены и клетки. 2022; 17 (3): 215.
- Попрыгина Т. Д., Пономарева Н. И., Гордеев С. К., Самодай В. Г. Импрегнирование углеродных наноструктурных имплантатов (УНИ) костным гидроксиапатитом. Прикладные информационные аспекты медицины. 2022; 25 (1): 51–7. DOI: 10.18499/2070-9277-2022-25-1-51-57.
- Панкратов А. С., Фадеева И. С., Юрасова Ю. Б., Гринин В. М., Черкесов И. В., Коршунов В. В., и соавт. Остеоиндуктивный потенциал частично деминерализованного костного матрикса и возможности его использования в клинической практике. Вестник РАМН. 2022; 77 (2): 143–51.

## ORIGINAL RESEARCH I TRAUMATOLOGY

- Liu J, Yang L, Liu K, Gao F. Hydrogel scaffolds in bone regeneration: their promising roles in angiogenesis. Front Bioeng Biotechnol. 2023; 11: 1217874. DOI: 10.3389/fbioe.2023.1217874.
- Cichoń E, Guzik M. Bacterial-derived polyhydroxyalkanoate/ bioceramic composites in clinical practice: state of the art and future perspectives. ACS Biomater Sci Eng. 2025; 11 (8): 4653–70.
- Fan D, Liu Y, Wang Y, Wang Q, Guo H, Cai Y, et al. 3D printing of bone and cartilage with polymer materials. Front Pharmacol. 2022; 13: 1044726.
- Марченко Е. С., Гордиенко И. И., Козулин А. А., Байгонакова Г. А., Борисов С. А., Гарин А. С., и др. Исследование биосовместимости пористых 3D-TiNi имплантатов в условиях *in vivo*. Сибирский журнал клинической и экспериментальной медицины. 2024; 39 (1): 184–93. DOI: 10.29001/2073-8552-2024-39-1-184-193.
- Crovace AM, Lacitignola L, Forleo DM, Staffieri F, Francioso E, Di Meo A, et al. 3D biomimetic porous titanium (Ti6Al4V ELI) scaffolds for large bone critical defect reconstruction: an experimental study in sheep. Animals (Basel). 2020; 10 (8): 1389.
- 17. Мартынов Р. С., Пак А. Я., Волокитин О. Г., Никитин Д. С., Ларионов К. Б., Поваляев П. В., и др. Синтез порошка карбида бора безвакуумным электродуговым методом и получение объемной керамики методом искрового плазменного спекания. Вестник Пермского национального исследовательского политехнического университета. Машиностроение, материаловедение. 2023; 25 (3): 65–76. DOI: 10.15593/2224-9877/2023.3.07.
- Хахалкин В. В., автор. Способ получения легкого керамического композита. Патент РФ № RU2836825C1. 24.03.2025.
- 19. ГОСТ ISO 10993-12-2023. Изделия медицинские. Оценка биологического действия медицинских изделий. Часть 12. Отбор и подготовка образцов для проведения исследований: межгосударственный стандарт: введен 2024-06-01. Межгосударственный совет по стандартизации, метрологии и сертификации. Москва: Стандартинформ, 2023.
- 20. ГОСТ ISO 10993-5-2023. Изделия медицинские. Оценка биологического действия медицинских изделий. Часть 5. Исследования на цитотоксичность методами in vitro: межгосударственный стандарт: введен в действие 01.06.2024. Межгосударственный совет по стандартизации, метрологии и сертификации. Москва: Стандартинформ, 2023.

- Singh P, Kaur G, Singh K, Kaur M, Kumar M, Meena R, et al. Nanostructured boron carbide (B4C): A bio-compatible and recyclable photo-catalyst for efficient wastewater treatment. Materialia. 2018; 1: 258–64.
- 22. Stodolak-Zych E, Gubernat A, Ścisłowska-Czarnecka A, Chadzińska M, Zych L, Zientara D, et al. The influence of surface chemical composition of particles of boron carbide powders on their biological properties. Appl Surf Sci. 2022; 582: 152380.
- Wróblewska A, Szermer-Olearnik B, Szczygieł A, Węgierek-Ciura K, Mierzejewska J, Kozień D, et al. Macrophages as carriers of boron carbide nanoparticles dedicated to boron neutron capture therapy. J Nanobiotechnol. 2024; 22 (1): 183.
- Öksüz KE. Macro-porous aluminum oxide-boron carbide ceramics for hard tissue applications. Recep Tayyip Erdoğan Üniv Fen Mühendis Bilim Derg. 2023; 4 (2): 65–75.
- Boccaccio A, Fiorentino M, Uva AE, Laghetti LN, Monno G. Rhombicuboctahedron unit cell based scaffolds for bone regeneration: geometry optimization with a mechanobiologydriven algorithm. Mater Sci Eng C Mater Biol Appl. 2018; 83: 51–66. DOI: 10.1016/j.msec.2017.09.004.
- Чупрунов К. О. Разработка метода получения наноструктурных сферических порошковых материалов на основе гидроксилапатита с регулируемыми фазовым составом и показателями дисперсности [диссертация]. М., 2022.
- 27. Некишева А. А., Абдулазизов Б. Д., Пешеходько Д. И. Обзор материалов для изготовления эндопротезов тазобедренного сустава. Медицина. Социология. Философия. Прикладные исследования. 2020; 6: 48–54.
- Marques A, Miranda G, Silva F, Pinto P, Carvalho Ö. Review on current limits and potentialities of technologies for biomedical ceramic scaffolds production. J Biomed Mater Res B Appl Biomater. 2021; 109 (3): 377–93. DOI: 10.1002/jbm.b.34706.
- Cai S, Wu C, Yang W, Liang W, Yu H, Liu L. Recent advance in surface modification for regulating cell adhesion and behaviors. Nanotechnol Rev. 2020; 9 (1): 971–89. DOI: 10.1515/ntrev-2020-0076.
- Deligianni DD, Katsala ND, Koutsoukos PG, Missirlis YF. Effect of surface roughness of hydroxyapatite on human bone marrow cell adhesion, proliferation, differentiation and detachment strength. Biomaterials. 2001; 22 (1): 87–96. DOI: 10.1016/S0142-9612(00)00174-5.

## SUSCEPTIBILITY OF THE NONTUBERCULOUS MYCOBACTERIA CIRCULATING IN RUSSIA TO BEDAQUILINE

Smirnova TG¹⊠, Andreevskaya SN¹, Larionova EE¹, Zaytseva AS¹, Kiseleva EA¹, Ustinova W¹, Chernousova LN¹, Ergeshov AE¹,

¹ Central Tuberculosis Research Institute, Moscow, Russia

The diseases caused by nontuberculous mycobacteria (NTM) are a public health problem all over the world due to increasing incidence and the associated mortality. Since it is difficult to treat mycobacteriosis, the search for drugs effective against NTM is relevant. Bedaguiline was approved in 2012 as a drug for tuberculosis treatment. The study aimed to determine susceptibility to bedaquiline of the main clinically significant NTM species that were common in the Russian Federation. In 2011-2024, a total of 345 NTM isolates were obtained: 289 isolates of slow growing NTM species (M. avium, M. intracellulare, M. chimaera, M. kansasii, M. xenopi) and 56 of the fast growing one (M. abscessus). Drug susceptibility testing for bedaquiline was performed by microdilution in a 96-well plate using the bedaquiline concentration range of 0.125–4  $\mu$ g/mL. The minimum inhibitory concentration of bedaquiline inhibiting 50% (MIC<sub>50</sub>) and 90% (MIC<sub>90</sub>) of NTM strains of each spesies was determined. It has been shown that the bedaquilline MIC<sub>50</sub> for *M. avium*, *M. intracellulare*, *M. chimaera*, *M. kansasii* is < 0.125 µg/mL, MIC<sub>90</sub> - $\text{from} < 0.125 \text{ to } 0.5 \text{ } \text{µg/mL, for } \textit{M. xenopi: MIC}_{50} -\!\!\!\! -4 \text{µg/mL, MIC}_{50} -\!\!\!\! -2 \text{µg/mL, } \textit{MIC}_{50} -\!\!\!\! -2 \text{µg/mL, } \textit{MIC}_{50} -\!\!\!\! -1 \text{µg/mL, } \textit{MIC}_{50} -\!\!\!\! -2 \text{µg/mL, } \textit{M$ 

Keywords: non-tuberculous mycobacteria, anti-tuberculosis drugs, bedaquilline, minimal inhibitory concentration, drug susceptibility

Funding: the study was conducted under the State Assignment of the Central Tuberculosis Research Institute, R&D project: 123061500080-6 "Developing an Import-Independent Technology to Determine Minimal Inhibitory Concentrations of Antibacterial Drugs Effective Against the Clinically Significant Nontuberculous Mycobacterial Species'

Author contribution: Chernousova LN, Ergeshov AE — study design; Ustinova W, Kiseleva EA — experimental procedure; Smirnova TG — data analysis, manuscript writing; Larionova EE — data analysis; Zaytseva AS — literature review, manuscript draft writing; Andreevskaya SN — data analysis; all authors contributed to the discussion.

Compliance with ethical standards: the study was conducted in accordance with the principles of the Declaration of Helsinki (1964) and its further revisions.

Correspondence should be addressed: Tatiana G. Smirnova

Yauzskaya alleya, 2, str. 1A, Moscow, 107564, Russia; s\_tatka@mail.ru

Received: 02.10.2025 Accepted: 18.10.2025 Published online: 30.10.2025

DOI: 10.24075/brsmu.2025.054

## ЧУВСТВИТЕЛЬНОСТЬ К БЕДАКВИЛИНУ НЕТУБЕРКУЛЕЗНЫХ МИКОБАКТЕРИЙ, ЦИРКУЛИРУЮЩИХ НА ТЕРРИТОРИИ РОССИИ

Т. Г. Смирнова<sup>1</sup>, С. Н. Андреевская<sup>1</sup>, Е. Е. Ларионова<sup>1</sup>, А. С. Зайцева<sup>1</sup>, Е. А. Киселева<sup>1</sup>, В. В. Устинова<sup>1</sup>, Л. Н. Черноусова<sup>1</sup>, А. Э. Эргешов<sup>1,2</sup>

Заболевания, вызываемые нетуберкулезными микобактериями (НТМБ), являются проблемой здравоохранения во всем мире из-за роста заболеваемости и связанной с этим смертности. В связи со сложностью лечения микобактериоза актуален поиск препаратов, эффективных в отношении НТМБ. Бедаквилин одобрен в 2012 г. как препарат для лечения туберкулеза. Целью исследования было определить чувствительность к бедаквилину основных клинических значимых видов НТМБ, распространенных в РФ. За период 2011–2024 гг. было выделено 345 изолятов НТМБ: 289 медленнорастущих видов HTMБ (M. avium, M. intracellulare, M. chimaera, M. kansasii, M. xenopi) и 56 — быстрорастущих (M. abscessus). Определение лекарственной чувствительности к бедаквилину проводили методом микроразведений в 96-луночном планшете, используя диапазон концентраций бедаквилина от 0.125 мкг/мл до 4 мкг/мл. Определяли минимальную подавляющую концентрацию бедаквилина, к которой чувствительны 50% (МПК...) и 90% (МПК<sub>ос</sub>) штаммов HTMБ каждого вида. Показано, что в отношении *M. avium, M. intracellulare, M. chimaera, M. kansasii* МПК<sub>эс</sub> бедаквилина 1 мкг/мл, МПК $_{\rm so}$  — 2 мкг/мл.

Ключевые слова: нетуберкулезные микобактерии, противотуберкулезные препараты, бедаквилин, минимальная подавляющая концентрация, лекарственная чувствительность

Финансирование: исследование проведено в рамках выполнения работ по Государственному заданию ФГБНУ «ЦНИИТ» Рег. № НИОКТР 123061500080-6 «Разработка импортонезависимой технологии определения минимальных ингибирующих концентраций антибактериальных препаратов, эффективных в отношении клинически значимых видов нетуберкулезных микобактерий».

Вклад авторов: Л. Н. Черноусова, А. Э. Эргешов — дизайн исследования; В. В. Устинова, Е. А. Киселева — проведение эксперимента; Т. Г. Смирнова анализ полученных данных, написание текста рукописи; Е. Е. Ларионова — анализ полученных данных; А. С. Зайцева — анализ литературы, подготовка черновика рукописи; С. Н. Андреевская — анализ полученных данных; все авторы участвовали в обсуждении результатов.

Соблюдение этических стандартов: работа проведена в соответствии с принципами Хельсинкской декларации (1964 г.) и дальнейших ее пересмотров.

Для корреспонденции: Татьяна Геннадьевна Смирнова ул. Яузская аллея, д. 2, стр. 1А, г. Москва, 107564, Россия; s\_tatka@mail.ru

Статья получена: 02.10.2025 Статья принята к печати: 18.10.2025 Опубликована онлайн: 30.10.2025

DOI: 10.24075/vramu 2025.054

<sup>&</sup>lt;sup>2</sup> Russian University of Medicine, Moscow, Russia

 $<sup>^{1}</sup>$  Центральный научно-исследовательский институт туберкулеза, Москва, Россия

<sup>&</sup>lt;sup>2</sup> Российский университет медицины, Москва, Россия

### ОРИГИНАЛЬНОЕ ИССЛЕДОВАНИЕ І МИКРОБИОЛОГИЯ

Nontuberculous mycobacteria (NTM) include representatives of the genus *Mycobacterium*, except the *Mycobacterium tuberculosis* complex (MTBC) and *Mycobacterium leprae* [1]. It is accepted to divide NTM into slow-growing and fast-growing ones based on the growth rate. Some species included in these groups can cause tuberculosis-like diseases of the lung and other organs [2–5].

The NTM infections represent a challenge faced by public health systems all over the world due to growing incidence and the associated mortality [6]. More than 90% of all registered cases of pulmonary diseases caused by NTM (mycobacteriosis) result from getting infected with the *Mycobacterium avium* complex (MAC) and *Mycobacterium abscessus* [7]. The diagnosis of the diseases caused by NTM is challenging due to symptoms and x-ray features similar to that of tuberculosis. Furthermore, NTM and MTBC show no differences when bacterioscopically examined. It is difficult to treat the diseases caused by NTM, since NTM show natural resistance to the majority of broadspectrum antibacterial drugs and anti-tuberculosis drugs [8, 9].

Considering the complexity of treating mycobacteriosis, it seems relevant to search for the drugs effective against NTM, for example, to study the activity of novel anti-tuberculosis drugs. One such drug is bedaquiline, which was approved by the U.S. FDA and included in the WHO list of three drugs for treatment of tuberculosis caused by a pathogen with multiple and pre-broad drug resistance after clinical trials [10].

The NTM susceptibility to bedaquiline that was described in a limited number of studies [11–14] can fail to reflect the biological specifics of the NTM isolates represented in Russia. Bedaquiline susceptibility of the NTM circulating in the Russian Federation has been studied in a small number of species, and it is necessary to accumulate data [15–17].

The study aimed to determine bedaquiline susceptibility of the main clinically significant NTM species that were common in Russia.

### **METHODS**

The study involved NTM isolates obtained from the patients examined at the Central Tuberculosis Research Institute in 2011–2024 at admission (one NTM isolate was obtained from each patient). The patients examined were residents of the following federal districts of Russia: Central (including Moscow and the Moscow region), Northwestern, Southern, Volga, and Urals regions.

NTM were identified to species by multiplex PCR, as previously reported [18]. The most common NTM species causing mycobacteriosis were included in the study: *M. avium*, *M. intracellulare*, *M. chimaera*, *M. kansasii*, *M. xenopi*, *M. abscessus*.

Bedaquiline susceptibility was determined by microdilution in a 96-well plate using the bedaquiline concentrations within the range of 0.125–4.000  $\mu$ L/mL [19]. The bedaquiline fumarate

Table. Bedaquiline MIC for the studied NTM species

substance containing 82.72% of the active ingredient (Janssen Pharmaceutica NV, Belgium) was used. The drug sample was dissolved in the chemically pure dimethyl sulfoxide to reach the necessary drug concentration, and the drug activity was taken into account.

A single-cell suspension was prepared from the NTM culture, while controlling CFU values using the spectrophotometer Ultraspec 10 (Ultraspec, USA) [20]. The resulting suspension was used to prepare a working suspension in the Middlebrook 7H9 medium with the concentration of  $5\times10^5$  CFU/mL and sown onto a plate, 100  $\mu\text{L}$  per well [21]. Plates were incubated at 37 °C in the microbiological incubator Binder (Binder, Germany). The culturing time was 14 days for slow-growing and 5 days for fast-growing NTM. The bedaquiline minimum inhibiting concentration (MIC) was determined in each test, which corresponded to the highest drug dilution inhibiting the culture growth. To characterize bedaquiline susceptibility of each studied NTM species, MIC $_{50}$  and MIC $_{90}$  were determined, i.e. the minimum bedaquiline concentrations, to which 50% and 90% of strains of each NTM species were susceptible [22].

### **RESULTS**

In 2011–2024, a total of 345 NTM isolates were obtained: 289 slow-growing NTM species (*M. avium*, *M. intracellulare*, *M. chimaera*, *M. kansasii*, *M. xenopi*) and 56 fast-growing ones (*M. abscessus*). Bedaquiline MIC values for the studied NTM species are provided in Table.

Such slow-growing NTM species, as M. avium, M. intracellulare, M. chimaera, M. kansasii, showed high susceptibility to bedaquiline: the bedaquiline MIC mode and MIC $_{50}$  for all species were < 0.125 µg/mL, MIC $_{90}$  was between < 0.125 and 0.5 µg/mL, depending on the species. One more slow-growing NTM species, M. xenopi, showed low susceptibility to bedaquiline with MIC $_{50}$  of 4 µg/mL and MIC $_{90}$  > 4 µg/mL. The fast-growing NTM species showed moderate susceptibility to bedaquiline with MIC $_{50}$  and MIC $_{90}$  of 1 µg/mL and 2 µg/mL, respectively.

When analyzing the resulting MIC distribution for all the studied slow-growing NTM species, a bimodal distribution was obtained allowing us to roughly determine that the bedaquiline tentative epidemiological cut-off value (ECOFF) for slow-growing NTM species did not exceed 1 µg/mL (Figure).

Based on this tentative ECOFF value it can be concluded that 208/210 (99.05%; 95% CI 96.59–99.74%) of the studied *M. avium* strains, 19/20 (95.00%; 95% CI 76.39–99.11) *M. intracellulare* strains, 24/24 (100%; 95% CI 86.20–100.00) *M. chimaera* strains, 27/27 (100%; 95% CI 87.54–100.00) *M. kansasii* strains are susceptible to bedaquiline. Among all the studied *M. xenopi* stains no strain was revealed susceptible to the proposed bedaquiline ECOFF.

NTM group	Number of		Number of isolates with MIC (μg/mL)					MIC mode	MO	Luc I		
	NTM species	isolates	<0.125	0.25	0.5	1	2	4	4	(µg/mL)	MIC <sub>50</sub>	MIC <sub>90</sub>
	M. avium	210	163	19	23	3	0	2	0	< 0.125	< 0.125	0.5
	M. intracellulare	20	18	0	1	0	0	0	1	< 0.125	< 0.125	< 0.125
Slow-growing	M. chimaera	24	24	0	0	0	0	0	0	< 0.125	< 0.125	< 0.125
	M. kansasii	27	24	1	2	0	0	0	0	< 0.125	< 0.125	0.25
	M. xenopi	8	0	0	0	0	0	6	2	4	4	> 4
Fast-growing	M. abscessus	56	5	3	13	29	6	0	0	1	1	2
	Total	345	234	23	39	32	6	8	3			

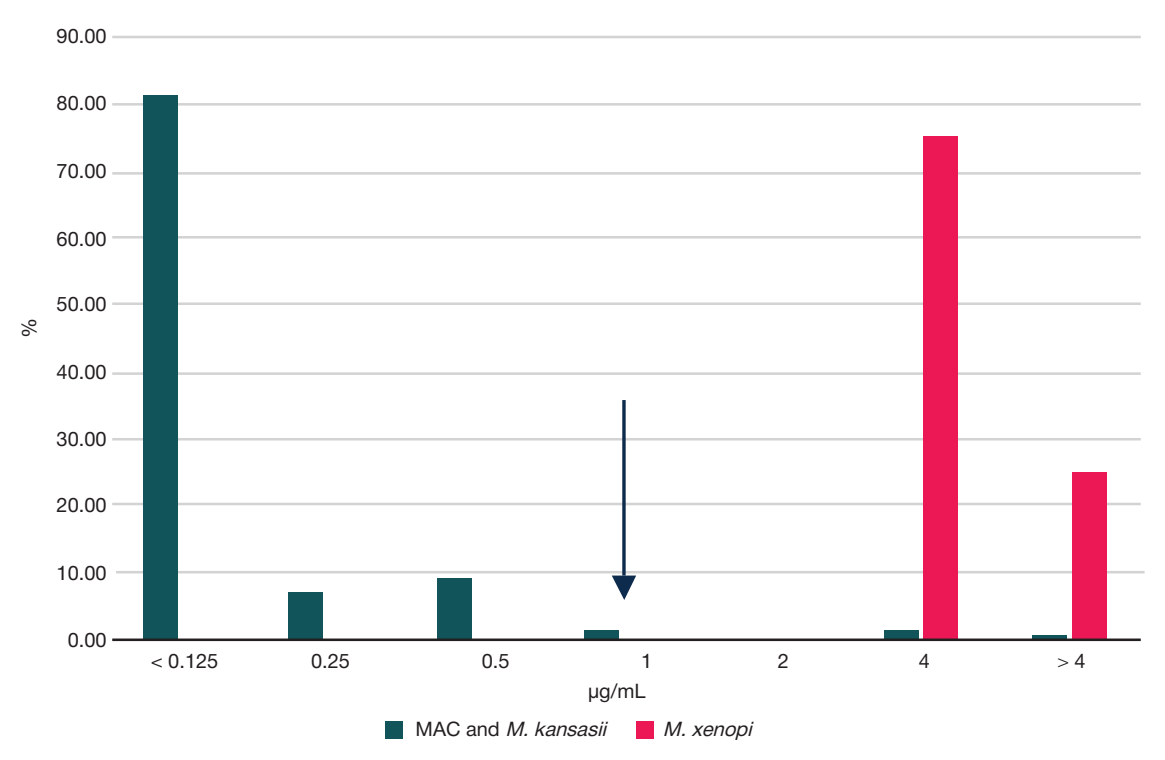


Fig. Bedaquiline MIC distribution for the studied slow-growing NTM species showing differences in drug susceptibility. MAC — M. avium complex mycobacteria (M. avium, M. intracellulare, M. chimaera); the resulting MIC value for the slow-growing NTM species showing high drug susceptibility (MAC and M. kansasii) are highlighted in green; MIC of M. xenopi, the slow-growing NTM species showing low bedaquiline susceptibility, is highlighted in red. The tentative ECOFF value is pointed by arrow

Among fast-growing NTM species, bedaquiline susceptibility was determined for only one species, *M. abscessus*, MIC distribution was unimodal, due to which bedaquiline ECOFF for fast-growing species was not determined.

## DISCUSSION

The NTM natural resistance to most antibacterial drugs makes the problem of finding new drugs effective against this group of mycobacteria relevant. The study presented provides the data on bedaquline susceptibility assessment for the main clinically significant NTM species. The bedaquline susceptibility distribution for each NTM species was unimodal, which suggested the species-specific susceptibility of the studied NTM species to this drug. *M. kansasii* and NTM of the *M. avium* complex (MAC) that includes *M. avium*, *M. intracellulare*, *M. chimaera*, turned out to be highly susceptible to bedaquline (MIC mode — < 0.125  $\mu$ g/mL). *M. abscessus* was less susceptible (MIC mode — 1  $\mu$ g/mL), and the lowest susceptibility was reported for *M. xenopii* (MIC mode — 4  $\mu$ g/mL).

The results obtained for the NTM species included in MAC and for *M. kansasii* matched the results obtained in a number of studies; these suggest that bedaquline shows high activity against these NTM species [12–14].

The data on bedaquline susceptibility of M. xenopi strains is insufficient. According to some reports, bedaquline susceptibility of one laboratory M. xenopi strain was > 2  $\mu$ g/mL, which is consistent with our results [12]. Another study describing bedaquline susceptibility of the NTM circulating in China involved assessment of four clinical M. xenopi strains, the bedaquline MIC for which varied broadly, from 0.0016  $\mu$ g/mL to 1  $\mu$ g/mL, which is significantly lower compared to the values we have determined [14].

In a number of studies the bedaquline ECOFF value for slow-growing NTM of 1  $\mu$ g/mL was proposed, which matched the bedaquline ECOFF value determined in our study [13, 23]. It is interesting to note that this ECOFF is higher, than the bedaquline ECOFF for *M. tuberculosis* equal to 0.125  $\mu$ g/mL, which also demonstrates higher NTM resistance to antituberculosis drugs relative to the tuberculosis pathogen [19].

The bedaquline susceptibility of the fast-growing NTM species M. abscessus was studied earlier [13]. According to the results of this study, the bedaquline MIC for M. abscessus had a bimobal distribution with the MIC modes of 0.13  $\mu$ g/mL and > 16  $\mu$ g/mL; the bedaquline MIC $_{50}$  and MIC $_{90}$  were 0.13  $\mu$ g/mL and >16  $\mu$ g/mL, respectively. In our study involving 56 M. abscessus strains, unimodal MIC distribution with the mode of 1  $\mu$ g/mL was reported, and MIC $_{90}$  was 2  $\mu$ g/mL. The differences revealed can indicate unique characteristics of the M. abscessus populations distinguished in Russia (the study presented) and China [13].

## CONCLUSIONS

The study presented provides important information about the antibacterial drug susceptibility of the main clinically significant NTM strains circulating in the Russian Federation. Based on the data obtained it has been found that bedaquline is highly effective against MAC being the main causative agents of mycobacteriosis in the world and against *M. kansasii*. Other NTM species turned out to be less susceptible to this drug. Further research is necessary to accumulate the data on bedaquline susceptibility of various NTM species and determine the correlation between NTM susceptibility *in vitro* and bedaquline clinical efficacy when used to treat mycobacteriosis.

## ОРИГИНАЛЬНОЕ ИССЛЕДОВАНИЕ І МИКРОБИОЛОГИЯ

#### References

- Tortoli E. Microbiological features and clinical relevance of new species of the genus *Mycobacterium*. Clin Microbiol Rev. 2014; 27: 727–52.
- Raju RM, Raju SM, Zhao Y, Rubin EJ. Leveraging advances in tuberculosis diagnosis and treatment to address nontuberculous mycobacterial disease. Emerg Infect Dis. 2016; 22 (3): 365–9.
- Otten TF, Vasilev AV. Mikobakterioz. SPb: Medicinskaya pressa, 2005; 224 s. Russian.
- Litvinov VI, Makarova MV, Krasnova MA. Netuberkuleznye mikobakterii. M.: MNPCBT, 2008; 256 s. Russian.
- Litvinov VI, Bogorodskaya EM, Borisov SE. Netuberkuleznye mikobakterii, mikobakteriozy M.: MNPCBT, 2014; 256 s. Russian.
- Brode SK, Daley CL, Marras TK. The epidemiologic relationship between tuberculosis and non-tuberculous mycobacterial disease: a systematic review. Int J Tuberc Lung Dis. 2014; 18: 1370–7.
- 7. Wu ML, Aziz DB, Dartois V, Dick T. NTM drug discovery: status, gaps and the way forward. Drug Discov Today. 2018; 23: 1502–19.
- Baldwin SL, Larsen SE, Ordway D, Cassell G, Coler RN. The complexities and challenges of preventing and treating nontuberculous mycobacterial diseases. PLoS Negl Trop Dis. 2019: 13: e0007083.
- Yilmaz N, Yilmazel Ucar E, Saglam L. Mycobacterium tuberculosis and nontuberculous mycobacteria coinfection of the lungs. Turk Thorac J. 2017; 18: 23–6.
- Mahajan R. Bedaquiline: first FDA-approved tuberculosis drug in 40 years. Int J App Basic Med Res. 2013; 3: 1–2.
- Aguilar-Ayala DA, Cnockaert M, André E, Andries K, Gonzalez-Y-Merchand JA, Vandamme P et al. In vitro activity of bedaquiline against rapidly growing nontuberculous mycobacteria. J Med Microbiol. 2017; 66: 1140–3.
- Martin A, Godino IT, Aguilar-Ayala DA, Mathys V, Lounis N, Villalobos HR. In vitro activity of bedaquiline against slow-growing nontuberculous mycobacteria. J Med Microbiol. 2019; 68 (8): 1137–9.
- Pang Y, Zheng H, Tan Y, Song Y, Zhao Y. In vitro activity of bedaquiline against nontuberculous mycobacteria in China. Antimicrob Agents Chemother. 2017; 61 (5): e02627–16.

- Yu X, Gao X, Li C, Luo J, Wen S, Zhang T. et al. In vitro activities of bedaquiline and delamanid against nontuberculous mycobacteria isolated in Beijing, China. Antimicrob Agents Chemother. 2019; 63 (8): e00031–19.
- Makarova MV, Mihajlova YuD, Hachaturyanc EN, Litvinov VI. Izuchenie lekarstvennoj chuvstvitel'nosti k bedakvilinu bystrorastushchih mikobakterij kompleksa M. chelonae–M.abscessus. Tuberkulez i social'no znachimye zabolevaniya. 2022; 10 (4): 42–49. Russian.
- 16. Makarova MV, Mihajlova YuD, Hachatur'yanc EN, Litvinov VI. Lekarstvennaya chuvstvitel'nost' k bedakvilinu shtammov M.kansasii, vydelennyh v protivotuberkuleznyh uchrezhdeniyah Moskvy. Epidemiologiya i vakcinoprofilaktika. 2023; 22 (3): 64–69. Russian.
- Makarova MV, Mihajlova YuD, Sviridenko MA, Hachatur'yanc EN, Litvinov VI. Izuchenie aktivnosti bedakvilina in vitro v otnoshenii Mycobacterium fortuitum complex. Tuberkulez i social'no znachimye zabolevaniya. 2024; 12 (1): 30–35. Russian.
- Smirnova T, Ustinova V, Andreevskaya S, Larionova E, Kiseleva E, Chernousova L, et al. Evaluation of a new assay for nontuberculous mycobacteria species identification in diagnostic material and cultures. Tuberculosis (Edinb). 2021; 130: 102124.
- Optimized broth microdilution plate methodology for drug susceptibility testing of Mycobacterium tuberculosis complex. Geneva: World Health Organization, 2022.
- Kralik P, Beran V, Pavlik I. Enumeration of Mycobacterium avium subsp. paratuberculosis by quantitative real-time PCR, culture on solid media and optical densitometry. BMC Res Notes. 2012; 5: 114.
- Jaffré J, Aubry A, Maitre T, Morel F, Brossier F, Robert J et al. Rational choice of antibiotics and media for Mycobacterium avium complex drug susceptibility testing. Front Microbiol. 2020; 11: 81.
- Susceptibility Testing of Mycobacteria, Nocardia spp., and Other Aerobic Actinomycetes, 3<sup>rd</sup> ed. CLSI standard document M24. Wayne (PA): Clinical and Laboratory Standards Institute; 2018.
- Wang M, Men P, Zhang W, Wu J, Gu Y, Wang F, et al. Bedaquiline susceptibility testing of *Mycobacterium abscessus* complex and *Mycobacterium avium* complex: A meta-analysis study. J Glob An-timicrob Resist. 2024: 37: 135–40.

## Литература

- Tortoli E. Microbiological features and clinical relevance of new species of the genus *Mycobacterium*. Clin Microbiol Rev. 2014; 27: 727–52.
- Raju RM, Raju SM, Zhao Y, Rubin EJ. Leveraging advances in tuberculosis diagnosis and treatment to address nontuberculous mycobacterial disease. Emerg Infect Dis. 2016; 22 (3): 365–9.
- 3. Оттен Т. Ф., Васильев А. В. Микобактериоз. СПб: Медицинская пресса, 2005; 224 с.
- 4. Литвинов В. И., Макарова М. В., Краснова М. А. Нетуберкулезные микобактерии. М.: МНПЦБТ, 2008; 256 с.
- 5. Литвинов В. И., Богородская Е. М., Борисов С. Е. Нетуберкулезные микобактерии, микобактериозы М.: МНПЦБТ, 2014: 256 с.
- Brode SK, Daley CL, Marras TK. The epidemiologic relationship between tuberculosis and non-tuberculous mycobacterial disease: a systematic review. Int J Tuberc Lung Dis. 2014; 18: 1370–7.
- Wu ML, Aziz DB, Dartois V, Dick T. NTM drug discovery: status, gaps and the way forward. Drug Discov Today. 2018; 23: 1502–19.
- 8. Baldwin SL, Larsen SE, Ordway D, Cassell G, Coler RN. The complexities and challenges of preventing and treating nontuberculous mycobacterial diseases. PLoS Negl Trop Dis. 2019; 13: e0007083.
- Yilmaz N, Yilmazel Ucar E, Saglam L. Mycobacterium tuberculosis and nontuberculous mycobacteria coinfection of the lungs. Turk Thorac J. 2017; 18: 23–6.
- Mahajan R. Bedaquiline: first FDA-approved tuberculosis drug in 40 years. Int J App Basic Med Res. 2013; 3: 1–2.
- Aguilar-Ayala DA, Cnockaert M, André E, Andries K, Gonzalez-Y-Merchand JA, Vandamme P et al. In vitro activity of bedaquiline against rapidly growing nontuberculous mycobacteria. J Med Microbiol. 2017; 66: 1140–3.

- Martin A, Godino IT, Aguilar-Ayala DA, Mathys V, Lounis N, Villalobos HR. In vitro activity of bedaquiline against slow-growing nontuberculous mycobacteria. J Med Microbiol. 2019; 68 (8): 1137–9.
- Pang Y, Zheng H, Tan Y, Song Y, Zhao Y. In vitro activity of bedaquiline against nontuberculous mycobacteria in China. Antimicrob Agents Chemother. 2017; 61 (5): e02627–16.
- Yu X, Gao X, Li C, Luo J, Wen S, Zhang T. et al. In vitro activities of bedaquiline and delamanid against nontuberculous mycobacteria isolated in Beijing, China. Antimicrob Agents Chemother. 2019; 63 (8): e00031–19.
- Макарова М. В., Михайлова Ю. Д., Хачатурьянц Е. Н., Литвинов В. И. Изучение лекарственной чувствительности к бедаквилину быстрорастущих микобактерий комплекса M. chelonae–M.abscessus. Туберкулез и социально значимые заболевания. 2022; 10 (4): 42–49.
- 16. Макарова М. В., Михайлова Ю. Д., Хачатурьянц Е. Н., Литвинов В. И. Лекарственная чувствительность к бедаквилину штаммов М. kansasii, выделенных в противотуберкулезных учреждениях Москвы. Эпидемиология и вакцинопрофилактика. 2023; 22 (3): 64–69.
- 17. Макарова М. В., Михайлова Ю. Д., Свириденко М. А., Хачатурьянц Е. Н., Литвинов В. И. Изучение активности бедаквилина *in vitro* в отношении *Mycobacterium fortuitum* complex. Туберкулез и социально значимые заболевания. 2024; 12 (1): 30–35.
- Smirnova T, Ustinova V, Andreevskaya S, Larionova E, Kiseleva E, Chernousova L, et al. Evaluation of a new assay for nontuberculous mycobacteria species identification in diagnostic material and cultures. Tuberculosis (Edinb). 2021; 130: 102124.
- Optimized broth microdilution plate methodology for drug susceptibility testing of Mycobacterium tuberculosis complex.

## ORIGINAL RESEARCH | MICROBIOLOGY

- Geneva: World Health Organization, 2022.
- Kralik P, Beran V, Pavlik I. Enumeration of Mycobacterium avium subsp. paratuberculosis by quantitative real-time PCR, culture on solid media and optical densitometry. BMC Res Notes. 2012; 5: 114.
- Jaffré J, Aubry A, Maitre T, Morel F, Brossier F, Robert J et al. Rational choice of antibiotics and media for Mycobacterium avium complex drug susceptibility testing. Front Microbiol. 2020; 11: 81.
- Susceptibility Testing of Mycobacteria, Nocardia spp., and Other Aerobic Actinomycetes, 3<sup>rd</sup> ed. CLSI standard document M24. Wayne (PA): Clinical and Laboratory Standards Institute; 2018.
- Wang M, Men P, Zhang W, Wu J, Gu Y, Wang F, et al. Bedaquiline susceptibility testing of *Mycobacterium abscessus* complex and *Mycobacterium avium* complex: A meta-analysis study. J Glob An-timicrob Resist. 2024; 37: 135–40.

### NEUROPHYSIOLOGICAL MARKERS OF THE ILLUSION CAUSED BY THE MIRROR VISUAL FEEDBACK

Mokienko OA<sup>1,2</sup> Bobrov PD<sup>1,3</sup>, Soloveva AA<sup>1</sup>, Isaev MR<sup>1,3</sup>, Kerechanin YaV<sup>1,3</sup>, Ratnikova VYu<sup>1</sup>, Kataitsev VA<sup>1</sup>, Shagina ED<sup>1</sup>, Nikishina VB<sup>1</sup>

- <sup>1</sup> Pirogov Russian National Research Medical University, Moscow, Russia
- $^{\rm 2}$  Russian Center of Neurology and Neurosciences, Moscow, Russia
- <sup>3</sup> Institute of Higher Nervous Activity and Neurophysiology of the Russian Academy of Sciences, Moscow, Russia

Neurophysiological mechanisms underlying the illusion caused by the mirror visual feedback are still poorly understood, despite the clinical use of mirror therapy for phantom pain and post-stroke hemiparesis. The study aimed to determine the mirror illusion neurophysiological correlates by the simultaneous use of electroencephalography (EEG) recording and near-infrared spectroscopy (NIRS). A total of 30 healthy volunteers (12 males, 18 females; average age  $24 \pm 8$  years) were assessed. The experimental procedure consisted of three blocks: bimanual movement without a mirror; moving one hand with the mirror; tactile stimulation with the mirror. We analyzed the degree of EEG alpha rhythm (8–13 Hz) desynchronization in primary sensorimotor areas, supplementary motor area, and the posterior parietal cortex. Furthermore, changes in the concentrations of oxy- and deoxyhemoglobin (HbO and HbR) were assessed by NIRS. When moving the hand with the mirror, bilateral activation of primary sensorimotor areas occurred in both hemispheres: mu rhythm desynchronization, 9.71 [2.82; 16.20]% in the contralateral and 5.64 [2.84; 12.13]% in the ipsilateral hemispheres (p = 0.797), along with the HbO concentration increase by 6.88 [3.07; 17.20] nmol/L in the contralateral and by 4.91 [0.11; 14.59] nmol/L in the ipsilateral hemispheres (p = 0.094). The correlations between EEG and NIRS parameters were reported for the posterior parietal cortex only ( $r_s = 0.527$ , p = 0.003). The illusion subjective characteristics were correlated to the emotional response, and only some of those showed a weak correlation with neurophysiological indicators. EEG and NIRS are complementary, rather than mutually exclusive, when used to study the mirror illusion resulting from the multi-level network organization of brain processes.

Keywords: mirror illusion, mirror visual feedback, electroencephalography, near-infrared spectroscopy, cerebral cortex, neurophysiological markers

Funding: the study was conducted under the State Assignment of the Ministry of Healthcare of the Russian Federation (No. 125022602910-2).

Acknowledhements: the authors express their gratitude to the study participants for their contribution to the scientific knowledge development.

Author contribution: Mokienko OA — research design, analysis of the results, manuscript writing; Bobrov PD — data analysis, manuscript writing; Soloveva AA — experimental procedure, analysis of the results; Isaev MR, Kerechanin YaV — data analysis; Ratnikova VYu, Kataitsev VA — experimental procedure; Shagina ED — research design, discussion; Nikishina VB — research conceptualization, discussion.

Compliance with ethical standards: the study was approved by the Ethics Committee of the Institute of Clinical Psychology and Social Work, Pirogov Russian National Research Medical University (protocol No. 28 dated 23 October 2024). All subjects signed the informed consent to take part in the study.

Correspondence should be addressed: Olesya A. Mokienko

Ostrovityanova, 1, stroenie 1, Moscow, 117997, Russia; o.mokienko@ihna.ru

Received: 29.09.2025 Accepted: 16.10.2025 Published online: 28.10.2025

DOI: 10.24075/brsmu.2025.052

Copyright: © 2025 by the authors. Licensee: Pirogov University. This article is an open access article distributed under the terms and conditions of the Creative Commons Attribution (CC BY) license (https://creativecommons.org/licenses/by/4.0/).

# НЕЙРОФИЗИОЛОГИЧЕСКИЕ МАРКЕРЫ ИЛЛЮЗИИ, ВЫЗВАННОЙ ЗЕРКАЛЬНОЙ ВИЗУАЛЬНОЙ ОБРАТНОЙ СВЯЗЬЮ

О. А. Мокиенко<sup>1,2</sup> ⊠, П. Д. Бобров<sup>1,3</sup>, А. А. Соловьева<sup>1</sup>, М. Р. Исаев<sup>1,3</sup>, Я. В. Керечанин<sup>1,3</sup>, В. Ю. Ратникова<sup>1</sup>, В. А. Катайцев<sup>1</sup>, Е. Д. Шагина<sup>1</sup>, В. Б. Никишина<sup>1</sup>

- 1 Российский национальный исследовательский медицинский университет имени Н. И. Пирогова, Москва, Россия
- <sup>2</sup> Российский центр неврологии и нейронаук, Москва, Россия
- <sup>3</sup> Институт высшей нервной деятельности и нейрофизиологии, Москва, Россия

Нейрофизиологические механизмы иллюзии, вызванной зеркальной визуальной обратной связью, остаются недостаточно изученными, несмотря на клиническое применение зеркальной терапии при фантомном болевом синдроме и при постинсультном гемипарезе. Цель исследования — определить нейрофизиологические корреляты зеркальной иллюзии у здоровых людей методами одновременной регистрации электроэнцефалографии (ЭЭГ) и ближней инфракрасной спектроскопии (БИКС). Обследовано 30 здоровых добровольцев (12 мужчин, 18 женщин; средний возраст  $24 \pm 8$  лет). Экспериментальная процедура включала три блока: бимануальное движение без зеркала, движение одной рукой с зеркалом; тактильная стимуляция с зеркалом. Анализировали степень десинхронизации ЭЭГ-ритмов альфа-диапазона (8–13 Гц) в первичных сенсомоторных областях, дополнительной моторной области и задней теменной коре, а также методом БИКС, изменение концентрации окси- и дезоксигемоглобина (HbO и HbR). При движении рукой с зеркалом происходила билатеральная активация первичных сенсомоторных областей обоих полушарий: десинхронизация мю-ритма 9,71 [2,82; 16,20]%, в контралатеральном и 5,64 [2,84; 12,13]% в ипсилатеральном полушарии (p = 0,797), а также увеличение концентрации Между ЭЭГ и БИКС-показателями выявлены лишь в задней теменной коре ( $r_{\rm s} = 0,527$ , p = 0,003). Субъективные характеристики иллюзии коррелировали с эмоциональной реакцией, и лишь отдельные из них слабо коррелировали с нейрофизиологическими показателями. ЭЭГ и БИКС дополняют, но не заменяют друг друга при изучении зеркальной иллюзии, формирование которой обусловлено многоуровневой сетевой организацией мозговых процессов.

**Ключевые слова:** зеркальная иллюзия, зеркальная визуальная обратная связь, электроэнцефалография, ближняя инфракрасная спектроскопия, кора головного мозга, нейрофизиологические маркеры

Финансирование: работа выполнена в рамках Государственного задания Министерства здравоохранения Российской Федерации № 125022602910-2. Благодарности: авторы признательны участникам исследования за их вклад в развитие научного знания.

Вклад авторов: О. А. Мокиенко — дизайн исследования, анализ результатов, написание статьи; П. Д. Бобров — анализ данных, написание статьи; А. А. Соловьева — проведение экспериментов, анализ результатов; М. Р. Исаев, Я. В. Керечанин — анализ данных; В. Ю. Ратникова, В. А. Катайцев — проведение экспериментов; Е. Д. Шагина — дизайн исследования, обсуждение результатов; В. Б. Никишина — концептуализация исследования, обсуждение результатов.

Соблюдение этических стандартов: исследование одобрено этическим комитетом Института клинической психологии и социальной работы РНИМУ им. Н. И. Пирогова (протокол № 28 от 23 октября 2024 г.). Все участники подписали добровольное согласие на участие в исследовании.

Для корреспонденции: Олеся Александровна Мокиенко

ул. Островитянова, д. 1, с. 1, г. Москва, 117997, Россия; o.mokienko@ihna.ru

Статья получена: 29.09.2025 Статья принята к печати: 16.10.2025 Опубликована онлайн: 28.10.2025

DOI: 10.24075/vrgmu.2025.052

Авторские права: © 2025 принадлежат авторам. Лицензиат: РНИМУ им. Н. И. Пирогова. Статья размещена в открытом доступе и распространяется на условиях лицензии Creative Commons Attribution (CC BY) (https://creativecommons.org/licenses/by/4.0/).

## ОРИГИНАЛЬНОЕ ИССЛЕДОВАНИЕ І НЕЙРОФИЗИОЛОГИЯ

The illusion caused by mirror visual feedback, or mirror illusion (MI), is a neurophysiological phenomenon that translates observed mirror-reflected movements of a limb into a feeling of corresponding movements in the contralateral limb that is behind the mirror or absent [1, 2].

It has been shown that mirror visual feedback activates the system of mirror neurons and motor structures of the brain in the hemisphere ipsilateral to the active arm, stimulating neuroplasticity [2, 3] and facilitating restoration of interhemispheric functional balance [4, 5]. These physiological mechanisms underpin mirror therapy, which employs MI to treat a number of chronic neurological pathologies. The clinical efficacy of mirror therapy has been established for post-amputation phantom limb pain [1, 6, 7] and stroke hemiparesis [8–10]. There is evidence for the effectiveness of the method in the treatment of a complex regional pain syndrome [11–14] and functional motor disorders [15]. Researchers and specialists are currently searching for new mirror therapy protocols to enhance its efficacy; one of the approaches under consideration is Graded Motor Imagery [16].

Electrophysiological correlates of the brain activity accompanying MI were studied in healthy individuals and patients using electroencephalography (EEG) [5, 17, 18], transcranial magnetic stimulation [19, 20] and magnetic encephalography [21, 22], and hemodynamic activity parameters have been assessed using functional magnetic resonance imaging [4, 23] and near-infrared spectroscopy (NIRS) [24, 25]. However, there are no reported studies that would have investigated electrophysiological and hemodynamic parameters simultaneously. We expect that simultaneous recording of EEG and NIRS will yield a better understanding of the physiology of MI and allow a comparison of the informative value of the two methods in identification of the MI's correlates. Moreover, the neurophysiology of MI during sensory stimulation remains largely unexplored.

This study aimed to determine the neurophysiological correlates of MI in healthy individuals by simultaneously registering brain activity using EEG and NIRS during a mirror procedure involving movement and tactile stimulation.

### **METHODS**

### Participants of the study

The study was conducted at N.I. Pirogov Russian National Research Medical University of the Ministry of Health of the Russian Federation. The inclusion criteria were: signed voluntary informed consent; age 18–80 years; any gender; right-handedness confirmed by the Edinburgh Handedness Inventory (score above 40). The exclusion criteria were: disagreement to participate in the study; intake of medications that affect the central nervous system at the time of the study; acute conditions or exacerbations of chronic diseases; chronic pain syndrome and disabling conditions (including amputations); serious vision problems that prevent seeing the reflection of the limb in the mirror; skin diseases in the head area; a desire to drop out of the study; deterioration of the health condition during the study.

The study included 30 healthy volunteers, 12 male and 18 female, median age 21 [20.0; 23.0] years, all right-handed. No participants dropped out of the study; the data describes the entire sample (n = 30).

### The procedure

The participants were randomized into two groups by the active arm, right or left. The active arm was the one placed in front of

the mirror and moved or subjected to sensory stimulation (Fig. 1A). The active left arm group included 18 people, the active right arm group 12 people.

The experiments were conducted in an electrically shielded and soundproof chamber (Neuroiconica Assistive, Russia, model EK-1). The participants were a cap with 21 EEG electrodes, 10 NIRS sources and 10 NIRS detectors. A conductive gel was applied under each electrode. The procedure included three blocks: 1) synchronous movement of two hands without a mirror; 2) imitation of mirror therapy with a motor paradigm; 3) imitation of mirror therapy with sensory stimulation. After the second and third blocks, the participants were offered to fill out questionnaires reflecting subjective parameters of MI.

For the first block of the experiment, the participants performed a bimanual synchronous movement "fist-edge-palm" (Fig. 1B) 20 times every 10 seconds, prompted by an audio signal.

For the second block, a mirror was placed before the participant so that it reflected the active arm, while the other hand was behind the mirror, relaxed. The participant performed the "fist-edge-palm" movement with only the active arm 20 times every 10 seconds, prompted by an audio signal; the gaze of the participant was focused on the reflection of the moving hand in the mirror.

The third block involved sensory stimulation of the participant's active arm: the first tool was a blunt needle, used from the middle of the forearm to the tip of the middle finger, the second tool — a brush, driven from the middle of the forearm to the tip of the middle finger in constant contact with the arm. The intensity of stimulation with a blunt needle was pre-calibrated by the experimenter to provide a comfortable tactile sensation without pain or discomfort. Each stimulation included alternating sequential use of the needle and the brush for a total of 20 times. The applications of the tools were 10 seconds apart from each other. The second arm was behind the mirror, relaxed; the participant watched the reflection of the stimulated arm in the mirror.

Hereinafter, the terms "contralateral" and "ipsilateral" are used in relation to the active arm when referring to the lateralization of sources of activity in the brain. For the bimanual movement stage, the active arm is that which performs movements in the second and third blocks of the experiment.

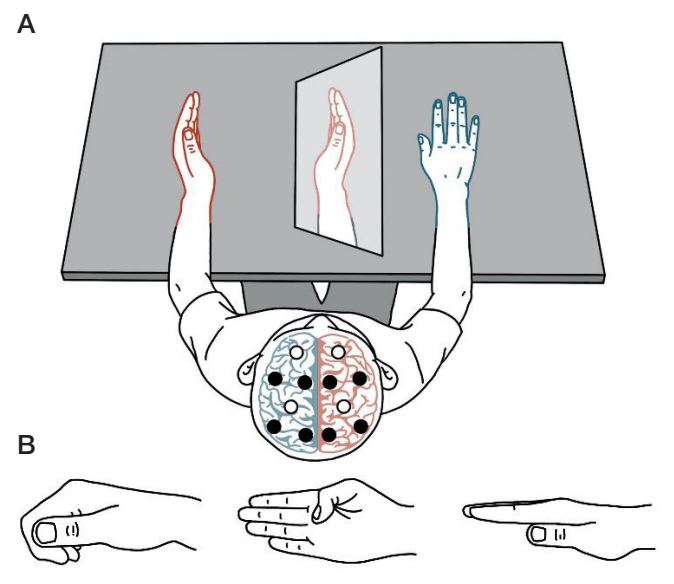


Fig. 1. A. The experimental setup: positions of the participant, the mirror, and the hands for the second and third blocks of the experiment. B. The "fist-edge-palm" movement

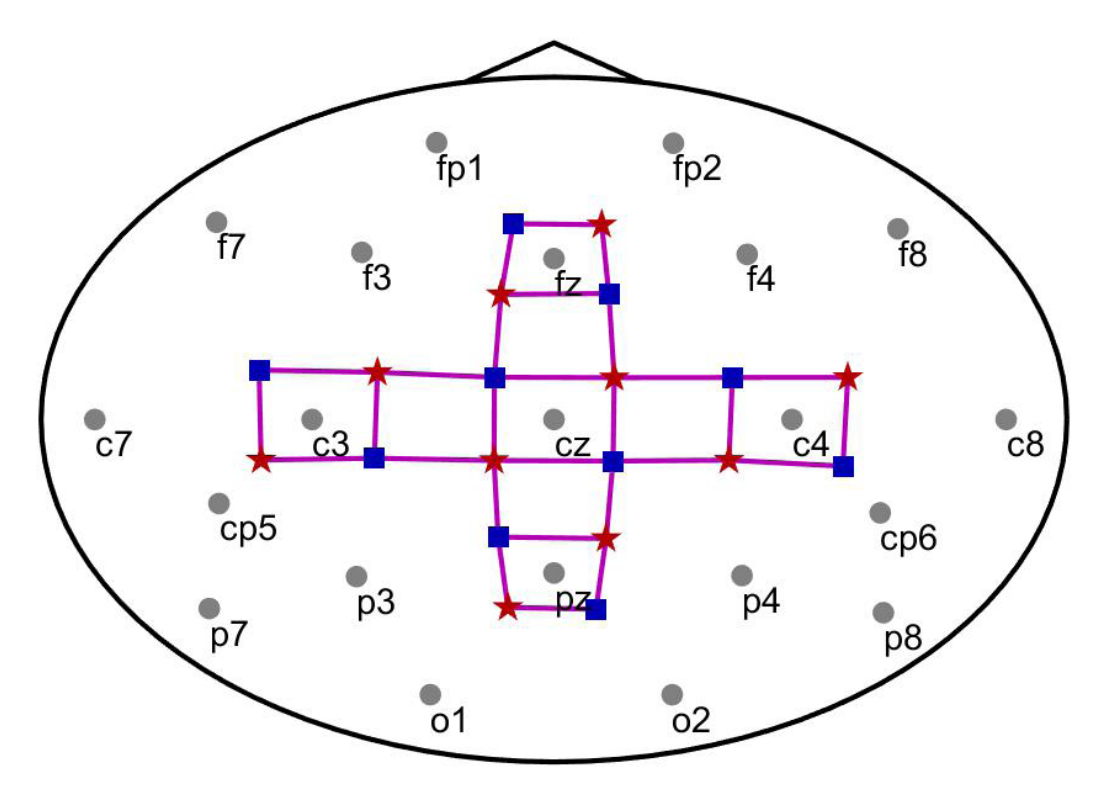


Fig. 2. The layout of the sensors. Circles indicate EEG electrodes, rectangles show NIRS detectors, asterisks are locations of NIRS sources; lines show source – detector pairs (NIRS channels)

### Assessment of the subjective parameters of the mirror illusion

After the second and third blocks, the participants assessed the following parameters of MI on a 10-point scale:

- vividness of the illusion: "I had a feeling of movement in the hand reflected in the mirror" (second block) or "I had a feeling of touch in the reflected hand" (third block);
- ownership: "I felt that the hand in the mirror was a part of my body, and not just a reflection of another hand" (second and third blocks);
- agency: "It seemed to me that I could directly control the movements of my hand in the mirror" (second block).

Additionally, the participants mentioned when the MI began to manifest: immediately or in the first seconds of the stimulation, or in the first, second, third or fourth quarter of the procedure.

After completing three blocks of the experiment, the participants assessed the intensity of the emotional reaction to MI in five domains: surprise, interest, delight, anxiety, and calmness (absence of a pronounced emotional reaction). They rated the intensity of each emotion on a scale from 0 (completely absent) to 10 (maximum intensity).

The questionnaire was developed specifically for this study.

### Registration of brain activity signals

NeoRec Cap 21 (Medical Computer Systems, Russia) was used to record EEG; the setup included 21 leads: Fp1, Fp2, F3, F4, C3, C4, P3, P4, O1, O2, F7, F8, C7, C8, P7, P8, Cp5, Cp6, Fz, Cz, Pz. The reference lead was Afz. The sampling rate was 250 Hz. The signal was not filtered during recording. We made EEG recordings for all 30 participants, one recording per block.

Photon Cap C20 NIRS spectroscope device (CortiVision, Poland) with 10 sources and 10 detectors was used to register the metabolic activity of the brain. Of all the source-detector pairs, we selected 28 channels corresponding to positions C5h, Fcc3, Ccp3, C3h, Ccp1, Fcc1, C1h, Fccz, Fc1h, Ccpz,

C2h, Ccp2, Cp2h, Fcc2, C4h, Fcc4, Ccp4, C6h, Cp1h, Cppz, P1h, P2h, Ppoz, Fc2h, Ffcz, F2h, F1h, Affz of the 10-5 system (Fig. 2). The NIRS sampling rate was about 5 Hz, reduced to this value by linear interpolation of the signal based on the timestamps sent by the device. There were NIRS recordings of 29 participants available, as one recording was lost.

Both devices transmitted data via the Lab Streaming Layer protocol using software provided by the manufacturers, NeoRec (version 1.6.19830, Medical Computer Systems, Russia) and CortiView (v1.11.5, CortiVision, Poland). The data were synchronized and recorded using a proprietary PsychoPy script (v2022.1.1, Open Science Tools Ltd, UK).

### Recording hand movements or sensory stimulation

The participant's hand movements and the experimenter's actions were recorded with a CW 870FHD video camera (CBR, China), resolution: 640  $\times$  480, horizontal FOV:75°, frame rate: 10 fps. The script that synchronously recorded the NIRS and EEG data assigned numbers of the frames to the saved data samples. The videos were analyzed frame-by-frame. In blocks with bimanual movements or mirrored movements, we distinguished the beginning of movement, complete clenching into a fist, full opening of the palm, touching the table with the palm, complete cessation of movements. In blocks with stimulation — the beginning of the experimenter's hand movement, the first touch with a hard object, the end of the last touch with a hard object, the beginning of the brush touch, the removal of the brush from the hand, the end of the experimenter's hand movement. The EEG and NIRS recordings were marked up in selected frames: the first data sample corresponding to the marked frame was taken as the beginning of the event.

## Processing of brain activity signals

We used the MATLAB 2023b environment to process EEG and NIRS data. A bidirectional notch filter suppressing 50 Hz

## ОРИГИНАЛЬНОЕ ИССЛЕДОВАНИЕ І НЕЙРОФИЗИОЛОГИЯ

Table 1. The degree of mu rhythm suppression under different conditions

Condition	Contralateral, %	Ipsilateral, %	р	
Bimanual movement	10.89 [4.59; 18.12]	8.72 [3.71; 16.02]	0.544	
Unimanual movement (active)	9.71 [2.82; 16.20]	5.64 [2.84; 12.13]	0.797	
Tactile stimulation	14.57 [6.39; 20.17]	5.49 [–5.00; 8.46]	< 0.001	

Table 2. The magnitude of the hemodynamic response under different conditions

Condition	Hk	HbO, nmol/l			HbR, nmol/I		
Condition	Contralateral, %	Ipsilateral, %	р	Contralateral, %	Ipsilateral, %	р	
Bimanual movement	6.92 [-0.21; 28.04]	7.02 [0.36; 28.61]	0.393	-2.66 [-7.80; -0.63]	-2.48 [-5.69; -0.13	0.393	
Unimanual movement	6.88 [3.07; 17.20]	4.91 [0.11; 14.59]	0.094	-0.68 [-4.32; 0.86]	-0.52 [-2.73; 0.80]	0.905	
Tactile stimulation	-0.76 [-16.59; 2.30]	-0.45 [-15.53; 6.18]	0.77	-0.09 [-1.02; 2.37]	0.27 [–1.19; 2.10]	0.787	

interference was used for EEG filtering; it was followed by a unidirectional FIR filter with a bandwidth of 0.5-40 Hz. The delay in bandpass filtering was compensated by sample shifts. To isolate artifacts, we analyzed 200 ms of the signal epoch: those with more than 1% of samples that exceeded ±200 microvolts on any of the channels were discarded. Only 3 out of 60 recordings had 0.5-0.8% of such epochs, and in the remaining recordings this figure was significantly smaller. The recordings of each participant were combined after filtering, and then the resulting signal was decomposed into independent components with the help of a proprietary implementation of the AMICA algorithm [26]. Based on the criteria described earlier [27], we selected components reflecting activity in the primary sensorimotor cortex of left and right hemispheres (mu rhythm sources), an additional motor region, and in the posterior parietal cortex/preclinium. If such components could not be identified, we used the LCMV beamforming method based on the averaged topographic maps of the components of the needed type, and thus searched for the activity.

For the selected components, we calculated the degree of desynchronization of rhythmic activity in the alpha range (8–13 Hz) during movements and stimulation: applied filtering using a unidirectional FIR filter with shift compensation, then the Hilbert transformation, and calculation of absolute values. The degree of desynchronization was calculated as follows:

where Arest is the average amplitude in the window (-6, -2) before the start of arm movement in blocks 1 and 2, and before the start of movement of the experimenter's hand in block 3; Atask is the average amplitude of the signal in the interval from the beginning of movement to its end for blocks 1 and 2, or the interval from the first to the last touch with a hard or soft object for block 3.

The NIRS signals, recorded as radiation intensities at two wavelengths, were converted into concentrations of oxy-(HbO) and deoxyhemoglobin (HbR). A filter with a bandwidth of 0.002–0.09 Hz was applied to the resulting data. In each session, we isolated 10-second segments with hemodynamic responses; the beginning was start of the movement for blocks 1 and 2, and first touch for block 3. The signal value th was average within the 5 seconds of the recording preceding the considered segment was subtracted therefrom. The value of the hemodynamic response was calculated as the response value averaged over all segments and over the four NIRS channels of the respective region. We considered four regions: those corresponding to the primary sensorimotor cortex of the

left (NIRS channels in positions C5h, Fcc3, Ccp3, C3h) and the right hemispheres (C4h, Fcc4, Ccp4, C6h), sources in the additional motor region (Ffcz, F2h, F1h, Affz), and those in the posterior parietal cortex/preclinium (Cppz, P1h, P2h, Ppoz).

### Statistical analysis

For statistical analysis, we used the STATISTICA 6.0 program (StatSoft, USA). The sample distribution normalcy hypothesis was checked with the help of the Shapiro–Wilk test. Spearman's rank correlation coefficient ( $r_s$ ) was used for correlation analysis, and the Wilcoxon test for comparison of related samples. The level of significance was set at p < 0.05. Quantitative data are given as median and interquartile ranges ( $25^{th}$  and  $75^{th}$  percentiles).

### **RESULTS**

### The degree of desynchronization of the mu rhythm

We managed to establish EEG laterality only for the mu rhythm sources, i.e. those localized in primary sensorimotor areas. In cases of bimanual movement, a comparable degree of desynchronization of the mu rhythm was observed over both hemispheres. A similar symmetrical desynchronization of the mu rhythm was recorded for the unimanual movement in front of the mirror both over the contralateral and ipsilateral hemispheres relative to the active limb (Table 1). In contrast, sensory stimulation of the active arm caused significantly more pronounced desynchronization of the mu rhythm over the contralateral hemisphere (Table 1).

### Hemodynamic response

In all experimental blocks, we registered a comparable intensity of the hemodynamic response in both hemispheres of the brain (Table 2). This pattern was evident in the concentration of both HbO and HbR. Tactile stimulation caused atypical changes in hemodynamic parameters: the concentration of HbO decreased during active stimulation, and the concentration of HbR decreased to a lesser extent or increased (Table 2).

## Correlation of quantitative characteristics of EEG and NIRS signals

The intensity of desynchronization of rhythmic activity in the alpha range also correlated with changes in HbO concentration ( $r_s = 0.527$ , p = 0.003) in the block involving unimanual movement

## ORIGINAL RESEARCH I NEUROPHYSIOLOGY

Table 3. Subjective perception of mirror illusions, unimanual movement or sensory stimulation

Illusion parameter			Condition		
iliusion parame	ter	Arm movement	Sensory stimulation	р	
Vividness of the illusion, 0-10 points		4.5 [1.0; 7.0]	2.0 [0.0; 6.0]	0.23	
Ownership, 0–10 points		6.0 [3.0; 8.0]	4.0 [3.0; 8.0]	0.192	
Agency, 0–10 points		4.5 [2.0; 7.0]	-	-	
	Immediately	8	9		
	First quarter	5	5		
	Second quarter	3	9		
Rate of onset, persons*	Third quarter	6	3		
	Fourth quarter	3	1		
	No onset	5	2	1	
	Surprise	6.0 [3	6.0 [3.0; 7.0]		
	Interest	8.0 [6	8.0 [6.0; 8.0]		
Emotional reaction, 0-10 points	Exaltation	3.0 [1	3.0 [1.0; 7.0]		
	Anxiety	1.0 [0	1.0 [0.0; 5.0]		
	Calmness	7.5 [4	.0; 9.0]	1	

Note: \* — one participant did not fill out the rate of onset of the illusion field for the sensory stimulation block.

in front of the mirror, as registered in the posterior parietal cortex. No further statistically significant correlations between the magnitude of desynchronization and hemodynamic response measures were observed for identical experimental conditions.

### Psychometric characteristics of the mirror illusion

The subjective intensity of the mirror illusion was comparable between hand movement and sensory stimulation conditions in terms of illusion vividness and sense of ownership (Table 3). The majority of participants noted the onset of MI during the first half of the corresponding block: 53% in block 2 and 79% in block 3 (Table 3).

The analysis of correlations between the subjective parameters of MI and the degree of desynchronization or a change in the concentration of HbO or HbR associated with unimanual movements in front of the mirror revealed only a weak correlation of the vividness of the illusion with the degree of desynchronization of the ipsilateral mu rhythm ( $r_s = 0.370$ , p = 0.044) and a change in the concentration of HbO in the area of the supplementary motor cortex ( $r_s = 0.425$ , p = 0.022), as well as a weak correlation of the sense of agency with a change in the concentration of HbO ( $r_s = 0.392$ , p = 0.036) and HbR ( $r_s = -0.413$ , p = 0.026) in the area of the supplementary motor cortex. This task yielded no other significant correlations.

As for the sensory stimulation of the arm in front of the mirror, we registered no significant correlations between the subjective parameters of MI and the degree of desynchronization of the mu rhythm (both contra- and ipsilateral).

Most of the subjective parameters of MI significantly positively correlated with the intensity of the emotional reaction to the illusion (Table 4).

For the unimanual movement in front of the mirror, the degree of interest in the emerging illusory sensations negatively correlated with the degree of desynchronization of the mu rhythm in the contralateral hemisphere ( $r_s = -0.471$ , p = 0.009) and in the area of the supplementary motor cortex ( $r_s = -0.419$ , p = 0.021), as well as with changes in the concentration of HbO in the area of the supplementary motor cortex ( $r_s = -0.444$ , p = 0.016). We registered no other statistically significant correlations between the vividness of emotional reactions and quantitative indicators of the EEG or NIRS response.

### DISCUSSION

The simultaneous recording of EEG and NIRS signals during perception of mirror visual feedback revealed that a unimanual movement reflected in the mirror and seen by a healthy individual activated both hemispheres of the brain, same as bimanual movement, as evidenced by electrophysiological and hemodynamic indicators. For the tactile stimulation, EEG registered activation of only the contralateral hemisphere relative to the stimulated arm, while NIRS showed comparable hemodynamic changes in both hemispheres, but atypical in the direction of changes of HbO and HbR concentrations. Most indicators of electrophysiological and hemodynamic response did not correlate with each other.

Other studies have shown bilateral activation of the brain associated with arm movement and visual mirror feedback using either EEG [17, 18] or NIRS [24, 25]. An unimanual movement in front of a mirror was accompanied (to a greater extent) by activation of the additional motor [24, 25], upper or lower parietal [18, 24], premotor [18, 25] and primary somatomotor [18] cortex of the ipsilateral hemisphere in relation to the active arm. These areas include, but are not limited to, the structures of the mirror neuron system. One of the explanations for the MI mechanism is the blockade of inhibitory processes in the ipsilateral (i.e., contralateral to the mirror image) frontal and parietal associative sensorimotor areas of the cortex, which leads to the disinhibition of these areas and the development of the illusion of movement of a stationary limb relaxed behind the mirror [18]. Perhaps this is due to a mirror feedbackinduced shift in the activation of cortical structures in the direction of the ipsilateral hemisphere, which helps to reduce the interhemispheric imbalance in unimanual movement [5].

EEG investigation of changes associated with tactile stimulation with a mirror [28] has shown stronger activation on the contralateral side of the stimulated arm, which is consistent with our data. Another finding was the activation of the secondary sensorimotor cortex and areas of the mirror neuron system in the ipsilatreal hemisphere, which justified the expectation of changes in the amplitude of the mu rhythm on the ipsilateral side depending on the intensity of the illusion; however, no such changes have been detected. The observed changes in HbO and HbR concentrations may reflect the

## ОРИГИНАЛЬНОЕ ИССЛЕДОВАНИЕ І НЕЙРОФИЗИОЛОГИЯ

Table 4. Subjective perception of mirror illusions, unimanual movement or sensory stimulation

Illusian navamentar		Emotional reaction						
Illusion parameter	Surprise	Interest	Exaltation	Anxiety	Calmness			
Illusion vividness – unimanual movement	$r_s = 0.523$	$r_s = 0.378$	$r_s = 0.469$	$r_s = 0.404$	$r_s = -0.199$			
	p = 0.003	p = 0.039	p = 0.008	p = 0.027	p = 0.291			
Ownership – arm movement	$r_s = 0.568$	$r_s = 0.482$	$r_s = 0.551$	$r_s = 0.401$	$r_s = -0.305$			
	p = 0.001	p = 0.007	p = 0.002	p = 0.028	p = 0.101			
Agency – arm movement	r <sub>s</sub> = 0.626	$r_s = 0.502$	$r_s = 0.588$	$r_s = 0.391$	$r_s = -0.305$			
	p < 0.001	p = 0.005	p < 0.001	p = 0.032	p = 0.101			
Vividness of the illusion – sensory stimulation	$r_s = 0.227$	$r_s = 0.231$	$r_s = 0.303$	$r_s = -0.108$	$r_s = 0.268$			
	p = 0.226	p = 0.217	p = 0.104	p = 0.570	p = 0.152			
Ownership - sensory stimulation	$r_s = 0.487$	$r_s = 0.410$	$r_s = 0.499$	$r_s = 0.401$	$r_s = -0.173$			
	p = 0.006	p = 0.025	p = 0.005	p = 0.028	p = 0.358			

so-called "sensorimotor paradox": it is impossible to clearly determine the direction of the hemodynamic response to tactile stimulation due to the complexity of the pattern of simultaneous activation and deactivation of various neural populations [29]. This phenomenon poses a serious methodological problem for the use of NIRS in the context of investigation of brain activity within the framework of the mirror paradigm, especially taking into account the influence of stimulation parameters and the involvement of multiple sensory modalities [30]. It can be assumed that simpler stimulation protocols may be beneficial to further research and explanation of atypical changes in hemodynamic parameters during sensory stimulation with mirror feedback (exclusive use of either a hard item or a soft object).

In this study, we revealed no correlation between the majority of quantitative EEG and NIRS indicators for identical experimental conditions. The correlation between the degree of rhythm desynchronization in the alpha range and an increase in HbO concentration was observed only in the area of the posterior parietal cortex in the context of unimanual movement in front of the mirror. The available literature does not offer other works involving simultaneous registration of electrophysiological and hemodynamic parameters of brain activity during experiments with mirror visual feedback. Further analysis of additional indicators, such as lateralization or connectivity indices, is required. Overall, it can be concluded that in a comprehensive study of the neurophysiological mechanisms of MI, EEG and NIRS can complement but not replace each other.

Individual subjective parameters of MI weakly correlated with the degree of desynchronization of the ipsilateral mu and the activation of the additional motor cortex. However, most of them did not correlate with electrophysiological and hemodynamic parameters of the cerebral cortex activity but showed a significant correlation with the intensity of the emotional reaction to the illusion. The dissociation between objective neurophysiological indicators and subjective experiences of illusion may indicate a multilevel or network-based formation of the illusory experience rather than the activity of isolated cortical regions [18]. The emotional reaction to the illusion can serve as an integrative indicator reflecting not only the perceptual aspects but also the personal characteristics of the participants, their willingness to accept the illusory experience and their general emotional reactivity.

The revealed bilateral activation of primary sensorimotor areas associated with unimanual movement in front of the mirror has a potential clinical significance in the context of optimization of mirror therapy protocols. These findings support the rationale for applying the motor paradigm of mirror therapy in patients with stroke hemiparesis, as it provides activation of motor structures

in the ipsilateral hemisphere, which may facilitate restoration of interhemispheric functional balance. The revealed close relationship between the subjective parameters of the mirror illusion and the emotional reaction suggests that the positive emotional response of the patient in the first sessions can be a predictor of the effectiveness of therapy, reflecting the degree of involvement of the patient in the rehabilitation process. The demonstrated possibility of combining EEG and NIRS opens up prospects for the development of hybrid neurobiological control technologies. This enables prediction of treatment efficacy and individualization of rehabilitation programs based on neurophysiological biomarkers, including for patients with contraindications to conventional mirror therapy, such as bilateral amputation with phantom limb pain syndrome.

This study has the following limitations: the participants had no technical means to record the time of the MI onset; there were no control block that would involve unimanual movement without a mirror; the questionnaire collecting perception of MI was a simplified one. However, these limitations do not affect the main conclusions of the study. It should also be noted that in this experiment, it is impossible to completely separate the emotional reaction to MI and the reaction caused by the novelty of an unusual sensory experience: there was only one assessment, the measurements were not taken repeatedly. Some of the recorded emotional states (surprise, interest) may partially reflect an orientation reflex to a new perceptual experience. The differentiation of these components may be the subject of future longitudinal studies.

### **CONCLUSIONS**

Thus, arm movement in front of the mirror is accompanied by bilateral activation of the primary sensorimotor areas of both hemispheres. The correlations between EEG and NIRS indicators were found only in the posterior parietal cortex, which means that EEG and NIRS complement but not replace each other in the study of MI. The subjective characteristics of the illusion correlated with the emotional reaction, and only some of them weakly correlated with neurophysiological indicators, which corresponds to the concept of a multi-level network organization of the mechanisms behind the illusion. In subsequent studies, it is advisable to jointly register EEG and NIRS indicators during mirror therapy in patients with post-amputation phantom pain or post-stroke hemiparesis, as well as to evaluate the dynamics of the identified MI neuromarkers. The data obtained in such studies can be compared with the norm and taken into account when developing EEG and NIRS-backed neurobiocontrol technologies aimed at correcting these pathologies.

#### References

- Ramachandran VS, Rogers-Ramachandran D. Synaesthesia in phantom limbs induced with mirrors. Proc Biol Sci. 1996; 263: 377–86.
- Deconinck FJA, Smorenburg ARP, Benham A, Ledebt A, Feltham MG, Savelsbergh GJP. Reflections on Mirror Therapy: A Systematic Review of the Effect of Mirror Visual Feedback on the Brain. Neurorehabilitation and Neural Repair. 2015; 29: 349–61.
- Zhang JJQ, Fong KNK, Welage N, Liu KPY. The Activation of the Mirror Neuron System during Action Observation and Action Execution with Mirror Visual Feedback in Stroke: A Systematic Review. Neural Plast. 2018; 2018: 2321045.
- Zhang K, Ding L, Wang X, et al. Mirror therapy reduces excessive variability of motor network in stroke patients: a randomized controlled trial. Eur J Phys Rehabil Med. 2025; 61: 184–94.
- Zhuang J, Lei X, Guo X, Ding L, Jia J. Motor and parietal cortex activity responses to mirror visual feedback in patients with subacute stroke: An EEG study. Clin Neurophysiol Pract. 2025; 10: 12–21.
- Xie H-M, Zhang K-X, Wang S, et al. Effectiveness of Mirror Therapy for Phantom Limb Pain: A Systematic Review and Meta-analysis. Arch Phys Med Rehabil. 2022; 103: 988–97.
- 7. Мокиенко О. А., Ивкина М. В. Методы лечения фантомной боли с позиций доказательной медицины. Российский неврологический журнал. 2023; 28(6): 11–18.
- Thieme H, Morkisch N, Mehrholz J, et al. Mirror therapy for improving motor function after stroke. Cochrane Database Syst Rev. 2018; 7: CD008449.
- Jaafar N, Che Daud AZ, Ahmad Roslan NF, Mansor W. Mirror Therapy Rehabilitation in Stroke: A Scoping Review of Upper Limb Recovery and Brain Activities. Rehabil Res Pract. 2021; 2021: 9487319.
- Kim H, Lee E, Jung J, Lee S. Utilization of Mirror Visual Feedback for Upper Limb Function in Poststroke Patients: A Systematic Review and Meta-Analysis. Vision (Basel). 2023; 7.
- McCabe CS, Haigh RC, Ring EFJ, Halligan PW, Wall PD, Blake DR. A controlled pilot study of the utility of mirror visual feedback in the treatment of complex regional pain syndrome (type 1). Rheumatology (Oxford). 2003; 42: 97–101.
- Vladimir Tichelaar YIG, Geertzen JHB, Keizer D, Paul van Wilgen C. Mirror box therapy added to cognitive behavioural therapy in three chronic complex regional pain syndrome type I patients: a pilot study. Int J Rehabil Res. 2007; 30: 181–8.
- 13. Pervane Vural S, Nakipoglu Yuzer GF, Sezgin Ozcan D, Demir Ozbudak S, Ozgirgin N. Effects of Mirror Therapy in Stroke Patients With Complex Regional Pain Syndrome Type 1: A Randomized Controlled Study. Arch Phys Med Rehabil. 2016; 97: 575–81.
- 14. Machač S, Chasáková L, Kakawand S, et al. Mirror visual feedback as therapeutic modality in unilateral upper extremity complex regional pain syndrome type I: randomized controlled trial. Eur J Phys Rehabil Med. 2024; 60: 280–91.
- Bullock K, Won AS, Bailenson J, Friedman R. Virtual Reality-Delivered Mirror Visual Feedback and Exposure Therapy for FND: A Midpoint Report of a Randomized Controlled Feasibility Study. J Neuropsychiatry Clin Neurosci. 2020; 32: 90–4.
- 16. Limakatso K, Cashin AG, Williams S, Devonshire J, Parker R,

- McAuley JH. The Efficacy of Graded Motor Imagery and Its Components on Phantom Limb Pain and Disability: A Systematic Review and Meta-Analysis. Can J Pain. 2023; 7: 2188899.
- Rizzo M, Petrini L, Del Percio C, Lopez S, Arendt-Nielsen L, Babiloni C. Mirror visual feedback during unilateral finger movements is related to the desynchronization of cortical electroencephalographic somatomotor alpha rhythms. Psychophysiology. 2022; 59: e14116.
- Rizzo M, Del Percio C, Petrini L, Lopez S, Arendt-Nielsen L, Babiloni C. Cortical sources of electroencephalographic alpha rhythms related to the anticipation and experience of mirror visual feedback-induced illusion of finger movements. Psychophysiology. 2023; 60: e14281.
- Norris TA, Augenstein TE, Rodriguez KM, Claffin ES, Krishnan C. Shaping corticospinal pathways in virtual reality: effects of task complexity and sensory feedback during mirror therapy in neurologically intact individuals. J Neuroeng Rehabil. 2024; 21: 154
- Yarossi M, Manuweera T, Adamovich SV, Tunik E. The Effects of Mirror Feedback during Target Directed Movements on Ipsilateral Corticospinal Excitability. Front Hum Neurosci. 2017; 11: 242.
- Tai R-Y, Zhu J-D, Chen C-C, Hsieh Y-W, Cheng C-H. Modulation of Functional Connectivity in Response to Mirror Visual Feedback in Stroke Survivors: An MEG Study. Brain Sci. 2021; 11.
- Cheng C-H, Lin S-H, Wu C-Y, Liao Y-H, Chang K-C, Hsieh Y-W. Mirror Illusion Modulates M1 Activities and Functional Connectivity Patterns of Perceptual-Attention Circuits During Bimanual Movements: A Magnetoencephalography Study. Front Neurosci. 2019; 13: 1363.
- 23. Wang J, Fritzsch C, Bernarding J, et al. Cerebral activation evoked by the mirror illusion of the hand in stroke patients compared to normal subjects. NeuroRehabilitation. 2013; 33: 593–603.
- Bai Z, Fong KNK, Zhang J, Hu Z. Cortical mapping of mirror visual feedback training for unilateral upper extremity: A functional nearinfrared spectroscopy study. Brain Behav. 2020; 10: e01489.
- Tsou M-H, Chen P-Y, Hung Y-T, Lim Y-W, Huang S-L, Liu Y-C. Comparison of Brain Activation Between Different Modes of Motor Acquisition: A Functional Near-Infrared Study. Brain Behav. 2025; 15: e70238.
- 26. Delorme A, Palmer J, Onton J, Oostenveld R, Makeig S. Independent EEG sources are dipolar. PLoS One. 2012; 7: e30135.
- Frolov A, Bobrov P, Biryukova E, et al. Using Multiple Decomposition Methods and Cluster Analysis to Find and Categorize Typical Patterns of EEG Activity in Motor Imagery Brain-Computer Interface Experiments. Front Robot Al. 2020; 7: 88.
- Dubová D, Dvořáčková D, Pavlů D, Pánek D. Cerebral Projection of Mirrored Touch via sLORETA Imaging. Life (Basel). 2023; 13. DOI:10.3390/life13051201.
- Seiyama A, Seki J, Tanabe HC, et al. Circulatory basis of fMRI signals: relationship between changes in the hemodynamic parameters and BOLD signal intensity. Neuroimage. 2004; 21: 1204–14.
- Seiyama A, Miura T, Okahashi S, Konishi N, Cassim M. Visual effects on tactile stimulation and its perception: A pilot study using near-infrared spectroscopy. MethodsX. 2024; 13: 102849.

### Литература

- Ramachandran VS, Rogers-Ramachandran D. Synaesthesia in phantom limbs induced with mirrors. Proc Biol Sci. 1996; 263: 377–86.
- Deconinck FJA, Smorenburg ARP, Benham A, Ledebt A, Feltham MG, Savelsbergh GJP. Reflections on Mirror Therapy: A Systematic Review of the Effect of Mirror Visual Feedback on the Brain. Neurorehabilitation and Neural Repair. 2015; 29: 349–61.
- Zhang JJQ, Fong KNK, Welage N, Liu KPY. The Activation of the Mirror Neuron System during Action Observation and Action Execution with Mirror Visual Feedback in Stroke: A Systematic Review. Neural Plast. 2018; 2018: 2321045.
- Zhang K, Ding L, Wang X, et al. Mirror therapy reduces excessive variability of motor network in stroke patients: a randomized controlled trial. Eur J Phys Rehabil Med. 2025; 61: 184–94.
- Zhuang J, Lei X, Guo X, Ding L, Jia J. Motor and parietal cortex activity responses to mirror visual feedback in patients with subacute stroke: An EEG study. Clin Neurophysiol Pract. 2025; 10: 12–21.
- Xie H-M, Zhang K-X, Wang S, et al. Effectiveness of Mirror Therapy for Phantom Limb Pain: A Systematic Review and Meta-analysis. Arch Phys Med Rehabil. 2022; 103: 988–97.
- 7. Мокиенко О. А., Ивкина М. В. Методы лечения фантомной

## ОРИГИНАЛЬНОЕ ИССЛЕДОВАНИЕ І НЕЙРОФИЗИОЛОГИЯ

- боли с позиций доказательной медицины. Российский неврологический журнал. 2023; 28(6): 11–18.
- Thieme H, Morkisch N, Mehrholz J, et al. Mirror therapy for improving motor function after stroke. Cochrane Database Syst Rev. 2018; 7: CD008449.
- Jaafar N, Che Daud AZ, Ahmad Roslan NF, Mansor W. Mirror Therapy Rehabilitation in Stroke: A Scoping Review of Upper Limb Recovery and Brain Activities. Rehabil Res Pract. 2021; 2021: 9487319.
- Kim H, Lee E, Jung J, Lee S. Utilization of Mirror Visual Feedback for Upper Limb Function in Poststroke Patients: A Systematic Review and Meta-Analysis. Vision (Basel). 2023; 7.
- McCabe CS, Haigh RC, Ring EFJ, Halligan PW, Wall PD, Blake DR. A controlled pilot study of the utility of mirror visual feedback in the treatment of complex regional pain syndrome (type 1). Rheumatology (Oxford). 2003; 42: 97–101.
- Vladimir Tichelaar YIG, Geertzen JHB, Keizer D, Paul van Wilgen C. Mirror box therapy added to cognitive behavioural therapy in three chronic complex regional pain syndrome type I patients: a pilot study. Int J Rehabil Res. 2007; 30: 181–8.
- Pervane Vural S, Nakipoglu Yuzer GF, Sezgin Ozcan D, Demir Ozbudak S, Ozgirgin N. Effects of Mirror Therapy in Stroke Patients With Complex Regional Pain Syndrome Type 1: A Randomized Controlled Study. Arch Phys Med Rehabil. 2016; 97: 575–81.
- 14. Machač S, Chasáková L, Kakawand S, et al. Mirror visual feedback as therapeutic modality in unilateral upper extremity complex regional pain syndrome type I: randomized controlled trial. Eur J Phys Rehabil Med. 2024; 60: 280–91.
- Bullock K, Won AS, Bailenson J, Friedman R. Virtual Reality-Delivered Mirror Visual Feedback and Exposure Therapy for FND: A Midpoint Report of a Randomized Controlled Feasibility Study. J Neuropsychiatry Clin Neurosci. 2020; 32: 90–4.
- Limakatso K, Cashin AG, Williams S, Devonshire J, Parker R, McAuley JH. The Efficacy of Graded Motor Imagery and Its Components on Phantom Limb Pain and Disability: A Systematic Review and Meta-Analysis. Can J Pain. 2023; 7: 2188899.
- 17. Rizzo M, Petrini L, Del Percio C, Lopez S, Arendt-Nielsen L, Babiloni C. Mirror visual feedback during unilateral finger movements is related to the desynchronization of cortical electroencephalographic somatomotor alpha rhythms. Psychophysiology. 2022; 59: e14116.
- 18. Rizzo M, Del Percio C, Petrini L, Lopez S, Arendt-Nielsen L, Babiloni C. Cortical sources of electroencephalographic alpha rhythms related to the anticipation and experience of

- mirror visual feedback-induced illusion of finger movements. Psychophysiology. 2023; 60: e14281.
- Norris TA, Augenstein TE, Rodriguez KM, Claflin ES, Krishnan C. Shaping corticospinal pathways in virtual reality: effects of task complexity and sensory feedback during mirror therapy in neurologically intact individuals. J Neuroeng Rehabil. 2024; 21: 154
- Yarossi M, Manuweera T, Adamovich SV, Tunik E. The Effects of Mirror Feedback during Target Directed Movements on Ipsilateral Corticospinal Excitability. Front Hum Neurosci. 2017; 11: 242.
- Tai R-Y, Zhu J-D, Chen C-C, Hsieh Y-W, Cheng C-H. Modulation of Functional Connectivity in Response to Mirror Visual Feedback in Stroke Survivors: An MEG Study. Brain Sci. 2021; 11.
- Cheng C-H, Lin S-H, Wu C-Y, Liao Y-H, Chang K-C, Hsieh Y-W. Mirror Illusion Modulates M1 Activities and Functional Connectivity Patterns of Perceptual-Attention Circuits During Bimanual Movements: A Magnetoencephalography Study. Front Neurosci. 2019; 13: 1363.
- Wang J, Fritzsch C, Bernarding J, et al. Cerebral activation evoked by the mirror illusion of the hand in stroke patients compared to normal subjects. NeuroRehabilitation. 2013; 33: 593–603.
- 24. Bai Z, Fong KNK, Zhang J, Hu Z. Cortical mapping of mirror visual feedback training for unilateral upper extremity: A functional nearinfrared spectroscopy study. Brain Behav. 2020; 10: e01489.
- Tsou M-H, Chen P-Y, Hung Y-T, Lim Y-W, Huang S-L, Liu Y-C. Comparison of Brain Activation Between Different Modes of Motor Acquisition: A Functional Near-Infrared Study. Brain Behav. 2025; 15: e70238.
- Delorme A, Palmer J, Onton J, Oostenveld R, Makeig S. Independent EEG sources are dipolar. PLoS One. 2012; 7: e30135.
- 27. Frolov A, Bobrov P, Biryukova E, et al. Using Multiple Decomposition Methods and Cluster Analysis to Find and Categorize Typical Patterns of EEG Activity in Motor Imagery Brain-Computer Interface Experiments. Front Robot Al. 2020; 7: 88.
- Dubová D, Dvořáčková D, Pavlů D, Pánek D. Cerebral Projection of Mirrored Touch via sLORETA Imaging. Life (Basel). 2023; 13. DOI:10.3390/life13051201.
- Seiyama A, Seki J, Tanabe HC, et al. Circulatory basis of fMRI signals: relationship between changes in the hemodynamic parameters and BOLD signal intensity. Neuroimage. 2004; 21: 1204–14.
- Seiyama A, Miura T, Okahashi S, Konishi N, Cassim M. Visual effects on tactile stimulation and its perception: A pilot study using near-infrared spectroscopy. MethodsX. 2024; 13: 102849.

## MOLECULAR CYTOGENETIC CHARACTERIZATION OF A RARE RECOMBINANT CHROMOSOME 22 CAUSED BY A MATERNAL INTRACHROMOSOMAL INSERTION

Yurchenko DA <sup>™</sup>, Markova ZhG, Petukhova MS, Matyushchenko GN, Shilova NV

Research Centre for Medical Genetics, Moscow, Russia

The formation of recombinant chromosomes in the offspring of inversion and insertion carriers constitutes a significant challenge in clinical genetics due to the high risk of chromosomal abnormalities in children. Here, we present a clinical case. The aim of this study was to characterize the structure and origin of a chromosomal imbalance in a female patient presenting with delayed motor and speech development, craniofacial anomalies, and sensorineural hearing loss through molecular cytogenetic analysis of a recombinant chromosome 22. Chromosomal microarray analysis of the proband, who exhibited psychomotor delay and dysmorphic features, revealed three interstitial duplications: 22q11.21, 22q12.3–q13.1, and 22q13.2. Fluorescence in situ hybridization (FISH), using both commercial and homemade DNA probes, demonstrated that the mother carried a complex intrachromosomal rearrangement comprising an initial paracentric inversion of 22q11.21–q12.3, followed by an interstitial insertion of the 22q11.21 and 22q12.3–q13.1 segments into the nucleolar organizer region at 22p12. Accordingly, the recombinant chromosome identified in the proband resulted from meiotic segregation of the maternal complex intrachromosomal inversion and insertion. These findings highlight the diagnostic value of an integrated cytogenomic approach for the precise delineation of complex chromosomal rearrangements, determination of their origin, and assessment of genetic risk in clinical genetic counseling.

Keywords: intrachromosomal insertion, inversion, recombinant chromosome 22, FISH, homemade DNA probes, CNV, duplication

Funding: this research was supported by the Ministry of Science and Higher Education of the Russian Federation (#FGFF-2023-0003).

**Author contribution:** Yurchenko DA — study design, development of homemade DNA probes, conducting FISH analysis and interpreting the data, manuscript preparation; Markova ZhG — conducting FISH analysis using commercial DNA probes; Petukhova MS and Matyushchenko GN — clinical genetic counseling of the family; Shilova NV — study conception and design, discussion of results, and scientific editing of the manuscript.

Compliance with ethical standards: the study was approved by the Ethics Committee of the Research Centre for Medical Genetics (protocol No. 4/2 dated 19 April 2021). The informed consent for participation in the research study was obtained from the patients.

Correspondence should be addressed: Darya A. Yurchenko Moskvorechye, 1, Moscow, 115522, Russia; dashalbv@mail.ru

Received: 16.09.2025 Accepted: 06.10.2025 Published online: 26.10.2025

DOI: 10.24075/brsmu.2025.050

Copyright: © 2025 by the authors. Licensee: Pirogov University. This article is an open access article distributed under the terms and conditions of the Creative Commons Attribution (CC BY) license (https://creativecommons.org/licenses/by/4.0/).

## МОЛЕКУЛЯРНО-ЦИТОГЕНЕТИЧЕСКАЯ ХАРАКТЕРИСТИКА РЕДКОГО СЛУЧАЯ РЕКОМБИНАНТНОЙ ХРОМОСОМЫ 22 ВСЛЕДСТВИЕ МАТЕРИНСКОЙ ИНТРАХРОМОСОМНОЙ ИНСЕРЦИИ

Д. А. Юрченко ⊠, Ж. Г. Маркова, М. С. Петухова, Г. Н. Матющенко, Н. В. Шилова

Медико-генетический научный центр имени Н. П. Бочкова, Москва, Россия

Формирование рекомбинантных хромосом в потомстве носителей инверсий и инсерций представляет собой серьезную проблему клинической генетики в связи с высоким риском рождения детей с хромосомной патологией. Представлен клинический случай. Целью исследования было в ходе молекулярноцитогенетической диагностики рекомбинантной хромосомы 22 установить структуру и происхождение хромосомного дисбаланса у пациентки с задержкой моторного и психоречевого развития, черепно-лицевыми аномалиями и тугоухостью. При проведении хромосомного микроматричного анализа у пробанда с задержкой психомоторого развития и признаками дисморфогенеза были обнаружены три интерстициальные дупликации: 22q11.21, 22q12.3q13.1 и 22q13.2. FISH-анализ с использованием коммерческих и несерийных ДНК-зондов позволил установить, что у матери пациентки имеется сложная интрахромосомная перестройка: сочетание инициирующей парацентрической инверсии 22q11.21q12.3 и последующей межплечевой инсерции районов 22q11.21 и 22q12.3q13.1 в район ядрышкового организатора 22p12. Соответственно, выявленная у пробанда рекомбинантная хромосома является результатом сегрегации материнской сложной внутрихромосомной перестройки. Полученные результаты подчеркивают диагностическую ценность комплексного цитогеномного подхода для точной идентификации сложных хромосомных нарушений, определения их происхождения и оценки генетических рисков при медико-генетическом консультировании.

Ключевые слова: интрахромосомная инсерция, инверсия, рекомбинантная хромосома 22, FISH, несерийные ДНК-зонды, CNV, дупликация

Финансирование: исследование проведено в рамках темы НИР № 123052200006-7 «Оптимизация молекулярно-(цито)генетических подходов для верификации и интерпретации клинически значимых вариаций числа копий участков ДНК (CNV)» (#FGFF-2023–0003).

Вклад авторов: Д. А. Юрченко — дизайн исследования, разработка несерийных ДНК-зондов, проведение FISH-диагностики и интерпретация полученных данных, подготовка рукописи; Ж. Г. Маркова — проведение FISH-исследования с коммерческими ДНК-зондами; М. С. Петухова, Г. Н. Матющенко — медико-генетическое консультирование семьи; Н. В. Шилова — концепция и дизайн исследования, обсуждение результатов, научное редактирование рукописи.

Соблюдение этических стандартов: исследование одобрено этическим комитетом ФГБНУ «МГНЦ» (протокол № 4/2 от 19 апреля 2021 г.). Получено добровольное информированное согласие на участие пациентов в научном исследовании.

 Для корреспонденции: Дарья Александровна Юрченко ул. Москворечье, д. 1, г. Москва, 115522, Россия; dashalbv@mail.ru

Статья получена: 16.09.2025 Статья принята к печати: 06.10.2025 Опубликована онлайн: 26.10.2025

DOI: 10.24075/vrgmu.2025.050

Авторские права: © 2025 принадлежат авторам. Лицензиат: РНИМУ им. Н. И. Пирогова. Статья размещена в открытом доступе и распространяется на условиях лицензии Creative Commons Attribution (CC BY) (https://creativecommons.org/licenses/by/4.0/).

## ОРИГИНАЛЬНОЕ ИССЛЕДОВАНИЕ І ГЕНЕТИКА

Recombinant chromosomes (rec) are detected in the offspring of carriers with balanced structural chromosomal rearrangements (CRs), such as inversions and insertions, and are associated with genomic imbalances — copy number variations (CNVs) in the form of deletions and duplications — linked to abnormal phenotypes [1, 2].

The majority of pathogenic microdeletions and microduplications represent the recurrent CNVs, which arise due to specific features of the genomic architecture and lead to sporadic cases of chromosomal imbalance [3]. In contrast, nonrecurrent CNVs may result from other mechanisms of formation, for example, from the recombination events occurring during in meiosis I in phenotypically normal heterozygous carriers of inversion, as well as from intra- and interchromosomal insertions. A between-arm intrachromosomal insertion represents a segment of chromatin from one arm inserted into a breakpoint site on the opposite arm [4]. Thus, after bivalent formation between the chromosome carrying a between-arm insertion and its normal homologue, the inserted segment becomes reoriented to ensure the maximum degree of synapsis within the bivalent. A single (or any odd number of) crossovers within the centromeric segment (the chromosome region containing the centromere) results in the formation of recombinant chromosomes — one with a duplication of the inserted segment and the other with a deletion. Gametes (and subsequently zygotes) carrying recombinant chromosomes give rise to interstitial CNVs in the offspring (Fig. 1).

The contribution of balanced intrachromosomal insertions to the spectrum of chromosomal abnormalities is significant, as the genetic risk is expected to be high and, in theory, could approach 50%, which is of crucial importance for medical genetic counseling [4, 5]. In this context, chromosome 22 characterized by a high concentration of low-copy repeats (LCRs) — is of particular interest. This genomic architecture predisposes the region to a broad spectrum of balanced and unbalanced chromosomal rearrangements (CRs) mediated by non-allelic homologous recombination (NAHR) [6]. The beststudied examples are the 22q11.2 reciprocal deletion and duplication syndromes, also known as genomic sister disorders [7, 8]. However, non-recurrent copy number variations (CNVs) in chromosome 22 are also of significant value. Such cases, which reveal complex and diverse mechanisms of genomic structural organization — including replication-mediated and multi-step genomic events — may present with multiple regions of chromosomal imbalance [9, 10]. These observations not only expand our understanding of the structural variability of chromosome 22 but are also of practical importance for medical genetic counseling, particularly in selecting strategies for prenatal and preimplantation genetic diagnosis in families with an affected child [11].

In this paper, we present a unique case of a recombinant chromosome 22 in a patient with an abnormal phenotype. The study aimed to characterize, using molecular cytogenetic methods, a rare rec(22) with three interstitial duplications resulting from meiotic crossing over during gametogenesis in the mother, who was a carrier of a complex intrachromosomal rearrangement.

### **METHODS**

### Clinical data

The patient was a 7-month-old girl referred to the Research Centre for Medical Genetics because of psychomotor developmental delay and craniofacial dysmorphism. The family history revealed an older child, a 5-year-old girl, who was healthy and had no apparent clinical abnormalities (as reported by the parents). Both parents were healthy and nonconsanguineous. The mother's obstetric history included two missed miscarriages (Fig. 2A).

The patient was born at 36 weeks of gestation. The Apgar score was 7/7. Birth weight was 2260 g, body length 45 cm, and head circumference 32 cm. After birth, she was admitted to the neonatal pathology unit with a diagnosis of grade I-II cerebral ischemia and motor dysfunction syndrome. From birth, delayed motor development and bilateral sensorineural hearing loss were noted. At the first examination (age 7 months), the following phenotypic features were observed: orbital hypertelorism, epicanthus inversus, short palpebral fissures, bulbous nasal tip, trapezoid-shaped upper lip, long philtrum, high-arched palate, and long fingers. Anthropometric parameters: body length 68 cm (between the 50th and 75th centiles), body weight 6000 g (below the 3rd centile). Gross motor development was markedly delayed: the patient could hold her head only in the prone position and was unable to roll over. At follow-up at the age of 2 years, she continued to show a pronounced delay in motor development: she could sit unsupported at 1.5 years and began standing and stepping with support at 2 years. Self-care skills were absent, and speech development was mildly delayed — she could pronounce a few simple words.

## Molecular cytogenetic studies

To detect CNV, the chromosomal microarray analysis of the DNA sample from the patient's peripheral blood was conducted using the CytoScan HD Array oligonucleotide microarrays (Affymetrix, Santa Clara, USA) in accordance with the manufacturer's protocols. The analysis of CNVs was performed using the Chromosome Analysis Suite (ChAS) ver.

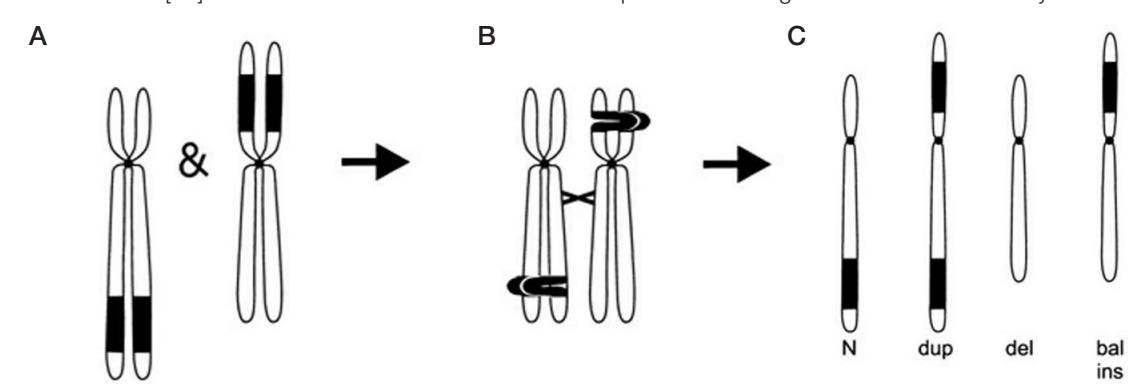


Fig. 1. Gamete production following recombination between the sites of rearrangement in a between-arm intrachromosomal insertion. A. Normal chromosome (left) and chromosome with insertion (right); B. Crossover event; C. Types of gametes. (Adapted from Gardner R. J., Amor D. J., 2018.)

### ORIGINAL RESEARCH | GENETICS

**Table.** Nucleotide sequences of the primers used in the study

Name	DNA primer sequences, 5'-3'	PCR product length (bp)	Genomic coordinates (hg19)		
dum00a10.0.1	F:GTGGGGTGGAAATAGAGGAGGAAAAGTG	9118			
dup22q12.3_1	R: ACACAATAACGCAGAGAGTGAAATGGGT	9116			
dum00~10.0	F: ACCCATTTCACTCTCTGCGTTATTGTGT	9818	sh-20,26 011 060 26 020 207		
dup22q12.3_2	R: CCAGCTTCATCTCATTCCTCTCTTGTCC	9010	chr22:36,911,962-36,938,387		
dus00a10.0.0	F: CACTCTTGCTGCTCTAGGGTTTCTTCTC	9964			
dup22q12.3_3	R: ATGGGAATCTATTTTGTCTCCTGTCGCC	9964			
00~10.1	F: GTCTCCCCCTCAAAAATGCTGGTGATAA	9874			
22q13_1	R: CAAGTAGCCTTCAGAGTTCCATCTGCTC	9074			
00~10.0	F: AAGACAGACGGATGGAAAACCTAGTTGC	9002	chr22:41,525,966-41,555,314		
22q13_2	R: GACATACTTGAGACACTGGAGCTTGACC	9002	CHIZZ:41,525,900-41,555,314		
22q13 3	F: AACTCTCCTATAATGCCTCCAGGGTCTC	0500			
22q13_3	R: GCAACACACAAGTTCAGCAAAAACCAAC	9520			
22g-invG-1	F: GTTCAAAGCCCCCACAGTCTTCCCAATG	9890			
22q-invG-1	R: AGGAGGAGGTCACAAGTCCCATACCACT	9090			
00g inuC 0	F: AGTGGTATGGGACTTGTGACCTCCTCCT	9643	chr22:24,426,053–24,452,928		
22q-invG-2	R: ACATGCTGGCGGGGAAAGAGACAGTTTA	9043	C11122:24,420,053-24,452,926		
00 10	F: GAGTAGGGAGGGATGCTGCTGGGTTAAG	9182			
22q-invG-3	R:GAGGAGACCAGAGAAGAGGGTGGCAATG	9182			
00 - i D 1	F: GTGGAGAGAGAGTGTGAATAGGGAAGT	9068			
22q-invR-1	R: GGTTGTTGCGAGATGAATGAAGCCAAAT	9066			
22g invP 2	F: CACCCACATTCCTGAAGATGACACTAC	9095	ohr00:24 100 000 24 100 001		
22q-invR-2	R: TGAGTGAGTGATCGCCTCCTTTATGAGA	9095	chr22:34,120,020-34,162,291		
OOm invD O	F: AAACCTCTACCTCCAAAACCTATCCCCA	0050			
22q-invR-3	R: TCCCACATTCTCTCCATCCTCTTCTTGT	9259			

4.0 software (Thermo Fisher Scientific Inc.; USA), and the results were interpreted in accordance with the International System for Human Cytogenomic Nomenclature (ISCN, 2020). The CNV identified was matched to the data published in the scientific literature and the information from the publicly available databases: Database of Genomic Variants (DGV) (http://dgv.tcag.ca/dgv/app/home), DECIPHER (http://decipher.sanger.ac.uk/), and OMIM (http://www.ncbi.nlm.nih.gov/omim). Genomic coordinates are provided in accordance with the Human Genome February 2009 assembly (GRCh37/hg19). Clinical significance of variants was assessed in accordance with the standards of the American College of Medical Genetics and Genomics (ACMG) [12].

Fluorescence *in situ* hybridization (FISH) on chromosomal preparations from cultured peripheral blood lymphocytes was performed using commercially available locus-specific (22q11.2 LSI *TBX1*/22q13 *SHANK3*) and sub-telomere (22qter) DNA probes (Kreatech, Netherlands), as well as a DNA probe specific to the short arms of acrocentric chromosomes (Acro-p) (MetaSystems, Germany), in accordance with the manufacturers' protocols. Denaturation and hybridization were performed using the ThermoBrite hybridization system (StatSpin, USA), and assessment was conducted using the Axiolmager M.1 epifluorescence microscope (Carl Zeiss, Germany) and the Isis softwate tool for digital image processing (MetaSystems, Germany).

The development of homemade DNA probes to refine the structure of the patient's recombinant chromosome 22 and assess the parental chromosomes parents represented an important stage of the study. Primers were selected using the Primer-BLAST NCBI software tool (https://www.ncbi.nlm. nih.gov/tools/primer-blast/) and the UCSC Genome Browser database (http://genome.ucsc.edu). The OligoAnalyzer™

Tool (https://eu.idtdna.com/pages/tools/oligoanalyzer/) was used to verify specificity of the selected primers. Primers were synthesized by Evrogen (Russia). The nucleotide sequences of the primers selected are provided in Table.

Sequences of the selected DNA primers were used to conduct LR-PCR using the BioMaster LR HS-PCR (2x) (BiolabMix, Russia) in the GeneAmp PCR System 9700 (Applied Biosystems, USA) in accordance with the manufacturer's protocol. The resulting amplicons were purified on the columns using the diaGene DNA purification kit for DNA isolation from reaction mixtures (Dia-M, Russia) in accordance with the manufacturer's instructions, with subsequent combining of purified PCR products in one test tube aimed at obtaining a DNA probe approximately 30 kb in length. A nick-translation method was used to introduce a fluorescent label into a DNA probe. FISH with homemade DNA probes involved separate denaturation of DNA in the chromosomal preparation and the DNA probe [13–15].

Chromosomes were counterstained with DAPI I (Abbott Molecular, USA) in Vectashield mounting medium (Vector Laboratories, USA) at a 1:20 ratio. Metaphase chromosome images were analyzed using the ISIS digital imaging system (MetaSystems, Germany) integrated with an Axio Imager M1 epifluorescence microscope (Carl Zeiss, Germany).

### **RESULTS**

In the first stage of molecular cytogenetic testing of the patient with motor and speech developmental delay, craniofacial anomalies, and hearing loss, chromosomal microarray analysis (CMA) was performed. The analysis revealed three interstitial micrtoduplications located in the long arm of chromosome 22: arr[hg19] 22q11.21(18037572\_21915207)

## ОРИГИНАЛЬНОЕ ИССЛЕДОВАНИЕ І ГЕНЕТИКА

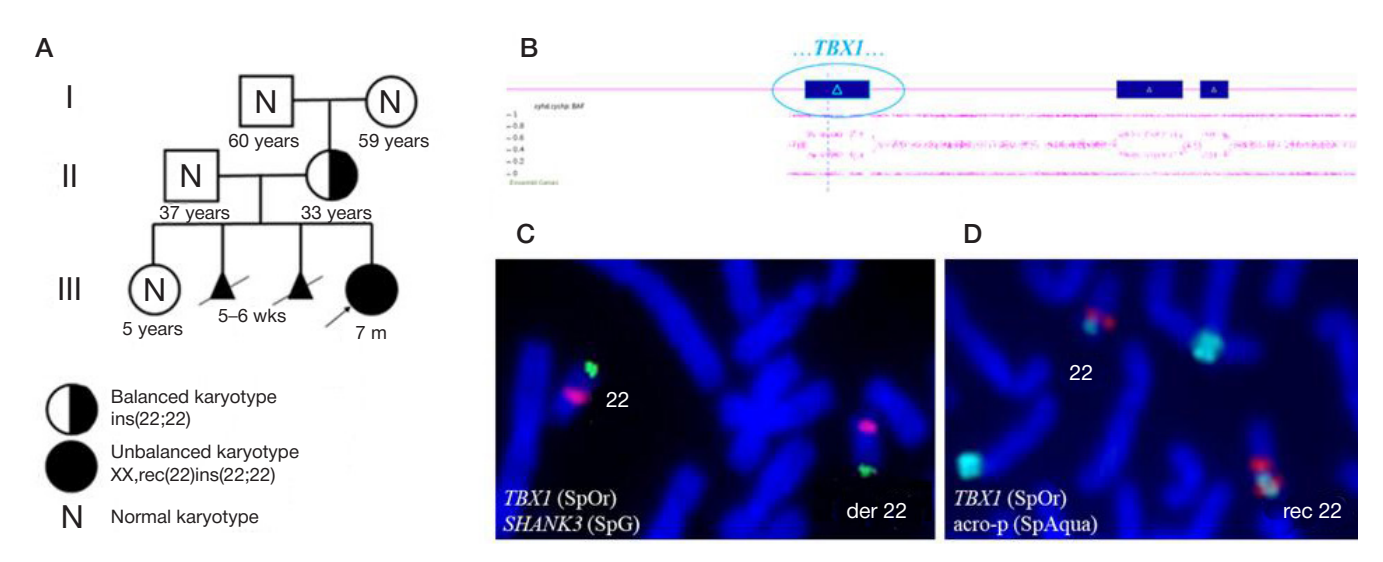


Fig. 2. Familial case of intrachromosomal ins(22;22). A. Three-generation pedigree of the family with the *de novo* heterozygous carrier of the intrachromosomal insertion on chromosome 22. B. CMA hybridization profile of chromosome 22 demonstrating three duplications in the patient. C. FISH results for the patient's mother showing hybridization with the DNA probe for the 22q11.2 region (*TBX1*, SpOrange) and the control probe for SHANK3 (SpGreen), which is not involved in the rearrangement. D. FISH results for the patient showing the recombinant chromosome 22, in which the duplicated fragment containing *TBX1* (SpOrange) is inserted into the nucleolar organizer region (p12) (acro-p, SpAqua).

x3,22q12.3q13.1(36793141\_40756125)x3,22q13.2 (41818449\_43449759)x3 (Fig. 2B) sized 3.9 Mb, 4 Mb, and 1.6 Mb, respectively.

To verify the data obtained, FISH analysis of the chromosomal preparations of the patient, her sister and parents was conducted that involved the use of the commercially available DNA probe for the 22q11.21 chromosomal locus (*TBX1* gene). It was found that the patient's mother was a carrier of an intrachromosomal between-arm insertion involving the 22q11.2 region inserted into the nucleolar organizer region (p12) (Fig. 2C). Thus, the duplication including the *TBX1* gene resulted from the maternal meiotic crossing over event within the centromeric segment of chromosome 22, which led to the formation of the recombinant chromosome 22 observed in the patient (Fig. 2D). Examination of the maternal grandparents revealed no insertion, indicating that the mother's chromosomal rearrangement occurred *de novo*.

To verify the second and third microduplications, it was hypothesized that there was a "single" duplication in the 22q12.3q13.2 region. For this purpose, homemade locus-specific DNA probes were designed for two regions of chromosome 22: (hg19):36,911,962–36,938,387 and (hg19):41,525,966–41,555,314. The primer design is provided in Table. The FISH analysis showed that the patient's mother carried an intrachromosomal insertion involving the 22q12.3q13.1 region into the nucleolar organizer region (p12) of chromosome 22 (Fig. 3B). Thus, the patient's recombinant chromosome 22 contains both the duplication including the *TBX1* gene (22q11.2) and the 22q12.3q13.1 duplication of maternal origin (Fig. 3C).

Based on the data obtained, we proposed a hypothesis regarding the complex mechanism underlying the chromosomal rearrangement in the patient's mother. A long disomic region of 14.9 Mb was identified between the proband's first (22q11.21) and second (22q12.3) duplications (Fig. 3A). This suggested that the 22q11.21 and 22q12.3q13.1 regions on the maternal chromosome 22 were likely close together due to a paracentric inversion (chr22(hg19):18,037,572–36,793,141). Therefore, both of these regions were inserted together into the nucleolar organizer region (p12) of chromosome 22 as a result of the initial de novo rearrangement that occurred during meiosis in one of her parents, whose karyotypes were assessed and turned out to

be normal. To verify this hypothesis, two additional homemade locus-specific DNA probes for the 22q11.23 and 22q12.3 regions were designed (chr22(hg19):24,426,053–24,452,928 and chr22(hg19):34,120,020–34,162,291 (Table). The schematic representation of the complex chromosomal rearrangement is shown in Fig. 4.

The comprehensive molecular cytogenetic analysis involving the use of both commercially available and homemade DNA probes confirmed the hypothesis about the complex mechanism underlying the maternal chromosomal rearrangement. It was shown that the patient's recombinant chromosome 22 with two microduplications resulted from two consecutive events that occurred during the maternal meiosis: an initial paracentric inversion in 22q11.21q12.3 and the subsequent betweenarm insertion of the regions 22q11.21 and 22q12.3q13.1 into the nucleolar organizer region 22p12. In this study, we did not assess the third duplication; further analysis is planned to clarify the complete mechanism underlying the formation of the complex CR in the patient's mother.

Thus, combining CMA and FISH with both the commercially available and homemade DNA probes made it possible to visualize the mechanism underlying the development of chromosomal imbalance. According to the family's three-generation pedigree, the estimated empirical risk of giving birth to a child with a chromosomal/genomic imbalance or spontaneous abortion is 75%, which is considered a high genetic risk (Fig. 2A).

### DISCUSSION

The present case demonstrates a rare instance of recombinant chromosome 22 formation resulting from the meiotic segregation of a complex maternal intrachromosomal rearrangement, specifically a combination of inversion and insertion. Similar mechanisms have been previously described in studies on rec(22) derived from maternal intrachromosomal rearrangements. For example, several rec(22) cases have been reported in which such maternal rearrangements led to duplications of distal 22q regions in the offspring [16, 17]. One report describes a female patient with a 7 Mb duplication in 22q13.1q13.2, which was subsequently identified as a meiotic segregation product of a maternal insertion [18].

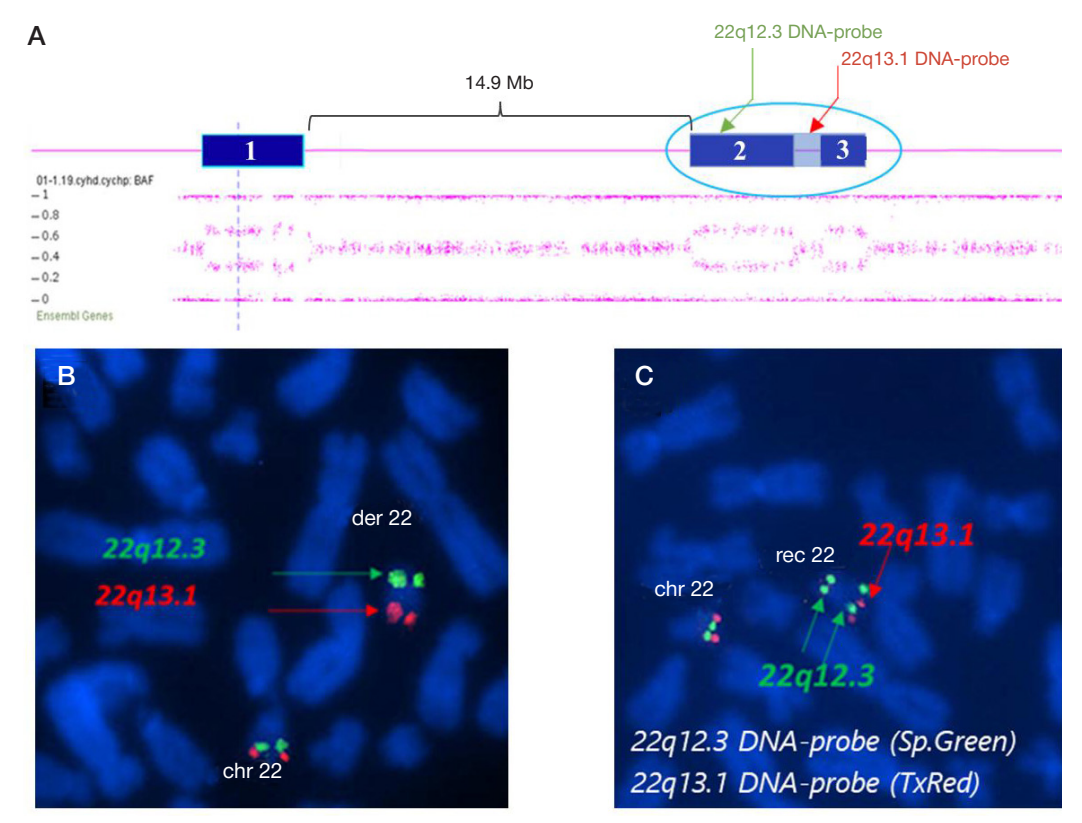


Fig. 3. FISH analysis with homemade DNA probes disproving the hypothesis of a "single" duplication. A. CMA hybridization profile of chromosome 22 in the patient and schematic representation of the genomic localization of the homemade DNA probes designed to test the "single duplication" hypothesis. B. FISH results with homemade DNA probes on maternal metaphase chromosomes, showing that the derivative chromosome 22 resulted from insertion of the 22q12.3 fragment into the nucleolar organizer region (p12). The 22q13.1 region is not involved in the rearrangement. C. FISH results with homemade DNA probes on the patient's metaphase chromosomes, showing that the recombinant chromosome 22 contains an insertion of the duplicated 22q12.3 fragment into the nucleolar organizer region (p12). The 22q13.1 region is not duplicated and is represented by a single copy on each homologue

Our case extends these observations by demonstrating that a recombinant chromosome 22 containing multiple CNVs can arise from the inheritance of a complex maternal intrachromosomal between-arm insertion combined with an inversion.

The acrocentric chromosome 22 is one of the shortest human chromosomes and contains the highest density of lowcopy repeats (LCRs) within its long arm. LCRs are DNA blocks ranging in size from 10 to 400 kb that share a high degree (95–97%) of nucleotide sequence identity. This homology facilitates non-allelic homologous recombination (NAHR), the mechanism underlying typical 22q11.2 deletions and duplications [6, 19]. Optical genome mapping has confirmed a high degree of LCR22 variability in the population, which increases the likelihood of non-recurrent and complex chromosomal rearrangements [20]. At the same time, more complex, multi-stage events like the one we report here are thought to be explained by other replication-mediated

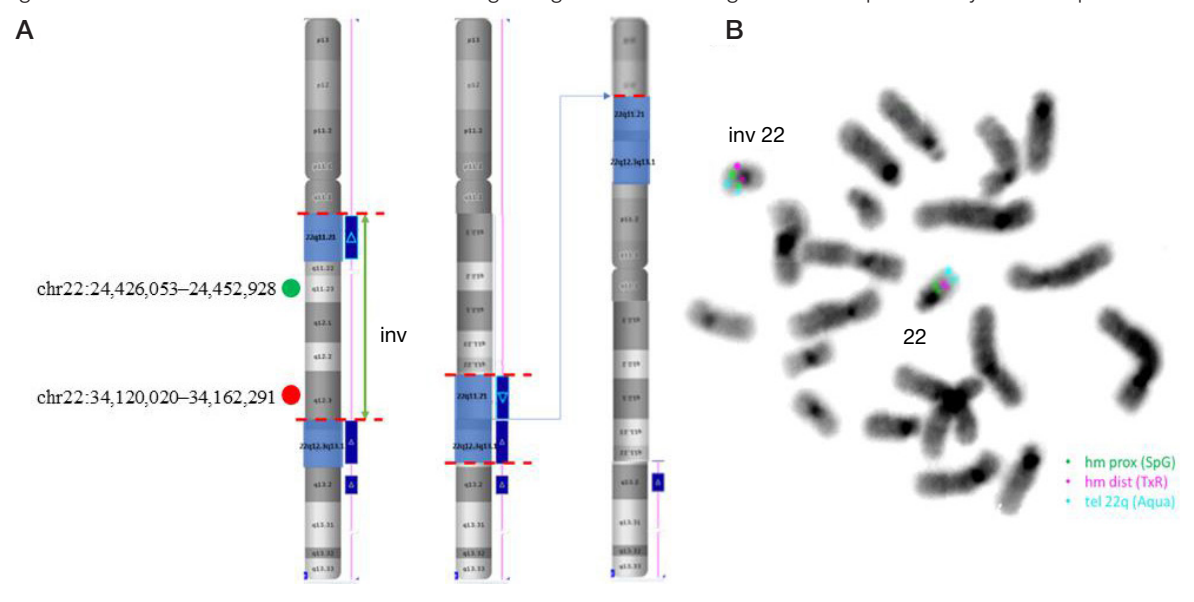


Fig. 4. A. Schematic representation of the mechanism underlying formation of the complex maternal *de novo* CR. B. Results of FISH analysis using the distal homemade DNA probe (TxRed), the proximal DNA probe (SpGreen) for the inversion region (chr22(hg19):18,037,572–36,793,141) and the commercially available DNA probe for the subtelomeric region of the long arm of chromosome 22 (SpAqua)

## ОРИГИНАЛЬНОЕ ИССЛЕДОВАНИЕ І ГЕНЕТИКА

mechanisms, specifically Fork Stalling and Template Switching (FoSTeS) and Microhomology-Mediated Break-Induced Replication (MMBIR) [3, 9, 10, 21].

In this case, we identified a complex intrachromosomal rearrangement in the mother, consisting of a paracentric inversion in 22q11.21q12.3 (chr22(hg19):18,037,572–36,793,141), followed by a between-arm intrachromosomal insertion of the 22q11.21 and 22q12.3q13.1 regions into the nucleolar organizer region at 22p12. The proximal inversion breakpoint is located within LCR22 A-B (~18-21 Mb), a well-known genomic instability "hot spot" that results in NAHR-mediated chromosomal rearrangements. According to the literature, inversions spanning the LCR22A-B or LCR22B-D/C blocks can initiate non-recurrent chromosomal rearrangements [6, 22]. The distal inversion breakpoint on the long arm (~36.8 Mb) lies outside the classic LCR22 boundaries in a region of unique sequences at 22q12.3, making the involvement of replication-mediated mechanisms (FoSTeS/MMBIR) more likely [21-23]. The insertion of a large 22g segment into the short arm (22p) is also consistent with known genomic architecture. The p-arms of acrocentric chromosomes, which contain the nucleolar organizer regions (NORs) and multiple repetitive blocks, represent highly dynamic genomic regions [24]. Therefore, the combination of an LCR22-associated inversion and an insertion into the 22p NOR creates a unique structural background predisposing to multiple duplications during meiotic segregation.

Our case expands the spectrum of previously reported rec(22) cases and demonstrates that the presence of a complex maternal CR can lead to multiple interstitial duplications in the offspring. This mechanism integrates two key factors: the variable genome architecture resulting from the abundance of low-copy repeats on chromosome 22, and the dynamic nature of the ribosomal repeat arrays within the nucleolar organizer region on its short arm.

The clinical manifestations in our patient, who carries multiple CNVs on chromosome 22, include motor and speech developmental delay, craniofacial dysmorphism, hypotonia, and hearing loss. These clinical features align with the phenotypic spectrum of 22q11.2 duplication syndrome, which is characterized by developmental delay, behavioral disorders, hearing loss, craniofacial anomalies, and variable degrees of cognitive impairment. The phenotypic abnormalities associated

with 22q11.2 duplication are highly heterogeneous. This variability is thought to be associated with dose-dependent effects of key genes such as *TBX1*, as well as the influence of additional duplicated segments in the 22q12–q13 region, which may contribute to neurodevelopment and hearing function [8, 25, 26].

In terms of methods, this case emphasizes the need for a comprehensive cytogenomic approach. Standard karyotyping cannot detect CNVs smaller than 10 Mb; therefore, CMA and FISH were pivotal in this study. CMA revealed three interstitial microduplications but did not clarify the mechanism underlying their formation. Only FISH, using both commercially available and homemade DNA probes, enabled us to determine the topology of the chromosomal rearrangement and demonstrate that two of the three duplications resulted from the abnormal meiotic segregation of a complex maternal intrachromosomal rearrangement. It is important to emphasize that the use of homemade locus-specific DNA probes, obtained by longrange PCR, was critical: this allowed us to distinguish between the hypothesis of a "single" duplication and the presence of two distinct duplications, and to confirm a paracentric inversion in the long arm of chromosome 22 as the key starting point for the formation of the complex chromosomal rearrangement in the mother.

Thus, the applied cytogenomic strategy—integrating CMA and FISH with both commercial and homemade DNA probes—enabled us to determine the origin and mechanism of formation, and to reconstruct the complex intrachromosomal rearrangement in a patient presenting with motor and speech developmental delay and dysmorphic features. These findings also indicate a high genetic risk for the family to have another child with a chromosomal abnormality.

### **CONCLUSIONS**

This study describes a rare case of multiple interstitial duplications on chromosome 22 resulting from meiotic segregation of a complex intrachromosomal rearrangement that arose *de novo* in the proband's mother. Our findings show that a combination of a paracentric inversion and subsequent insertion events can generate recombinant chromosomes harboring multiple CNVs, leading to a clinically significant chromosomal imbalance.

### References

- Liehr T, Weise A, Mrasek K, Ziegler M, Padutsch N, Wilhelm K, et al. Recombinant chromosomes resulting from parental pericentric inversions — two new cases and a review of the literature. Front Genet. 2019; 10: 1165. DOI: 10.3389/fgene.2019.01165.
- Madan K, Menko FH. Intrachromosomal insertions: a case report and a review. Hum Genet. 1992; 89 (1): 1–9. DOI: 10.1007/BF00207032.
- Carvalho CM, Lupski JR. Mechanisms underlying structural variant formation in genomic disorders. Nat Rev Genet. 2016; 17 (4): 224–38. DOI: 10.1038/nrg.2015.25.
- Gardner RJ, Amor DJ. Gardner and Sutherland's Chromosome Abnormalities and Genetic Counselling. 5th ed. Oxford: Oxford University Press, 2018; 440 p.
- Nowakowska BA, de Leeuw N, Ruivenkamp CA, Sikkema-Raddatz B, Crolla JA, Thoelen R, et al. Parental insertional balanced translocations are an important cause of apparently de novo CNVs in patients with developmental anomalies. Eur J Hum Genet. 2012; 20 (2): 166–70. DOI: 10.1038/ejhg.2011.157.
- Vervoort L, Vermeesch JR. The 22q11.2 low copy repeats. Genes (Basel). 2022; 13 (11): 2101. DOI: 10.3390/genes13112101.

- Demaerel W, Hosseinzadeh M, Nouri N, Sedghi M, Dimitriadou E, Salehi M, et al. Reciprocal 22q11.2 deletion and duplication in siblings with karyotypically normal parents. Cytogenet Genome Res. 2016; 148 (1): 1–5. DOI: 10.1159/000445089.
- Portnoï MF. Microduplication 22q11.2: a new chromosomal syndrome. Eur J Med Genet. 2009; 52 (2–3): 88–93. DOI: 10.1016/j.ejmg.2009.02.008.
- Arlt MF, Wilson TE, Glover TW. Replication stress and mechanisms of CNV formation. Curr Opin Genet Dev. 2012; 22 (3): 204–10. DOI: 10.1016/j.gde.2012.01.009.
- Liu P, Carvalho CM, Hastings PJ, Lupski JR. Mechanisms for recurrent and complex human genomic rearrangements. Curr Opin Genet Dev. 2012; 22 (3): 211–20. DOI: 10.1016/j.gde.2012.02.012.
- 11. Li S, Han X, Ye M, Chen S, Shen Y, Niu J, et al. Prenatal diagnosis of microdeletions or microduplications in the proximal, central, and distal regions of chromosome 22q11.2: ultrasound findings and pregnancy outcome. Front Genet. 2019; 10: 813. DOI: 10.3389/fgene.2019.00813.
- 12. Riggs ER, Andersen EF, Cherry AM, Kantarci S, Kearney H, Patel A,

## ORIGINAL RESEARCH | GENETICS

- et al. Technical standards for the interpretation and reporting of constitutional copy-number variants: a joint consensus recommendation of ACMG and ClinGen. Genet Med. 2020; 22 (2): 245–57. DOI: 10.1038/s41436-019-0686-8.
- Minzhenkova ME, Yurchenko DA, Semenova NA, Markova ZG, Tarlycheva AA, Shilova NV. Characterization of a complex chromosomal rearrangement in a girl with PURA syndrome. Genet Mol Res. 2022; 21 (4). DOI: 10.4238/gmr19065.
- 14. Yurchenko DA, Minzhenkova ME, Tveleneva AA, Voroncova EO, Harchenko TV, Shilova NV. Citogenomnyj podhod v diagnostike invertirovannyh duplikacij so smezhnymi terminal'nymi deleciyami. Medicinskaya genetika. 2023; 22 (5): 54–62. Russian.
- Yurchenko DA. Molekulyarno-citogeneticheskie harakteristiki i osobennosti diagnostiki variacij chisla kopij uchastkov DNK (CNV) [dissertaciya]. M., 2022. Russian.
- Tonk VS, Jesurun CA, Morgan DL, Lockhart LH, Velagaleti GVN. Molecular cytogenetic characterization of a recombinant chromosome rec(22)dup(22q)inv(22)(p13q12.2). Am J Med Genet A. 2004; 124A (1): 92–95. DOI: 10.1002/ajmg.a.20384.
- Boyd LJ, Livingston JS, Brown MG, Lawce HJ, Gilhooly JT, Wildin RS, et al. Meiotic exchange event within the stalk region of an inverted chromosome 22 results in a recombinant chromosome with duplication of the distal long arm. Am J Med Genet A. 2005; 138 (4): 355–60. DOI: 10.1002/ajmg.a.30895.
- Pramparo T, de Gregori M, Gimelli S, Ciccone R, Frondizi D, Liehr T, et al. A 7 Mb duplication at 22q13 in a girl with bipolar disorder and hippocampal malformation. Am J Med Genet A. 2008; 146A (13): 1754–60. DOI: 10.1002/ajmg.a.32326.
- 19. Stankiewicz P, Lupski JR. Genome architecture, rearrangements

- and genomic disorders. Trends Genet. 2002; 18 (2): 74–82. DOI: 10.1016/s0168-9525(02)02592-1.
- Pastor S, Tran O, Jin A, Carrado D, Silva BA, Uppuluri L, et al. Optical mapping of the 22q11.2DS region reveals complex repeat structures and preferred locations for NAHR. Sci Rep. 2020; 10 (1): 12235. DOI: 10.1038/s41598-020-69134-4.
- Zhang F, Khajavi M, Connolly AM, Towne CF, Batish SD, Lupski JR.
  The DNA replication FoSTeS/MMBIR mechanism can generate
  genomic, genic and exonic complex rearrangements in humans.
  Nat Genet. 2009: 41 (7): 849–53. DOI: 10.1038/ng.399.
- Demaerel W, Mostovoy Y, Yilmaz F, Vervoort L, Pastor S, Hestand MS, et al. The 22q11 low copy repeats are characterized by unprecedented size and structural variability. Genome Res. 2019; 29 (9): 1389–401. DOI: 10.1101/gr.248682.119.
- Guo T, Diacou A, Nomaru H, McDonald-McGinn DM, Hestand M, Demaerel W, et al. Deletion size analysis of 1680 22q11.2DS subjects identifies a new recombination hotspot on chromosome 22q11.2. Hum Mol Genet. 2018; 27 (7): 1150–63. DOI: 10.1093/hmg/ddy028.
- van Sluis M, van Vuuren C, Mangan H, McStay B. NORs on human acrocentric chromosome p-arms are active by default and can associate with nucleoli independently of rDNA. Proc Natl Acad Sci USA. 2020; 117 (19): 10368–77. DOI: 10.1073/pnas.2001812117.
- Purow J, Waidner L, Ale H. Review of the pathophysiology and clinical manifestations of 22q11.2 deletion and duplication syndromes. Clin Rev Allergy Immunol. 2025; 68 (1): 23. DOI: 10.1007/s12016-025-09035-4.
- Deepika M, Tella S, Avvari S, Pratibha N, Ananthapur V. A rare case of dysmorphism with duplication in chromosome 22. Indian J Clin Biochem. 2022; 37 (4): 504–6. DOI: 10.1007/s12291-020-00945-y.

### Литература

- Liehr T, Weise A, Mrasek K, Ziegler M, Padutsch N, Wilhelm K, et al. Recombinant chromosomes resulting from parental pericentric inversions — two new cases and a review of the literature. Front Genet. 2019; 10: 1165. DOI: 10.3389/fgene.2019.01165.
- Madan K, Menko FH. Intrachromosomal insertions: a case report and a review. Hum Genet. 1992; 89 (1): 1–9. DOI: 10.1007/BF00207032.
- Carvalho CM, Lupski JR. Mechanisms underlying structural variant formation in genomic disorders. Nat Rev Genet. 2016; 17 (4): 224–38. DOI: 10.1038/nrg.2015.25.
- Gardner RJ, Amor DJ. Gardner and Sutherland's Chromosome Abnormalities and Genetic Counselling. 5th ed. Oxford: Oxford University Press, 2018; 440 p.
- Nowakowska BA, de Leeuw N, Ruivenkamp CA, Sikkema-Raddatz B, Crolla JA, Thoelen R, et al. Parental insertional balanced translocations are an important cause of apparently de novo CNVs in patients with developmental anomalies. Eur J Hum Genet. 2012; 20 (2): 166–70. DOI: 10.1038/ejhg.2011.157.
- Vervoort L, Vermeesch JR. The 22q11.2 low copy repeats. Genes (Basel). 2022; 13 (11): 2101. DOI: 10.3390/genes13112101.
- Demaerel W, Hosseinzadeh M, Nouri N, Sedghi M, Dimitriadou E, Salehi M, et al. Reciprocal 22q11.2 deletion and duplication in siblings with karyotypically normal parents. Cytogenet Genome Res. 2016; 148 (1): 1–5. DOI: 10.1159/000445089.
- Portnoï MF. Microduplication 22q11.2: a new chromosomal syndrome. Eur J Med Genet. 2009; 52 (2–3): 88–93. DOI: 10.1016/j.ejmg.2009.02.008.
- Arlt MF, Wilson TE, Glover TW. Replication stress and mechanisms of CNV formation. Curr Opin Genet Dev. 2012; 22 (3): 204–10. DOI: 10.1016/j.gde.2012.01.009.
- Liu P, Carvalho CM, Hastings PJ, Lupski JR. Mechanisms for recurrent and complex human genomic rearrangements. Curr Opin Genet Dev. 2012; 22 (3): 211–20. DOI: 10.1016/j.gde.2012.02.012.
- 11. Li S, Han X, Ye M, Chen S, Shen Y, Niu J, et al. Prenatal diagnosis of microdeletions or microduplications in the proximal, central, and distal regions of chromosome 22q11.2: ultrasound findings and pregnancy outcome. Front Genet. 2019; 10: 813. DOI: 10.3389/fgene.2019.00813.
- Riggs ER, Andersen EF, Cherry AM, Kantarci S, Kearney H, Patel A, et al. Technical standards for the interpretation and reporting

- of constitutional copy-number variants: a joint consensus recommendation of ACMG and ClinGen. Genet Med. 2020; 22 (2): 245–57. DOI: 10.1038/s41436-019-0686-8.
- Minzhenkova ME, Yurchenko DA, Semenova NA, Markova ZG, Tarlycheva AA, Shilova NV. Characterization of a complex chromosomal rearrangement in a girl with PURA syndrome. Genet Mol Res. 2022; 21 (4). DOI: 10.4238/gmr19065.
- Юрченко Д. А., Миньженкова М. Е., Твеленева А. А., Воронцова Е. О., Харченко Т. В., Шилова Н. В. Цитогеномный подход в диагностике инвертированных дупликаций со смежными терминальными делециями. Медицинская генетика. 2023; 22 (5): 54–62.
- Юрченко Д. А. Молекулярно-цитогенетические характеристики и особенности диагностики вариаций числа копий участков ДНК (CNV) [диссертация]. М., 2022.
- Tonk VS, Jesurun CA, Morgan DL, Lockhart LH, Velagaleti GVN. Molecular cytogenetic characterization of a recombinant chromosome rec(22)dup(22q)inv(22)(p13q12.2). Am J Med Genet A. 2004; 124A (1): 92–95. DOI: 10.1002/ajmg.a.20384.
- Boyd LJ, Livingston JS, Brown MG, Lawce HJ, Gilhooly JT, Wildin RS, et al. Meiotic exchange event within the stalk region of an inverted chromosome 22 results in a recombinant chromosome with duplication of the distal long arm. Am J Med Genet A. 2005; 138 (4): 355–60. DOI: 10.1002/ajmg.a.30895.
- Pramparo T, de Gregori M, Gimelli S, Ciccone R, Frondizi D, Liehr T, et al. A 7 Mb duplication at 22q13 in a girl with bipolar disorder and hippocampal malformation. Am J Med Genet A. 2008; 146A (13): 1754–60. DOI: 10.1002/ajmg.a.32326.
- Stankiewicz P, Lupski JR. Genome architecture, rearrangements and genomic disorders. Trends Genet. 2002; 18 (2): 74–82. DOI: 10.1016/s0168-9525(02)02592-1.
- Pastor S, Tran O, Jin A, Carrado D, Silva BA, Uppuluri L, et al. Optical mapping of the 22q11.2DS region reveals complex repeat structures and preferred locations for NAHR. Sci Rep. 2020; 10 (1): 12235. DOI: 10.1038/s41598-020-69134-4.
- 21. Zhang F, Khajavi M, Connolly AM, Towne CF, Batish SD, Lupski JR. The DNA replication FoSTeS/MMBIR mechanism can generate genomic, genic and exonic complex rearrangements in humans. Nat Genet. 2009; 41 (7): 849–53. DOI: 10.1038/ng.399.

## ОРИГИНАЛЬНОЕ ИССЛЕДОВАНИЕ І ГЕНЕТИКА

- Demaerel W, Mostovoy Y, Yilmaz F, Vervoort L, Pastor S, Hestand MS, et al. The 22q11 low copy repeats are characterized by unprecedented size and structural variability. Genome Res. 2019; 29 (9): 1389–401. DOI: 10.1101/gr.248682.119.
- Guo T, Diacou A, Nomaru H, McDonald-McGinn DM, Hestand M, Demaerel W, et al. Deletion size analysis of 1680 22q11.2DS subjects identifies a new recombination hotspot on chromosome 22q11.2. Hum Mol Genet. 2018; 27 (7): 1150–63. DOI: 10.1093/ hmg/ddy028.
- 24. van Sluis M, van Vuuren C, Mangan H, McStay B. NORs on human
- acrocentric chromosome p-arms are active by default and can associate with nucleoli independently of rDNA. Proc Natl Acad Sci USA. 2020; 117 (19): 10368–77. DOI: 10.1073/pnas.2001812117.
- Purow J, Waidner L, Ale H. Review of the pathophysiology and clinical manifestations of 22q11.2 deletion and duplication syndromes. Clin Rev Allergy Immunol. 2025; 68 (1): 23. DOI: 10.1007/s12016-025-09035-4.
- Deepika M, Tella S, Avvari S, Pratibha N, Ananthapur V. A rare case of dysmorphism with duplication in chromosome 22. Indian J Clin Biochem. 2022; 37 (4): 504–6. DOI: 10.1007/s12291-020-00945-y.

## THE TERMS "DOMINANT" AND "RECESSIVE" SHOULD BE AVOIDED DUE TO GENE THERAPY

Gamisonia AM <sup>™</sup>, Rebrikov DV

Pirogov Russian National Research Medical University (Pirogov University), Moscow, Russia

The accumulation of scientific data can conflict with theoretical propositions, requiring their revision. Ptolemy's model of celestial motion was repeatedly "upgraded" until the paradigm fundamentally changed. Today, we not only understand the structure of the solar system but also see the universe across fourteen billion light-years. Similarly, phenotype-based medical genetics still operates with concepts such as dominance, recessiveness, penetrance, expressivity, complementarity, epistasis, and so on. These are descriptive terms of limited accuracy, which are redundant and often confounding in clinical settings. This opinion article re-examines the relationship between molecular inheritance and its phenotypic manifestations in light of the growing role of gene editing and gene therapy. We believe that the use of the classical terms "dominant" and "recessive" in a medical context should be avoided as non-informative and possibly misleading in terms of clinical decisions and treatment choices.

Keywords: dominant, recessive, genotype, phenotype, loss-of-function, gain-of-function, haploinsufficiency, dominant-negative effect, clinical genetics, compensatory gene therapy, genome editing

Funding: This work was supported by the State Assignment of the Ministry of Health of the Russian Federation, Registration No. 123021500064-0, "Development of technology for personalized gene therapy drugs based on the AAV platform and drugs for the treatment of Sanfilippo syndrome and multiple epiphyseal dysplasia."

Acknowledgements: The authors are grateful to Sergey Glagolev for his critical comments

**Author contribution:** Gamisoniya AM — analysis and summary of literature data, manuscript writing, manuscript design; Rebrikov DV — critical revision and editing of the manuscript.

Correspondence should be addressed: Alina Mukhadinovna Gamisoniya Ostrovityanova, 1, Moscow, 117997, Russia; amgamisoniya@mail.ru

Received: 23.10.2025 Accepted: 30.10.2025 Published online: 31.10.2025

DOI: 10.24075/brsmu.2025.055

Copyright: © 2025 by the authors. Licensee: Pirogov University. This article is an open access article distributed under the terms and conditions of the Creative Commons Attribution (CC BY) license (https://creativecommons.org/licenses/by/4.0/).

# В МЕДИЦИНЕ СЛЕДУЕТ ИЗБЕГАТЬ ТЕРМИНОВ «ДОМИНАНТНЫЙ» И «РЕЦЕССИВНЫЙ» ИЗ-ЗА РАЗВИТИЯ ГЕННОЙ ТЕРАПИИ

А. М. Гамисония ⊠, Д. В. Ребриков

Российский национальный исследовательский медицинский университет (Пироговский Университет), Москва, Россия

Понимание устройства системы ведет к оптимизации описывающей ее модели. Модель движения небесных тел Птолемея многократно усложнялась с целью подгонки под реальность, пока точка зрения исследователей кардинально не изменилась. Аналогично и «фенотипическая генетика» до сих пор пытается описывать наблюдаемое в терминах XIX в.: доминантность, рецессивность, пенетрантность, экспрессивность, комплементарность, эпистаз и т. д. Сегодня мы не просто понимаем устройство Солнечной системы, но видим Вселенную на четырнадцать миллиардов световых лет. Использовать в клинической генетике описательную фенотипическую терминологию — то же самое, что определять расположение небесных тел по гороскопу. В статье рассмотрено соотношение некоторых молекулярных механизмов наследования и их фенотипических проявлений. На фоне возрастающей роли геноредактирующей, генозаместительной и генокомпенсаторной терапии использование фенотипических терминов «доминантный» и «рецессивный» становится нежелательным, поскольку не отражает молекулярный профиль заболевания и может вводить врачей в заблуждение при выборе метода лечения.

**Ключевые слова:** доминантный, рецессивный, генотип, фенотип, потеря функции, возрастание функции, гаплонедостаточность, доминантно-негативный эффект, клиническая генетика, генозаместительная терапия, генокомпенсаторная терапия, геномное редактирование

Финансирование: работа выполнена в рамках Государственного задания МЗ РФ Рег № 123021500064-0 «Разработка технологии персонализированных генотерапевтических лекарственных препаратов на платформе ААВ и препаратов для лечения синдрома Санфилиппо и множественной эпифизарной дисплазии».

Благодарности: авторы признательны Сергею Глаголеву за критические комментарии.

**Вклад авторов:** А. М. Гамисония — анализ и обобщение данных литературы, написание текста и оформление рукописи; Д. В. Ребриков — критический пересмотр и редактирование текста рукописи.

Для корреспонденции: Алина Мухадиновна Гамисония ул. Островитянова, д. 1, г. Москва, 117997, Россия; amgamisoniya@mail.ru

Статья получена: 23.10.2025 Статья принята к печати: 30.10.2025 Опубликована онлайн: 31.10.2025

DOI: 10.24075/vrgmu.2025.055

Авторские права: © 2025 принадлежат авторам. **Лицензиат:** PHИMУ им. Н. И. Пирогова. Статья размещена в открытом доступе и распространяется на условиях лицензии Creative Commons Attribution (CC BY) (https://creativecommons.org/licenses/by/4.0/).

Establishing the relationship between a genotype and its manifestation (phenotype) is a key task in genetics, which for diploid organisms is complicated by the interaction of two complete sets of (different) genetic information. Gregor Mendel termed a parental trait expressed in the offspring "dominant", as opposed to cryptic "recessive" traits prone to vanishing. Today, we know that traits represent the realization of the function of proteins (or regulatory RNAs) encoded in DNA, and a dominant phenotype can result from either increased or decreased protein activity/concentration due to various genetic and epigenetic factors: allelic polymorphism of the protein-coding sequence, DNA methylation profile, histone modification and promoter activity, small regulatory RNAs, post-translational protein modification, polygenic interactions, etc. In medical genetics, loss-of-function (LOF) mutations are typically associated with recessive inheritance, while gainof-function (GOF) mutations are associated with dominant inheritance. However, there are numerous exceptions to this simplistic rule, highlighting the importance of understanding the functional context and biological role of the affected protein or the corresponding regulatory mechanism, particularly in view of gene therapy options.

The rapid development of genetic programming technologies (including the modulation of gene activity by delivering additional copies, CRISPR editing, or using small RNAs) has led to the emergence of a wide range of high-tech drugs prescribed to compensate for genetic disorders (if a function is deficient, it obviously needs to be enhanced; if it is excessive, it needs to be attenuated). At the same time, the "phenotypic" terms dating from the mid-19<sup>th</sup> century continue to appear in medical records, clinical treatment guidelines, laboratory test reports, and even in gene therapy protocols. According to our estimates, up to 8% of laboratory test reports describing specific molecular events in monogenic diseases are misinterpreted by medical geneticists because of confounding "phenotypic" descriptions.

## Terminology: inheritance types and corresponding molecular mechanisms

Autosomal dominant (AD) and autosomal recessive (AR) diseases have clearly distinct patterns of occurrence in a genetic pedigree. With AD inheritance, a single mutant copy of the gene (heterozygous state) is sufficient for the development of the disease, which is characterized by a 50% risk of vertical transmission from generation to generation (examples include Huntington's disease, Thomsen disease, Creutzfeldt-Jakob disease, and over 4,000 other conditions) [1–3].

With AR inheritance, a mutation in both copies of the gene is required for the development of the disease (homozygous/compound heterozygous state). In such cases, the parents are usually healthy carriers, and the disease in the offspring occurs due to the coincidence of nonfunctional alleles with a 25% probability (examples include hereditary hearing loss, cystic fibrosis, phenylketonuria, and over 3,000 other conditions) [4–6].

In the case of X-linked recessive inheritance, the trait is phenotypically manifested in males in the hemizygous state, while homozygosity/compound heterozygosity for the mutation is required for manifestation in females. Classic examples of this group of diseases are hemophilia A and color blindness, and over 100 similarly inherited conditions have been described [7, 8].

In X-linked dominant inheritance, the presence of a single mutant allele is sufficient for manifestation. This type of inheritance is characterized by more severe consequences in males, sometimes lethal early in development. An affected

woman has a 50% chance of transmitting the disease to offspring of both sexes, while an affected man transmits the mutant allele to all of his daughters and none of his sons. About 40 diseases have this pattern of inheritance. A striking example of X-linked dominant condition is Rett syndrome [9]. Importantly, in women, the pathogenic allele in each individual cell will be either active or not as a result of X-inactivation; the ratio can vary, which explains the phenomenon of varying symptom severity in heterozygous carriers.

The classical Mendelian scheme assumes 100% phenotypic expression of any allele (penetrance) with full strength (expressivity), and that the presence of a mutant variant in a particular number of copies is unambiguously linked to the phenotype. However, for many hereditary conditions, both autosomal dominant and X-linked, so-called incomplete penetrance is observed (when some carriers of a pathogenic allele remain clinically asymptomatic throughout their lives due to the genomic landscape and environmental factors). Incomplete penetrance creates significant difficulties for medical genetic counseling, as a phenotypically healthy individual can transmit a mutant allele to an offspring who unexpectedly develops the disease. Agedependent penetrance and variable expressivity are recognized as well; it should be noted that manifestation of any trait is agedependent and variable in strength, even in identical twins. For example, for autosomal dominant neurofibromatosis type 1 or hereditary cancer syndromes caused by mutations in tumor suppressor genes (such as BRCA1 or TP53), the penetrance is considered age-dependent, while the expressivity varies [10].

## Conventionality of "dominance" and "recessiveness" in the context of gain- and loss-of-function mutations

From a molecular perspective, different inheritance patterns are typically associated with functional types of mutations. Gain-of-function mutations confer a new or enhanced function to the protein, which is pathogenic even with a normal second allele. This mechanism most often underlies dominant diseases. However, the disease typically occurs only in heterozygotes, as homozygosity for such critical defects leads to embryonic death early in development.

By contrast, loss-of-function mutations result in complete or partial loss of protein function (for example, due to promoter inactivation or severe disruption of protein structure) and are usually associated with recessive diseases [11, 12].

However, under certain conditions, LOF mutations can lead to dominant pathologies (in heterozygotes). This occurs through two main mechanisms: haploinsufficiency and dominant-negative effects. Haploinsufficiency occurs when the level of normal protein synthesized from a single functioning allele is insufficient to fully implement the necessary functions, leading to the development of disease (examples include Marfan syndrome, DiGeorge syndrome, Williams syndrome, and approximately 500 other diseases) [13–15]. In the context of incomplete penetrance, haploinsufficiency can predispose to disease (examples include tumor suppressor genes, such as TP53 in Li-Fraumeni syndrome, BRCA1 in ovarian cancer, etc.) [16, 17].

A dominant-negative effect is observed when the LOF mutant protein not only loses function but also actively disrupts the functioning of intracellular systems, for example, through inclusion in multimeric complexes, changes in receptor titer, and other methods of competitive inhibition. Thus, LOF mutations can manifest as either recessive or dominant mutations (examples include Brugada syndrome, Culler-Jones syndrome, and approximately 700 other diseases) [18, 19].

Thus, comparing the heterozygous GOF effect of protein hyperactivity/overconcentration and the heterozygous dominant-negative LOF effect of competitive inhibition of multicomplexes, it can be argued that the key factor in understanding the molecular mechanisms of pathology and choosing the correct pathogenetic therapy (gene delivery or genome editing) is the deficiency or excess of function, not homo/heterozygosity (and, especially, not the phenotype).

Incomplete penetrance adds uncertainty to the decision to use a gene therapy, especially when prescribing treatment before the clinical manifestation of a monogenic hereditary disease [20]. In such cases, it is necessary to weigh the reversibility of pathological processes with delayed phenotypic manifestation against the safety of the gene therapy.

#### CONCLUSION

Thus, in modern medical genetics, the phenotypic terms "dominant" and "recessive" are losing their diagnostic and prognostic value. Their persistent use can mislead the clinical interpretation of molecular-genetic findings and critically undermine the choice of therapeutic strategy. With the rapid development of gene replacement, gene compensatory therapy, and genome editing, the emphasis should be shifted from formally classifying the mode of inheritance to accurately determining the molecular routes of pathogenesis — whether the cause of a disease is a consequence of a deficiency or excess of a specific macromolecule (protein, tRNA, etc.). This functional approach is essential for the prescription of pathogenetically based and personalized therapy.

#### References

- McColgan, P., & Tabrizi, S. J. (2018). Huntington's disease: a clinical review. European journal of neurology. 25 (1): 24–34. Available from: https://doi.org/10.1111/ene.13413.
- Suetterlin K, Matthews E, Sud R, McCall S, Fialho D, Burge J, et al. Translating genetic and functional data into clinical practice: a series of 223 families with myotonia. Brain: a journal of neurology. 2022; 145 (2): 607–20. Available from: https://doi.org/10.1093/brain/awab344.
- Chen C, Dong XP. Epidemiological characteristics of human prion diseases. Infectious diseases of poverty. 2016; 5 (1): 47. Available from: https://doi.org/10.1186/s40249-016-0143-8.
- Sommen M, Schrauwen I, Vandeweyer G, Boeckx N, Corneveaux JJ, van den Ende J, et al. DNA Diagnostics of Hereditary Hearing Loss: A Targeted Resequencing Approach Combined with a Mutation Classification System. Human mutation. 2016; 37 (8): 812–9. Available from: https://doi.org/10.1002/humu.22999.
- Polgreen PM, Comellas AP. Clinical Phenotypes of Cystic Fibrosis Carriers. Annual review of medicine. 2022; 73: 563–74. Available from: https://doi.org/10.1146/annurev-med-042120-020148.
- van Spronsen FJ, Blau N, Harding C, Burlina A, Longo N, Bosch AM. Phenylketonuria. Nature reviews. Disease primers. 2021; 7 (1): 36. Available from: https://doi.org/10.1038/s41572-021-00267-0.
- Berntorp E, Fischer K, Hart DP, Mancuso ME, Stephensen D, Shapiro AD, et al. Haemophilia. Nature reviews. Disease primers. 2021;
   7 (1): 45. Available from: https://doi.org/10.1038/s41572-021-00278-x.
- larossi G, Coppè AM, Passarelli C, Maltese PE, Sinibaldi L, Cappelli A, et al. Blue Cone Monochromatism with Foveal Hypoplasia Caused by the Concomitant Effect of Variants in OPN1LW/OPN1MW and GPR143 Genes. International journal of molecular sciences. 2021; 22 (16): 8617. Available from: https://doi.org/10.3390/ijms22168617.
- Renieri A, Meloni I, Longo I, Ariani F, Mari F, Pescucci C, Cambi F. Rett syndrome: the complex nature of a monogenic disease. Journal of molecular medicine (Berlin, Germany). 2003; 81 (6): 346–54. Available from: https://doi.org/10.1007/s00109-003-0444-9.
- Chen S, Parmigiani G. Meta-analysis of BRCA1 and BRCA2 penetrance. Journal of clinical oncology: official journal of the American Society of Clinical Oncology. 2007; 25 (11): 1329–33.
   Available from: https://doi.org/10.1200/JCO.2006.09.1066.
- 11. Jiao SY, Yang YH, Chen SR. Molecular genetics of infertility: loss-

- of-function mutations in humans and corresponding knockout/mutated mice. Human reproduction update. 2021; 27 (1): 154–89. Available from: https://doi.org/10.1093/humupd/dmaa034.
- Malik I, Kelley CP, Wang ET, Todd PK. Molecular mechanisms underlying nucleotide repeat expansion disorders. Nature reviews. Molecular cell biology. 2021; 22 (9): 589–607. Available from: https://doi.org/10.1038/s41580-021-00382-6.
- Judge DP, Biery NJ, Keene DR, Geubtner J, Myers L, Huso DL, et al. Evidence for a critical contribution of haploinsufficiency in the complex pathogenesis of Marfan syndrome. The Journal of clinical investigation. 2004; 114 (2): 172–81. Available from: https://doi.org/10.1172/JCl20641.
- 14. Lindsay EA, Vitelli F, Su H, Morishima M, Huynh T, Pramparo T, et al. Tbx1 haploinsufficieny in the DiGeorge syndrome region causes aortic arch defects in mice. Nature. 2001; 410 (6824): 97–101. Available from: https://doi.org/10.1038/35065105.
- Metcalfe K, Simeonov E, Beckett W, Donnai D, Tassabehji M. Autosomal dominant inheritance of Williams-Beuren syndrome in a father and son with haploinsufficiency for FKBP6. Clinical dysmorphology. 2005; 14 (2): 61–65.
- Bougeard G, Renaux-Petel M, Flaman JM, Charbonnier C, Fermey P, Belotti M, et al. Revisiting Li-Fraumeni Syndrome From TP53 Mutation Carriers. Journal of clinical oncology: official journal of the American Society of Clinical Oncology. 2015; 33 (21): 2345– 52. Available from: https://doi.org/10.1200/JCO.2014.59.5728.
- Chu DT, Vu Ngoc Suong M, Vu Thi H, Vu TD, Nguyen MH, Singh V. The expression and mutation of BRCA1/2 genes in ovarian cancer: a global systematic study. Expert review of molecular diagnostics. 2023; 23 (1): 53–61. Available from: https://doi.org/10.1080/147 37159.2023.2168190.
- Doisne N, Grauso M, Mougenot N, Clergue M, Souil C, Coulombe A. In vivo Dominant-Negative Effect of an SCN5A Brugada Syndrome Variant. Frontiers in physiology. 2021; 12: 661413. Available from: https://doi.org/10.3389/fphys.2021.661413.
- Bertolacini CD, Ribeiro-Bicudo LA, Petrin A, Richieri-Costa A, Murray JC. Clinical findings in patients with GLI2 mutations phenotypic variability. Clinical genetics. 2012; 81 (1): 70–75. Available from: https://doi.org/10.1111/j.1399-0004.2010.01606.x.
- Shubina J, Tolmacheva E, Maslennikov D, Kochetkova T, Mukosey I, Sadelov I, et al. WES-based screening of 7,000 newborns: A pilot study in Russia. HGG Adv. 2024; 10; 5 (4): 100334. Available from: https://doi.org/10.1016/j.xhgg.2024.100334.

### Литература

- McColgan, P., & Tabrizi, S. J. (2018). Huntington's disease: a clinical review. European journal of neurology. 25 (1): 24–34. Available from: https://doi.org/10.1111/ene.13413.
- Suetterlin K, Matthews E, Sud R, McCall S, Fialho D, Burge J, et al. Translating genetic and functional data into clinical practice: a series of 223 families with myotonia. Brain: a journal of neurology. 2022; 145
- (2): 607–20. Available from: https://doi.org/10.1093/brain/awab344.
  3. Chen C, Dong XP. Epidemiological characteristics of human prion diseases. Infectious diseases of poverty. 2016; 5 (1): 47. Available from: https://doi.org/10.1186/s40249-016-0143-8.
- Sommen M, Schrauwen I, Vandeweyer G, Boeckx N, Corneveaux JJ, van den Ende J, et al. DNA Diagnostics of Hereditary Hearing

## МНЕНИЕ І ГЕНЕТИКА

- Loss: A Targeted Resequencing Approach Combined with a Mutation Classification System. Human mutation. 2016; 37 (8): 812–9. Available from: https://doi.org/10.1002/humu.22999.
- Polgreen PM, Comellas AP. Clinical Phenotypes of Cystic Fibrosis Carriers. Annual review of medicine. 2022; 73: 563–74. Available from: https://doi.org/10.1146/annurev-med-042120-020148.
- van Spronsen FJ, Blau N, Harding C, Burlina A, Longo N, Bosch AM. Phenylketonuria. Nature reviews. Disease primers. 2021; 7 (1): 36. Available from: https://doi.org/10.1038/s41572-021-00267-0.
- Berntorp E, Fischer K, Hart DP, Mancuso ME, Stephensen D, Shapiro AD, et al. Haemophilia. Nature reviews. Disease primers. 2021;
   7 (1): 45. Available from: https://doi.org/10.1038/s41572-021-00278-x.
- larossi G, Coppè AM, Passarelli C, Maltese PE, Sinibaldi L, Cappelli A, et al. Blue Cone Monochromatism with Foveal Hypoplasia Caused by the Concomitant Effect of Variants in OPN1LW/OPN1MW and GPR143 Genes. International journal of molecular sciences. 2021; 22 (16): 8617. Available from: https://doi.org/10.3390/ijms22168617.
- Renieri A, Meloni I, Longo I, Ariani F, Mari F, Pescucci C, Cambi F. Rett syndrome: the complex nature of a monogenic disease. Journal of molecular medicine (Berlin, Germany). 2003; 81 (6): 346–54. Available from: https://doi.org/10.1007/s00109-003-0444-9.
- Chen S, Parmigiani G. Meta-analysis of BRCA1 and BRCA2 penetrance. Journal of clinical oncology: official journal of the American Society of Clinical Oncology. 2007; 25 (11): 1329–33.
   Available from: https://doi.org/10.1200/JCO.2006.09.1066.
- Jiao SY, Yang YH, Chen SR. Molecular genetics of infertility: loss-of-function mutations in humans and corresponding knockout/mutated mice. Human reproduction update. 2021; 27 (1): 154–89. Available from: https://doi.org/10.1093/humupd/dmaa034.
- Malik I, Kelley CP, Wang ET, Todd PK. Molecular mechanisms underlying nucleotide repeat expansion disorders. Nature reviews. Molecular cell biology. 2021; 22 (9): 589–607. Available from:

- https://doi.org/10.1038/s41580-021-00382-6.
- Judge DP, Biery NJ, Keene DR, Geubtner J, Myers L, Huso DL, et al. Evidence for a critical contribution of haploinsufficiency in the complex pathogenesis of Marfan syndrome. The Journal of clinical investigation. 2004; 114 (2): 172–81. Available from: https://doi.org/10.1172/JCl20641.
- 14. Lindsay EA, Vitelli F, Su H, Morishima M, Huynh T, Pramparo T, et al. Tbx1 haploinsufficieny in the DiGeorge syndrome region causes aortic arch defects in mice. Nature. 2001; 410 (6824): 97–101. Available from: https://doi.org/10.1038/35065105.
- Metcalfe K, Simeonov E, Beckett W, Donnai D, Tassabehji M. Autosomal dominant inheritance of Williams-Beuren syndrome in a father and son with haploinsufficiency for FKBP6. Clinical dysmorphology. 2005; 14 (2): 61–65.
- Bougeard G, Renaux-Petel M, Flaman JM, Charbonnier C, Fermey P, Belotti M, et al. Revisiting Li-Fraumeni Syndrome From TP53 Mutation Carriers. Journal of clinical oncology: official journal of the American Society of Clinical Oncology. 2015; 33 (21): 2345– 52. Available from: https://doi.org/10.1200/JCO.2014.59.5728.
- Chu DT, Vu Ngoc Suong M, Vu Thi H, Vu TD, Nguyen MH, Singh V. The expression and mutation of BRCA1/2 genes in ovarian cancer: a global systematic study. Expert review of molecular diagnostics. 2023; 23 (1): 53–61. Available from: https://doi.org/10.1080/147 37159.2023.2168190.
- Doisne N, Grauso M, Mougenot N, Clergue M, Souil C, Coulombe A. In vivo Dominant-Negative Effect of an SCN5A Brugada Syndrome Variant. Frontiers in physiology. 2021; 12: 661413. Available from: https://doi.org/10.3389/fphys.2021.661413.
- Bertolacini CD, Ribeiro-Bicudo LA, Petrin A, Richieri-Costa A, Murray JC. Clinical findings in patients with GLI2 mutations phenotypic variability. Clinical genetics. 2012; 81 (1): 70–75. Available from: https://doi.org/10.1111/j.1399-0004.2010.01606.x.
- Shubina J, Tolmacheva E, Maslennikov D, Kochetkova T, Mukosey I, Sadelov I, et al. WES-based screening of 7,000 newborns: A pilot study in Russia. HGG Adv. 2024; 10; 5 (4): 100334. Available from: https://doi.org/10.1016/j.xhgg.2024.100334.